ENHANCEMENT OF TRIBOLOGICAL PROPERTIES OF MINERAL OIL BY ADDITION OF SORBITAN MONOSTEARATE AND ZINC BORATE

A Thesis Submitted to
the Graduate School of Engineering and Sciences of
İzmir Institute of Technology
in Partial Fulfillment of the Requirements for the Degree of

DOCTOR OF PHILOSOPHY

in Chemical Engineering

by
Sevdiye ATAKUL SAVRIK

July 2010
İZMİR

ACKNOWLEDGMENTS

ABSTRACT

ENHANCEMENT OF TRIBOLOGICAL PROPERTIES OF MINERAL OIL BY ADDITION OF SORBITAN MONOSTEARATE AND ZINC BORATE

The development of modern automobile and engine industries requires lubricants that can withstand high temperatures and pressures. Recent advances made in the chemistry provide the use of inorganic particles as lubricant additives. Therefore inorganic boron-based additives have been the focus of much attention, as they posses a good combination of properties, such as wear resistance, friction-reducing ability. In this study, the state of art in the field of inorganic particle, zinc borate synthesis and its employment in tribology were investigated. The synthesis of zinc borate was achieved not just by precipitation, but also production methods such as inverse emulsions. The products were characterized by SEM, FTIR, TGA, DSC, EDX. In lubrication part, the friction reducing and antiwear ability of the particles as an additive in the mineral oil was focused. Sorbitan monostearate was used to cover the surfaces of inorganic particles in order to provide better dispersion of additives in the oil. Friction and wear behavior of the lubricants were measured by four-ball wear test machine. The effects of dispersing agent, zinc borate type as well as surfactant concentration on the tribological properties of the lubricants were investigated. Sorbitan monostearate not only outperformed as a dispersing agent of inorganic particles, but also it proved to be an efficient antiwear agent. The lowest wear scar diameter was obtained by the lubricant containing zinc borate synthesized via coordination precipitation method. The addition of this sample with the surfactant in the oil reduced the wear scar diameter from 1.402 mm to 0.550 mm.

ÖZET

MİNERAL YAĞLARININ TRİBOLOJİK ÖZELLİKLERİNİN SORBİTAN MONOSTEARAT VE ÇİNKO BORAT KATKISI İLE GELİŞTİRİLMESİ

Otomobil ve motor endüstrisindeki gelişmeler yüksek sıcaklık ve basınca dayanıklı kaydırıcılar gerektirmektedir. Kimya bilimindeki son gelişmeler inorganik parçacıkların tribolojide kaydırıcı katkısı olarak kullanılmasını sağlamaktadır. Bor bazlı inorganik katkılar sürtünmeyi azaltıcı, aşınma önleyici gibi özelliklerinden dolayı çalışmaların odak noktasını oluşturmaktadırlar. Bu çalışmada çinko borat sentezi ve bu malzemenin triboloji alanında uygulanması araştırılmıştır. Çinko borat sadece çöktürme ile değil, aynı zamanda özel bir üretim yöntemi olan ters emülsiyon tekniği ile de üretilmiştir. Parçacıkların tanımlanması SEM, FTIR, TGA, DSC, EDX ile yapılmıştır. Kaydırıcılar bölümünde ise, sentezlenen parçacıkların mineral yağ içinde sürtünmeyi ve aşınmayı önleyici özellikler sağlayıp sağlamadığı araştırılmıştır. Yağın içine sentezlenen parçacıkların yanı sıra bu parçacıkların yüzeyini kaplayan ve yağ içinde daha homojen olarak dağılmasını sağlayan sorbitan monostearat da eklenmiştir. Kaydırıcıların sürtünme ve aşınma testleri dört top aşınma cihazında yapılmıştır. Kaydırıcılarda dispersiyon ajanı, farklı çinko borat türlerinin ve yüzey aktif madde derişiminin etkileri tribolojik özellikleri göz önünde bulundurularak değerlendirilmiştir. Sorbitan monostearat, sadece dispersiyon ajanı olarak değil aynı zamanda aşınma önleyici katkı olarak da kullanılabilineceğini kanıtlamıştır. En düşük aşınma iz çapı koordinasyon çöktürme yöntemi ile üretilen çinko boratı içeren kaydırıcıda gözlenmiştir. Bu katkının yüzey aktif madde ile saf yağda 1.402 mm olan aşınma iz çapını 0.550 mm'ye düşürdüğü belirlenmiştir.

Dedicated to My Mother

Sebahat ATAKUL

TABLE OF CONTENTS

LIST OF FIGURES

LIST OF TABLES

CHAPTER 1

INTRODUCTION

Lubrication is an art that has been practiced for thousands of years from the early days of the human civilization. The study of lubrication as a science began in the 17th century with the development of bearings and axles. In the early 21st century, the advent of automobiles and steam engines caused the development of modern complex lubricants consisting of base oils and chemical additives (Hsu, 2004). Such additives include dispersants, surfactants, oxidation inhibitors, and antiwear agents (Smiechowski and Lvovich, 2002). Friction and surface damage can be reduced by applying extreme pressure and anti-wear additives. These tend to be suphur-, chlorine-, and phosphorous-containing compounds designed to react chemically with the metal surfaces, forming easily sheared layers of sulphides, chlorines or phoshides and thereby preventing severe wear and seizure. As an environmental protection measure, the use of chlorine- and phosphorous-containing compounds used as lubricant additives has been restricted, and so developing new additives that pollute less has therefore become the target researchers. Therefore organic and inorganic boron-based additives have been the focus of much attention, as they posses a good combination of properties, such as wear resistance, friction-reducing ability, oxidation inhibition, low toxicity, pleasant odor and compatibility with frictional pairs (Battez et al., 2006; Zheng et al., 1998). Among boron compounds, hexagonal boron nitride (BN) has a lamellar crystalline structure, in which the bonding between molecules within each layer is strong covalent, while the binding between layers is almost entirely by means of weak van der Waals forces. This structure is similar to that of graphite and molybdenum disulfide which are highly successful solid lubricants, and the mechanism behind their effective lubricating performance is understood to be owing to easy shearing along the basal plane of the hexagonal crystalline structures (Pawlak et al., 2009; Kimura et al., 1999). In addition the employment of hexagonal boron nitride in lubricating oils, metal borates which are extraordinary ceramic and functional materials find in use as an antiwear and anticorrosion material. In literature, numerous studies have been carried out in recent

years on the effects of various metal borate particles as lubricating oil additives on wear and friction (Hu and Dong, 1998; Dong and Hu, 1998; Hu et al., 2000). Their effectiveness can be related to the formation of a borate glass as a tribochemical film or the deposition of particles on the rubbing surface (Varlot et al., 2001). The friction-reduction and anti-wear behaviors are dependent on the characteristics of nanoparticles, such as size, shape, and concentration.

Water-in-oil inverse emulsions are formed by mixing small amounts of water and surfactant with oil. The inverse emulsion droplets consist of a water core surrounded by a single layer of surfactant molecules act as micro/nano reactors. These reactors are used to synthesize metal, organic and inorganic particles and the excellent ability of emulsion-assisted precipitation provides to control the shape and the size of the synthesized particles. Moreover, the precipitated particles in emulsions are stabilized by the surfactant monolayer which surrounds each microemulsion droplet and thereby particle agglomeration is suppressed. In general, two different modes for the initialization of the precipitation reaction can be distinguished in emulsions. For the first case, one reactant is transported from the continuous phase into the emulsion droplets which already contain the other reactant, whereas for the second case, two separate emulsions are prepared containing the aqueous solution of the reactants then these two microemulsions are mixed. In both operating modes, the two reactants are contacted within the emulsion droplets and consequently a chemical reaction starts which is followed by particle nucleation and growth (Niemann and Sundmacher, 2010).

Zinc borate is a synthetic hydrated metal borate. There are various kinds of crystalline hydrated zinc borate. These have compositions $4ZnO \cdot B_2O_3 \cdot H_2O$, $ZnO \cdot B_2O_3 \cdot 1.12H_2O$, $ZnO \cdot B_2O_3 \cdot 2H_2O$, $6ZnO \cdot 5B_2O_3 \cdot 3H_2O$, $2ZnO \cdot 3B_2O_3 \cdot 7H_2O$, $2ZnO \cdot 3B_2O_3 \cdot 3H_2O$. In these products, B_2O_3/ZnO mole ratios changes from 0.25 to 5 and it determines the characteristics of product (Schubert, 1995). The production techniques of zinc borate generally include the reaction between zinc source materials (zinc oxide, zinc salts, zinc hydroxide) and the boron source materials (boric acid and borax) (Nies et al., 1972, Shi et al., 2008; Eltepe et al., 2007). In literature the studies have demonstrated that zinc borate is commonly used as flame-retardant filler in polyvinylcloride (PVC), polyamides, and epoxy resins.

This study attempts not only to enhance the tribological properties of mineral oil by employment of sorbitan monostearate and zinc borate additives but also to

synthesize boron based lubricant additives by precipitation and inverse emulsion technique. Moreover, the other objective is to characterize the synthesized particles in order to estimate the ranges of application of zinc borate used as a lubricating oil additive and to understand the mechanism under the lubrication theory of zinc borate. This study also aims to present a new lubrication preparation technique in the field of both colloidal systems and nano-size particle preparation since the prepared inverse emulsions are directly used as lubricants without any further processes.

In Chapter 2, wear, friction and lubrication in tribology are introduced. Mechanical-dynamic testing methods for lubrication and the types of lubricants are defined. Besides them, recent studies related to the preparation and testing of lubricating oil additives are reviewed. Chapter 3 summarizes the boron-based lubricating oil additives. In Chapter 4, emulsions and the synthesis of nano-sized particles by inverse emulsion technique are explained. Chapter 5 includes the production of zinc borate and its characterization. Chapter 6 describes the materials used in the production of zinc borate samples, experimental procedure of synthesis and the preparation of lubricants. This chapter explains the characterization techniques for both zinc borate particles and the lubricants, as well. Chapter 7 includes results of zinc borate production by inverse emulsion and precipitation techniques and it indicates the tribological characterization of the prepared lubricants.

CHAPTER 2

TRIBOLOGY, FRICTION, WEAR AND LUBRICATION

Tribology (derived from the Greek tribein, or tribos meaning rubbing) is the science of interacting surfaces in relative motion. Even though the term tribology was first introduced in 1967 by a committee of the Organization for Economic Cooperation and Development and it has been used globally since 1985, early civilizations, especially Egyptians developed quite sophisticated tribological devices such as wheels, door hinges and wheeled carriages before 2400 BC. After, this science was developed by Leonardo da Vinci in the late 15th century by postulating a scientific approach to drilling holes (Stachowiak and Batchelor, 2005).

The study of friction, wear, lubrication and contact mechanics are all important parts of tribology. The tribological system consists of four elements; two contacting partners, the interface between the two and the medium in the interface and the environment. The variables are the type of movement, the forces involved, temperature, speed, and duration of stress. Tribometric parameters such as friction, wear and temperature data can be gathered from the stress area. Tribological stress is the result of numerous criteria of the surface and contact geometry, surface loading or lubricant thickness. Tribological processes can occur in the contact area between two friction partners which can be physical and physicochemical (adsorption, desorption), or chemical in nature (tribochemistry) and the tribology progress is based on the concept of friction as a multi-scale process taking place in the surface layers of solids and lubricant under the combined effects of deformation and shear with the simultaneous action of chemical reactions, structural and phase transformations in lubricating layer, surface films, and adjacent materials (Mang and Dresel, 2001; Myshkin, 2000). The factors affecting the tribological properties are summarized as;

- Mechanical, physical and chemical properties of the materials

- Mating conditions

- Type of processing (heat treatment, plastic forming etc.)

- Metallic inclusions etc (Leśniewski and Krawiec, 2008).

Nowadays, tribological studies related to the engineering surfaces at scales ranging from atomic and molecular to microscales are gaining importance to understand the lubrication theory and predict some of the many challenging problems in the fundamental research of tribology. The development of surface force apparatus (SFA), scanning tunneling microscope (STM), atomic force microscope (AFM) and friction force microscope (FFM) microscopes provides the nanotribological and nanomechanic studies needed to find out interfacial phenomena on a small scale and surface interactions (Bhushan, 2005; Bhushan, 1999).

2.1. Friction

Friction can be defined as the net resistant force for one surface to move against another when two objects are in contact. The coefficient of friction is defined by the ratio of the tangential force over the normal force acting on the surface (Ruina and Pratap, 2002; Hsu, 1996). Friction occurs in all mechanical systems; bearings, transmissions, hydraulic and pneumatic cylinders, valves, brakes and wheels. Friction appears at the physical interface between two surfaces in contact. Lubricants such as grease or oil are often used but there may also be a dry contact between the surfaces. Friction is strongly influenced by contaminations. There is a wide range of physical phenomena that cause friction this includes elastic and plastic deformations, fluid mechanics and wave phenomena, and material sciences. The coefficient of friction (COF), also known as a frictional coefficient or friction coefficient, symbolized by the Greek letter μ, is a dimensionless scalar value which describes the ratio of the force of friction between two bodies and the force pressing them together and represents the friction between two surfaces. Between two equal surfaces, the coefficient of friction will be the same. The maximum frictional force, F (when a body is sliding or is in limiting equilibrium) is equal to the multiplication of the coefficient of friction with the normal reaction force (N) as demonstrated in Equation 1.

$$F = \mu N \qquad\qquad\qquad (2.1)$$

Sliding and rolling frictions are the types of kinetic friction and they occur when the contact surfaces are moving. Especiall y, sliding friction occurs in a pure sliding motion with no rolling and no spin as shown in Figure 2.1. Rolling friction is the friction generated by rolling contact. In roller bearings, rolling friction mainly occurs between the rolling elements and the raceways, whereas sliding friction occurs between the rolling elements and the cage. The main cause of friction in roller bearings is sliding in the contact zones between the rolling elements and the raceways. It is also influenced by the geometry of the contacting surfaces and the deformation of the contacting elements (Figure 2.1) (Mang and Dresel, 2001).

| (a) | (b) |
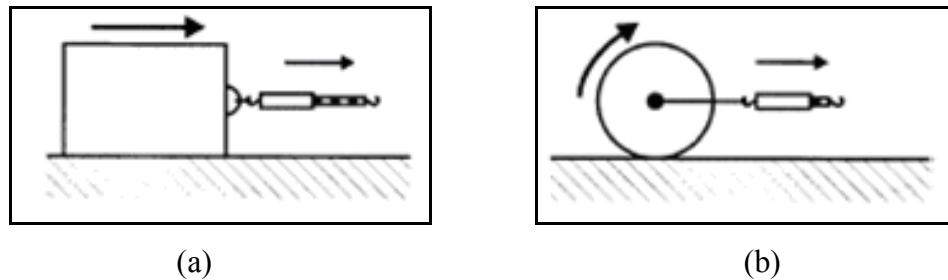
Figure 2.1. Friction of a) sliding and b) rolling
(Source: Mang and Dresel, 2001).

2.2. Wear

Wear is the loss of material from one or both of the contacting surfaces when subjected to relative motion. Film failure impairs the relative movement between solid bodies and inevitably causes severe damage to the contacting surfaces. The consequence of film failure is severe wear. It is created by the process of abrasion, adhesion, erosion, tribochemical reactions, and metal fatigue which are important to lubrication technology. The reduction of wear depends on interfacial conditions such as normal load, geometry, relative surface motion, sliding speed, surface roughness, lubrication and vibration (Zhang et al., 2009). Wear can be measured gravimetrically, volumetrically or in terms of area over a period of time or against increasing load and there are eight types of wear as indicated in below (Mang and Dresel, 2001).

Adhesive wear: It is the result of adhesion between contacting bodies

Fatigue wear: When the intervening films are partially effective then milder forms of wear occur and these are often initiated by fatigue processes due to repetitive stresses under either sliding or rolling.

Abrasive wear: If the film material consists of hard particles or merely flows against one body without providing support against another body then abrasive wear occurs.

Erosive wear: It is caused by the impact of particles of solid or liquid against the surface of an object.

Cavitation wear: It is caused by fast flowing liquids.

Corrosive wear: In some practical situations the film material is formed by chemical attack of either contacting body and while this may provide some lubrication, significant wear is virtually inevitable. This form of wear is known as corrosive wear.

Oxidative wear: When atmospheric oxygen is the corroding agent, then oxidative wear is said to occur.

Fretting wear: When the amplitude of movement between contacting bodies is restricted to, for example, a few micrometers, the film material is trapped within the contact and may eventually become destructive. Under these conditions fretting wear may result.

Jacobson and Hogmark (2009) summarized the surface modifications of the surfaces due to its tribological action by four categories (Figure 2.2);

- Modification of the original surface without any material transfer (Figure 2.2a)
- Modification of the original surface involving material transfer (Figure 2.2b)
- Formation of tribofilm or coating on top of the original surface (Figure 2.2c)
- Wear (loss of particles or atoms from the surface) (Figure 2.2d)

2.3. Surface Roughness

Two of the most important surface properties are surface roughness and topography. The evaluation of surface roughness is of great importance to obtain the surface topography for many fundamental problems such as friction, contact deformation and conduction. The real surface geometry is so complicated that many

parameters according to functionality are used to describe the surface evaluation. In fact the roughness parameters can be calculated in either two-dimensional (2D) or three-dimensional (3D) forms. Among the surface roughness parameters; arithmetic average height (Ra) is defined as the average absolute deviation of the roughness irregularities from the mean line over one sampling length as shown in Figure 2.3. This parameter is easy to define, easy to measure and gives a good general description of height variation (Sedlaček et al., 2009). However it is not sensitive to small changes in profile (Gadelmawla et al., 2002). The mathematical definition of Ra is indicated as follows;

(a)	(b)

(c)	(d)
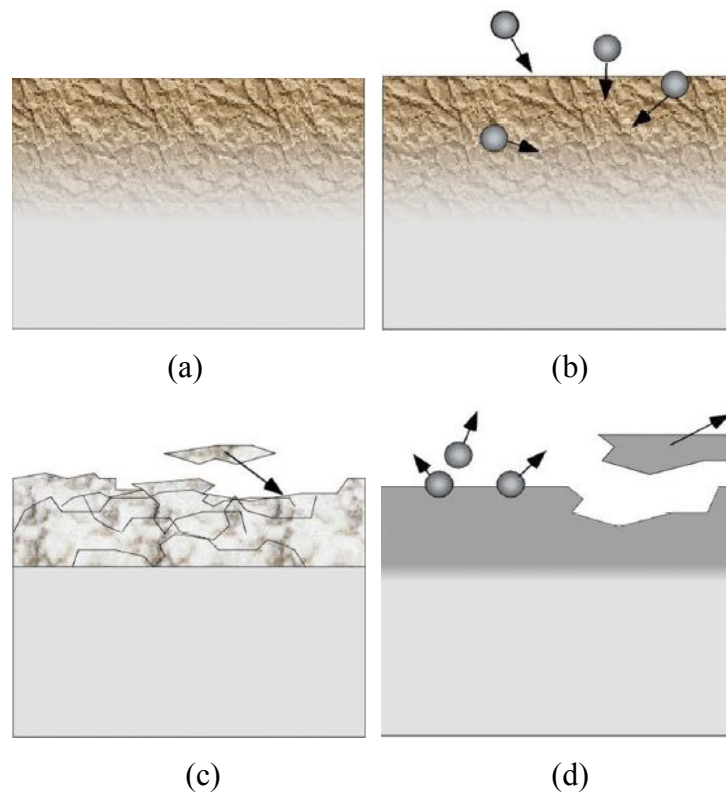
Figure 2.2. The four basic categories of tribological surface modification
(Source: Jacobson and Hogmark, 2009).

$$R_a = \frac{1}{l} \int_0^l |y(x)| dx \qquad (2.2)$$

$$R_a = \frac{1}{n} \sum_{i=1}^n |y_i| \qquad (2.3)$$
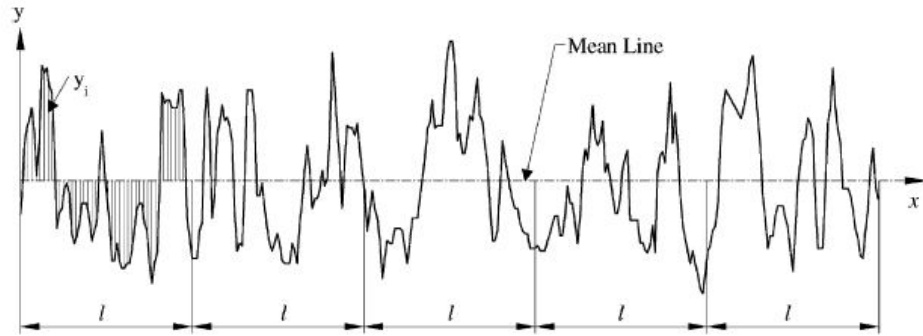
Figure 2.3. Definition of the arithmetic average height (Ra)
(Source: Gadelmawla et al., 2002).

In addition to Ra, maximum height of peaks (Rp) and maximum depth of valleys (Rv) are used to define the surface properties. As shown in Figure 2.3. Rp is above the mean line within the assessment length, whereas Rv is below the mean line. By using Rp and Rv, maximum height of the profile (Ry (R_t) or Rmax) which is defined as the vertical distance between the highest peak and the lowest valley along the assessment length of the profile can be evaluated (Figure 2.4). This parameter is very sensitive to the high peaks or deep scratches (Gadelmawla et al., 2002).
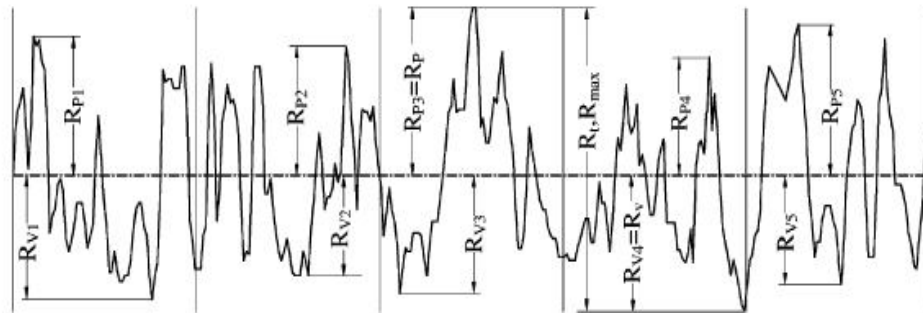
Figure 2.4. Definition of parameters, Rp, Rv, Rmax
(Source: Gadelmawla et al., 2002).

2.4. Lubrication

The main purpose of lubrication is to reduce the friction between the interacting surfaces in relative motion by introducing a third body called lubricant between them. The third body should have very low shear strength so that the mating surfaces do not

undergo wear or damage. The effectiveness of the lubricant is measured by its ability to prevent wear and reduce friction. This prevention can be achieved by providing a protective film or a coating on the surfaces. In literature four different liquid lubrication regimes; such as hydrodynamic, elastohydrodynamic (EHD), mixed and boundary lubrication regimes are defined depending up on the thickness of lubricant film present between the interacting surfaces. These four regimes are clearly understood from the Stribeck/Hersey curve in Figure 2.5. Knowing the magnitude of the coefficient of friction, the curve allows one to determine the various lubricating regimes in a metal forming process. In this figure, h denotes the thickness of the lubricant film and their magnitudes are listed in Table 2.1 according to the regimes. In the first portion, where the viscosity of the lubricant and the relative velocity of the contacting surfaces are low and the interfacial pressure is high, boundary lubrication is observed, in which metal-to-metal contact is predominant in addition to some lubricant-to-metal contact. Boundary lubrication is highly complex, and it involves chemical interactions between the contacting surfaces and the liquid lubricant. The lubrication mechanisms depend on the load-carrying capacity and limiting frictional temperature, and are controlled by the additives in the lubricant, leading to the formation of a low-friction tribofilm by physisorption and/or chemisorption (Kim et al., 2000). The transition between the elastohydrodynamic and boundary regimes is not sharp, and there exists a region, called the mixed lubrication regime, which consists of some elastohydrodynamic and some boundary lubrication. Elastohydrodynamic lubrication comes into effect where loads are high enough to cause elastic deformation of the surfaces, but speed and viscosity are not high enough to produce film thicknesses greater than about 0.25 μm. In this regime, the ability of the fluid to develop a lubricant film to support the load is directly related to the viscosity of the fluid and the relative speed (Hsu, 2004). The minimum film thickness in an elestohydrodynamic lubrication contact is a function of the applied load, surface speed and geometry, elasticity of the material and the viscosity and pressure–viscosity coefficient of the lubricant (Höglund, 1999). Hydrodynamic lubrication is characterized by complete separation of the surfaces by a fluid film that is developed by the flow of the fluid through the contact region (Sathyan et al., 2009).
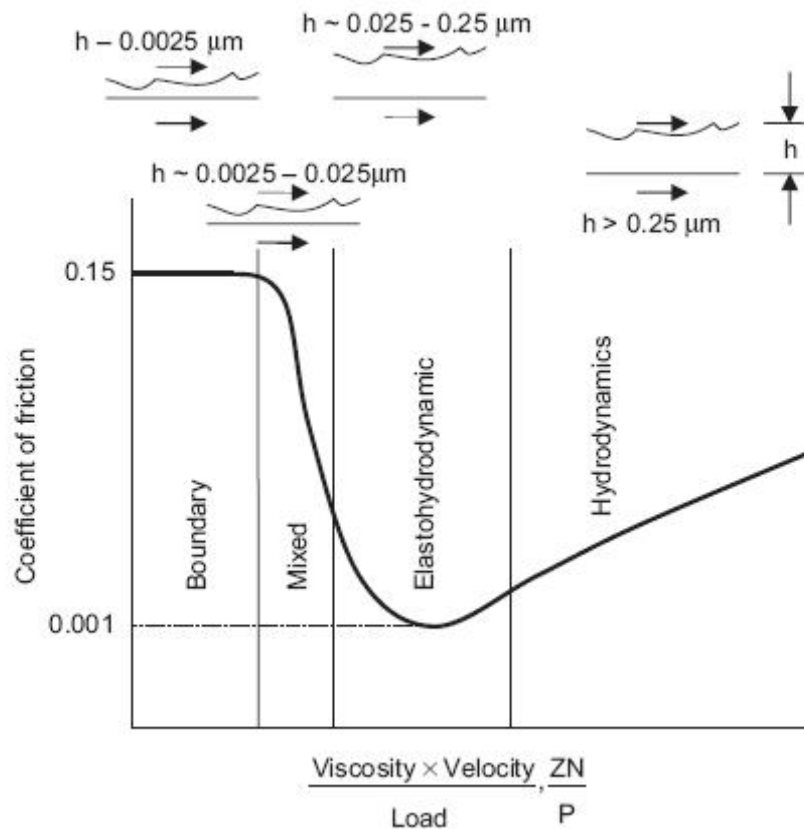
Figure 2.5. Stribeck/Hersey curve
(Source: Sathyan et al., 2009)

Table 2.1. Thickness of the lubricant film according to lubrication regimes
(Source: Sathyan et al., 2009).

Lubrication Regime	h (µm)	Deformation
Hydrodynamic	> 0.25	Negligible
Elastohydrodynamic	0.025-0.25	Elastic
Mixed	0.0025-0.025	Elastic
Boundary	≈ 0.0025	Contact, elastic and plastic

2.5. Mechanical-Dynamic Testing Methods for Lubrication

Mechanical-dynamic lubricant testing has become an essential element in the development of modern lubricants. In this respect, standardized tribological, mechanical-dynamic testers and test methods play a decisive role in the development of

lubricants. These testers and test methods include small laboratory instruments and field tests under real conditions. The most important test methods, used worldwide by many laboratories, are ISO, CEC, ASTM, IP and DIN standards, listed in Table 2.2. The most common characterization tool is the tribometer having several configurations such as pin-on-disk, ball on flat, and flat on flat, etc. (Hu et al., 2002).

The four ball geometry was first developed in 1933 and has become one of the most widely used wear test procedures. The diagram in Figure 2.6 explains the test principle. A roller bearing ball rotates under pressure and at a constant speed on three fixed steel balls of the same type in an oil bath or lubricated with a solid lubricant. The gradual increase in pressure enables the determination the weld loads, supplies key values concerning loadability, or enables the determination of the friction or start up behavior in relation to the lubricant. In other words, the test may be used to evaluate the friction, extreme pressure and wear-control ability of liquid lubricants or greases in sliding contact. The point contact interface is obtained by rotating a 12.7 mm diameter steel ball under load against three stationary steel balls immersed in the lubricant (Figure 2.6). During these tests, the surface of the ball surface will produce wear impressions and the measurements will lead to information on the effects of additives. The normal load, frictional force, and temperature can be monitored using software. The rotating speed, normal load, and temperature can be adjusted in accordance with published ASTM and IP test standards. For evaluating the wear preventive characteristics of lubricants, the subsequent wear scar diameters on the balls can be measured using a graduated-scale microscope. The wear scar can also be captured using an optional digital camera and measured using wear scar analysis software. For evaluating the extreme-pressure (load-carrying) capacity of lubricants, the normal load at which welding occurs at the contact interface can be recorded (Mang and Dresel, 2001).

Table 2.2. Common model testers and test standards
(Source: Mang and Dresel, 2001).

Tester	Application	Test Method
Four-ball apparatus	Standard test method for wear-preventive characteristics of lubricating fluids	ASTM D 4172-88
	Standard test method for wear-preventive characteristics of lubricating grease	ASTM D 2266-86
	Standard test method for determination of the friction coefficient of lubricants using the four-ball apparatus	ASTM D 5183-95
	Standard test method for measurement of lubricating fluids- four-ball method	ASTM D 2783-88
	Standard test method for measurement of lubricating grease- four-ball method	ASTM D 2596-87
	Standard test method for determination of load carrying capacity and mean hertz load	FTMS No 791 b
	Determination of extreme pressure and anti-wear properties of lubricants-four ball apparatus	IP 239/85
	Standard test method for lubricants using the Shell four ball apparatus	DIN 51350, part 1
	General principles	DIN 51350, part 2
	Weld load of liquid lubricants	DIN 51350, part 3
	Wear key values of liquid lubricants	DIN 51350, part 4
	Weld load of solid lubricants	DIN 51350, part 5
	Wear key values of liquid lubricants	DIN 51350, part 6
	Viscosity shear stability of transmission lubricants-taper roller bearing rig	CEC L-45-T-98
Brugger test rig	Testing under boundary lubricating conditions with the Brugger lubricant tester	DIN 51347, part 1
	General principles	DIN 51347, part 2
Reichert friction wear tester	Standard test method for determining the pressure compensation capacity	VKIS No.6
Almen Wieland oil tester	Standard test method for determining the frictional behavior and pressure loadability	Internal specifications
Falex tester	Standard test method for the calibration and operation of the Falex block on ring friction and wear tester	ASTM D 2714-94
	Standard test method for the extreme pressure properties of liquid lubricants	ASTM D 3233-93
	Standard test method for measuring the wear properties of liquid lubricants	ASTM D 2670-94
Tannert slide indicator	Standard test method for determining sliding behavior using the Tannert slide indicator	DIN 51387, part 1
Translatory oscillation apparatus	Tribological test method using a linear oscillation tester	E-DIN 51834, part1
	Determination of measured friction and wear quantities for lubricating oils	E-DIN 51834, part5
Timken tester	Standard test method for measuring the loadability of lubricating greases	ASTM D 2509-86
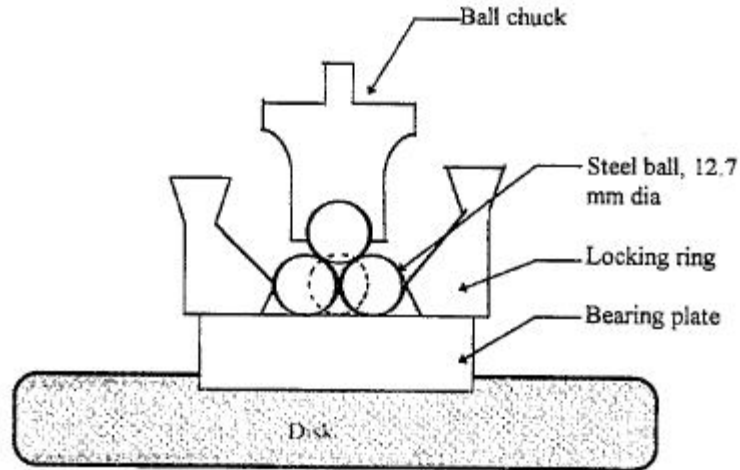
Figure 2.6. Schematic diagram of the four ball wear machine
(Source: Masjuki and Maleque, 1997).

2.6. Lubricants

Lubricants serve an important function in preserving machine components and extending machine operating lifetimes of contacts (Erdemir, 2000; Mazuyer et al., 2001). They are the substances introduced between two moving surfaces to reduce the friction and wear between them. The most important function of lubricants is the reduction of friction and wear. A lubricant provides a protective film which allows for two touching surfaces to be separated, thus lessening the friction between them. Moreover, lubricants also perform the following key functions.

- Keep moving parts apart
- Transfer heat
- Carry away contaminants and debris
- Transmit power
- Prevent corrosion.

Mineral oil components continue to form the quantitatively most important foundation of lubricants. Petrochemical components and increasingly derivatives of natural and harvestable raw materials from the oleo-chemical industry are finding increasing acceptance because of their environmental capability and some technical advantages. Typically lubricants contain 90% base oil (most often petroleum fractions, called mineral oils) and less than 10% additives. Vegetable oils or synthetic liquids such as hydrogenated polyolefins, esters, silicone, fluorocarbons and many others are

sometimes used as base oils. Additives deliver reduced friction and wear, increased viscosity, improved viscosity index, resistance to corrosion and oxidation, aging or contamination, etc. The production of simple lubricants normally involves blending processes but specialties often require the use of chemical processes such as saponification (in the case of greases), esterification (when manufacturing ester base oils or additives) or amidation (when manufacturing components for metalworking lubricants). Further manufacturing processes include drying, filtration, homogenizing, dispersion or distillation (Mang and Dresel, 2001). Apart from the most common lubricant oils, different lubricant systems are used such as emulsions. Oil in water emulsions are central to water-miscible cutting fluids, rolling emulsions. In these cases, the concentrations of these emulsions with water are generally between 1 and 10%. The annual consumption of such emulsions in industrialized countries is about the same as all other lubricants together (Mang and Dresel, 2001). The next group of lubricants systems is water-in-oil emulsion (inverse emulsion). Their most important application is in metal forming. These products are supplied ready to use or as dilutable concentrates. Grease is one of the most important semi-solid lubricants used in tribosystems. It is thickened oil (basic oil).Greases are two phase lubricants with complex structure and rheological characteristics (Zhou and Vincent, 1999). The thickeners used for greases are based on soaps or other organic and inorganic substances. Special equipment is required for their production (Mang and Dresel, 2001). Solid lubricant suspensions normally contain solid lubricants in stable suspension in a fluid such as water or oil. These products are often used in forging, extrusion and other metal working processes.

Lubricants are generally composed of a majority of base oil and a minority of additives to impart desirable characteristics. Types of lubricants are divided into five different groups as indicated below;

- Gas
- Liquid (including emulsions and suspensions)
- Solid
- Greases
- Adhesive

2.6.1. Gaseous Lubricants

Gaseous lubricants have a much lower viscosity and higher compressibility compared to liquid lubricants, but the fluid-film principles apply analogous to gases. Some examples for gaseous lubricants are air, technical gases, steam or liquid-metal vapours.

2.6.2. Liquid Lubricants

Liquid lubricants may be characterized in many different ways. One of the most common ways is by the type of base oil used. Followings are the types of liquid lubricants.

- Lanolin (wool grease, natural water repellent)
- Water
- Mineral oils
- Vegetable (natural oil)
- Synthetic oils
- Other liquids.

Lanolin : A natural water repellent, lanolin is derived from sheep wool grease, and is an alternative to the more common petro-chemical based lubricants. This lubricant is also a corrosion inhibitor, protecting against rust, salts and acids.

Water: Water can be used on its own, or as a major component in combination with one of the other base oils. Commonly it is used in engineering processes such as milling.

Mineral oil: This term is used to encompass lubricating base oil derived from crude oil. The American Petroleum Institute (API) designates several types of lubricant base oil identified as: Group I, Group II, Group III, Group IV and Group V. The sulphur content and the saturate amount are listed in Table 2.3.

Table 2.3. API Base Oil Categories
(Source: Pulcu, 2008).

Group	Sulphur wt%	Saturates %	Common base oil
I	>0.03	<90	SN150, SN500
II	≤0.03	≥90	Water-white color oil
III	≤0.03	≥90	Synthetic lubricants
IV			Polyalphaolefins (PAO)
V			Pale oils and non-PAO synthetics

There are three basic classes of refined mineral oils:

- paraffinic oils, based on *n*-alkanes
- naphthenic oils, based on cycloalkanes
- aromatic oils, based on aromatic hydrocarbons.

Vegetable (natural) oils: These are primarily triglyceride esters derived from plants and animals. For lubricant base oil use, the vegetable derived materials are preferred. Common ones include high oleic canola oil, castor oil, palm oil, sunflower seed oil and rapeseed oil from vegetable, and tall oil from animal sources. Many vegetable oils are often hydrolyzed to yield the acids which are subsequently combined selectively to form special synthetic esters.

Synthetic Oils: These oils are polyalpha-olefin (PAO), synthetic esters, polyalkylene glycols (PAG), phosphate esters, Alkylated naphthalenes (AN), silicate esters, ionic fluids (Marsh and Kandil, 2002).

2.6.3. Solid Lubricants

Solid lubricants possess lamellar structure preventing direct contact between the sliding surfaces even at high loads. Graphite and molybdenum disulfide particles are common solid lubricants. Boron nitride, tungsten disulfide and polytetrafluorethylene (PTFE) are other solid lubricants. Solid lubricants are mainly used as additives to oils

and greases. Solid lubricants are also used in form of dry powder or as constituents of coatings (Donnet and Erdemir, 2004; Zhou and Vincent, 1999).

2.6.4. Viscosity of Lubricants

Viscosity is a measure of the internal friction of a fluid. It is the most important physical property of a fluid in the context of lubrication. The viscosity of a lubricant varies with temperature and pressure and, in some cases, with the rate at which it is sheared (Neale, 1995). For the parallel plate situation illustrated in Figure 2.7, coefficient of dynamic viscosity of the lubricant (μ) equals to the ratio of shear stress (τ) to the gradient of velocity (U) as expressed in Equation 2.4.

$$\tau = \mu \frac{\partial U}{\partial y} \tag{2.4}$$
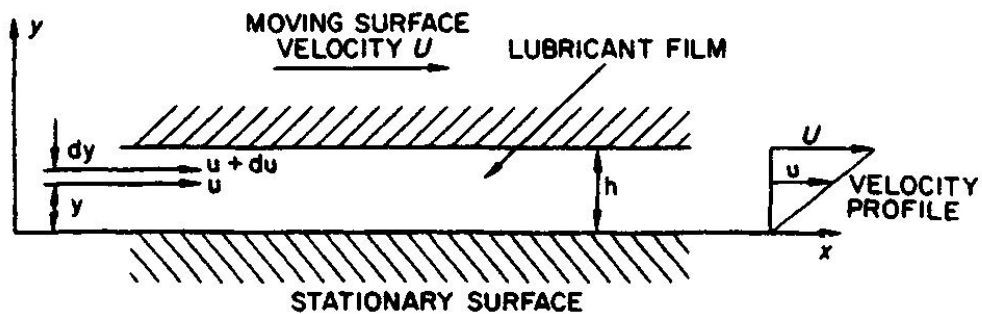
Figure 2.7. Lubricant film between parallel plates
(Source: Neale, 1995).

If the viscosity of a fluid is independent of its rate of shear, the fluid is said to be Newtonian. Information on the viscosity of oil fractions and their mixtures is of considerable importance for estimating transport properties in petroleum processing (Wakabayashi, 1997). In order to reduce the costs of crude oil production, the petroleum industry must anticipate crude oil properties and behavior. One of the main properties relevant to the choice of equipment and its sizing is viscosity. It is a characteristic property of fluids that allows measurement of the forces hindering movement or flow when a shear stress is applied. This property is influenced by external conditions such as temperature and pressure and internal characteristics of crudes. Measurement of

viscosity, modification of this property if needed and testing of oil field behavior can be performed by several methods:

• simulation of production steps with small-scale oilfield equipment;

• chemical and rheological tests in the laboratory;

• modelling and prediction (Burg et al., 1997).

It is found that the mineral lubricating oils and synthetic oils of low molecular weight are Newtonian under almost all practical working conditions, whereas greases are non-Newtonian.

2.6.5. Market Research for Lubricants

Lubricants today are classified in two major groups:

• Automotive lubricants

• Industrial lubricants

Moreover industrial lubricants can be sub-divided into industrial oils and industrial specialties; ie., greases, metalworking lubricants, and solid lubricant films (Mang and Dresel, 2001). It is reported that there are about 180 multinational and national companies engaged in manufacturing lubricants in 2008 and China is the fastest growing lubricants market in the world and second largest market by volume is US (ResearchWikis, 2010). Figure 2.8 shows the lubricant demand by region in 2008 (Klinegroup, 2010). In 2004, 37.4 million tons of lubricants were consumed worldwide (53% automotive lubricants, 32% industrial lubricants, including related specialties, 5% marine oils, and 10% process oils). Amongst industrial lubricants, 37% were hydraulic oils, 7% industrial gear oils, 31% other industrial oils, 16% metalworking fluids, and 9% greases.

World demand for lubricants is forecast to advance 2.3% per year to 41.7 million metric tons at the end of 2010. Growth will be driven by increasing rates of motor vehicle ownership worldwide, and rising number of kilometers traveled per vehicle. Growth in worldwide manufacturing activity will boost the demand for industrial lubricants such as process oils and hydraulic fluids. Among major world regions, lubricant demand in the Asia/Pacific region is expected to grow at the fastest pace, with the market in China leading overall gains due to ongoing rapid industrialization as well as rising car ownership rates. Growth in the mature markets of

North America and Western Europe will be well below the global average, due to slower economic growth and an increased emphasis on extended drain intervals for lubricants.

Others
11%

North America
26%

Africa and
Middle East
3%

South
America
7%

Asia-Pasific
35%

Europe
18%
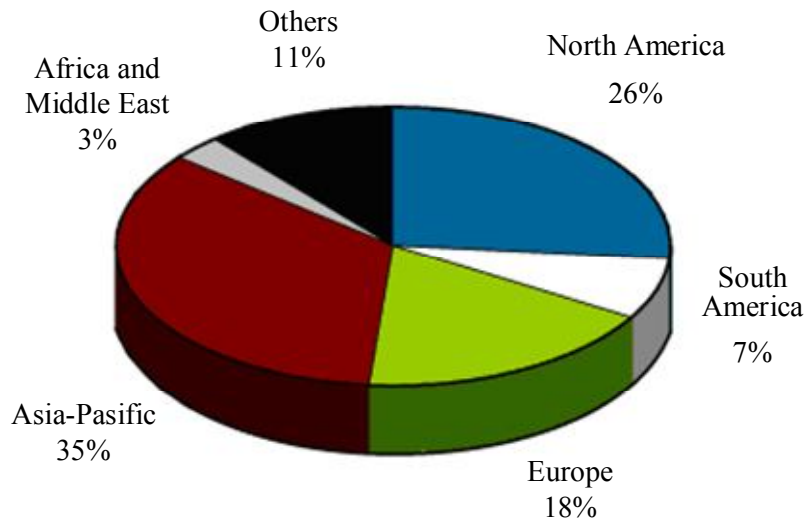
Figure 2.8. Lubricant demand by region in 2008
(Source: Klinegroup, 2009)

2.6.6. Lubricating Oil Additives

While lubricants for use in internal combustion engines may solely consist of one of the above-mentioned oil groups, it is not desirable in practice. Additives to reduce oxidation and improve lubrication are added to the final product. The main constituent of such lubricant product is called the base oil. While it is advantageous to have a high-grade base oil in a lubricant, proper selection of the lubricant additives is equally as important. The types of additives used for the preparation of lubricants are;

- Extreme pressure (EP) additives
- Anti-wear (AW) additives
- Friction modifiers
- Corrosion inhibitors
- Anti-oxidants
- Dispersants
- Detergents
- Anti-foaming agents
- Pour point depressant.

The additives in lubricating oils tend to overpower the base oil to produce desirable characteristics. For these purposes many lubricant additives have been improved and their tribological properties are tested. The materials having antiwear and extreme pressure functions and used for the modification of the surfaces in the lubricating oils can be divided into three basic groups;

- sulphur-, chlorine-, and phosphorous-containing compounds
- boron-containing compounds (boric acid, metal borates)
- zinc containing materials.

Sulphur-, chlorine-, and phosphorous-containing compounds tend to be designed to react chemically with the metal surfaces, forming easily sheared layers of sulphides, chlorines or phoshides and thereby preventing severe wear and seizure. However, the use of these compounds used as lubricant additives has been restricted due to their significant negative impacts on environment. Therefore, developing new additives that pollute less has become the target for the researchers. Choundary and Pande, claimed that boron-containing lubricants have major tribological advantages, such as antiwear efficiency, good film strength, high temperature resistance, and self-lubricating properties (Choundary and Pande, 2006; Shen et al., 2000). Among the boron compounds, boric acid and boric acid in dry powder form are found as a potential environmentally solid lubricant for sliding metal contacts and it is revealed that the lubricity of conventional oils and greases can be improved by adding concentrates of boric acid. (Erdemir, 1995; Barton et al., 2004; Rao and Xie, 2006; Deshmukh et al., 2006). Although boric acid ester is liable to hydrolyze, the results demonstrated that the friction coefficients were reduced by 10 to over 100% below those of the unmixed lubricant itself (Erdemir, 1995). Besides the boric acid, organic and inorganic borate-based additives have been the focus of much attention, as they posses a good combination of properties, such as wear resistance, friction-reducing ability, oxidation inhibition, low toxicity, pleasant odor and compatibility with frictional pairs (Zheng et al., 1998). Antiwear and antifriction capabilities of metal borates, such as zinc borate, magnesium borate, and titanium borate were studied by many researchers (Dong and Hu, 1998; Hu et al., 2002; Hu and Dong, 1998). The main idea of the employment of borates in lubricating oils is explained as the formation of amorphous film on wear scar surface and the reaction of this film with the substrate due to extreme pressure as shown in Figure 2.9. Nanoparticle magnesium borate with a particle size of about 10 nm produced by ethanol supercritical fluid drying with adsorbing dispersing agent deposits

or adsorbs on wear scar surface at first, then forms an amorphous film due to the shearing effect. At the same time, the boron containing antiwear film reacts with the substrate due to extreme pressure effect. Tribological reactions occurred in the surface (Hu et al., 2002).
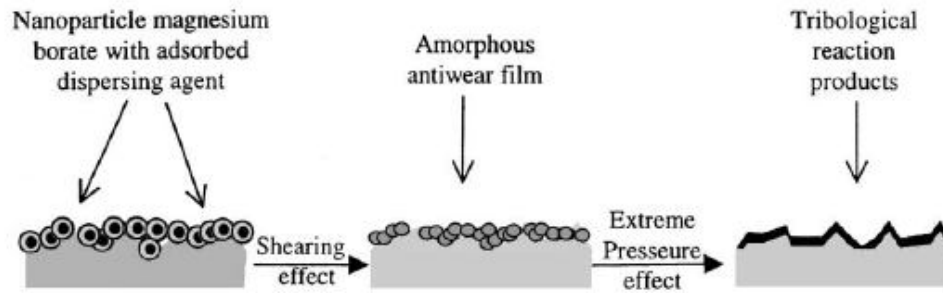
Figure 2.9. A diagram of antiwear mechanism of the magnesium borate
(Source: Hu et al., 2002).

Besides boron containing materials, zinc containing materials, especially zinc oxides, are used as lubricant additive (Wang et al., 2009; Battez et al., 2008). Battez et al., examined the antiwear behavior of CuO, ZnO, and ZrO_2 nanoparticles in a polyalphaolefin (PAO 6) by a block-on-ring tribometer. 20-50 nm diameter nanoparticles have been tested as lubricating oil additive and the friction coefficient is reduced for the lubricant containing ZnO suspensions (Battez et al., 2008). Another study performed by the same researchers disclosed the antiwear behavior of ester based dispersing agent (OL 300) in polyalphaolefin (PAO6). Figure 2.10 shows the antiwear properties of a number of lubricants including OL300 and/or ZnO suspensions. Wear scar diameters using these lubricants were smaller than those obtained with base oil (PAO6). However, when 0.3% ZnO nanoparticles were added to PAO6 + 1% OL300 and PAO6 + 1.5% OL300 lubricants, wear scar diameter increased. In contrast, adding 0.3% of ZnO in PAO6 + 3% OL300 failed to change the wear scar diameter. The results proved that ester based dispersing agent OL300 had an antiwear ability (Battez et al., 2006).
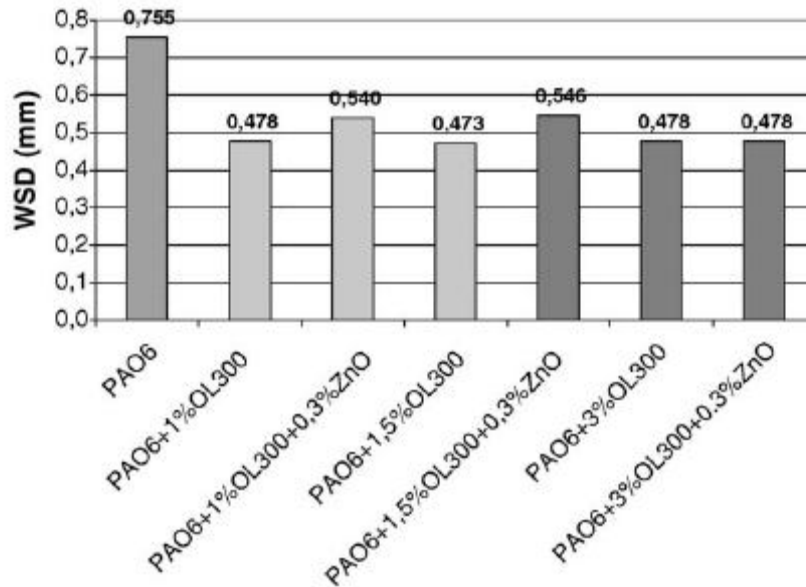
Figure 2.10. Results of anti-wear tests of PAO6 + OL300 + ZnO suspensions
(Source: Battez et al., 2006).

Among these additives nano-sized particles are promising materials for lubrication since they offer a better understanding of the interfacial properties of fluid-solid interfaces. The tribological properties of the nanoparticles as lubricant additives are studied and the results show that the addition of the nanoparticles can be used as anti-wear and extreme pressure additives with excellent performances since the dispersion stability of nanoparticles in base oil is superior to micron particles in lubrication systems (Li et al., 2006). A variety of mechanisms has been proposed to explain the lubrication enhancement of the nanoparticles suspended in lubricating oil. The first is the direct effect of the nanoparticles on lubrication enhancement. The nanoparticles suspended in lubricating oil play the role of ball bearings between the friction surfaces (Figure 2.11a). In addition, they also make a protective film to some extent by coating the rough friction surfaces (Figure 2.11b). The others, mending and polishing effects are the secondary effects of the presence of nanoparticles on surface enhancement. The nanoparticles deposit on the friction surface and compensate for the loss of mass, which is known as mending effect (Figure 2.11c). Furthermore, the roughness of the lubricating surface is also reduced by nanoparticle-assisted abrasion, which is known as a polishing effect (Figure 2.11d) (Lee et al., 2009).

(a) (b)

(c) (d)
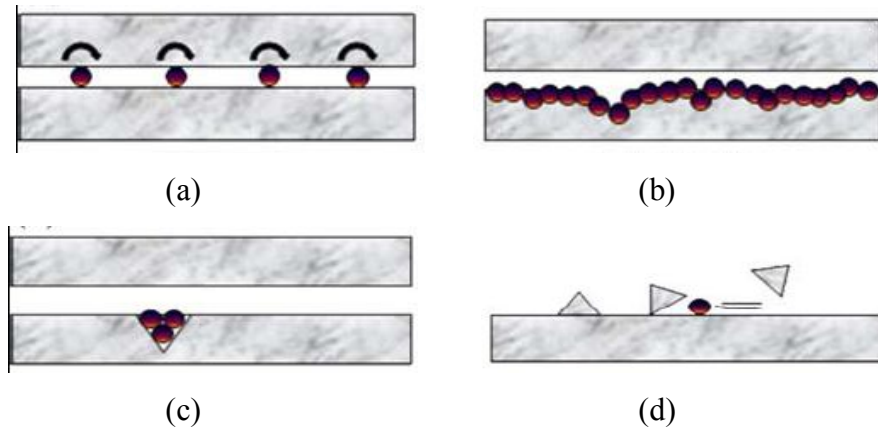
Figure 2.11. Possible lubrication mechanism between the frictional surfaces a) Rolling
effect b) protective film, c) Mending effect d) Polishing effect (Source:
Lee et al., 2009).

Wasilewski and Sulek (2006) have chosen paraffin mixtures of sorbitan
monolaurate and ethoxylated sorbitan monolaurate as lubricant additive since they are
environment-friendly. Tribological tests of the lubricants are performed using a four-
ball tester and friction coefficients for mixtures of sorbitan monolaurate and ethoxylated
sorbitan monolaurate in paraffin oil were evaluated. Figure 2.12 indicates the change in
friction coefficient values with respect to time.
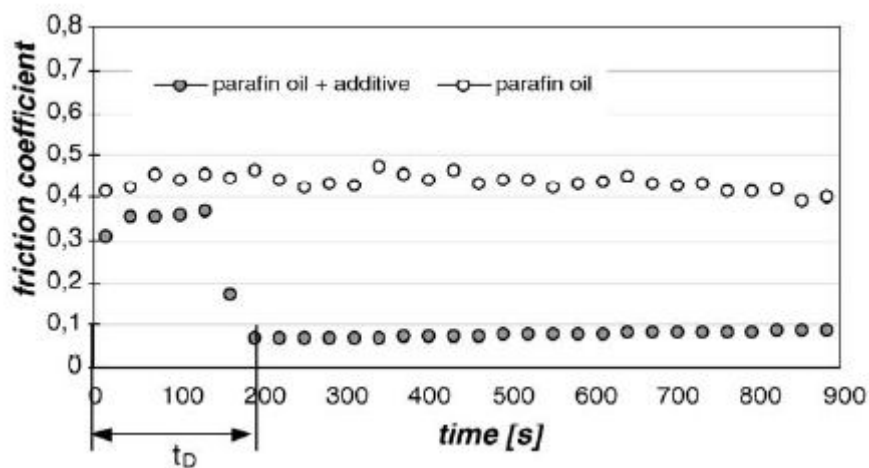
Figure 2.12. Friction coefficient vs. time for paraffin oil and for paraffin oil containing 1
% mixture of sorbitan monolaurate and ethoxylated sorbitan monolaurate
(Source: Wasilewski and Sulek, 2006).

The base oil containing additive shows stable friction coefficient with increasing

time. Therefore introduction of the mixture containing ester and its ethoxylated sorbitan

monolaurate into the base oil significantly influences the motion of resistance due to their strong interaction with surfaces and formation of ordered structures (Wasilewski and Sulek, 2006). Moreover, it was reported that ester compounds behave as corrosion inhibitors in lubricating oil (Schick, 1966).

Besides the organic particles, inorganic materials are also used as antiwear additive in base oil. Serpentine which describes a common rock-forming hydrous magnesium iron phyllosilicate $((Mg,Fe)_6Si_4O_{10}(OH)_8)$ minerals proves to be an effective additive which enhances the tribological properties of the base oil. Yu and coworkers tested the tribological properties of diesel engine oil suspended serpentine particles having 1μm particle size by sliding friction tribotester. Wear resistance ability of the oils including different amounts of serpentine particles for various applied loads are shown in Figure 2.13.
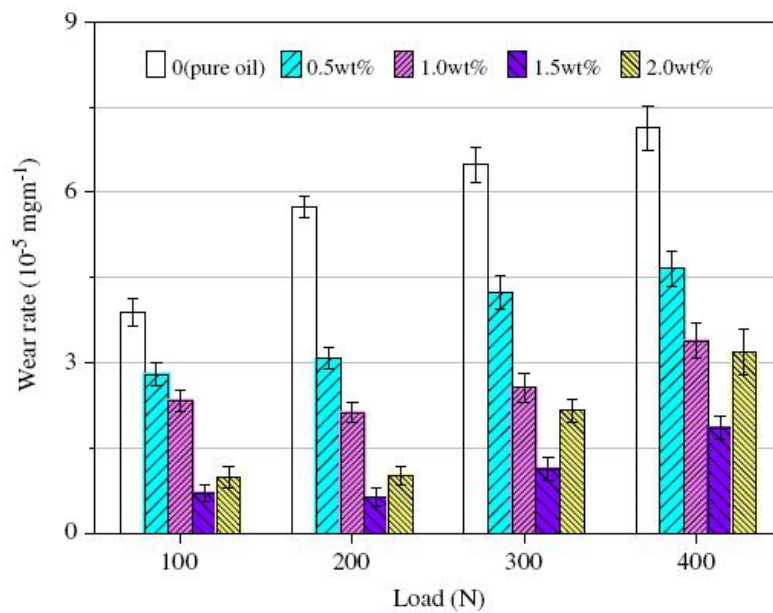
Figure 2.13. Wear rate of disk specimens under the lubrication of oil with and without serpentine particles (Source: Yu et al., 2010).

As presented in Figure 2.13, wear of disk specimens under the lubrication of oil with and without serpentine particles increases with increasing the load, accordingly. The addition of serpentine particles into the oil decreases the wear of steel. The addition of 1.5 wt% serpentine to oil is found most efficient in reducing wear (Yu et al., 2010)

CHAPTER 3

BORON COMPOUNDS AS LUBRICATING
OIL ADDITIVES

Boron-containing compounds, such as boric acid, boric oxide, and other organic and inorganic borates have been used for lubrication purposes since they have major tribological advantages such as antiwear efficiency, good film strength, friction reducing ability, high temperature resistance. Table 3.1. summarizes the studies in literature dealing with the addition of boron-based compounds into the various base oils. The tribological tests are generally carried out by four-ball tester to exhibit the wear and friction property of the lubricants. All the additives including boron element show considerable behavior to reduce the friction coefficient and improve the wear property. The typical reasons why boron element shows excellent tribological properties are listed as below;

- It is an electron-deficient non-metallic element
- It has a layered crystal structure
- It has a small atomic diameter (1-1.5 Å)
- It has a high affinity for oxygen
- It has a vacant p-orbital.

In this part of the study, the tribological behaviors of boron-based materials are explained in detail and the literature of the studies related to the employment of boron compounds into the base oil is reviewed.

Table 3.1. Studies related to employment of boron based additives in base oil.

Boron Based Additives	Base Oil	Dispersing Agent	Type of Tribometer	Results	Reference
Borate ester	Rapeseed oil	-	Four ball	Friction coefficient is decreased	Li et al., 2010
Hexagonal boron nitride	Transformer oil	-	KEWAT-6	Friction coefficient is decreased	Pawlak et al., 2009
Magnesium borate (120-180 nm)	Mobilube gear	-	Wear tester	Wear resistance is improved Friction coefficient is decreased	Zeng et al., 2008
Barium borate (20 nm)	Base oil	-	Wear tester	Wear resistance is improved Friction coefficient is decreased	Liu et al., 2008
Sodium borate	Water	-	Four ball	Poor wear performance Friction coefficient is decreased	Chen et al., 2008
Zinc borate (50-500 nm)	Base oil	-	Pin-on-disc	Friction coefficient is decreased	Tian et al., 2006
Boric acid (100 μm)	Transmission oil	-	Pin-on-disc	Wear resistance is improved	Deshmukh et al., 2006
N-modified borate (20-500nm)	Liquid paraffin	-	Four ball	Wear resistance is improved Friction coefficient is decreased	Qiao et al., 2003
Magnesium borate (10 nm)	500 SN	Sorbitol monostearate	Four ball	Wear resistance is improved Friction coefficient is decreased	Hu et al., 2002

(cont. on next page)

Table 3.1. (cont.).

Lanthanum borate (20-40 nm)	500 SN	Sorbitol monostearate	Four ball	Wear resistance is improved	Hu et al., 2000
Hexagonal boron nitride	Mineral oil	-	Ring-on-roller	Eliminate fluctuation of friction coefficient	Kimura et al., 1999
Zinc borate (20-50 nm)	500 SN	Sorbitol monostearate	Four ball	Wear resistance is improved Friction coefficient is decreased	Dong and Hu, 1998
Titanium borate (10-70 nm)	500 SN	Sorbitol monostearate	Four ball	Wear resistance is improved Friction coefficient is decreased	Hu and Dong, 1998

3.1. Hexagonal Boron Nitride

Hexagonal boron nitride (h-BN) has captured attention as a solid lubricant for general use due to its easy shearing along the basal plane of the hexagonal crystal structure. Many studies in literature indicate the excellent lubricating property of this material and they claim that it show very low friction coefficient and slow wear rate (Pawlak et al., 2009; Shi et al., 2008; Wood et al., 2005; Kimura et al., 1999). This material is constructed from layers consisting of a flat or nearly flat network of B_3N_3 hexagons and the layers stacked one over the other along the [0 0 1] direction. Hexagonal nitride powder produced by spray drying technique is shown in Figure 3.1. HBO_3, $Na_2B_4O_7$ and $(NH_2)_2CO$ were used as raw materials. The crystals had plate-like shapes, where the (002) atomic planes of the hexagonal structure of BN align paralleled to the particle's major flat surface. Mean particle sizes of the fully crystallized powders could be estimated in the following ranges, 100–400 nm in diameter, and 30–90nm in thickness (Shi et al.,2008). Kimura et al. (1999) describes the behavior of hexagonal boron nitride when added to oil. A paraffinic mineral oil was used in this study and friction with respect to sliding distance was determined by a ring-on-roller tribometer. Figure 3.2 shows the examples of friction traces. The addition of 2 wt% hexagonal

boron nitride to the oil eliminated the fluctuation of friction coefficient which occurred as a result of the poor boundary lubrication and markedly lowered the stationary value of friction coefficient.
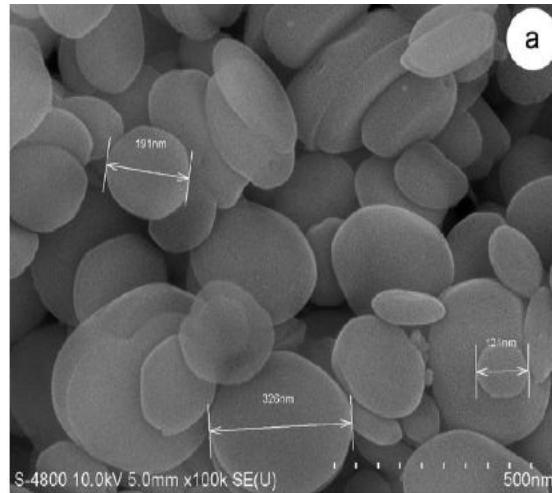
Figure 3.1. FESEM micrographs of h-BN powder
(Source: Shi et al., 2008).

| (a) | (b) |
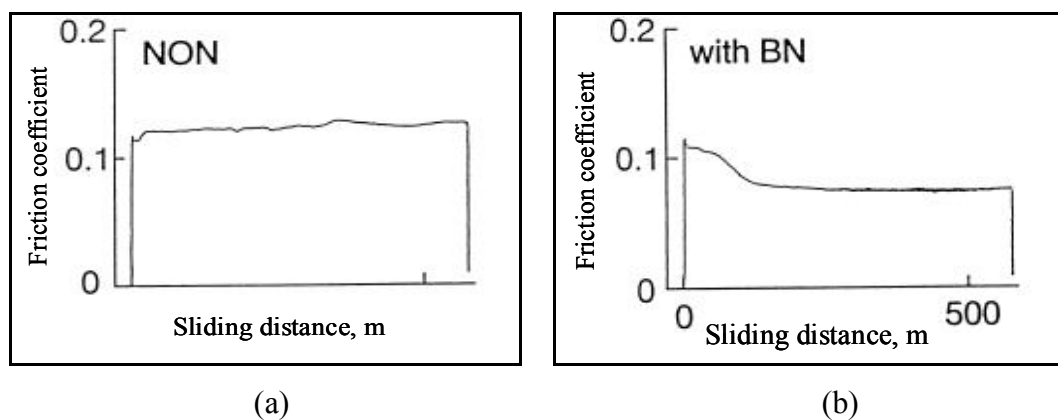
Figure 3.2. Friction traces of a) lubricated with oil b) lubricated with oil including 2 wt % h-BN (Source: Kimura et al., 1999).

3.2. Boric Acid

Boric Acid (H_3BO_3) is one of the most popular solid lubricants and has excellent lubrication properties without calling for expensive disposal techniques. The most important characteristics of boric acid for use as a lubricant are that it is readily available and environmentally safe. Several studies related to the lubrication properties

of boric acid are carried out over the past several decades (Damera and Pasam, 2008; Erdemir, 2008; Jallad et al., 2002). These works have primarily focused on the performance of boric acid and indicated that boric acid's unique layered inter-crystalline structure made it a very promising solid lubricant material because of its relatively high load carrying capacity and low steady state friction coefficient (0.02). In addition, boric acid was found to help in reducing friction and corrosion when mixed with cutting and grinding fluids during machining processes. However, boric acid alone was found as an ineffective lubricant particularly when considering wear. Deshmukh et al. (2006) measured the boric acid performance as a lubricant by pin-on disk apparatus. The experiments were performed at room temperature and the worn surface of the pin was investigated by SEM. Figure 3.3 exhibits the worn surfaces of the pin without a lubricant, with boric acid lubricant and transmission fluid including boric acid. The boric acid crystal size was 100 μm. The wear volume of the pin were evaluated as 0.01338, 3.7246, and 0.0033 (mm^3) for unlubricated, lubricated with boric acid and lubricated transmission oil including boric acid, respectively. The poor wear performance of boric acid as a lubricant could be attributed to the fact that without replenishment, the boric acid was quickly forced out of the contact interface.

3.3. Borates

In addition the employment of boric acid in lubricating oils, metal borates that are extraordinary ceramic and functional materials find in use as an antiwear and anticorrosion material (Zeng et al., 2008; Hu et al., 2002; Hu and Dong, 1998; Dong and Hu, 1998). Zeng and his colleagues (2008) synthesized single crystalline magnesium borate ($Mg_2B_2O_5$) nanowires with typical diameter of 120-180 nm and length about 0.2 mm and they examined its tribological properties by means of friction reducing ability. The synthesized nanowires were added to gear lubricant oil and lubricating property was tested by terminal face friction apparatus. Figure 3.4 shows the effect of magnesium borate nanowires on the friction coefficient of lubricating oil. It can be seen that the friction coefficients of the base oil and the oil containing the $Mg_2B_2O_5$ nanowires become larger with the increase of the load. The oil containing $Mg_2B_2O_5$ nanowires gets a smaller friction coefficient than the base oil under the same load. The oil containing 5.0 wt% $Mg_2B_2O_5$ nanowires has the smallest friction

coefficient, which indicates that the increase of the content of $Mg_2B_2O_5$ nanowires in the oil can further reduce the friction coefficient.

In lubrication industry, the lubricants can be water based, therefore water is used instead of oil products. Metal borates also have potential use in that kind of products. Chen et al. (2008) obtained the wear and friction performances of sodium and potassium borates ($Na_2B_4O_7 \cdot 10H_2O$ and $K_2B_4O_7 \cdot 5H_2O$) in water. The antiwear and friction properties of the additives were evaluated by four ball tribotester. The experimental condition and the results were tabulated in Table 3.2. When sodium borate or potassium borates were introduced into water, friction-reducing capacity of water was improved, whereas, anti-wear capacity was decreased. The friction reducing ability of potassium borate was higher than the sodium borate.

(a)   (b)

(c)
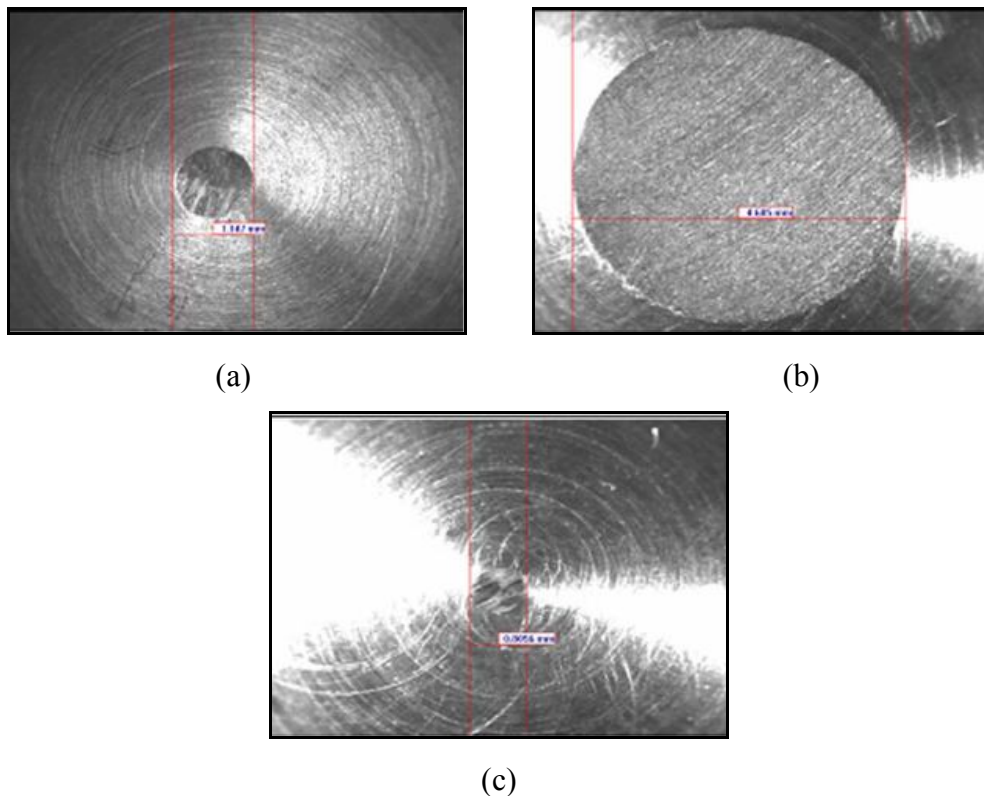
Figure 3.3. SEM images of the worn surfaces of the pin a) without lubrication b) lubricated with boric acid c) lubricated with transmission oil having boric acid (Source: Deshmukh et al., 2006).
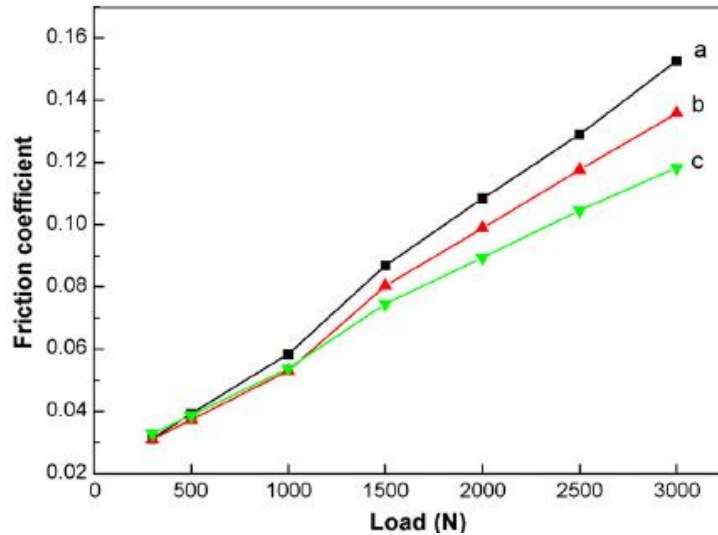
Figure 3.4. Effect of magnesium borate nanowires on the friction coefficient of lubricating oil a) base oil, b) oil containing 1.0 wt.% $Mg_2B_2O_5$ nanowires and c) oil containing 5.0 wt.% $Mg_2B_2O_5$ nanowires (Source: Zeng et al., 2008).

Table 3.2. Friction and wear behaviors of borates
(Source: Chen et al., 2008).

Additive	Concentration	Load (N)	Test Duration (min)	Wear Scar Diameter (mm)	Average friction coefficient
Distilled water	-	59	10	0.46	0.583
$Na_2B_4O_7 \cdot 10H_2O$	2	137	10	0.63	0.463
$K_2B_4O_7 \cdot 5H_2O$	2	137	10	0.59	0.451

Qiao et al. (2003) synthesized N-modified nano/micrometer borate as an oil additive by an ultrasonic dispersion and emulsion reaction in the microemulsion phase. The tribological properties of N-modified nano/micrometer borate particles 20-50 nm in diameter were analyzed by a four-ball tester. It was demonstrated that these borate particles decrease the wear scar diameter and when the additive concentration was 0.05 wt %, minimum wear scar diameter was obtained. Figure 3.5 explains the change in wear scar diameter by increasing the additive concentration.
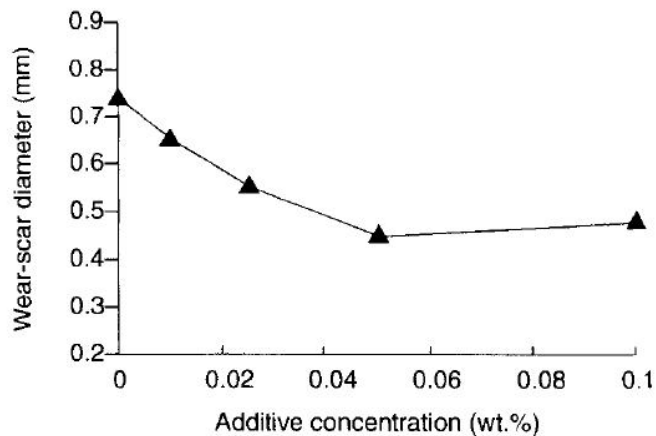
Figure 3.5. Effect of concentration of additive on antiwear properties
(Source: Qiao et al., 2003).

Nowadays, tribological studies related to the engineering surfaces at scales ranging from atomic and molecular to microscales are gaining importance to understand the lubrication theory and predict some of the many challenging problems in the fundamental research of tribology. The development of surface force apparatus (SFA), scanning tunneling microscope (STM), atomic force microscope (AFM) and friction force microscope (FFM) provides the nanotribological and nanomechanic studies needed to find out interfacial phenomena on a small scale and surface interactions (Bhushan, 2005; Bhushan, 1999). Surface topography is a key factor affecting the function and reliability of a component and the characterization of surface topography has become increasingly important in many fields, such as tribology and machine condition monitoring. Li and his colleagues synthesized a novel borate ester derivative containing benzothiazol-2-yl and disulfide (BTSB) and they examined its tribological properties in rapeseed oil by a four-ball tribometer. In order to analyze the morphology of the worn surfaces and the extent of the wear, AFM was used and 3D surface topographies were obtained as shown in Figure 3.6. It was observed that there were more scratches and deeper furrows on the wear scar obtained from the test lubricated by rapeseed oil alone than that of rapeseed oil containing 1.5 wt% BTSB additives, which indicated that BTSB additives possessed good antiwear ability (Li et al., 2010).

<div align="center">(a)   (b)</div>
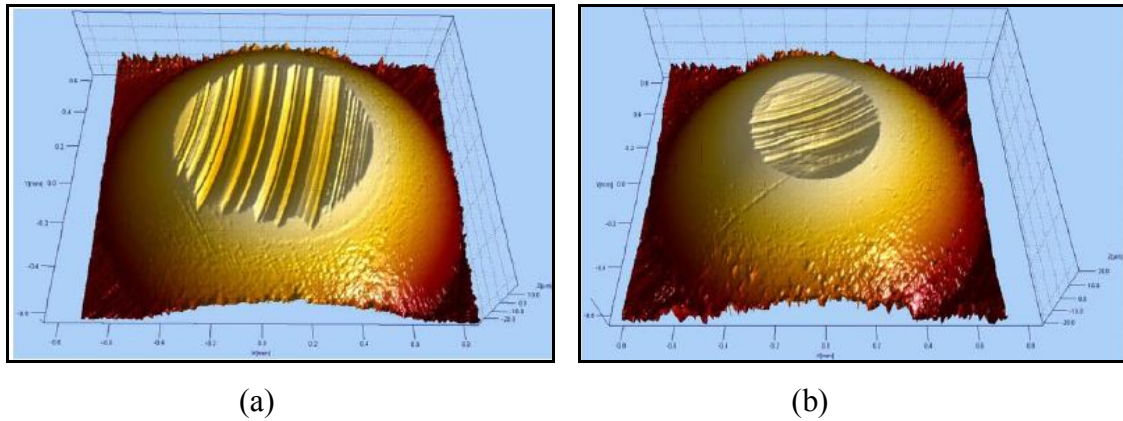
Figure 3.6. 3D plot of the worn surface lubricated with a) rapeseed oil alone b) rapeseed oil containing 1.5 wt% BTSB additives under 392 N (Source: Li et al., 2010).

Tribological properties of SN 500 base oil containing different types of metal borates prepared by ethanol supercritical fluid drying were investigated (Hu and Dong, 1998; Dong and Hu, 1998; Hu et al., 1999; Hu et al., 2002). The lubricants were prepared by adding 0.757 wt % metal borate and 1 wt.% sorbitol monostearate. The content of these lubricants, and their tribologic property are given in Table 3.3. The wear scar diameters of the worn surfaces were determined by four-ball tribotester under 294 N. The wear scar diameter of the ball running in base oil was evidently larger than that running in the oil with nano-sized metal borates. However, the dispersing agent effect on the wear scar diameter was not tested therefore it was not clear to understand the antiwear ability of metal borates. Larger wear scar diameter was obtained when zinc borate nanoparticles were added to the base oil. Besides them, it was observed that the wear scar diameter was reduced by decreasing the particle size of the metal borates, accordingly.

Friction coefficient of the lubricants described in Table 3.3 were measured by a HQ-1 block-on-ring tribotester in which the ring was a quenched CrWMn steel ring (Cr: 0.9–1.2 wt%, C: 0.9–1.05 wt%, W: 1.2–1.6 wt%, Mn: 0.8–1.1 wt%, Si: 0.15–0.35 wt%) of 49 mm diameter, 13 mm height, 62 HRC hardness and a surface roughness of Ra=0.27 mm, which was rotating against 45 steel block (12.64 mm in breadth) with a hardness of 44.8 HRC and a surface roughness of Ra = 0.35 mm. The rotating speed of the ring was 1500 rpm; in other words, the friction velocity was 3.85 m/s. It was found that oil with nano-sized metal borates gave a smaller friction coefficient than base oil (Figure 3.7).

Table 3.3. The properties of the lubricants containing metal borates
(Source: Hu et al., 2000; Hu et al., 1999; Dong and Hu, 1998)

Additive	Particle size (nm)	Amount of additive in base oil (wt. %)	Wear Scar Diameter (mm)	Reference
-	-	-	0.69	Hu et al., 1999
Magnesium borate	10	0.757	0.43	Hu et al., 2002
Lanthanum borate	20-40	0.757	0.46	Hu et al., 2000
Titanium borate	10-70	0.757	0.48	Hu et al., 1999
Zinc borate	20-50	0.757	0.62	Dong et al., 1998

(a)   (b)
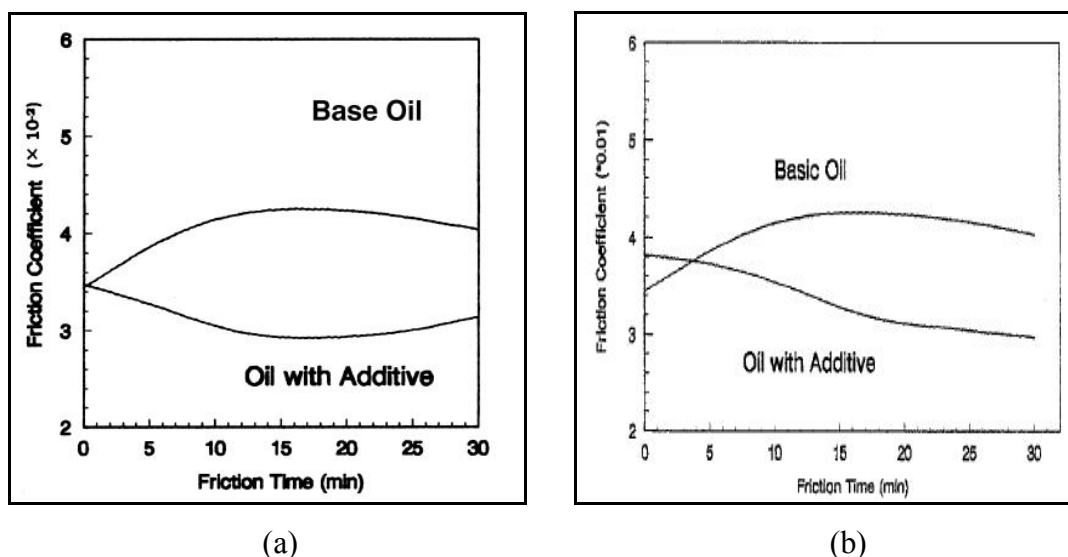
Figure 3.7. Effect of a)nano-sized zinc borate b) nano-sized titanium borate on friction coefficient of oil (Source: Dong and Hu, 1998; Hu and Dong, 1998).

The enhancement of the wear resistance and load carrying capacity of 500 SN base oil by metal borates is explained by the tribochemical reaction formed on the surface. Hu and his coworkers (2000) claimed that diboron trioxide and FeB were formed on the wear scar surface. These tribochemical reaction products as well as some depositions of the metal borate formed a wear resistant film on the rubbing surface, which provided the oil with an excellent load carrying capacity. A schematic diagram of the wear resistance mechanisms is given in Figure 3.8. First of all, nanoparticle metal borate with adsorbing dispersing agent is deposited on the rubbing surface. Then, diboron trioxide is formed by the decomposition of the metal borate due to shear effect

and extreme-pressure effect. Finally FeB is produced by a further tribochemical reaction between the diboron trioxide and substrate iron. These depositions and the tribochemical reaction products form a wear resistance film on the rubbing surface, which provides the oil with an excellent load carrying capacity.
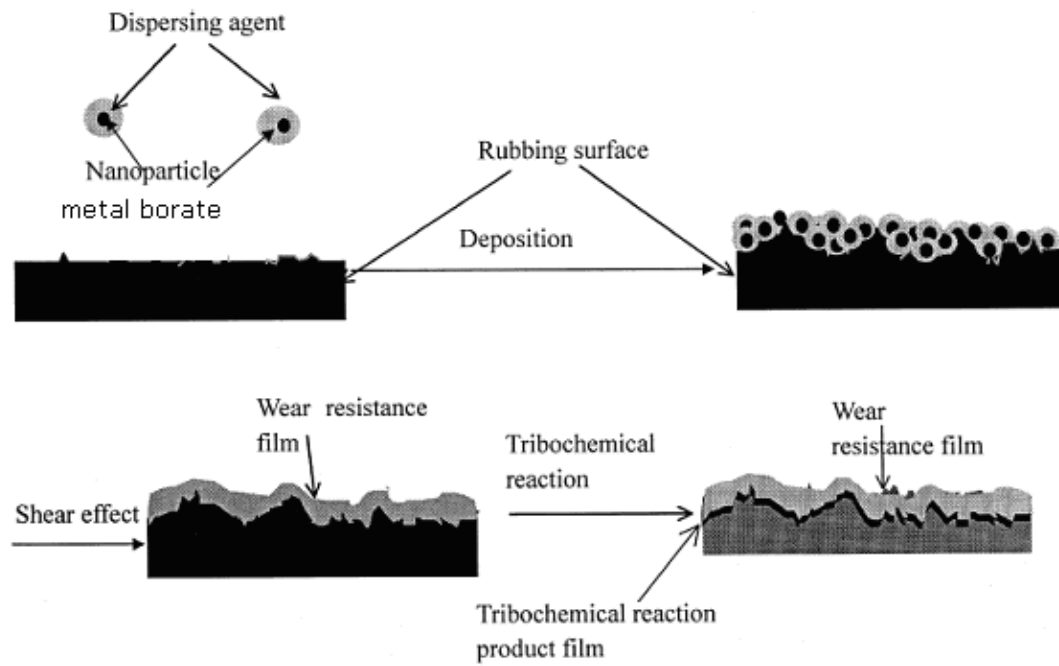
Figure 3.8. Schematic diagram of the wear resistance mechanisms of the lanthanum borate (Source: Hu et al., 2000).

The crystal and hydrophobic zinc borate ($2B_6O_{11}.3H_2O$) was prepared by a wet method using $Na_2B_4O_7 \cdot 10H_2O$ and $ZnSO_4 \cdot 7H_2O$ as raw materials in situ aqueous solution, and oleic acid was used as the modifying agent. TEM images demonstrate that the surfactant has an effect on the shape of zinc borate particles as shown in Figure 3.9. Pure zinc borate without surfactant presented polyhedral shape with particle size of around 50-500 nm, while hydrophobic zinc borate had disc-like shape. The diameters of the nanodiscs were from 100 to 500 nm. It was observed that the morphologies transform from irregular to regular, indicating that oleic acid adjusted the shape of the particles (Tian et al., 2006). The friction coefficient of the base oil with zinc borate nanodiscs was measured with MMU-10G pin-on-disc tester, in comparison to the base oil and the base oil with the addition of pure zinc borate powder. The results of their friction test are shown in Figure 3.10.

a   b
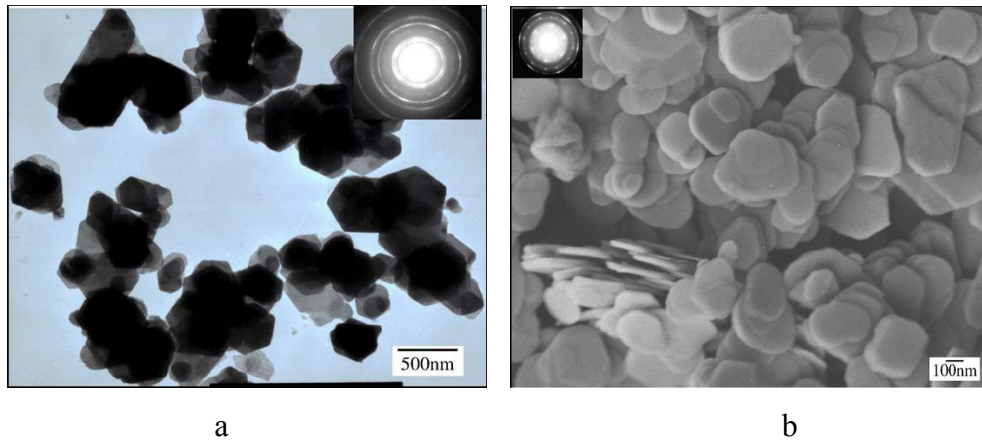
Figure 3.9. a) TEM image of pure zinc borate particles b) SEM image of the hydrophobic zinc borate nanodiscs (Source: Tian et al., 2006).
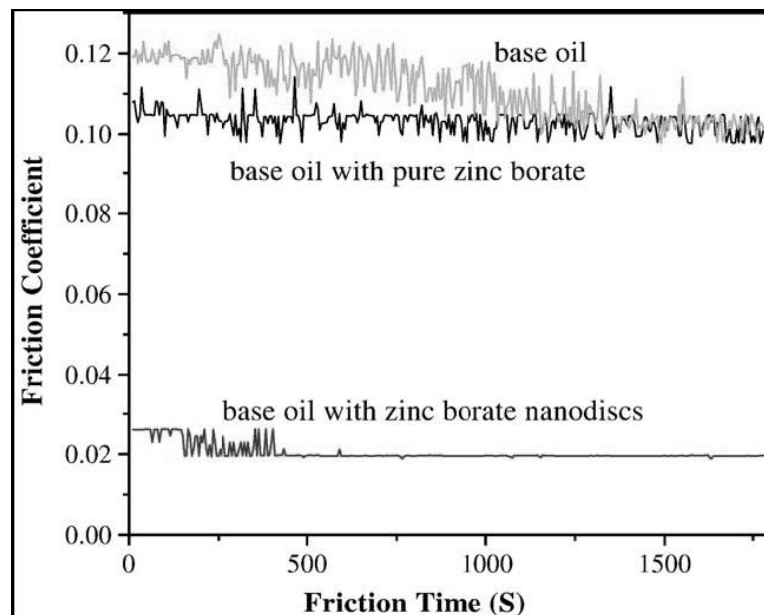
Figure 3.10. Effect of zinc borate nanodiscs and pure zinc borate on friction coefficient of the base oil (Source: Tian et al., 2006).

It can be seen that the base oil with zinc borate nanodiscs gives a smaller and more stable friction coefficient than the base oil and the base oil with pure zinc borate powder since pure zinc borate powder accumulates and cohers in the front of the leading face of a steel board and its size is larger, it is hardly dispersed in the base oil. However the hydrophobic zinc borate nanodiscs more easily penetrated into the interface of the base oil and formed a continuous film in concave of rubbing face, which could decrease shearing stress, therefore, gave a low friction coefficient (Tian et al., 2006).

CHAPTER 4

EMULSIONS

Emulsions are heterogeneous mixtures of at least one immiscible liquid dispersed in another in the form of droplets, the diameters of which are, in general, greater than 0.1 μm (Myers, 1991). The dispersed liquid is present in the form of droplets in the continuous phase (Ulmeanu, 2008). Emulsions are divided into two types, water-in-oil and oil-in-water (Ichikawa, 2007). Water-in oil systems (o/w) are sometimes called as normal emulsion. Important oil-in-water food emulsions, ones in which oil or fat is the dispersed phase and water is the continuous phase, include milk, cream, ice cream, salad dressings, cake batters, flavor emulsions, meat emulsions, and cream liquors. However, it is also possible to form an inverse or water in oil (w/o) emulsion. In an inverse emulsion, the water droplets are dispersed in a continuous phase of oil. Many medicinal creams and butter are water in oil emulsions. Schematic diagrams of normal emulsion (oil-in-water) and inverse emulsion (water-in oil) are given in Figure 4.1. Emulsions are inherently unstable because free energy is associated with the interface between the two phases. As the interfacial area increases, either through a decrease in particle size or the addition of more dispersed phase material, i.e. higher fat, more energy is needed to keep the emulsion from coalescing. Some molecules act as surface active agents (called surfactants or emulsifiers) and can reduce this energy needed to keep these phases apart (Rosen, 1989). In literature qualitative theory behind the emulsion formation is explained on the basis of difference in contact angles at the oil-water-emulsifier boundary as shown in Figure 4.2. If oil contact angle (measured in the oil phase) at the contact between oil, water, and emulsifier (θ) is less than 90°, then the oil surface is concave toward the water, producing a water-in-oil emulsion (Figure 4.2a). The emulsifier is more hydrophobic than hydrophilic for this case. On the other hand, the water contact angle at the same contact is less than 90°, and then the water surface is concave toward the oil, forming an oil-in-water emulsion (Figure 4.2b). Therefore, the emulsifier is more hydrophilic than hydrophobic (Rosen, 1989).
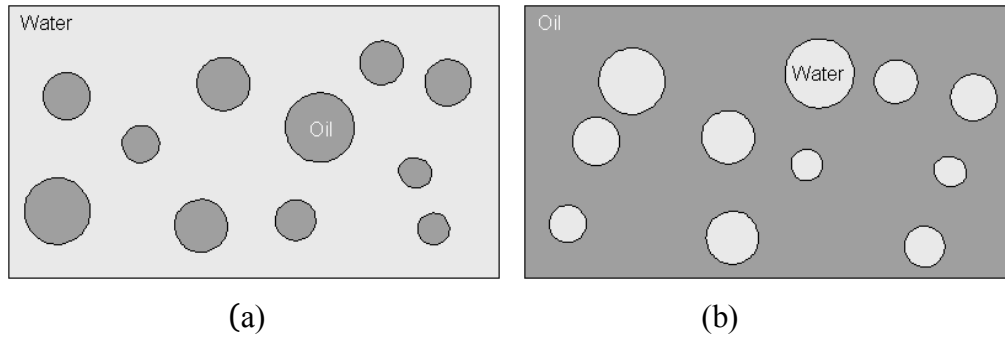
Figure 4.1. Schematic diagram of a) normal emulsion b) inverse emulsion.
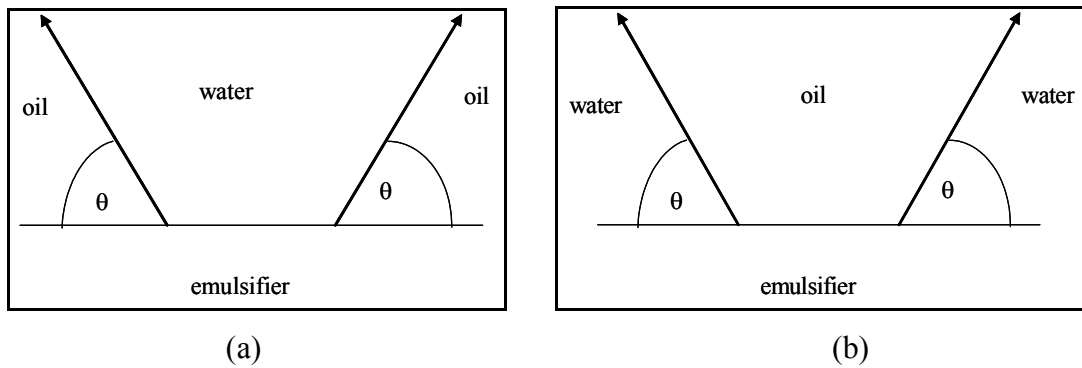
Figure 4.2. Effect of contact angle on emulsion type
(Source: Rosen, 1989).

4.1. Emulsifiers and Stabilizers for Emulsions

There are four general classes of materials that can act as emulsifiers and/or stabilizers for emulsions. They are common ionic materials, colloidal solids, polymers and surfactants. The surfactants adsorb at interfaces, lower the interfacial tension, and impose a stabilizing barrier between emulsion drops. Surfactant molecule is formed by two parts with different affinities for the solvents. One of them has affinity for water (polar solvents) and the other for oil (non-polar solvents) as shown in Figure 4.3a. The surfactant molecules are formed by the agglomeration of micelles. A typical micelle in aqueous solution forms an aggregate with the hydrophilic head regions in contact with surrounding solvent, and the hydrophobic tail regions are in the micelle centre. This type of micelle is known as a normal phase micelle (oil-in-water micelle). Inverse micelles have the headgroups at the centre with the tails extending out (water-in-oil micelle). Figures 4.3b and 4.3c show oil-in-water micelle and water-in-oil micelle, respectively. In other words, micelles are like drops of oil in water and reverse micelles

39

are like drops of water in oil. They are approximately spherical in shape. Other phases, including shapes such as ellipsoids, cylinders, and bilayers are also possible. The shape and size of a micelle are the functions of the molecular geometry of its surfactant molecules and solution conditions such as surfactant concentration, temperature, pH, and ionic strength (Schick and Fawkers, 1966).
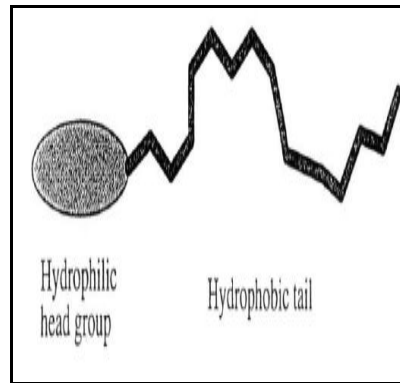
(a)
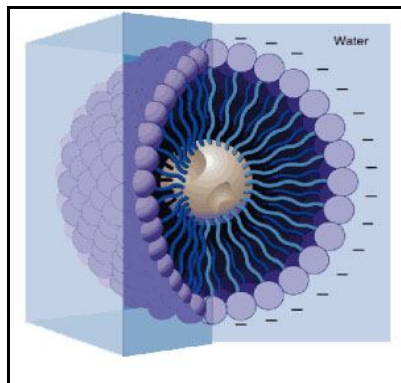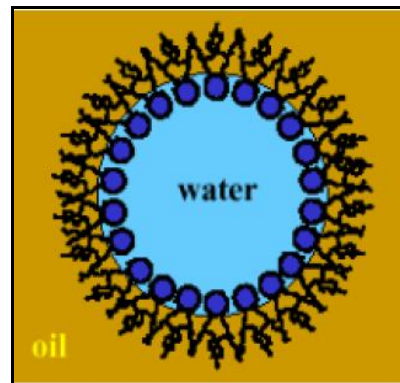
….(b)   ..(c)

Figure 4.3. The schematic illustration of a) a surfactant b) normal phase micelle c) inverse phase micelle.

There are four main types of surfactants used in laundry and cleaning products. Depending on the type of the charge of the head, a surfactant belongs to the anionic, cationic, non-ionic or amphoteric/zwitterionic family. For anionic surfactants, the head is negatively charged. This is the most widely used type of surfactant for laundering, dishwashing liquids and shampoos because of its excellent cleaning properties. The surfactant is particularly good at keeping the dirt away from fabrics, and removing residues of fabric softener from fabrics. The most commonly used anionic surfactants are alkyl sulphates, alkyl ethoxylate sulphates and soaps. In solution, the head of

cationic surfactants is positively charged. Noninonic surfactants do not have an electrical charge, which makes them resistant to water hardness deactivation. The most commonly used non-ionic surfactants are ethers of fatty alcohols and sorbitan esters. Sorbitan fatty acid ester surfactants are effective reducers of interfacial tension. At the oil-water interface the hydrocarbon chains of sorbitan monostearate molecule orientate the oil and the sorbitan ring to the aqueous side of the interface. The properties of sorbitan monoester surfactants (sorbitan monolaurate, sorbitan monopalmitate, sorbitan monostearate and sorbitan monooleate) at air-water and oil-water interfaces were studied (Korhonen et al., 2004; Peltonen et al., 2001; Peltonen et al., 2000). The surface pressure-molecular area curves of sorbitan monoesters are given in Figure 4.4. In comparisons of surface pressure–molecular area curves of Span 60 (saturated) and 80 (unsaturated), the molecular area of Span 80 is larger than that of Span 60. When stearic and oleic acids are compared (Span 60 is a sorbitan ester of stearic acid and Span 80 a sorbitan ester of oleic acid), the surface pressure–molecular area curves behave in the same way, the molecular area of stearic acid being smaller at the same surface pressure compared to that of oleic acid (Peltonen et al., 2000). Figure 4.5. shows the plot of the interfacial tension of sorbitan ester surfactants versus their bulk-phase concentrations in n-haptane at the water-n-heptane interface. From the interfacial tension measurements the following values were calculated: critical micelle concentration (cmc) which were the concentration at which micellization started, the interfacial tension at the cmc (γ_{cmc}), surface pressure at the cmc (π_{cmc}), area per molecule at the cmc (A_{cmc}). These values evaluated for sorbitan monostearate in different alkane solvent are listed in Table 4.1. The cmc value increased slightly when the length of the hydrocarbon chain decreased (Peltonen et al., 2001). Furthermore, it was obtained that sorbitan monoester surfactants had no effect on the interfacial tension of n-hexane against air and the surface tension of mineral oil against air did not change after the addition of the sorbitan monoester surfactants (Peltonen et al., 2000). This phenomenon was explained by the fact that in the absence of a hydrophilic phase there was no driving force for interfacial adsorption and multilayer formation.
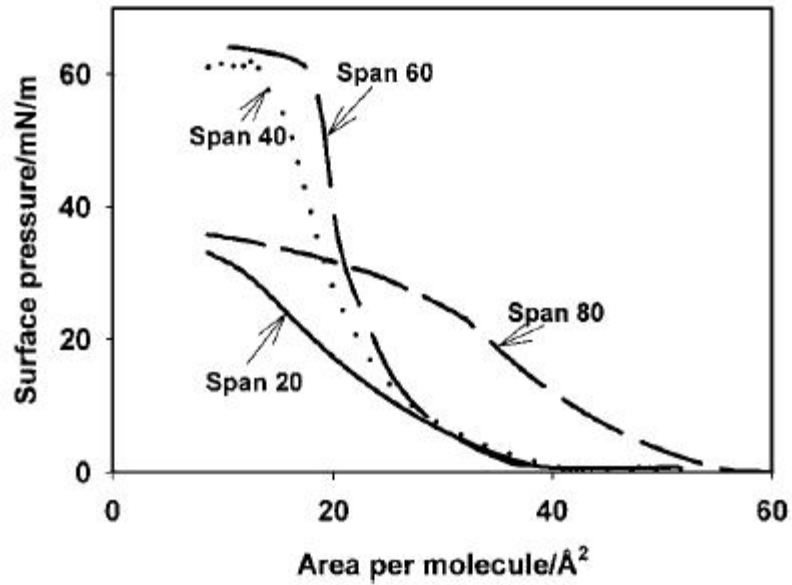
Figure 4.4. The surface pressure-molecular area curves of sorbitan monoesters (T= 295K) (Source: Peltonen et al., 2000).
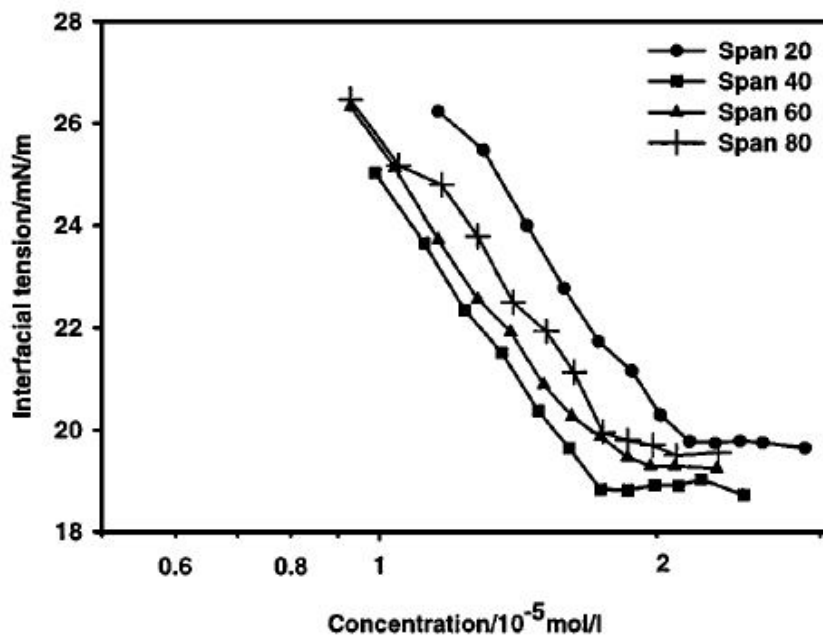
Figure 4.5. The interfacial tension (mN/m) vs concentration (mol/L) of sorbitan monoesters at the water–heptane interface (Source: Peltonen et al., 2001).

Table 4.1. Cmc (mol/L), γ_{cmc} (mN/m), π_{cmc} (mN/m), and A_{cmc} (A^2) values at the different oil phases for sorbitan monoesters (Source: Peltonen, 2001).

	Pentane	Hexane	Heptane	Octane	Nonane	Decane	Dodecane
cmc (10^{-5} mol/L)	1.6	1.7	1.7	1.8	1.8	1.8	1.9
γ_{cmc} (mN/m)	14.4	18.9	19.3	19.8	20.1	21.2	22.4
π_{cmc} (mN/m)	34.0	31.9	31.9	31.9	31.9	31.2	30.5
A_{cmc} (A^2)	38.0	38.0	33.0	31.0	28.0	27.0	30.0

A related rule concerning surfactant structure and the type of emulsion formed is related to the solubility of the surfactant in the two liquids. The rule states that the liquid in which the surfactant is most soluble will be continuous phase in the final emulsion. For example, if the surfactant is more soluble in the oil phase a water-in-oil emulsion will result (Myers, 1991). On the other hand hydrophile-lipophile balance (HLB) number classifies the surfactants according to their chemical structure by using numbers in between 0 and 20 on an arbitrary scale. At the high end of the scale (8-18) lie hydrophilic surfactants which posses high water solubility and generally act as good aqueous solubilizing agents, detergents and stabilizers for oil-in-water emulsions, whereas at the low end (3-6) are surfactants with low water solubility which act as solubilizers of waters in oils and good water-in-oil emulsion stabilizers. For noninonic surfactants HLB may be calculated from the formula;

$$HLB=20(1-S/A)$$
(3.1)

where S is the saponification number of the ester and A is the acid number of the acid. The HLB value of nonionic surfactant sorbitan monostearate is reported as 4.7, indicating a good water-in-oil stabilizer (Myers, 1991).

4.2. Emulsion Preparation

Besides the importance of surfactant type and its concentration, the energy needed to produce the droplets play an important role in the formation of emulsion. High-speed stirrers and high-pressure homogenizers are preferred to prepare the

emulsions (Porras et al., 2008). A water-in-oil emulsion is prepared by homogenizing an oil phase and an aqueous phase together in the presence of a suitable oil-soluble emulsifier (low HLB number) (Surh et al., 2007). One of the main problems in the preparation of the emulsions is the mixing of oil and water phases. Jafari and his colleagues have examined the techniques of emulsification in four different groups as;

- Rotor-stator system
- High-pressure system
- Ultrasonic system
- Membrane system (Jafari et al., 2008).

The reason for using different emulsification techniques is to produce emulsion droplets as small as possible in order to obtain stable systems. Coarse emulsion having droplet size between 0.5-100μm can be obtained by using rotor-stator system whereas, nanoemulsions can be prepared by high pressure system. In a high pressure homogenizer, the dispersed and continuous phases are subjected to intense turbulence and shear by the conversion of pressure to kinetic energy, thereby leading to breakup of the dispersed phase into small droplets. Collisions brought about by the relative motion of the droplets lead to their coalescence. The drop size distribution of the emulsion is influenced by the rates of breakage and coalescence in the homogenizer during emulsion formation

Jafari et al. (2008) have studied the comparison of different emulsifying devices in terms of emulsion droplet size. As it can be seen in Figure 4.6, normal mixer (IKA) gives the biggest emulsion droplet size since the forces in this case are shear stresses in Laminar flow and it can not cause adequate droplet disruption. Rotor stator system (Silverson) is much better than the mixer and it produce 1μm emulsion droplet. The other emulsification systems, microfluidizer and ultrasound, droplets as small as 500 nm are produced.
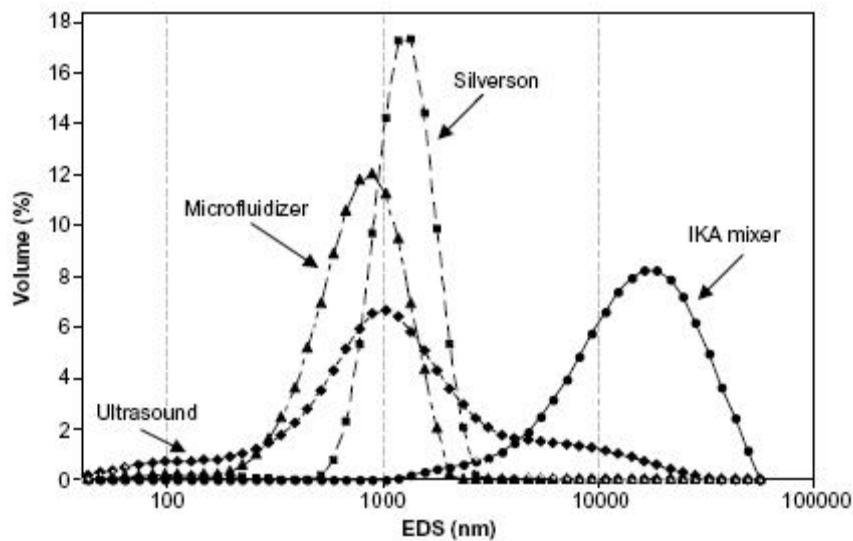
Figure 4.6. Emulsion droplet size distribution for different emulsification method
(Source: Jafari et al., 2008).

4.3 Emulsion Stability

The term stability is used for practical applications, usually refers to the resistance of emulsions to the coalescence of their dispersed droplets. In literature, it is indicated that the stability may be sustained by the activation energy much higher than the thermodynamic energy difference (Fukishima et al., 2009). The aggregation of droplets and the coalescence cause the separation of emulsions into two phases. The rate of the coalescence of the droplets in the emulsion depends on a number of factors:

- The physical nature of interfacial film
- The existence of an electrical and steric barrier on the droplets
- The viscosity of the continuous phase
- The size distribution of the droplets
- The phase volume ratio
- The temperature (Rosen, 1989; Elwell et al., 2004).

The prediction of emulsion stability is very important since it effects the formulation, quality control and the technical service of the products (metal working fluids, lubricants etc.). There are two mechanisms to achieve emulsion stability; electrostatical stabilization and sterical stabilization as shown in Figure 4.7. In many oil-in-water emulsions both electrostatic and steric forces play roles in the stability of

the emulsions, whereas, a water-in-oil emulsion can be mainly stabilized by the steric mechanism because of the low dielectric medium of the continuous oil phase. Moreover, it was reported that the emulsions containing nonionic polymeric surfactants, the system is stabilized by steric mechanism (Zhao, 2006).

<div align="center">(a)   (b)</div>
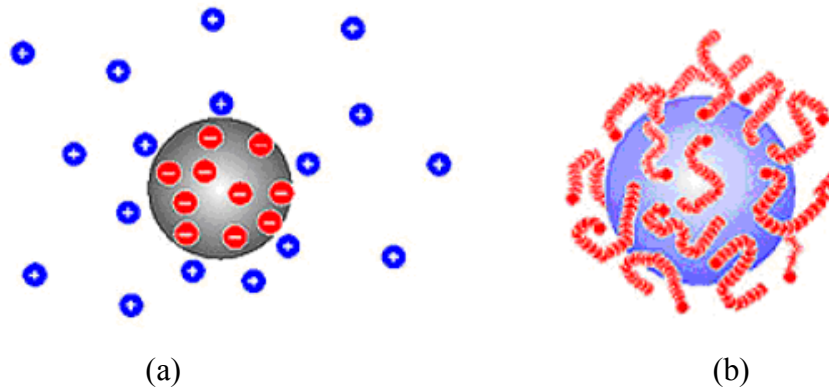
Figure 4.7. Illustration of emulsion stability mechanisms a) Electrostatically stabilized b) Sterically stabilized (Source: Zhao, 2006).

4.4. Microemulsions

Depending on the emulsion droplet size, emulsions can be divided into micro (10-100 nm), mini (100-1000 nm), and macro (0.5-100 μm) emulsions (Jafari et al., 2008; Zhao et al., 2006; Windhab et al., 2005). Microemulsions were first introduced by an English chemist J.H. Schulman in 1950, and he converted the turbid unstable emulsions to optically transparent and thermodynamically stable mixtures by adding alcohol and called the system as microemulsion. Therefore, the term microemulsion is applied to thermodynamically stable systems prepared by emulsifying an oil in aqueous surfactant and then adding a fourth component, called a cosurfactant, generally an alcohol of intermediate chain length (Palla and Shah, 1999; Lu and Guo, 2009). Benzene, water, potassium oleate, and hexanol might be the components of typical microemulsion formulation. Light scattering and an assortment of other techniques reveal that the resulting system consists of either oil-in-water or water-in-oil dispersions with particles having diameters in the 10-100 nm size range (Hiemenz and Rajagopalan, 1997). The most significant advantages of microemulsion method in the production of nanoparticles are better size distribution of particles and the controlling of the shape of

particles (Tai and Chen, 2008; Qiu et al., 1999). However, the utilization of great amount of surfactant and co-surfactant increases the preparation cost.

4.5. Synthesis of Nano-Sized Particles by Microemulsion

Microemulsion has become important in the synthesis of nanoparticles. Synthesis of particles in microemulsion systems can be carried out inside the emulsion droplets which act as micro/nano reactors (KeLong et al., 2007). Many researchers have studied the synthesis of metal, organic and inorganic nanoparticles in microemulsion systems (Capek, 2004; Shi and Weweij, 2005; Zhang et al., 2007, Tai and Chen, 2008, Öncül et al., 2008; Adityawarman, 2007) as shown in Table 4.2. The advantages of the utilization of microemulsion system in the particle synthesis lie in the fact of the controlling the particle size and shape. Also the microemulsion method requires no extreme pressure- temperature control, and no special or expensive equipment. Figure 4.8 illustrates possible qualitative structures that can be formed in the composition triangle of the ternary mixture water/oil/surfactant. According to this illustration the microstructures can be divided into two main groups. The first one is characterized by roughly spherical objects such as micelles and nanodroplets, whereas the second one is the aggregates having one, two and three dimensions (Adityawarman, 2007).

In literature the particles synthesis in microemulsions are achieved by two different methods. The first method is called as one-microemulsion method and the reaction is carried out by directly adding the aqueous solutions of raw materials into single microemulsion. If the reaction is initiated by implementing a triggering agent such as pulse radiolysis and laser photolysis into the single microemulsion, it is called as energy-triggering one-microemulsion method. The one-microemulsion method is driven by the diffusion-based process since the second aqueous solution of the reactant diffuses into the droplets containing the first reactant in microemulsion system. The second method is called as two-microemulsion method and is based on the mixing of two separate microemulsions prepared by the aqueous solutions of the raw materials (Adityawarman, 2007). This method relies on fusion-fission events between the droplets. The schematic illustrations of these methods are shown in Figure 4.9.

Table 4.2. Studies related to synthesis of particles in inverse microemulsions.

Particle	Oil Phase	Aqueous phase	Surfactant	Co-surfactant	Reference
Zinc borate	Kerosene	$Na_2B_4O_7 \cdot 10H_2O$ ZnSO4·7H$_2$O H_3BO_3	Span 80	Propanol-2	Köytepe et al., 2009
$CaAl_{12}O_{19}$	Hexane	$Ca(NO_3)_3 \cdot 4H_2O$ $Al(NO_3)_3 \cdot 9H_2O$	Poly (oxyethylene) nonylphenyl ether	-	Chandradass et al., 2009
Copper oxide	Isooctane	$CuCl_2$ NaOH	AOT	-	Nassar and Husein, 2007
Al_2O_3	Hexane	$Al\,(NO_3)_3 \cdot 9H_2O$ $NH_3 \cdot H_2O$	Triton X-100	n-buthyl alcohol	Ke-Long et al., 2007
$BaSO_4$	Hexane	$BaCl_2$ K_2SO_4	Marlipal O13/40		Adityawarman et al., 2005
Cu	Hexane	$CuSO_4$ $NaBH_4$	Sodium dodecyl sulfate	isopenthanol	Qiu et al., 1999
ZrO_2	n-heptane	$C_8H_{12}O_8Zr$ NH3	Span 40 Span 80 Span 85 Arlacel 83	-	Lee et al., 1999

In literature, various nano-sized inorganic particles such as calcium carbonate, barium sulphate, barium hydroxide, aluminum trioxide, zinc borate etc are synthesized using inverse microemulsion systems. Niemann and Sundmacher (2010) explained the particle formation in two-microemulsion system by three steps which are droplet exchange, nucleation and particle growth as shown in Figure 4.10. Droplet exchange starts after the mixing of the separate microemulsions. When mixing leads to the situation that both reactants appear in significant amounts inside one droplet, nucleation can occur. If further droplet exchanges provide new reactants to a droplet containing a

particle, this particle can grow. Also it is claimed that the surfactant monolayer protects the particles against agglomeration.
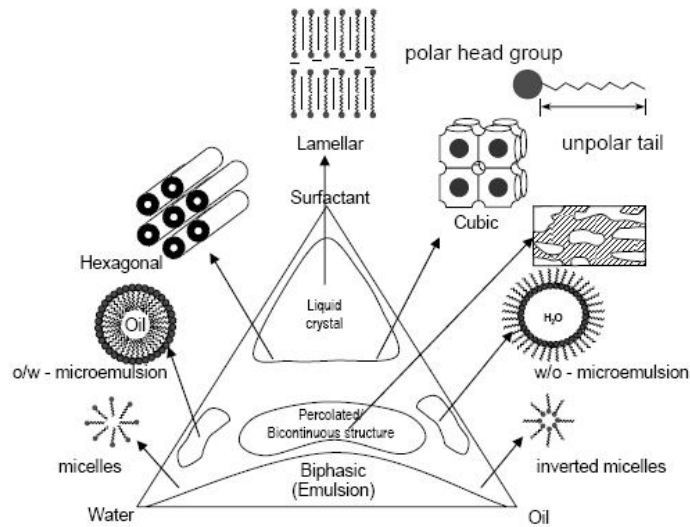
Figure 4.8. Schematic diagram illustrating the phase behavior of an oil/water/surfactant system (Source: Adityawarman, 2007).

(a)   (b)
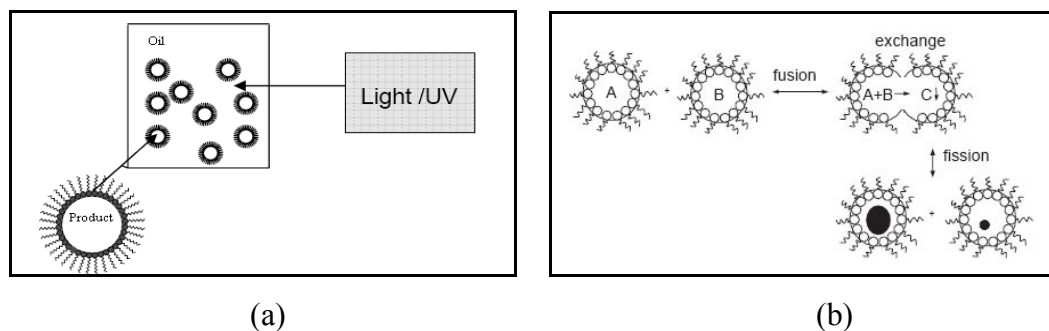
Figure 4.9. Schematic illustrations of the methods of particle synthesis a) Energy triggering one-microemulsion method b) Two-microemulsion method (Source: Adityawarman, 2007 and Adityatarwan et al., 2005).

Tai and Chen (2008), carried out the synthesis of $CaCO_3$ with different shapes and sizes because of their corresponding potential applications. In order to control the morphology, habit and size of the particles, inverse microemulsion techniques having different ω (water/surfactant molar ratio), S (water/oil molar ratio) and R (molar ratio of raw materials) were used. The synthesis of $CaCO_3$ consisted of the reparation of two inverse microemulsions of $CaCl_2$ and Na_2CO_3 solutions by mixing isooctane (oil phase),

sodium bis(2-ethylhexyl) sulfosuccinate (AOT) (surfactant), and a certain amount of aqueous $CaCl_2$ and Na_2CO_3 solutions. Figure 4.11 indicates SEM images of calcium carbonate powders. For these samples, the concentrations of $CaCl_2$ and Na_2CO_3 were 0.05 M, and the reaction time was recorded as 30 min. Rod-like particles were synthesized when ω and S values were adjusted as 15.96 and 3.16, respectively as shown in Figure 4.11a. However, spherical powders were obtained for lower ω (11.30) and higher S (4.65) values as pointed out in Figure 4.11b.
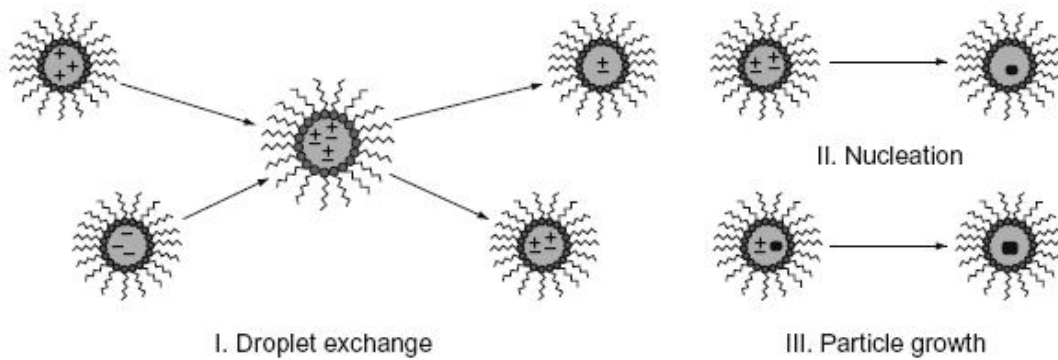
Figure 4.10. Particle formation mechanism in water in oil microemulsion
(Source: Niemann and Sundmacher, 2010).

(a)   (b)
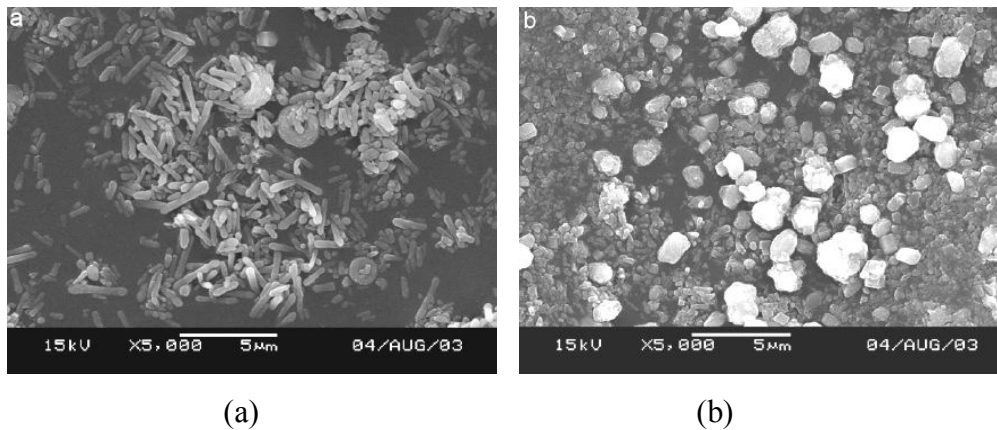
Figure 4.11. SEM images of $CaCO_3$ particles a) ω=15.96 S=3.16 b) ω=11.30 S=4.65
(Source: Tai and Chen, 2008).

Zinc borate ($Zn_2B_6O_{11} \cdot 3H_2O$) nanoparticles were prepared by precipitation in microemulsion. Microemulsions were prepared by dispersing aqueous phases (boric acid, borax decahydrate and zinc sulphate) in continuous oil phase (kerosene) and the

stabilization is achieved using Span 80 (sorbitan monooleate) as a surfactant and propanol-2 as a co-surfactant. Two microemulsions were mixed under constant stirring, allowing the reacting species to come in contact with each other due to dynamic nature of the dispersed droplets. The obtained nano-sized particles were characterized and XRD pattern of the zinc borate is given in Figure 4.12. The sharp peaks indicate the zinc borate particles are crystalline and all the diffraction peaks are consistent with the data of JCPDS files No. 21-1473. No characteristic peaks of impurities of the other unreacted compounds were observed (Köytepe et al., 2009).
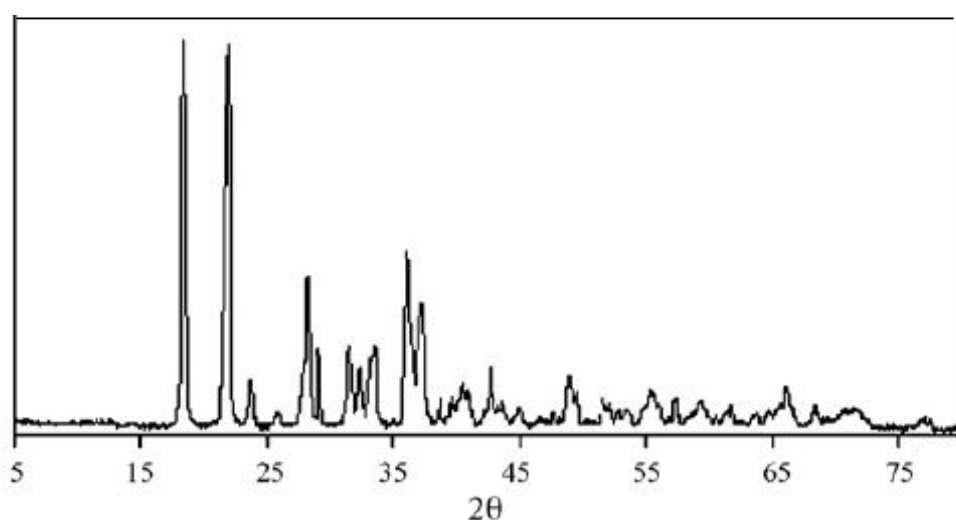
Figure 4.12. XRD of $Zn_2B_6O_{11} \cdot 3H_2O$ powders.
(Source: Köytepe et al., 2009).

4.5.1. Effect of Co-Surfactant in Particle Synthesis in Microemulsion

The formation of a microemulsion requires the presence of a cosurfactant and it is also known that addition of cosurfactant can reduce the surfactant concentration in microemulsion preparation (Lopez et al., 2004; Luo et al., 2004). In literature, especially low molecular weight alcohols, are used for this purpose. Their short hydrophobic chain and terminal hydroxyl group is known to enhance the interaction with surfactant monolayers at the interface, which can influence the curvature of the interface and internal energy. The amphiphilic nature of cosurfactants could also enable them to distribute between the aqueous and oil phases. The formation and various

physicochemical properties of the microemulsions are influenced by the alkyl chain length of alcohol and hydrocarbons (Bayrak, 2004).

Nanoscale yttrium–barium–copper oxide (Y_2BaCuO_5) particles were synthesized using the emulsion method and the solution method. The basic water-in-oil (w/o) emulsion system consisted of n-octane (continuous oil phase), cetyltrimethylammonium bromide (cationic surfactant), butanol (cosurfactant) and water. The composition of the emulsion system was varied and characterized by measuring the conductivity of the solutions and droplet size. The droplet size of emulsion was determined by using the dynamic light scattering method (DLS). Without the addition of cosurfactant, no water in oil phase was observed, however, the conductivity decreases with the addition of co-surfactant (butanol). Additionally, it is found that the sizes of droplets reduce due to the addition of the co-surfactant as shown in Figure 4.13. Droplet size initially decreases with addition of co-surfactant and reaches a limited value and the droplet size is 3.5 nm. The droplet size remains almost unchanged with further addition of cosurfactant (Li and Vipulanandan, 2007).
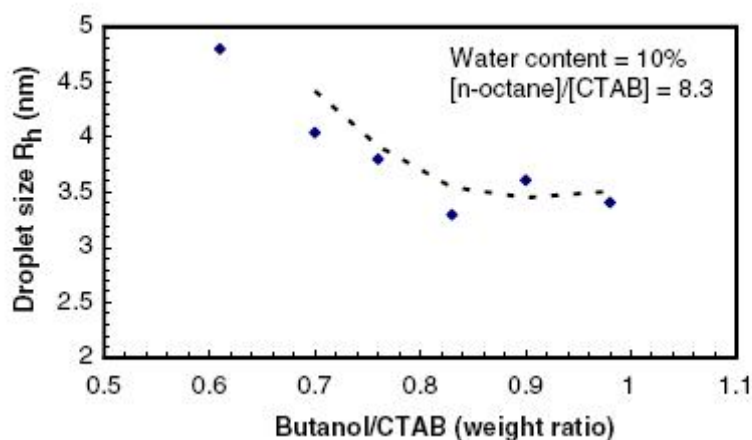
Figure 4.13. Effect of co-surfactant concentration on the water droplet size
(Source: Li and Vipulanandan, 2007).

Charinpanitkul et al. (2005), indicate the effect of co-surfactant type on the size and the morphology of ZnS nanoparticles obtained by two microemulsion method. Three different alcohols were used as co-surfactant in the microemulsion system and the synthesized particles were compared with each other by means of their morphology as demonstrated in Figure 4.14. When n-hexanol was employed as a co-surfactant, ZnS nanoparticles were obtained as quantum dots with diameters less than 5 nm. These quantum dot particles could agglomerate to form secondary particles with larger

diameters of between 40–100 nm (Figure 4.14a). However, the utilization of n-pentanol might result in ZnS nanorods with some agglomerations as shown in Figure 4.14b. On the other hand, ZnS nanotubes with some quantum dot depositing on their surface could again be successfully grown when n-butanol was introduced as a cosurfactant in the system (Figure 4.14c).

(a)　　　　　　　　　　　　　　(b)

(c)
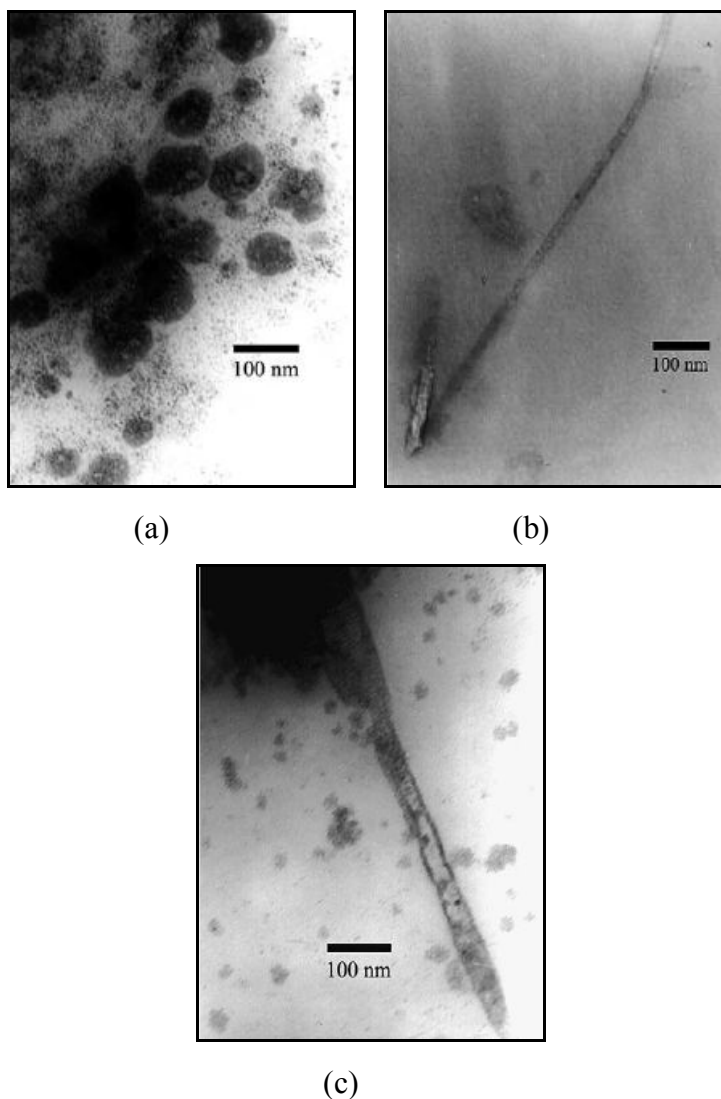
Figure 4.14. TEM images of ZnS nanoparticles synthesized in microemulsions with a) n-hexanol b) n-pentanol c) n-butanol as cosurfactants (Source: Charinpenitkul et al., 2005).

4.6. Emulsion Lubrication

Oil-in-water emulsions are commonly used in the manufacturing processes, particularly, in metalworking fluids such as rolling, cutting, ironing and grinding. The oil-in water emulsion systems in these processes are some advantages since they have;

- Stability against creaming

- Low cost

- Fire resistance

- Corrosion inhibition

- Ability to remove heat

- Hydrophobic surfactant film which protects the metal surface (Lu and Guo, 2009; Cambiella et al., 2006).

Therefore, understanding of the tribology of emulsions is of principal importance to the application of the emulsions as lubricants (Januszkiewicz et al., 2004). Yan and Kuroda (1997) have proposed two types of lubrication with emulsions. The illustrations related to lubrication are given in Figure 4.15. Figure 4.15a shows the thick film type and for this type, the diameters of droplets of the disperse phase are smaller than the minimum film thickness, so the droplets suspend in the continuous phase in the whole contact area. For the thin film type (Figure 4.15b), the diameters of the majority of droplets are larger than the minimum film thickness, thus the droplets deform and sandwiched between two solid surfaces at the thin film zone.

(a)   (b)
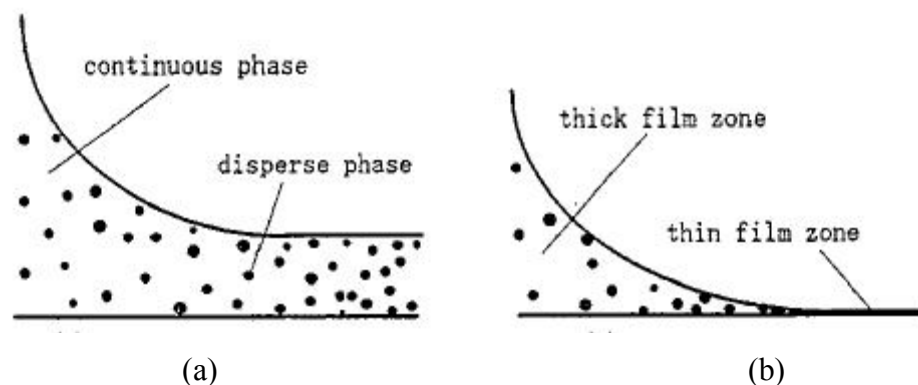
Figure 4.15. The types of emulsion lubrication a) thick film type b) thin film type
(Source: Yan and Kuroda, 1997).

Even though there are some studies dealing with the application of oil-in-water emulsion, there are few studies related to the employment of water-in-oil emulsions in lubrication processes according to our knowledge.

CHAPTER 5

ZINC BORATE

Zinc borates have been typically used as fire retardant additives, smoke and afterglow suppressants, char promoters, lubricating oil additives and nonlinear optical materials. There are major advantages in using zinc borate because of its high thermal stability, no toxicity and low cost (Schubert et al., 2003; Shi et al., 2008). Several unique crystalline zinc borates have been developed and are being used. The physical properties and the application areas of zinc borate are fundamentally related to its water content, size and morphology. The chemical formulations of the most important commercial products are $2ZnO·3B_2O_3·3.5H_2O$, $ZnO·B_2O_3·2H_2O$, $ZnO·3B_2O_3·7-7.5H_2O$, $2ZnO·3B_2O_3·9H_2O$, $3ZnO·2B_2O_3·5H_2O$, $ZnO·B_2O_3·1.5H_2O$, $4ZnO·B_2O_3·H_2O$, $2ZnO·3B_2O_3$ (Gürhan et al., 2009). Extensive research has been carried out in the design and preparation of nanostructures with different shapes and sizes because of their corresponding novel properties and potential applications. In order to obtain a high performance, it is imperative that the morphology and size of the materials should be controlled. Even if there are various studies related to the zinc borate synthesis, unfortunately, there are few reports on nanosized zinc borate. Table 5.1 summarizes the studies related to the production of zinc borate.

The production techniques of zinc borate generally include the reaction between zinc oxide and boric acid or the reaction between aqueous solution of alkali metal borate and a water soluble zinc salt (Eltepe et al., 2007; Nies et al., 1972).

Table 5.1. Studies related to zinc borate production

Raw Materials	Production Method	Product Type	Particle morphology	Reference
Zinc oxide Boric acid	Precipitation	$2ZnO \cdot 3B_2O_3 \cdot 3.5H_2O$	Flake-like	Li et al., 2010
Zinc nitrate Borax	Precipitation	$4ZnO \cdot B_2O_3 \cdot H_2O$	Nanowhisker	Zheng et al., 2009
Zinc sulphate Boric acid	Precipitation	$2ZnO \cdot 2B_2O_3 \cdot 3H_2O$	Rhombohedral	Liu et al., 2009
Zinc sulphate Borax Boric acid	Inverse microemulsion	$Zn_2B_6O_{11} \cdot 3H_2O$	Undefined	Köytepe et al., 2009
Zinc Sulphate Borax PEG 300	Surfactant-assisted Hydrothermal	$4ZnO \cdot B_2O_3 \cdot H_2O$	Lamellar-like	Shi et al., 2009
Zinc oxide Zinc sulphate Borax	Precipitation	$Zn_2B_6O_{11} \cdot 7H_2O$	Undefined	Gao et al., 2009a
Zinc sulphate Borax Boric acid	Precipitation	$Zn_3B_{10}O_{18} \cdot 14H_2O$	Undefined	Gao et al., 2009a
Zinc oxide Boric acid	Precipitation	$2ZnO \cdot 3B_2O_3 \cdot 3.5H_2O$	Undefined	Gürhan et al., 2009

Table 5.1. (cont.)

Zinc nitrate Borax	Homogeneous precipitation with ammonia	$2ZnO \cdot 2.2B_2O_3 \cdot 3H_2O$	Flake-like	Ting et al., 2009
Zinc Sulphate Borax	Precipitation	$4ZnO \cdot B_2O_3 \cdot H_2O$	Unidentified	Gao et al., 2009b
Zinc sulfate Borax Oleic acid	Precipitation	$Zn_2B_6O_{11} \cdot 3H_2O$	Nanoplatelet	Tian et al., 2006, 2008
Zinc Sulphate Borax PEG 300	Surfactant-assisted Hydrothermal	$4ZnO \cdot B_2O_3 \cdot H_2O$	Rod-like Lamellar-like	Shi et al., 2008
Zinc oxide Boric acid	Homogeneous precipitation	$ZnO \cdot 0.3B_2O_3 \cdot H_2O$ $ZnO \cdot 0.4B_2O_3 \cdot 1.4H_2O$	Fiber like	Ting et al., 2008
Zinc oxide Boric acid	Rheological phase reaction	$2ZnO \cdot 3B_2O_3 \cdot 3H_2O$	Plate like	Shi et al., 2008
Zinc oxide Boric acid	Precipitation	$2ZnO \cdot 3B_2O_3 \cdot 3H_2O$	Needle shape	Eltepe et al., 2007.
Zinc oxide Boric acid	Precipitation	$2ZnO \cdot 3B_2O_3 \cdot 3H_2O$ or $Zn[B_3O_4(OH)_3]$	Undefined	Schubert et al., 2003
Zinc nitrate Borax	Precipitation Supercritical fluid drying	Undefined	Spherical	Hu and Dong, 1998
Zinc oxide Boric acid	Precipitation	$4ZnO \cdot B_2O_3 \cdot H_2O$	Undefined	Schubert, 1995

5.1. Zinc Borate Production from Zinc Oxide and Boric Acid

Zinc borate having a chemical formula ($2ZnO \cdot 3B_2O_3 \cdot 3H_2O$) is one of the several types of zinc borates. This compound has the unusual property of retaining its water of hydration at temperatures up to 290 $^\circ$C. This thermal stability makes it attractive as a fire retardant additive for plastics and rubbers that require high processing temperatures. It is also used as an anticorrosive pigment in coatings. Zinc borate is produced by reaction between aqueous boric acid and zinc oxide in the solid state above 70 ^{o}C (Shete et al., 2004). Eltepe et al. (2007) developed the synthesis of $2ZnO \cdot 3B_2O_3 \cdot 3H_2O$ by using zinc oxide and boric acid. The synthesis was performed according to the reaction given in Equation 5.1. Firstly the boric acid was dissolved in pure water and then zinc oxide was added and also zinc borate seed crystals were used. The reaction was carried out in closed Schott bottles in two steps by stirring at 60 °C for 1.5 h and 90 °C for 4 h.

$$2ZnO(s) + 6H_3BO_3 \text{ (aq)} \rightarrow 2ZnO \cdot 3B_2O_3 \cdot 3H_2O \text{ (s)} + 6H_2O \qquad (5.1)$$
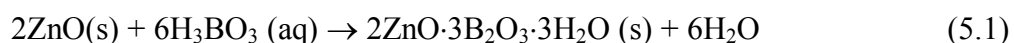
Gao et al. (2009c) synthesized and characterized $2ZnO \cdot 3B_2O_3 \cdot 3H_2O$ by using zinc oxide and boric oxide as raw materials at 368 K for 5 days. The FTIR spectrum of sample exhibits the following absorption bands in Figure 5.1. The bands at 3204 cm^{-1} and 3461 cm^{-1} are the stretching of O-H. The band at 2520 cm^{-1} is the O-H stretching because of hydrogen bond. The bands at 1249cm^{-1} and 1189cm^{-1} might be the in-plane bending of B-O-H. The bands at 1409 cm^{-1}, 1299cm^{-1}, and 953 cm^{-1} are the asymmetric and symmetric stretching of B(3)-O, respectively. The bands at 1114cm^{-1}, 1067cm^{-1}, 860 cm^{-1} and 800 cm^{-1} are the asymmetric and symmetric stretching of B(4)-O respectively. Additionally, Eltepe and his colleagues (2007) reported that these stretching peaks of tetrahedral B(4)-O and trihedral borate groups B(3)-O at the same wavelength values. The bands at 745 cm^{-1} and 658 cm^{-1} are the out-of-plane bending mode of B(3)-O. The band at 546 cm^{-1} is the bending of B(3)-O and B(4)-O.
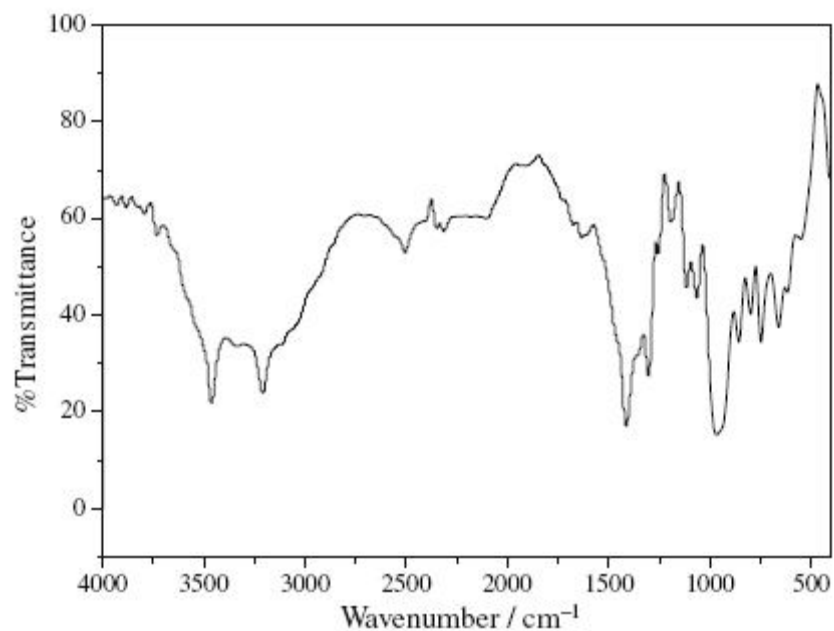
Figure 5.1. FTIR spectrum of $2ZnO \cdot 3B_2O_3 \cdot 3H_2O$
(Source: Gao et al., 2009c).

Another recent study dealing with the synthesis of zinc borate was carried out by Li et al. (2010). They prepared hydrophobic nanoflakes having molecular formula of $2ZnO \cdot 3B_2O_3 \cdot 3.5H_2O$ by using boric acid and zinc oxide. Besides the raw materials, oleic acid was used as a modifying agent. Figure 5.2 implies the XRD pattern of hydrophobic zinc borate. All diffraction peaks were quite similar to those of bulk $2ZnO \cdot 3B_2O_3 \cdot 3.5H_2O$.
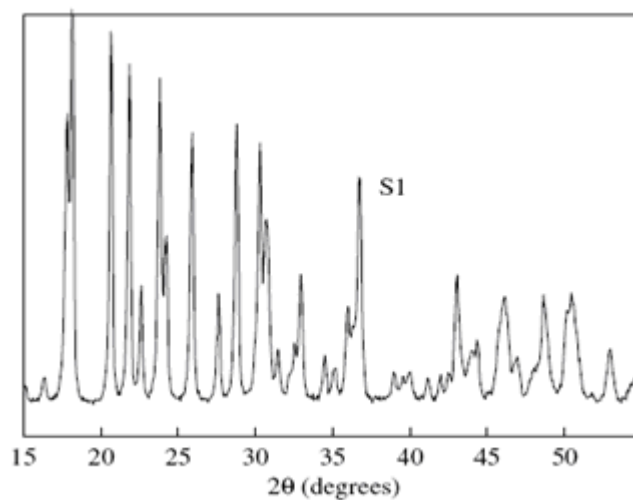
Figure 5.2. XRD patterns of the hydrophobic zinc borate
(Source: Li et al., 2010).

Figure 5.3 demonstrates SEM images of the zinc borates without and with oleic acid as the modifying agent. The images showed that oleic acid did not affect the morphology and the size of the crystals. Despite that, irregular nanoflakes were formed for both cases (Li et al., 2010).

| (a) | (b) |
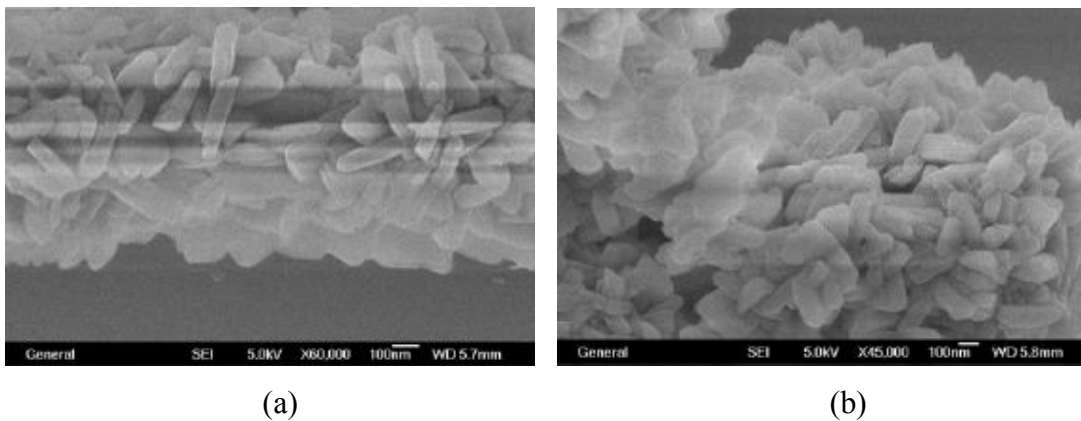
Figure 5.3. SEM images of zinc borate a) without oleic acid b) with oleic acid
(Source: Li et al., 2010).

5.2. Zinc Borate Production from Zinc Salt and Borax

Zinc borate can also be prepared by forming an aqueous solution of an alkali metal borate with a water-soluble zinc salt at least about 70 °C. The zinc salt used in this process is water soluble, preferably an inorganic zinc salt, such as zinc sulphate, zinc bromide, zinc chloride, zinc nitrate etc. The alkali metal borate is generally sodium tetraborate, also known as borax ($Na_2B_4O_7$) or potassium tetraborate (Nies et al., 1972). In nature, borax is found as tincal as a mineral and it can be obtained by flocculating and separating of impurities and clays from tincal ores.

In order to prepare zinc borate by using borax and zinc salt, borax solution is firstly prepared by considering the solubility of the borax at the temperature of $70^{o}C$. Then aqueous solution of zinc salt at the same temperature is added into borax solution under vigorous mixing. The possible reactions related to the production of zinc borate from zinc salts (zinc sulphate and zinc nitrate) and borax decahydrate are shown below (Nies et al., 1972);

$$Na_2B_4O_7\cdot10H_2O + ZnSO_4 \rightarrow 2ZnO\cdot3B_2O_3\cdot7H_2O + 2Na_2SO_4 + 2H_3BO_3 \qquad (5.2)$$

$$Na_2B_4O_7\cdot10H_2O + ZnSO_4 \rightarrow 2ZnO\cdot3B_2O_3\cdot14H_2O + 2Na_2SO_4 + 2H_3BO_3 \qquad (5.3)$$

$$Na_2B_4O_7\cdot10H_2O + ZnSO_4 \rightarrow 2ZnO\cdot3B_2O_3\cdot3H_2O + 2Na_2SO_4 + 2H_3BO_3 +4H_2O \quad (5.4)$$

$$2Na_2B_4O_7\cdot10H_2O + 2Zn(NO_3)_2\cdot6H_2O \rightarrow 2ZnO\cdot3B_2O_3\cdot3H_2O$$
$$+ 4NaNO_3 + 2H_3BO_3 + 10H_2O \qquad (5.5)$$

$$Na_2B_4O_7\ 10H_2O + Zn(NO_3)_2\cdot6H_2O \rightarrow ZnB_4O_7\cdot10H_2O + 2NaNO_3 \qquad (5.6)$$
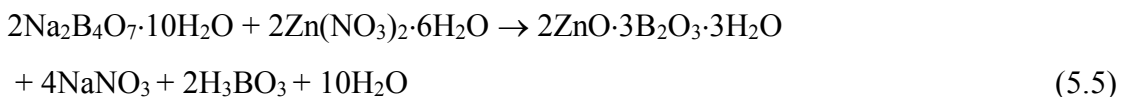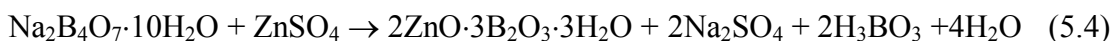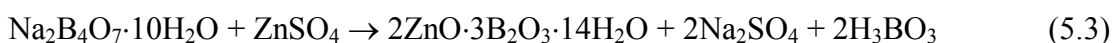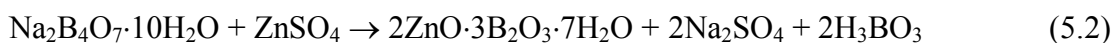
As inorganic flame retardants, $4ZnO\cdot B_2O_3\cdot H_2O$ offers significant advantages for compounding polymers requiring processing at high temperatures owing to its relatively high dehydration temperature (415 °C). However, it is reported that there are some difficulties in the employment of zinc borate in polymer matrix since the uniform dispersion behavior of the zinc borate powder is poor and it needs to be improved. Shi et al. (2009) tried to overcome this problem by using organic compound as templates to produce nanostructured materials. Besides the raw materials (zinc sulfate and borax decahydrate), polyethylene glycol-300 (PEG-300) was used as a surfactant. This surfactant was a non-ionic polymer and has hydrophilic –O- and hydrophobic –CH_2-CH_2- on the long chains. The synthesized products in the absence and in the presence of PEG-300 are shown in Figure 5.4. The product formed in the absence of PEG-300 only consisted of irregular crystals in μm range (Figure 5.4a). The effects of PEG-300 on the morphology of zinc borate are shown in Figures 5.4b and 5.4c. Leaf-like lamellar particles and nanorods were obtained at 90°C, whereas, rod-like nanoparticles were formed at higher temperatures.

Same type zinc borate ($4ZnO\cdot B_2O_3\cdot H_2O$) was produced via one-step precipitation reaction in aqueous solution of sodium borate ($Na_2B_4O_7\cdot10H_2O$) and zinc nitrate ($Zn(NO_3)_2\cdot6H_2O$) with phosphate ester as the modifying agent. Figure 5.5 exhibits a set of typical SEM images corresponding to the samples obtained from the solution with pH=8.0 at different reaction temperatures for 7 h. Irregular crystals were obtained in the absence of modifying agent at 70 °C (Figure 5.5a) and this result is consistent with literature (Shi et al., 2009). On the other hand, whiskers were the major products when the reaction was controlled with phosphate ester and at 60 °C (Figure 5.5b) (Zheng et al., 2009).
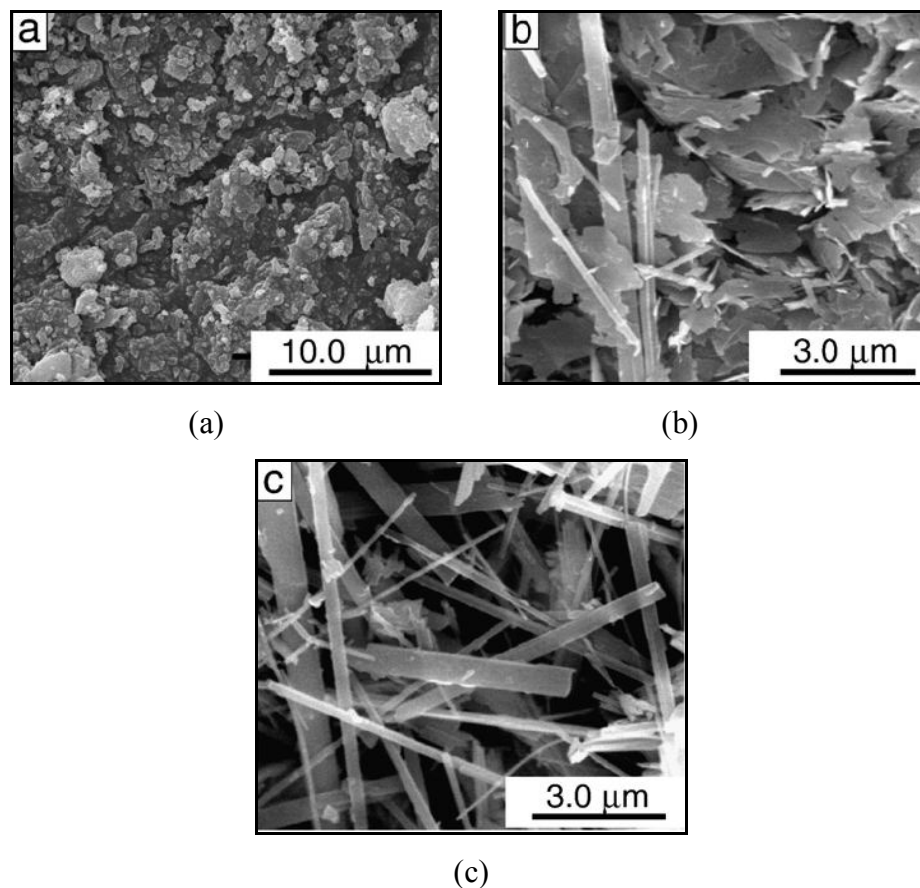
Figure 5.4. SEM images of zinc borate obtained at a)90 °C, without PEG-300, b)90 °C in the presence of PEG-300, c) 120 °C in the presence of PEG (Source: Shi et al., 2009).

The surface characteristics of the zinc borate nanowhiskers materials were measured by a contact angle analyzer. Figure 5.6 presents the changes of the contact angle containing the unmodified products (without added phosphate ester) and the modified products (with added phosphate ester) from the low synthesis temperature to the high synthesis temperature. The pure products have the smallest contact angle (Figure 5.6d). When the synthesis temperature was enhanced from 30 °C to 70 °C (Figure 5.6a-c), the wettability of products was decreased. The reason of this result could be explained by the increase in contact angle with increasing temperature (Zimmerman et al., 2003). The biggest contact angle was 115.26° when the whiskers were synthesized at 70 °C for 7 h. From these results, it was deduced that the contact angle increased while the synthesis temperature increased. It was also proposed that the hydrophobic products could be easily combined with polymers (Zheng et al., 2009).

<table>
<tr><td>(a)</td><td>(b)</td></tr>
</table>
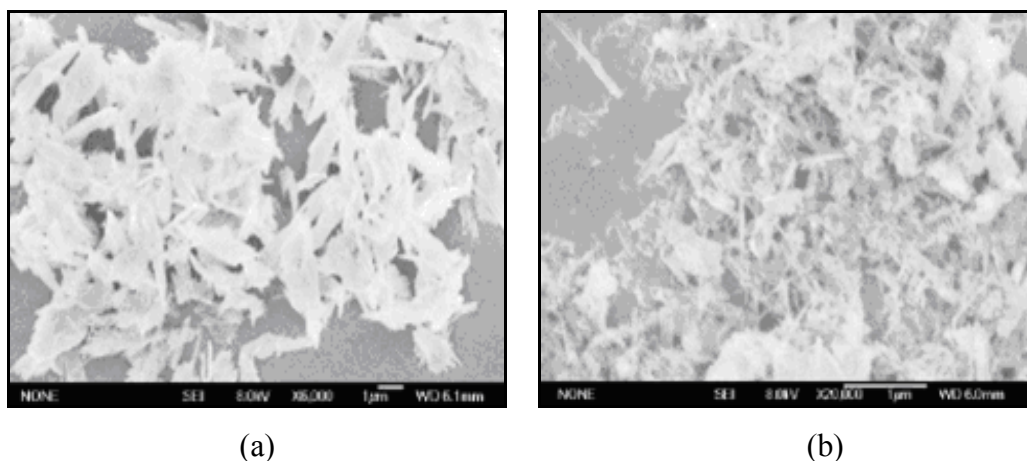
Figure 5.5. SEM images of samples prepared at pH = 8 for 7 h: (a) at 70 °C without phosphate ester; b) at 60 °C with phosphate ester (Source: Zheng et al., 2009).

Besides the other production techniques such as precipitation, microemulsion techniques, coordination homogenous precipitation method which is developed by Ting et al. (2009) was used for zinc borate synthesis. This method requires the employment of ammonia in reaction medium and it is relatively simple and inexpensive so that it has potential for application in industry. The key factor of the method is how to control the chemical reaction in solution and competitive balance. The authors summarize the mechanism of the precipitation method with ammonia as follows; firstly, zinc ions react with an appropriate coordination agent (ammonia) forming a complex solution. Then the complex dissociates to release the metal ions via changing the conditions of the solution such as concentration or temperature. Therefore zinc ions reach a certain amount which ensures the sedimentation of desired nanoparticles yielding and a precipitate is formed in the aqueous solution. A nano-flake-like zinc borate species $2ZnO \cdot 2.2 \ B_2O_3 \cdot 3H_2O$ were prepared for different mixing hours and the morphologies of the products are given in Figure 5.7. For 6 and 8 hours mixing periods the products have relatively unstable morphology as shown in Figure 5.7a and Figure 5.7b. However, when the reaction time prolonged the samples had stable crystals having sizes of around 100-200 nm. In addition to morphology of the crystals, the functional groups of the products were investigated. IR spectra of the products are shown in Figure 5.8. According to the spectra, the characteristic peaks of B(3)-O and B(4)-O are observed at 1343 cm^{-1} and 1078 cm^{-1}, respectively. The crystal structures of the products were determined by XRD analysis and XRD pattern of the products are indicated in Figure 5.9.
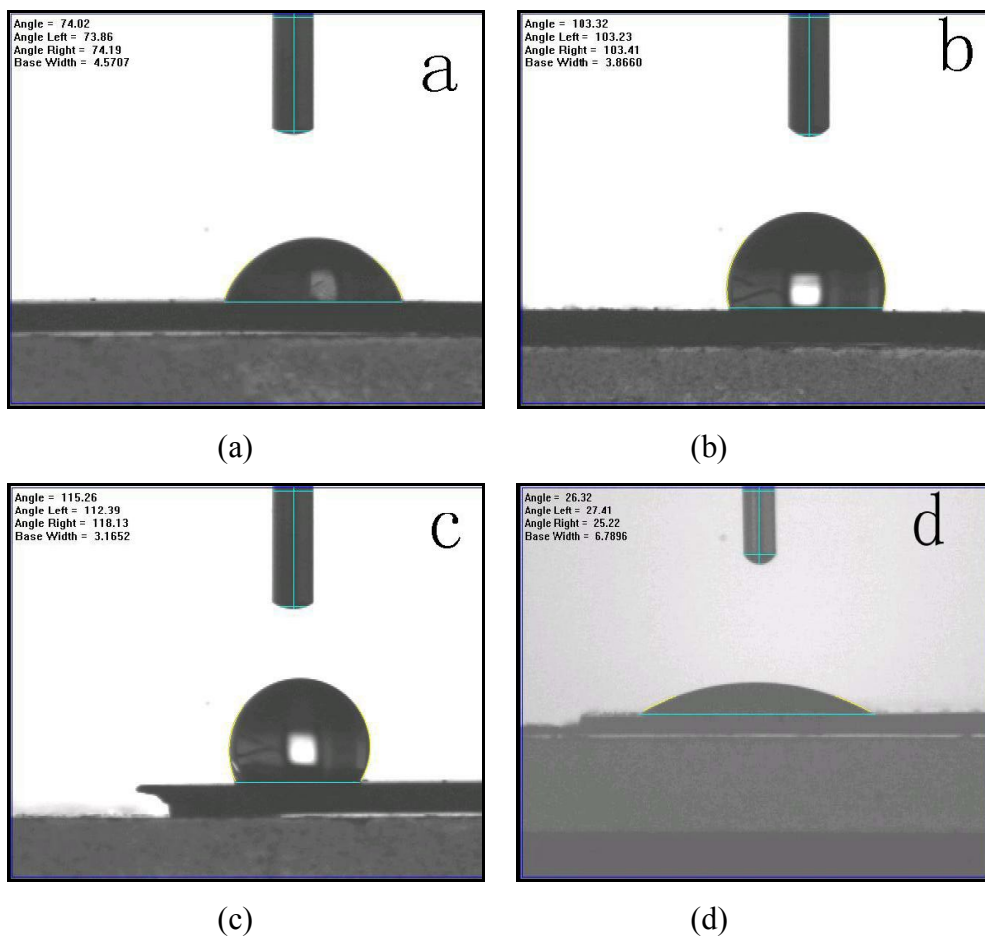
Figure 5.6. Contact angle of samples prepared at pH=8 for 7h: a) at 30 °C with phosphate ester; b) at 50 °C with phosphate ester; c) at 70 °C with phosphate ester and d) at 70 °C without phosphate ester (Source: Zheng et al., 2009).

(a)   (b)

(c)   (d)
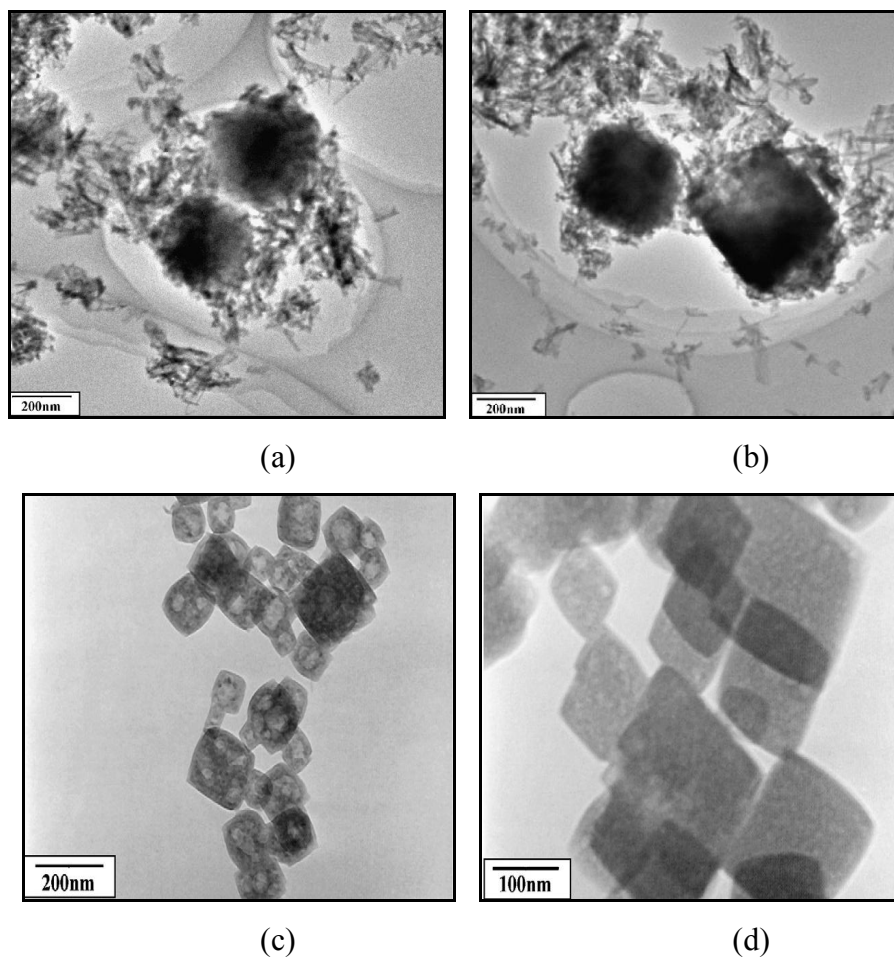
Figure 5.7. TEM images of the products having a) 6 , b) 8, c) 12 and d) 15 hours mixing periods (Source: Ting et al., 2009).
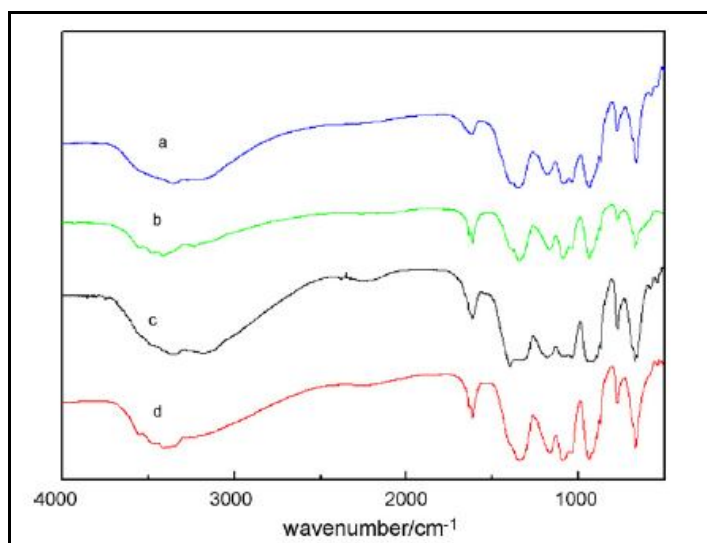
Figure 5.8. IR spectra of the products having a) 6 , b) 8, c) 12 and d) 15 hours mixing periods (Source: Ting et al., 2009).
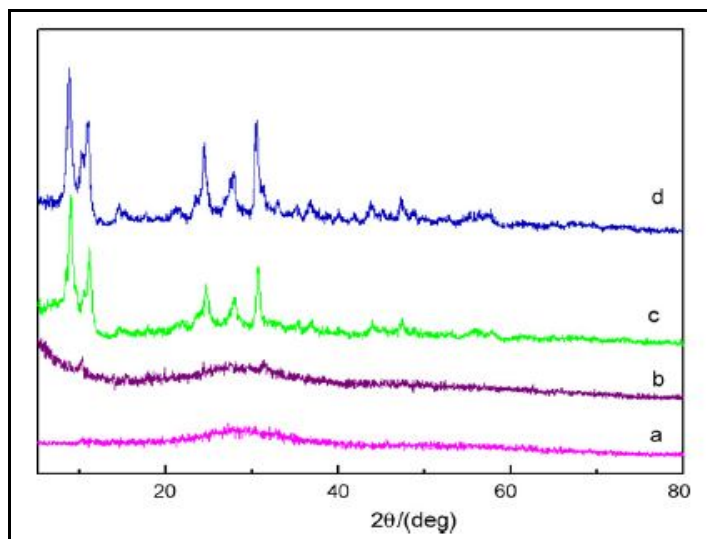
Figure 5.9. XRD patterns of the products having a)6 , b)8, c)12 and d)15 hours mixing periods (Source: Ting et al., 2009).

Amorphous structure is obtained for low mixing times (6 and 8 hours), whereas the structure becomes crystalline after 12 and 15 hours. Even tough the authors call the products as zinc borate, XRD pattern of the products does not reflect any type of zinc borate pointed out in JCPDS cards (Ting et al., 2009; Guan and Deng., 2007).

CHAPTER 6

MATERIALS AND METHOD

6.1. Materials

In this study, zinc borate was produced by borax decahydrate ($Na_2B_4O_7 \cdot 10H_2O$) produced by Etibor (purity 99.9%) and zinc nitrate hexahydrate ($Zn(NO_3)_2 \cdot 6H_2O$) (Sigma Aldrich) were used to produce zinc borate. Light neutral oil (SN 150) produced by Tüpraş A.Ş., and supplied by Petrofer Company was used as base oil for the preparation of inverse emulsions and lubricants. The typical properties of light neutral oil are tabulated in Table 6.1.

Table 6.1. Physical properties of light neutral oil
(Source: Tüpraş, 2010).

Chemical Composition	Hydrocarbon (C_{20}-C_{50}), heavy parafinic hydrotreated base oil
Density @15 °C (kg/m^3)	0.86-0.89
Viscosity @100 °C (cSt)	5.0-5.7
Pour point (°C)	-12
Boiling point (°C)	400-500

Sorbitan monostearate (Span 60, Sigma Aldrich) ($C_{24}H_{46}O_6$) was employed in inverse emulsions to stabilize the system and also it was used for the lubricants to disperse the inorganic particles in the base oil. In addition to sorbitan monostearate as a surfactant, propanol-2 (Merck) was introduced in microemulsions as a co-surfactant. Washing liquids to obtain zinc borate particles were methyl ethyl ketone (MEK) (Kimetsan), ethanol (Riedel-de Haën), propanol-2 (Merck) and distilled water. In order to form the lubricants, different types of zinc borate samples synthesized by different

raw materials were added to the mineral oil (Gönen, 2009; Gönen et al., 2009). Moreover, Firebrake zinc borate ($2ZnO \cdot 3B_2O_3 \cdot 3.5H_2O$) was obtained from US Borax Inc. and added to mineral oil to understand its lubricating property. The other additives used to obtain better dispersion of inorganic particles in mineral oil were Viscobyk 5025 and Disperbyk 1161 (BYK Chemie). Viscobyk 5025 is a volatile carboxylic acid derivative and it improves the wetting and dispersing properties of the materials whereas Disperbyk 1161 contains multifunctional deflocculating groups for wetting and stabilizing of inorganic solids in oils. The amount of Viscobyk and Disperbyk were 5 wt% of zinc borate added to lubricants. In addition to boron based lubricants, clinoptilolite rich mineral was also used as an additive for the enhancement of tribological properties of the light neutral oil. The particle size of the purified clinoptilolite is nearly 5 μm and it consists of 74.73% SiO_2, 12.70 Al_2O_3, 0.73% Fe_2O_3, 7.78 %K_2O, 2.00% Na_2O, 1.76% CaO and 0.28% MgO by weight. Clinoptilolite rich mineral obtained from mineral deposits located in Manisa Gördes region having 2-5 mm particle size was also used to remove the water content of a lubricant prepared by inverse emulsion. The chemical composition of the water adsorber mainly contains 65.19% SiO_2, 12.94% Al_2O_3, 1.45% Fe_2O_3, 0.92% Na_2O, 3.99% K_2O, 1.99% CaO and 1.39% MgO.

PVC-zinc borate composite films were formed by using poly vinyl chloride (Petkim, PETVİNİL 38/74) and tetrahydrofurane (THF) (Merck) and zinc borates obtained by inverse emulsion technique.

6.2. Method

In this part of the study, preparation of inverse emulsions, synthesis of zinc borate, lubricant preparation and the characterization techniques used to determine the properties of obtained samples will be mentioned.

6.2.1. Preparation of Control Inverse Emulsions

Inverse emulsions were formed by light neutral oil, water and sorbitan monostearate. The surfactant amount in the control emulsions were changed between 0.1-10 wt %. Firstly, the surfactant was dissolved in the oil and mixed with a magnetic

stirrer at 70 °C, secondly the water was added to oil and finally the emulsion was stirred for 2 hours. The mixing of the control emulsions, C1, C2, C3, C4 and C5 was achieved by magnetic stirrer, whereas the control emulsion C6 and C7 were mixed by both a rotor-stator homogenizer (OMNI GLH) and magnetic stirrer (Yellowline MSH Basic). The homogenizer had a variable speed (5000-30000 rpm) and it combined 700 Watt with a rotor-stator generator probe of 10 mm diameter. The mixing rates of homogenizer and magnetic stirrer were 13500 and 1000 rpm, respectively. The detailed preparation conditions of inverse emulsions are listed in Table 6.2.

Table 6.2. The preparation conditions of control inverse emulsion.

Sample	H_2O wt.%	Span 60 wt%	Mixing temperature (°C)	Mixing period	Mixing
C1	10	1	25	2h	Magnetic stirrer
C2	20	1	70	2h	Magnetic stirrer
C3	10	1	70	2h	Magnetic stirrer
C4	10	0.1	70	2h	Magnetic stirrer
C5	10	10	70	2h	Magnetic stirrer
C6	10	1	70	10 min + 2h	Homogenizer + Magnetic stirrer
C7	10	1	70	2 min + 2h	Homogenizer + Magnetic stirrer

6.2.2. Preparation of Zinc Borate Inverse Emulsions by One Microemulsion Method

One microemulsion method applied for zinc borate synthesis consisted of light neutral oil, non-ionic surfactant sorbitan monostearate and pure water in which borax decahydrate and zinc nitrate were dissolved. One water-in oil microemulsions containing different amounts of reactants in the aqueous phase were prepared. 1 M aqueous borax decahydrate and 1 M aqueous zinc nitrate solutions were added to mineral containing sorbitan monostearate at 70 °C. The samples were heated at 70 °C for 2 hours. Table 6.3 shows the amounts of starting materials (by volume) for producing the microemulsions and the mixing temperatures and periods. 100 cm^3 light neutral oil was used for all the samples indicated in Table 6.3. The water content of the emulsions was removed by heating the samples at 160 °C via water-oil separation apparatus in Figure 6.1. The products settled down at the bottom of Schott bottles were separated and the oily phase was removed by washing them with methyl ethyl ketone, ethanol and water. Then the samples were dried at 110 °C in an oven for 2 hours and characterized.

Table 6.3. The preparation conditions of inverse emulsions prepared by one microemulsion method

Sample	Span 60%	Zinc nitrate solution %	Borax solution%	Mixing temperature (°C)	Mixing period	Mixing
E1	1	5	5	70	2h	Magnetic stirrer
E1-1	1	5	5	160	2h	oil-water separation set-up
E2	1	5	5	70	2 min + 2h	Homogenizer + Magnetic stirrer
E2-1	1	5	5	160	2h	oil-water separation set-up
E3	1	2.5	2.5	70	2 min + 2h	Homogenizer + Magnetic stirrer
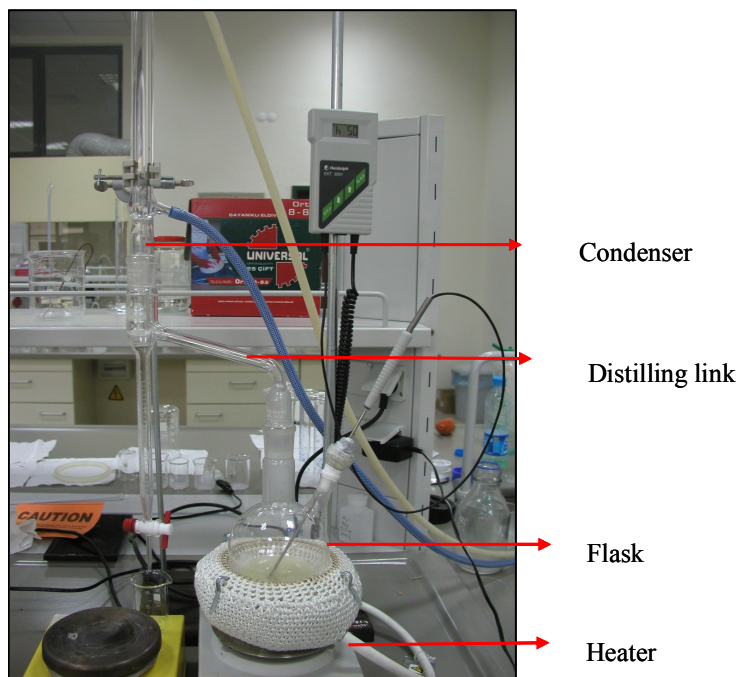
Figure 6.1. Water-oil separation apparatus

6.2.3. Preparation of Zinc Borate Inverse Emulsions by Two Microemulsion Method

Unlike the one microemulsion method, two microemulsions technique required the preparation of two separate inverse emulsions by borax decahydrate and zinc nitrate. Compositions of the emulsion system used for the synthesis of zinc borate particles are indicated in Table 6.4. 100 cm^3 light neutral oil was used for each case. In order to obtain zinc borate particles in nano scale, the droplets of the inverse emulsions were tried to produce as small as possible. For this reason, different emulsification systems such as rotor stator homogenizer and ultrasonic systems were applied for the mixing of the inverse emulsions. SU-1 inverse emulsions were prepared by a magnetic stirrer (Yellowline MSH Basic) and the rate of mixing was 1000 rpm. After stirring the emulsions, both borax decahydrate and zinc nitrate emulsions were put in an ultrasonic bath (Everest) at 70 °C for 10 min to disperse particles in continuous phase. Final zinc borate emulsion was obtained by mixing these two emulsions and this final emulsion was mixed by a magnetic stirrer and ultrasonic bath for 2 hours and 10 min, respectively. A rotor-stator homogenizer (OMNI GLH) was used to prepare the SH-1 inverse emulsions. In this case, the homogenizer was used instead of ultrasonic bath.

The final zinc borate emulsion was mixed by a homogenizer and a magnetic stirrer for 2 minutes and 2 hours, respectively. Besides them, the cosurfactant, propanol-2 was employed to the two microemulsion system, and its concentration effect on the morphology and the structure of obtained particles were also investigated. The compositions of the inverse emulsions (SC-1, SC-2, SC-3 and SC-4) are tabulated in Table 6.4. For this case, the molarities of raw materials were decreased from 1 M to 0.1 M to obtain more stable and transparent emulsions. Same mixing procedure was applied to these microemulsions as indicated for SH-1 emulsion.

The stability of these emulsions was measured by using graduated cylinders having 50 cm^3 volume. A simple ruler was sticked on the surface of the graduated cylinders to observe the height of precipitates. During 20 minutes, the height of the precipitate was reported to understand the settling of particles in continuous phase.

.

Table 6.4. Compositions of the two microemulsions system used for the synthesis of zinc borate particles

| Sample | Aqueous Phase | | Mixing Type | Mixing period | Surfactant (g) | Co-surfactant (cm^3) |
| | Emulsion I | Emulsion II | | | | |
	Na$_2$B$_4$O$_7$·10H$_2$O (10 cm^3)	Zn(NO$_3$)$_2$·6H$_2$O (10 cm^3)				
SU-1	1 M	1 M	Magnetic stirrer + Ultrasonic bath	2 h + 10 min	1	-
SH-1	1 M	1 M	Homogenizer + Magnetic stirrer	2 min + 2 h	1	-
SC-1	0.1 M	0.1 M	Homogenizer + Magnetic stirrer	2 min + 2h	10	30.0
SC-2	0.1 M	0.1 M	Homogenizer + Magnetic stirrer	2 min + 2h	10	51.5
SC-3	0.1 M	0.1 M	Homogenizer + Magnetic stirrer	2 min + 2h	10	80.0
SC-4	0.1 M	0.1 M	Homogenizer + Magnetic stirrer	2 min + 2h	10	102.2

6.2.4. Preparation of Zinc Borate by Precipitation Technique

One of the oldest unit operations, precipitation technique was also used to synthesize zinc borate. Zinc borate, ZBS-1 was prepared by mixing equal volumes (50 cm^3) of borax decahydrate and zinc nitrate hexahydrate solutions having 1 mol /dm^3 concentration and 1g sorbitan monostearate was added to system as demonstrated in Table 6.5. It was mixed at 70 °C by homogenizer and magnetic stirrer for 2 minutes and 2 hours, respectively. The separation of particles from the aqueous media was achieved by using a membrane separation unit, then, the particles were washed with 50 cm^3 water for three times and they were dried at 110 °C for 2 h in air circulating oven. However, the other precipitations of zinc borate in the bulk phase, ZB-3, ZB-6, ZB-12, ZB-15, ZB-W-3, ZB-W-6, ZB-W-12, and ZB-W-15 were carried out by homogeneous precipitation method which was reported by Ting et al. 0.05 mol zinc nitrate was dissolved in 40 cm^3 distilled water, then the solution obtained from 0.05 mol borax dissolved in 60 cm^3 water at 45 °C was slowly poured into it with constant stirring to form a homogenous mixture, and then 25 cm^3 concentrated ammonia (25 wt.%) was added into the system. When the sediment disappeared, the complex solution was added into 150 cm^3 distilled water, and then the reaction was carried out in open beaker having 8 cm diameter in water bath under magnetic stirring at 45 °C for 3, 6, 12 and 15h. When ammonia started to evaporate the samples, a large amount of white sediment was formed again. The precipitate was separated by centrifuge and rinsed with ethanol, then dried in a vacuum oven at 40 °C for 12 h. In order to examine the washing effect of water, the same samples were washed with water before ethanol (Ting et al., 2009). The preparation conditions of homogeneous precipitation method are listed in Table 6.5 and the flowchart related to the homogeneous precipitation method is given in Figure 6.2.

Table 6.5. The preparation conditions of zinc borate synthesis in aqueous phase.

Sample	$Na_2B_4O_7 \cdot 10H_2O$ Solution		$Zn(NO_3)_2 \cdot 6H_2O$ Solution		Surfactant (1 g)	Ammonia (7.20 mol/dm^3, 25cm^3)	Stirring time (h)
	mol.dm^{-3}	cm^3	mol.dm^{-3}	cm^3			
ZBS-1	1	50	1	50	+	-	2
ZB-3	0.83	60	1.25	40	-	+	3
ZB-6	0.83	60	1.25	40	-	+	6
ZB-12	0.83	60	1.25	40	-	+	12
ZB-15	0.83	60	1.25	40	-	+	15
ZB-W-3*	0.83	60	1.25	40	-	+	3
ZB-W-6*	0.83	60	1.25	40	-	+	6
ZB-W-12*	0.83	60	1.25	40	-	+	12
ZB-W-15*	0.83	60	1.25	40	-	+	15

* Samples were washed with water and ethanol
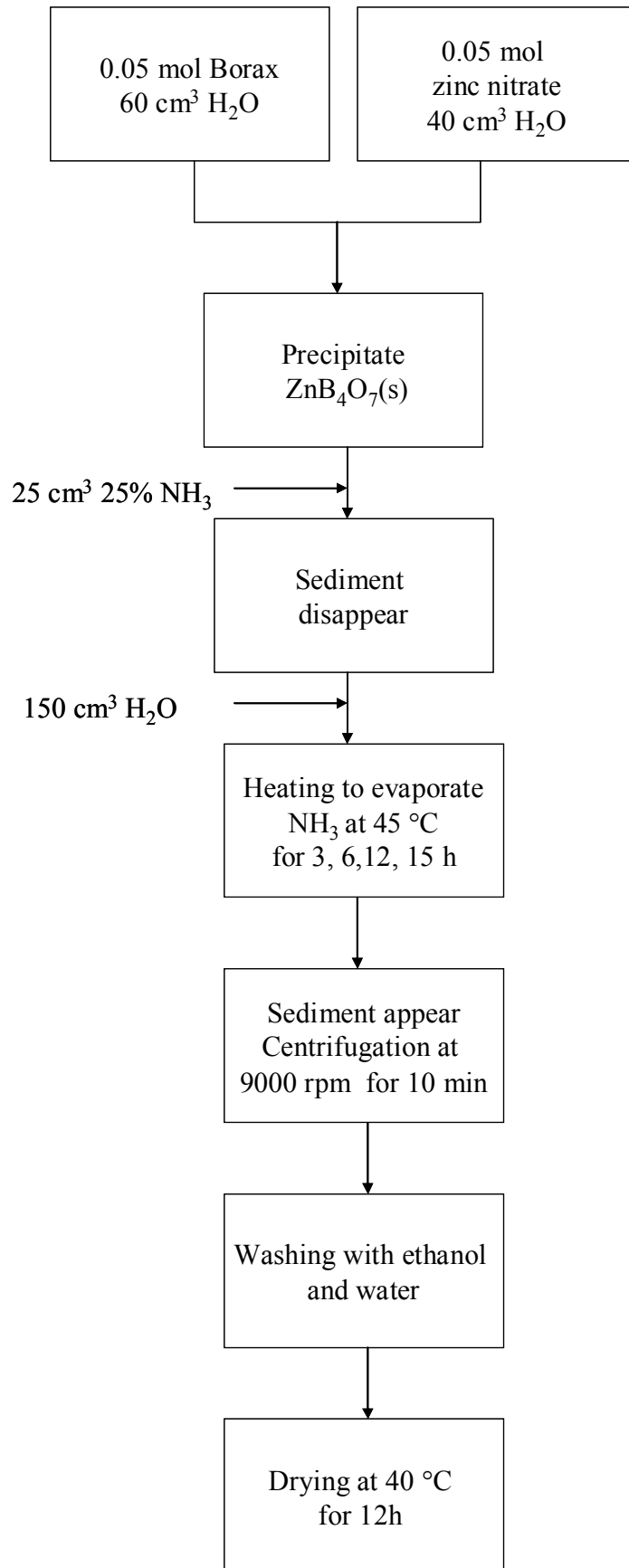
Figure 6.2. Flowchart of zinc borate production by homogeneous precipitation technique.

6.2.5. Preparation of Lubricants

The lubricants except L16 and L17 were prepared via the following method, in which sorbitan monostearate was used as a surfactant. Firstly, the sorbitan monostearate was dissolved in mineral oil and heated up to 70 °C, secondly, the additives were dispersed in the mineral oil. The lubricants were mixed at 150 °C by homogenizer and magnetic stirrer for 2 minutes and 2 hours, respectively. The additives used for 100 cm^3 light neutral oil are listed in Tables 6.6, 6.7, 6.8 and 6.9. As seen from these tables, the control lubricants are L1 and L2 which are light neutral oil and light neutral oil with surfactant. Commercial zinc borate, Firebrake 2335 ($2ZnO \cdot 3B_2O_3 \cdot 3.5H_2O$) obtained from US Borax Inc was used to prepare L7 and L8 lubricants. Viscobyk and Disperbyk (BYK) were added into the lubricants L5, L7 and L8 with the surfactant in the initial step in order to obtain better dispersion behavior of inorganic particles. The details of the lubricants prepared by commercial zinc borate and other additives are tabulated in Table 6.6. The lubricants containing zinc borates prepared by different techniques and raw materials were formed as indicated in Table 6.7. L3, L4 lubricants were prepared by the zinc borate species synthesized by Gönen (Gönen, 2009), whereas ZBS-1 zinc borate which was formed in the presence of surfactant was added to mineral oil to obtain L6 lubricant. In order to expose the effect of surfactant concentration in the mineral oil on the tribological properties of the oil, the lubricants L11, L12 and L13 were formed. The amount of the surfactants in L11, L12 and L13 were 1 g, 0.00005 g (which was below its critical micelle concentration) and 0.5 g for 100 cm^3 light neutral oil, respectively. The details of the lubricants prepared by different amount of surfactant are shown in Table 6.8. Unlike the other lubricants, L16 and L17 lubricants were prepared by only removing water content of the inverse emulsion (E2M) to understand whether the synthesized zinc borate particles could directly be used in the emulsion or not. Since the water caused harmful effects for corrosion in lubrication systems, the water content was tried to remove by two ways, therefore two different emulsions were formed. For the first one, the water content was evaporated by heating up to 160 °C via water-oil separation apparatus as shown in Figure 6.1 to obtain L16 lubricant, and for the second one, 10 g clinoptilolite having 2-5 mm particle size was put in 20 cm^3 inverse emulsion to adsorb the residual water in the emulsion and the zeolites were separated from the emulsion after two days and the prepared emulsion was used as the

lubricant L17. Moreover, the precipitate (SC-2) which was formed by two microemulsion method containing 51.5 cm^3 propanol-2 was also dispersed as an additive for mineral oil without using any surfactant (L14). The descriptions of lubricants prepared using inverse emulsions or the precipitates synthesized by emulsions are listed in Table 6.9 and 6.10. Besides the boron-based additives, clinoptilolite rich minerals having average 5 µm particle size. was also dispersed into the oil and hence L15 lubricant was obtained as presented in Table 6.10.

Table 6.6. The additives of lubricants prepared by commercial zinc borate.

Lubricant Code	Span 60 (g)	Zinc Borate (g)	Viscobyk (cm^3)	Disperbyk (cm^3)
L1	-	-	-	-
L2	1	-	-	-
L5	1	1g Firebrake 2335	-	-
L7	1	1g Firebrake 2335	0.05	-
L8	1	1g Firebrake 2335	-	0.05

Table 6.7. The additives of lubricants prepared by different types of zinc borate

Lubricant Code	Zinc Borate (g)	Explanation Zinc Borate Property
L3	1g ZBC	The B_2O_3/ZnO molar ratio of 2 and 4.7 mol.dm^{-3} 50 cm^3 boric acid and stoichiometric amount of ZnO, dried by conventionally, particle size:2-4 μm
L4	1g ZBE	The B_2O_3/ZnO molar ratio of 2 and 4.7 mol.dm^{-3} 50 cm^3 boric acid and stoichiometric amount of ZnO, dried by supercritical ethanol, particle size 20-40 nm
L6	1g ZBS-1	1.0 mol.dm^{-3}, 50 cm^3 $Na_2B_4O_7 \cdot 10H_2O$, 1.0mol.dm^3, 50cm^3 $ZnN_2O_6 \cdot 6H_2O$ and 1 g Span 60 dried by conventionally,
L9	1g ZB-W-6	0.83 mol.dm^{-3} 60 cm^3 $Na_2B_4O_7 \cdot 10H_2O$, 1.25 mol.dm^{-3} 40 cm^3 $ZnN_2O_6 \cdot 6H_2O$ and 25 cm^3 NH_3, 6h mixing time
L10	1g ZB-15	0.83 mol.dm^{-3} 60 cm^3 $Na_2B_4O_7 \cdot 10H_2O$, 1.25 mol.dm^{-3} 40 cm^3 $ZnN_2O_6 \cdot 6H_2O$ and 25 cm^3 NH_3, 15h mixing time
L11	1g ZB-W-12	0.83 mol.dm^{-3} 60 cm^3 $Na_2B_4O_7 \cdot 10H_2O$, 1.25 mol.dm^{-3} 40 cm^3 $ZnN_2O_6 \cdot 6H_2O$ and 25 cm^3 NH_3, 12h mixing time

Table 6.8. The additives of lubricants prepared by different surfactant concentration

Lubricant Code	Span 60 (g)	Zinc Borate (g)	Explanation Zinc Borate Property
L11	1	1g ZB-W-12	0.83 mol.dm^{-3} 60 cm^3 $Na_2B_4O_7 \cdot 10H_2O$, 1.25 mol.dm^{-3} 40 cm^3 $ZnN_2O_6 \cdot 6H_2O$ and 25 cm^3 NH_3, 12h mixing time
L12	0.00005	1g ZB-W-12	0.83 mol.dm^{-3} 60 cm^3 $Na_2B_4O_7 \cdot 10H_2O$, 1.25 mol.dm^{-3} 40 cm^3 $ZnN_2O_6 \cdot 6H_2O$ and 25 cm^3 NH_3, 12h mixing time
L13	0.1	1g ZB-W-12	0.83 mol.dm^{-3} 60 cm^3 $Na_2B_4O_7 \cdot 10H_2O$, 1.25 mol.dm^{-3} 40 cm^3 $ZnN_2O_6 \cdot 6H_2O$ and 25 cm^3 NH_3, 12h mixing time

Table 6.9. The additives of lubricants prepared by inverse emulsions

Lubricant Code	Light Neutral Oil (cm^3)	Span 60 (g)	Inverse emulsion or precipitate (g)
L14	100	-	0.5 g precipitate obtained by the microemulsion containing 51.5 cm^3 co-surfactant
L16	100	-	Inverse emulsion having 5 wt% aqueous phase (E3) and heated up to 160 °C

Table 6.10. The additives of lubricants prepared using clinoptilolite rich minerals

Lubricant Code	Light Neutral Oil (cm^3)	Span 60 (g)	Inverse emulsion or clinoptilolite (g)
L15	100	1	Clinoptilolite rich mineral (5 μm)
L17	100	1	Inverse emulsion having 5 wt% aqueous phase (E3) and water content was removed by clinoptilolite rich mineral (2-5 mm)

6.2.6. Preparation of PVC-Zinc Borate Composite Films

In order to determine the particle size of zinc borate particles produced by inverse emulsion technique, emulsions or precipitates obtained from inverse emulsions were dispersed in PVC films by solvent casting. In the formation of PVC-zinc borate composite films, 1.2 g polyvinyl chloride (PVC) was dissolved in 30 cm^3 tetarahydrofurane (THF). The suspension was stirred for 4 h by magnetic stirrer. Then the films were obtained by adding zinc borate particles into the suspension. The compositions of the prepared films are tabulated in Table 6.11. The suspensions contained additives poured into the petri dishes to cast the films and they were waited for 24 h for evaporation of THF in a fume cupboard.

Table 6.11. The compositions of the prepared films

Sample	Additive	Additive Amount
F1	-	-
F2	Light neutral oil having 1wt% Span 60	0.1 cm^3
F3	Inverse emulsion heated up to 160 °C (E1-1)	0.1 cm^3
F4	The bottom precipitate of E1-1	0.1 g
F5	Inverse emulsion heated up to 160 °C (E2-1)	0.1 cm^3

6.3. Characterization

The physico-chemical properties of raw materials (borax decahydrate, zinc nitrate, sorbitan monostearate, light neutral oil) and the obtained zinc borate particles were identified by Fourier transform infrared spectroscopy (FTIR), Thermal gravimetric analysis (TGA), Differential scanning calorimeter (DSC), X-Ray diffraction (XRD), Scanning electron microscopy (SEM), elemental analysis (EDX) (Philips XL30 SFEG) and CHNS elemental analysis (Leco Corporation St. Joseph MI U.S.A). The zinc borate samples produced by precipitation technique were also characterized by analytical titration in order to determine boron and zinc contents.

Fourier Transform Infrared Spectroscopy (FTIR)

Fourier Transform Infrared Spectrometer (Shimadzu 8601) was used to determine chemical structure of the raw materials and products. Zinc borate-KBr pellets were prepared by mixing 4.0 mg of zinc borate and 196 mg of KBr in an agate mortar and pressing the mixture under 8 tons. The FTIR spectra of the liquid samples (light neutral oil, lubricants and the emulsions) were measured by dripping a drop on the surface of KBr pellets. FTIR analysis of the lubricants which were tested by four ball wear test was also performed to understand if the chemical structure of the samples were stable or not when they were exposed to four ball wear test.

Thermogravimetric Analysis (TGA)

Thermogravimetric analyses (TGA) were carried out by using Shimadzu TGA-51. The samples (10-15 mg) were loaded into an alumina pan and heated from room temperature to 600 °C at 10 °C.min^{-1} under N_2 flow of 40 mL min^{-1}.

Differential Scanning Calorimetry (DSC)

DSC was performed on a calorimeter (Shimadzu, DSC 50). The sample (5-10 mg) was placed in an aluminum pan that was hermetically sealed. For conventional DSC measurements, samples were heated from room temperature to 600 °C at a rate of 10 °C.min^{-1}.

X-Ray Powder Diffraction (XRD)

XRD was carried out using a X-ray diffractometer (Philips Xpert-Pro). The incident CuK$_\alpha$ radiation at 45 kV and 40 mA with 1.54 Å was used in the analysis. The dried sample powders were prepared in a 0.5-mm thick holder. Diffraction patterns were used to determine the type of zinc borate samples as well as to understand whether the formed samples were amorphous or crystalline.

Analytical Titration

The B_2O_3 and ZnO contents of zinc borate samples were determined by analytical titration using 0.1 N NaOH and 0.01 mol.dm^{-3} EDTA, respectively.

NaOH Solution, 0.1 mol.dm^{-3} NaOH solution was used in analytical titration to determine boric acid content of zinc borate after it was dissolved by 6 M HCl.

EDTA Solution, 0.01 mol.dm^{-3} 3.80 g of disodium dihydrogen ethylenediaminetetraacetate dehydrate was dissolved in 1 dm^3 deionized water.

Buffer Solution, pH 10: 70 g NH_4Cl was dissolved in 325 cm^3 H_2O and 1135 cm^3 (25 wt %) ammonia solution was added and final solution diluted to 2 dm^3 by deionized water.

Indicators: Erichrome Black T indicator for Zn titration by EDTA, methyl red for HCl titration and phenolphthalein for B(OH)$_3$ by NaOH.

In the titration, firstly the samples prepared in aqueous phase was dissolved by 6 M HCl and completed to 100 cm^3 by deionized H_2O, secondly, 25 cm^3 of that solution was used to determine the Zn content with EDTA titration in the presence of Erichrome Black T

indicator and a buffer solution of pH 10. Another 25 cm^3 of that solution, that contains EDTA solution equivalent to zinc ions to prevent the precipitation of Zn with NaOH in the solution, was titrated by 0.1 N NaOH solution in the presence of methyl red till color changes from pale red to yellow. This first titration is attributed to the determination of free H$^+$ ions released by HCl. Mannitol was then added to form a complex with boric acid releasing 1 mol H$^+$ per 1 mol of boric acid and the resulting solution was titrated with 0.1 N NaOH solution using phenolphthalein as an indicator until color of mixture changes from yellow to deep pink. All the titration experiments were performed twice to obtain reliable results.

Particle Size Analysis

Particle sizes of zinc borate samples were determined using by particle size analyzer (Malvern Mastersizer 2000). The samples were dispersed in water by sonication for a while, and also calgon surfactant (1 wt%) was added to the zinc borate samples washed with water to enhance the dispersion property of the particles.

Optical Microscopy

The prepared inverse emulsions and lubricants were characterized by optical microscopes (Olympus CX31, Olympus CH40 and Olympus BX60M) and the microphotographs were taken by a digital camera (Olympus DP25 and Camedia C-4040). Olympus BX60M was a polarized microscope and the particles could be easily seen and the diameters of particles and droplets were evaluated by Olympus DP2-BSW program. Besides them, the effect of temperature on the morphology of emulsion was examined. C2 control emulsion and E1 zinc borate emulsion were heated up to 160 °C on the temperature controlled plate (INSTEC STC 200) and the microphotographs were taken at different temperatures. Additionally the worn surfaces of the balls used for four-ball tribotester were visualized by an optical microscope (Olympus CH40 and Olympus BX60M). The optical microphotographs were taken by a digital camera (Camedia C-4040).

Tensiometer and Rheometer

Surface tension of sorbitan monostearate was measured by KRÜSS digital tensiometer (K1OST) and the viscosities of the lubricants at 25 °C were determined by Brookfield programmable rheometer (Model DV-III).

UV Spectroscopy

UV spectroscopy (Perkin Elmer Lambda 45) was carried out to obtain the color change of the lubricants when they were exposed to four ball wear tester. For all lubricant samples, the reference was pure mineral oil.

Four-Ball Wear Test Machine

Tribological characterization of the lubricants containing zinc borate species was performed by a four-ball wear test machine (made by Falex Corp.). Test balls were chrome alloy steel, made from AISI standard steel No. E-52100 with a diameter of 12.7 mm. The test was performed according to ASTM D 4172-94 at 392 N and the test duration was 1h. The photographs of the balls and the whole machine are shown in Figure 6.3. These tribological tests were carried out at OPET Mineral Oil Factory.

(a)   (b)

Figure 6.3. a) Fixed balls of four-ball wear tester b) Whole machine of four-ball tester.

Profilometry

The roughnesses of the worn surfaces were measured by a profilometry (Mitutoyo SJ 301).

Cutting of fixed balls

Fixed balls for samples L1, L2 and L10 were cut with a microcutter (Metkon Microcut Precision Cutter) for closer examination of worn surfaces by SEM, AFM and microhardness testing. The rotating velocity of the microcutter was 2000 rpm and water was used to cool the system.

Scanning Electron Microscopy (SEM)

SEM (Philips XL30 SFEG and Zeiss DSM 940) images were used to examine the morphology of the raw materials, zinc borate samples and the worn surfaces of the balls used in four-ball tribometer. Conductive double sided tape was used to fix the particles to the specimen holder before sputtering them with a thin layer of gold. However, chrome alloy steel balls were put on the specimen holder of SEM directly before the analysis. For L1, L2 and L 10 a closer examination was made.

Microhardness Tester

The indentation tests were performed to obtain the hardness of the wear surfaces of the balls using a digital microhardness tester (TIME HVS-1000). The load and the indentation time were 4.9 N and 20 sec, respectively. For each sample three points were measured and the average value was considered as the final hardness of the sample.

Atomic Force Microscopy

The worn surfaces of the balls were also characterized by Multimode Atomic Force Microscopy (Digital Instrument, Nanoscope IV).

Commercial Lubricant BOR POWER Characterization

Commercial lubricant BORPOWER was characterized, as well. In order to separate the particles from the oil, the sample was centrifuged and the precipitate was washed with methyl ethyl ketene, water and ethanol. The obtained particles were dried at 110 °C and they were identified by X-Ray diffraction (XRD), scanning electron microscope (SEM), fourier transform infrared spectroscopy (FTIR) as well as elemental analysis (EDX). Additionally, the oil was characterized by FTIR.

PVC-Zinc Borate Composite Film Characterization

The obtained PVC-zinc borate composite films were characterized by optical microscopy (Olympus) BX60M, SEM (Philips XL30 SFEG) and EDX (Philips XL30 SFEG). The mapping of boron, carbon, and zinc elements on the film surfaces were achieved by energy dispersive spectrometry (EDX, Philips XL30 SFEG).

CHAPTER 7

RESULTS AND DISCUSSION

The results of this study are going to be introduced in four main sections: In the first part, the characterization of starting materials is going to be given in detail. In the second part, the results obtained from the zinc borate emulsions is going to be explained. In the third part, the characterization of zinc borate prepared by precipitation technique is going to be discussed, and finally the properties of lubricants are going to be shown in the final section.

7.1. Characterization of Raw Materials

The characterization of raw materials is of great importance to understand the properties of the final products and to determine the structure as well as the morphology of the obtained particles. The characterization of borax decahydrate and zinc nitrate hexahydrate, light neutral oil, sorbitan monostearate was carried out by FTIR spectroscopy, thermal gravimetric analysis (TGA), scanning electron microscopy (SEM) and elemental analysis (EDX).

Borax Decahydrate and Zinc Nitrate Hexahydrate:

Figure 7.1 shows FTIR spectra of borax decahydrate and zinc nitrate hexahydrate that were used in the zinc borate production. The broad band at 3500 cm^{-1} represents the OH groups in water of crystallization for borax decahydrate and zinc nitrate hexahydrate. FTIR spectrum of borax decahydrate in Figure 7.1, curve 1 indicates OH groups' coordination in borax structure and hydrogen bonding between OH groups at 3600-3200 cm^{-1}. The bands at 1695 and 1650 cm^{-1} is assigned to the H-O-H bending mode, which shows the sample containing water of crystallization. The bands at 1425-1360 cm^{-1} and 1000-950 cm^{-1} belong to the asymmetric and symmetric stretching vibrations of BO_3 group, respectively. The band at 1161 cm^{-1} indicates the vibrations of in-plane bending of B-O-H. The bands at 1145-1045 cm^{-1} and 837-829 cm^{-1} are assigned as the asymmetric and symmetric stretching of BO_4 group,

respectively. The bands at 781-670 cm^{-1} are the out-of-plane bending of B-O-H. The band at 632 cm^{-1} is assigned to symmetric pulse vibration of triborate anion. The bands at 545 and 460 cm^{-1} are due to the bending of BO_3 and BO_4 groups, respectively (Jun et al., 1995). The typical asymmetric stretching (ν_4), symmetric stretching (ν_1) of N-O are observed at 1390, 1360 cm^{-1} in Figure 7.1 curve 2. The band at 829 cm^{-1} belongs to asymmetric deformation (ν_2) of nitrate structure (Biswick et al., 2007).

SEM images of borax decahydrate are indicated in Figure 7.2. The crystal sizes of largest particles are nearly 500 µm, whereas the smallest particles have 20 µm crystal size. The small crystals were embedded on the surface of larger crystals.

According to chemical formula of borax decahydrate, the weight% of B, O and Na elements are 11.31%, 71.35% and 12.07%, respectively. EDX elemental analysis was used to determine borax decahydrate composition and the results together with the theoretical compositions are listed in Table 7.1. It was revealed that the elemental composition obtained from EDX was consistent with those obtained theoretically.
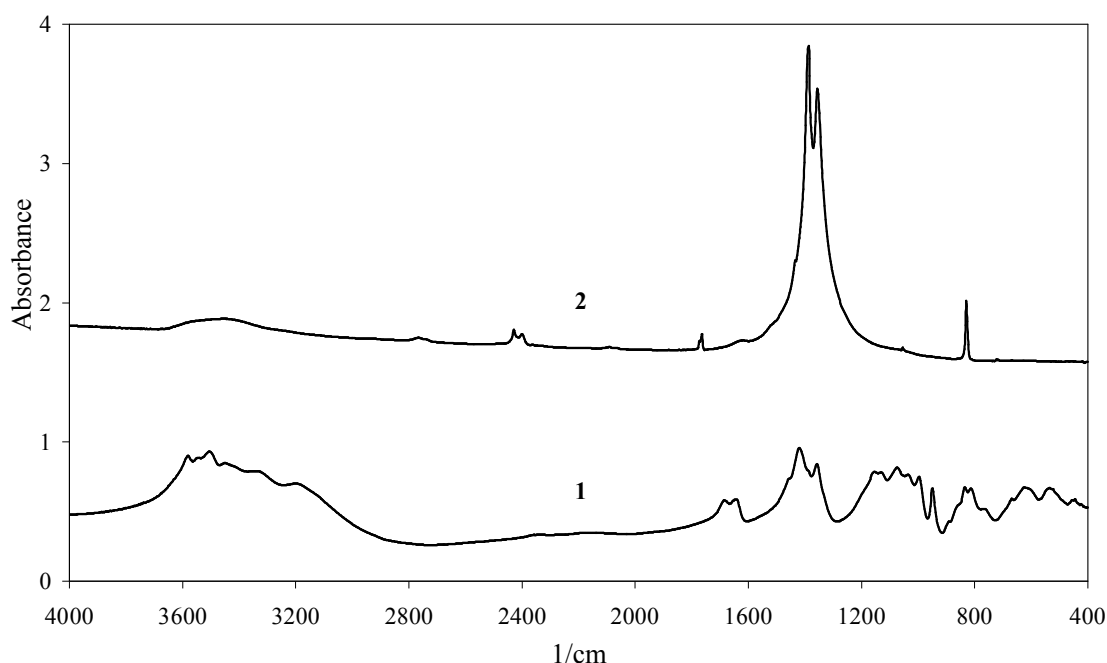
Figure 7.1. FTIR spectra of 1) borax decahydrate and 2) zinc nitrate hexahydrate.
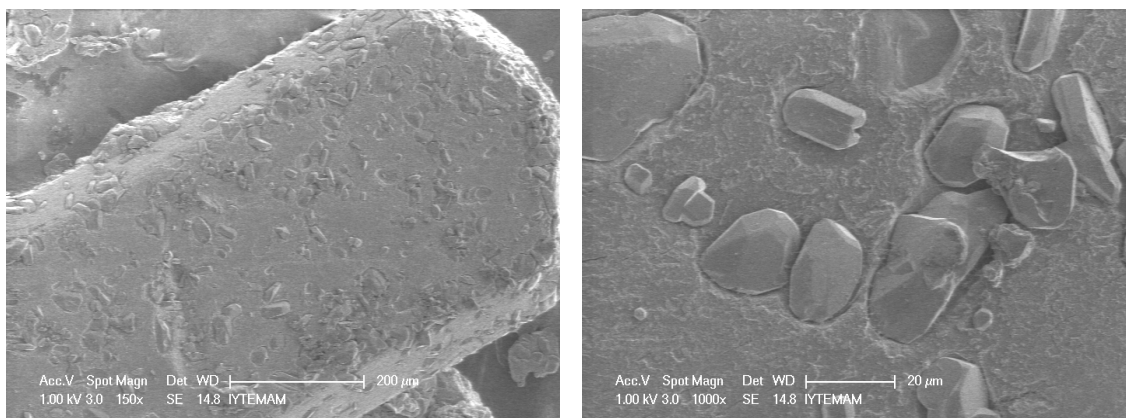
| | (a) | (b) |

Figure 7.2. SEM images of borax decahydrate a) 150x b) 1000x magnification.

Table7.1. Chemical composition of borax decahydrate.

Element	Weight %	
	EDX	Theoretical
B	10.69	11.31
O	70.76	71.35
Na	18.55	18.55

Light Neutral Oil and Sorbitan Monostearate

FTIR spectra of light neutral oil and sorbitan monostearate are given in Figure 7.3. FTIR spectrum of the sorbitan monostearate in Figure 7.3, curve 2 confirms all the characteristic peaks (at 2850, 2920, 1730, 1467 and 721 cm^{-1}) of the emulsifier related to partially fatty acid ester of polyol. The peak at 1730 cm^{-1} is attributed to C=O of esters, whereas the band at 1467 cm^{-1} shows CH$_2$ bending. On the other hand, FTIR spectrum of light neutral oil in Figure 7.3, curve 1 exhibits C-H stretching vibrations of hydrocarbons, C-H asymmetric and symmetric vibrations at 2930 and 2860 cm^{-1}, respectively.

Thermal behavior of light neutral oil and sorbitan monostearate determined by TGA are given in Figure 7.4. The onset temperature where the light neutral oil starts to loose its mass is 228 °C, while the surfactant starts to loose its mass at 148 °C.

For sorbitan monostearate, the endothermic peak at 50 °C is observed due to the melting of sorbitan monostearate and the heat of melting is evaluated as -3.50 J/g (Figure 7.5).
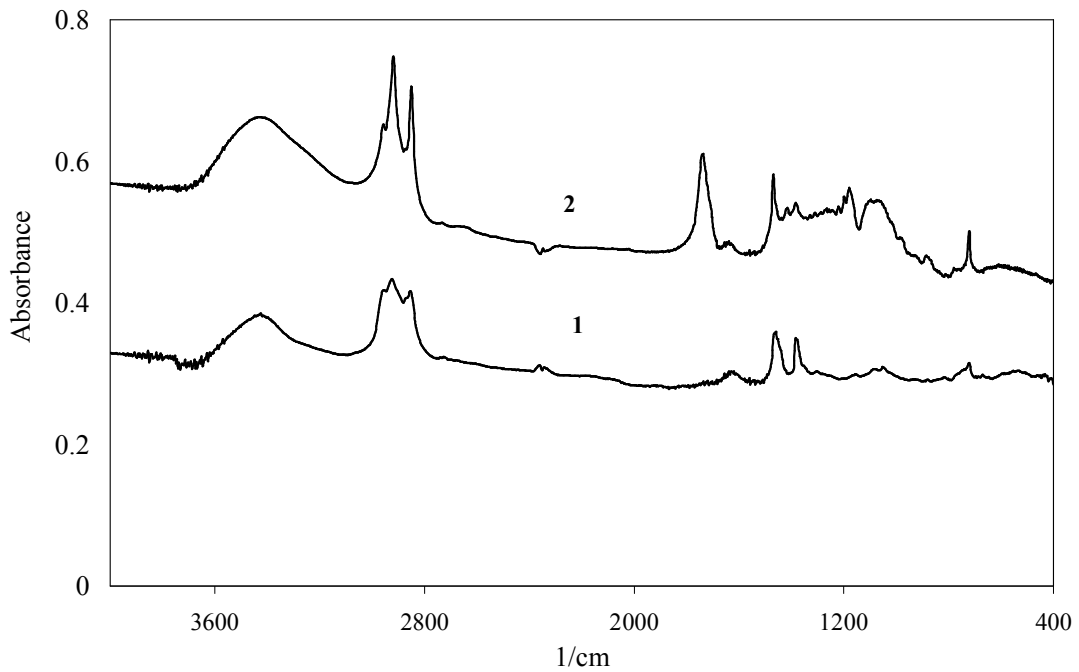
Figure 7.3. FTIR spectra of a) light neutral oil and b) sorbitan monostearate.
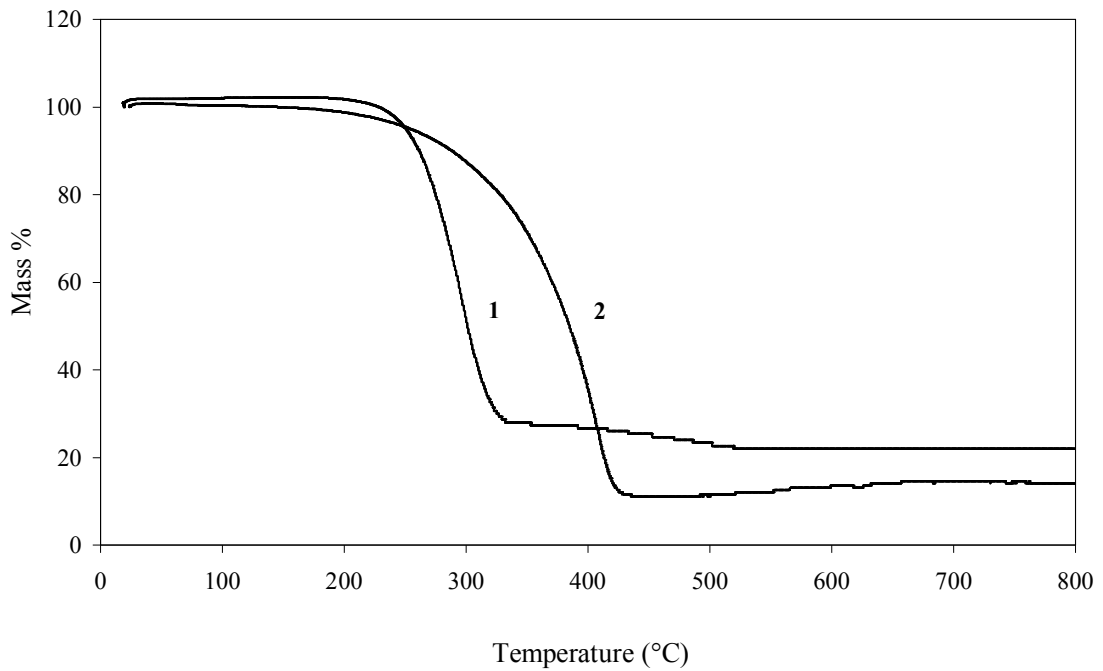
Figure 7.4. TGA thermogram of 1) light neutral oil 2) sorbitan monostearate.
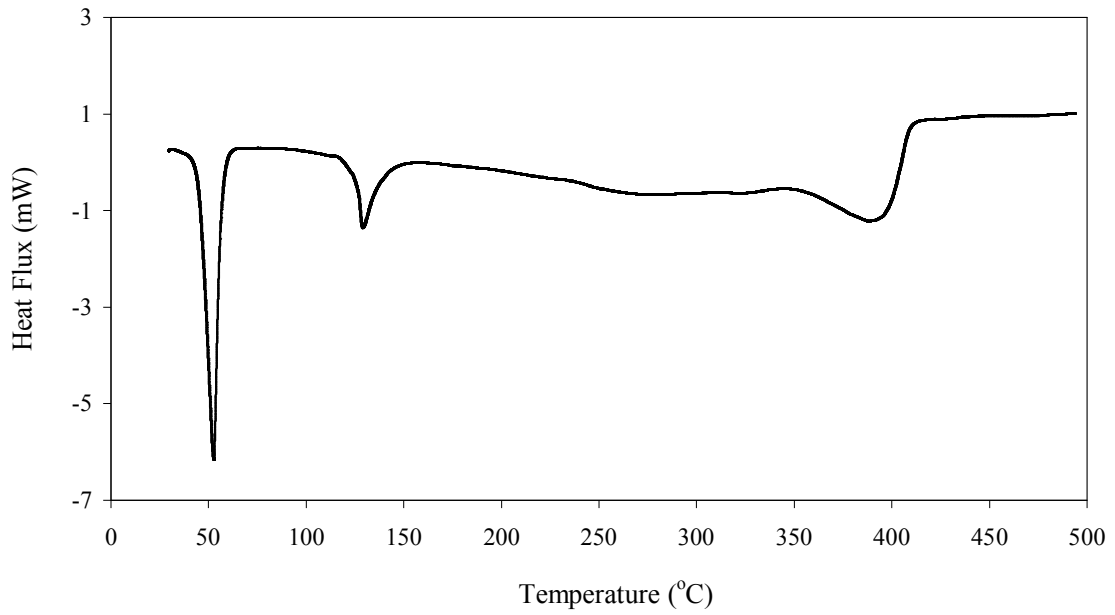
Figure 7.5. DSC curve of sorbitan monostearate.

The morphology of the emulsifier shows that the particles are spherical and they are one within the other. The particle size of the largest particle including the smaller ones is nearly 500 μm. As demonstrated in Figure 7.6b, the wall thickness of the largest particle is nearly 20 μm.

(a)   (b)
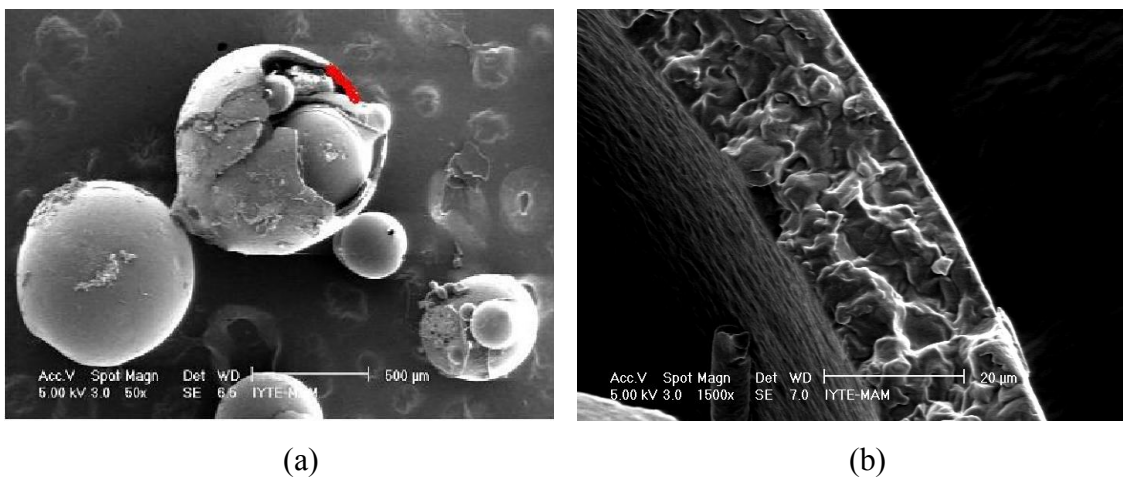
Figure 7.6. SEM images of sorbitan monostearate a) 50x b) 1500x magnification.

Zinc Borate Additives Used for Lubricant Preparation

The additives are vital constituents of most lubricant formulations that protect the equipment from wear and enable it to operate successfully under heavy loads. In this study, different types of zinc borate and clinoptilolite rich mineral were used as lubricating oil additives. Besides the zinc borates synthesized in the scope of this work, three different zinc borate species were dispersed into the base oil.

The morphology of these zinc borates are displayed in Figure 7.7. Zinc borate particles synthesized by precipitation technique using boric acid and zinc oxide as starting materials are in the shape of prism and the diameters of the particles are in the range of micro scale (Figure 7.7a). When these particles dried by supercritical ethanol, the particle size decreases and both rod-like and broccoli type species are observed (Figure 7.7b). SEM image of commercial product (Firebrake 2335) exhibits that the nano-sized particles agglomerate (Figure 7.7c) (Gönen, 2009).

Particle size distribution of zinc borate produced at 90 °C using boric acid and zinc oxide is shown in Figure 7.8. It has a bimodal distribution, smaller percent of particles has particle diameter lower than 1.0 µm and greater percent has particle diameter greater than 6 µm and volume-weighted mean diameter was found as 5.8 µm.

Clinoptilolite Rich Mineral Used for Lubricant Preparation

The two reasons for the employment of clinoptilolite rich minerals in this study are related to the enhancement of tribological properties of mineral oil and the water adsorbance property of zeolites. The clinoptilolite rich minerals having average 5 µm particle size (Figure 7.9) was also used as a lubricating oil additive and the crystal morphology of the zeolite was investigated by scanning electron microscope. SEM image which is given in Figure 7.10 indicates the classical clinoptilolite family of zeolite crystals. In order to adsorb the residual water in the emulsion the clinoptilolite rich mineral 2-3 mm particle size was put in inverse emulsion heated up to 160 °C to and the zeolites were separated from the emulsion after two days and the prepared emulsion was used as a lubricant.
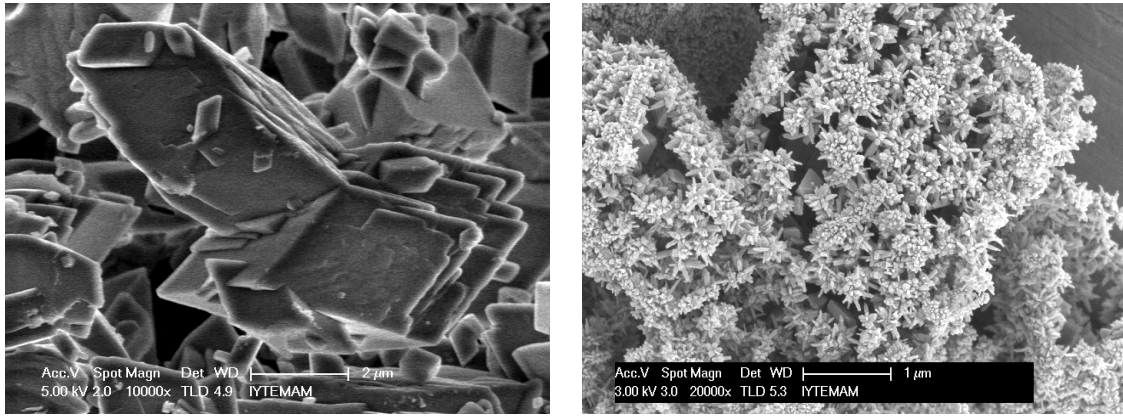
(a)   (b)
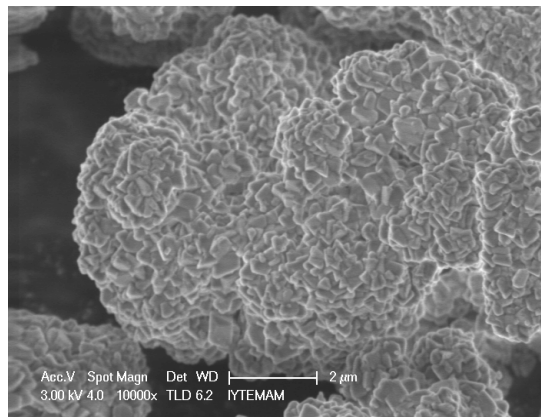
(c)

Figure 7.7. SEM images of a) zinc borate produced at 90 °C using boric acid and zinc oxide b) zinc borate produced at 90 °C using boric acid and zinc oxide dried by supercritical ethanol and c) commercial zinc borate (Firebrake 2335) (Source: Gönen, 2009).
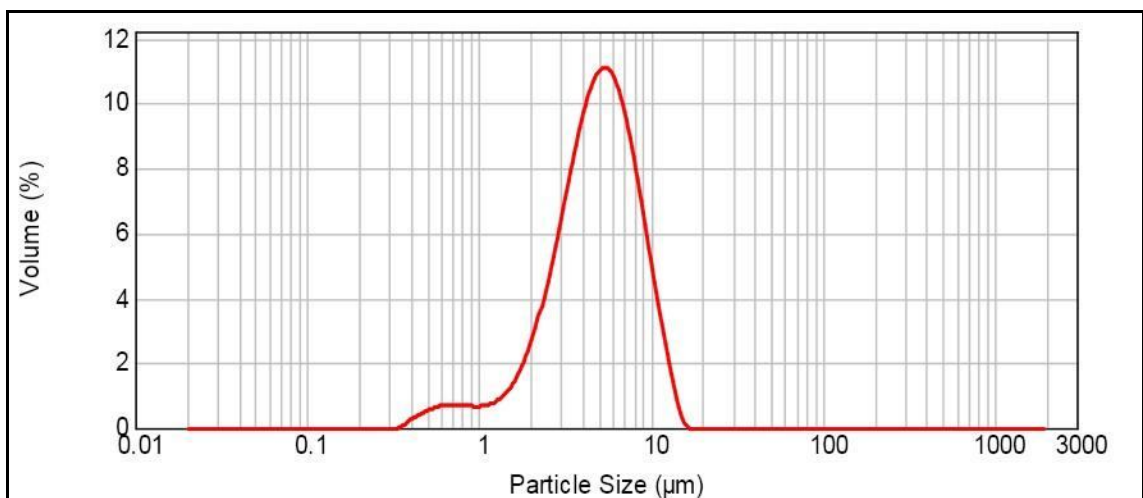
Figure 7.8. Particle size distribution of zinc borate produced at 90 °C using boric acid and zinc oxide (Source: Gönen, 2009).
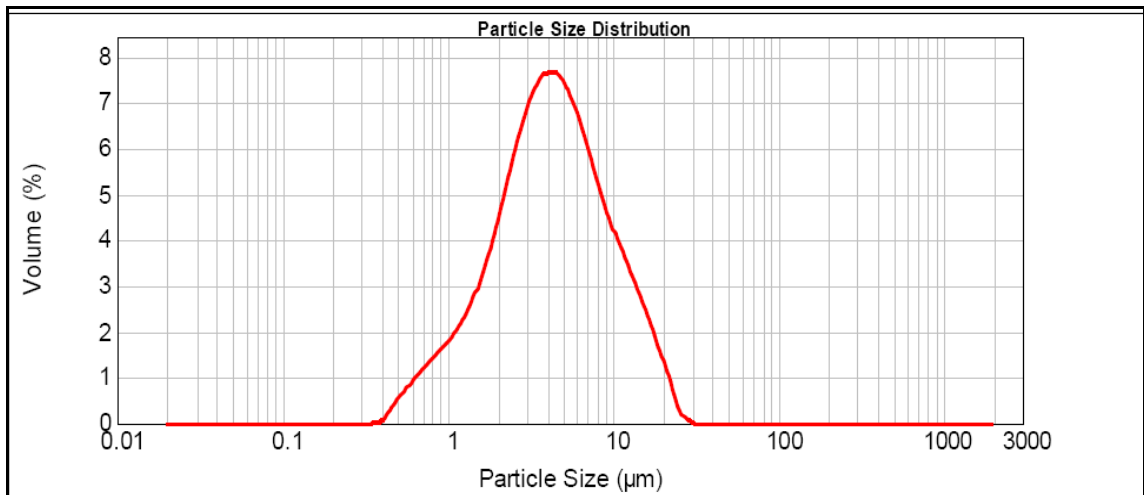
Figure 7.9. Particle size distribution of clinoptilolite rich mineral used as an anti-wear additive in the mineral oil
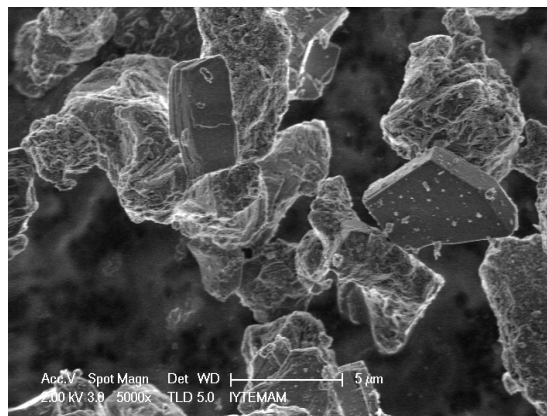
Figure 7.10. SEM images of clinoptilolite rich mineral having 5 μm

7.2. Characterization of Inverse Emulsions

7.2.1. Control Emulsions

Microscopes are very useful tools in the observation of emulsions and dispersions, and they can provide us a good picture of the structure, shapes and sizes of the particles. This part of the study includes the optical microphotographs of the prepared emulsions. For water-in-oil emulsions the water droplets are stabilized in the apolar solvent (oil) by a surfactant monolayer. The size of these droplets depends only on water concentration expressed as the water to surfactant molar ratio W. Water–filled

micelles were dispersed in the continuous oil phase as shown in Figure 7.11. Although spherical droplets were formed, neither the micelles nor their shapes could be observed in these microphotographs which were taken by Olympus CH40. It was reported that inverse emulsion droplets are slightly polydisperse which is a thermodynamically equilibrium property (Capek, 2004). In this figure, the effect of surfactant concentration in the morphology of inverse emulsions is indicated, as well. The emulsions indicated in Figure 7.11a, 7.11b, and 7.11c were prepared by magnetic stirrer. In inverse emulsions, oil diffusion is high, water diffusion as well as the surfactant mass transfer is low and corresponds to smaller water droplets than oil droplets (Koroleva and Yurtov, 2006). The water droplets can be seen clearly in Figure 7.11a, whereas, the black and spherical droplets in Figure 7.11c are air bubbles which are formed due to mixing. For all emulsion samples, droplets are slightly polydisperse. The average droplet diameters calculated from the microphotographs are listed in Table 7.2. The average diameters of the samples were evaluated taking ten different droplets' diameter. Therefore Figure 7.12 was plotted to point out the effect of surfactant concentration on the droplet size. It is seen that the average diameter of droplets decreases with increasing the amount of surfactant in the oil.

The utilization of a rotor-stator homogenizer for emulsion mixing reduces the diameters of the droplets since rotor knife spins within the tube, creates a pumping action, forcing the sample out through the windows in the tube. The microphotographs of the control emulsions containing 1 wt% surfactant and prepared by a magnetic stirrer and a homogenizer are compared with each other to expose the effect of emulsification mixing on the size of the droplets (Figure 7.13).

In order to find out the temperature effect on the morphology of the control emulsions, they were heated up to 160 °C, and the microphotographs of them were taken at different temperatures as seen in Figure 7.14.The microphotographs were taken by Olympus CHX microscope. It was observed that the air bubbles disappeared when the temperature was increased and transparent droplets formed.

(a)

(b)

(c)
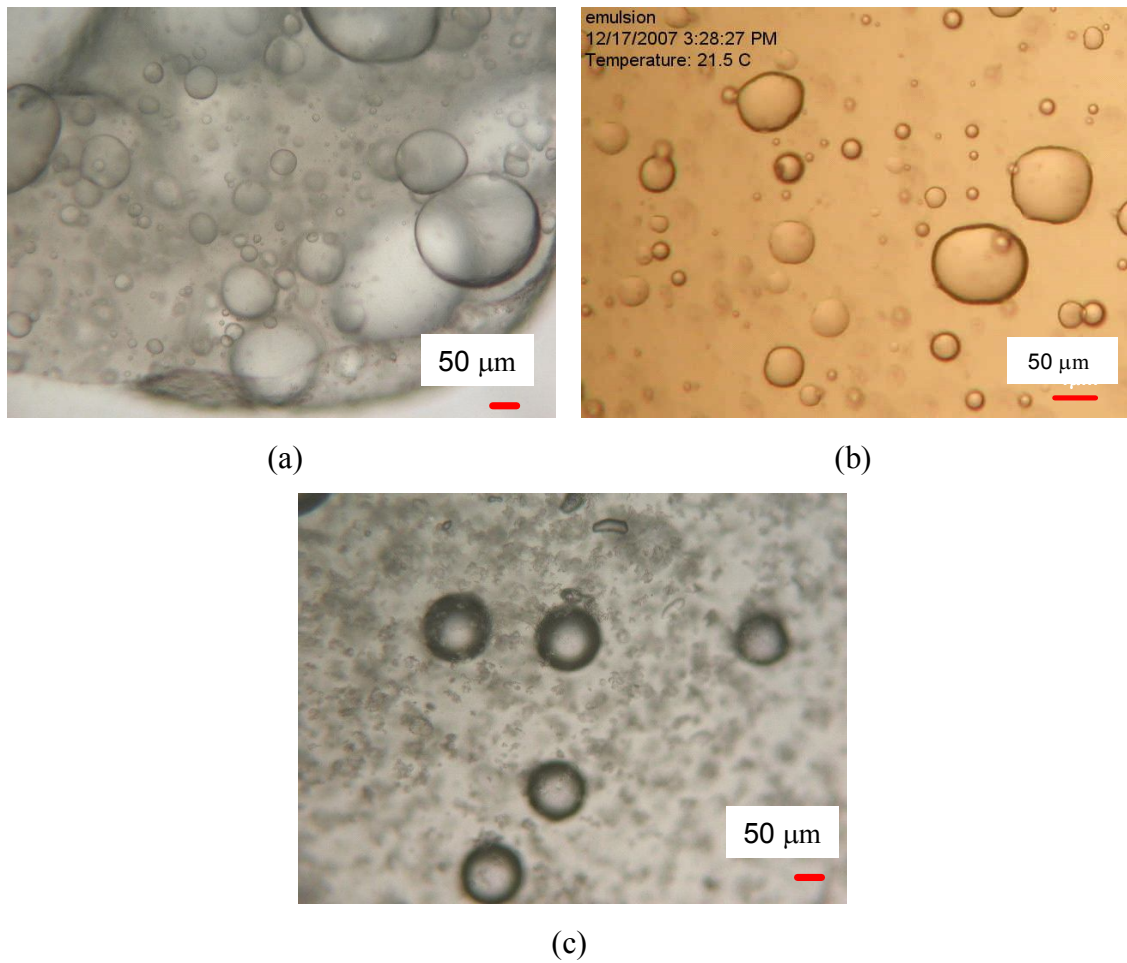
Figure 7.11. The microphotographs of control emulsion having a) 0.1% (C4) b) 1% (C3) c) 10% (C5) surface active agent.

Table 7.2. Avarage droplet diameter for control emulsions.

Control Emulsion	Average Droplet Diameter (μm)
C4	51.82
C3	31.36
C5	1.02
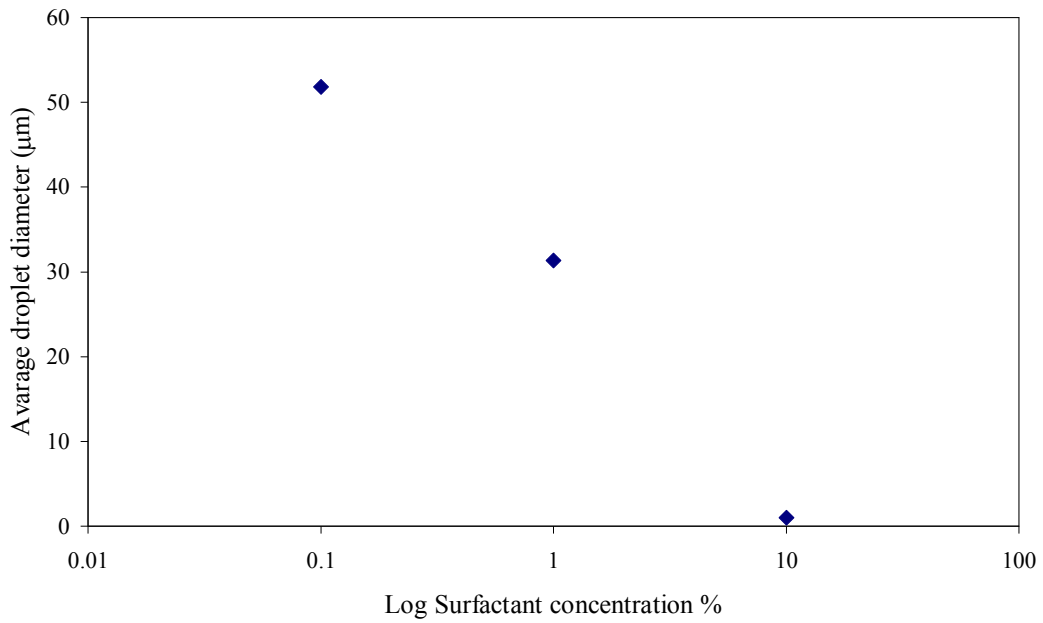
Figure 7.12. Effect of surfactant concentration on the average size of the droplets.

(a)	(b)
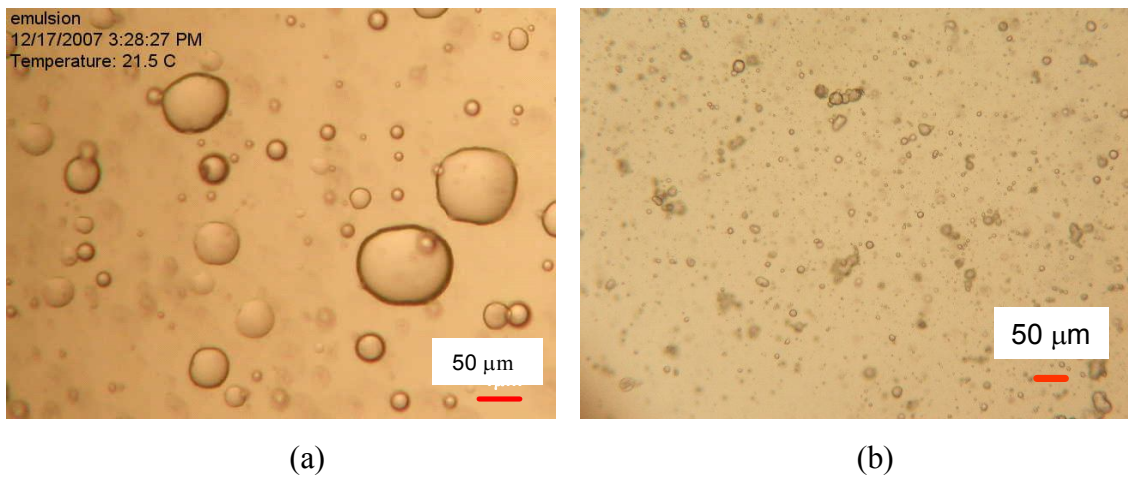
Figure 7.13. The microphotographs of control emulsion having 1 wt % surfactant and prepared by a) a magnetic stirrer (C3) and b) a homogenizer (C7).
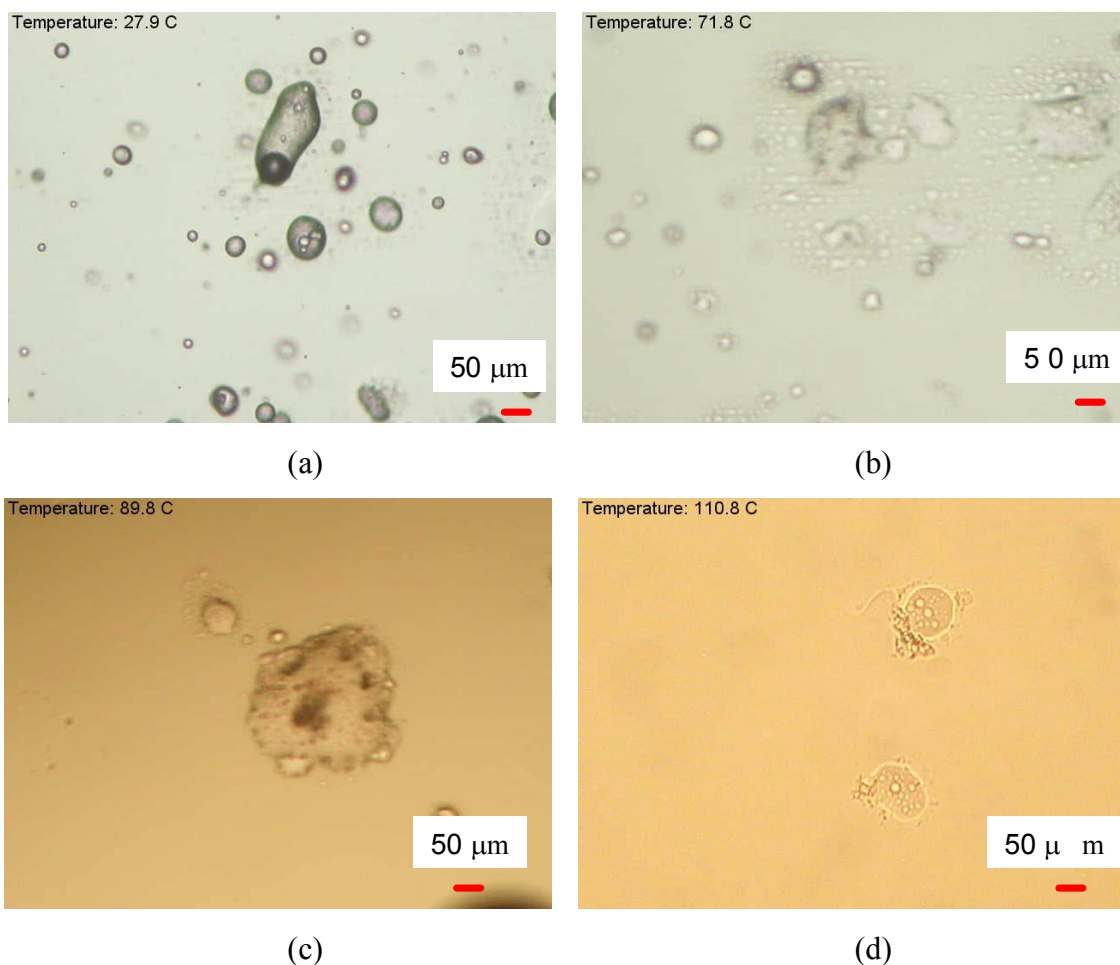
Figure 7.14. The microphotographs of control emulsion having 1% (C3) surface active agent at a) 27.9°C, b) 71.8°C, c) 89.8°C, d) 110.8 °C.

7.2.2. Zinc Borate Inverse Emulsions

In this part of the project, the morphological study was performed not only to investigate the morphology of the control emulsions, but also to expose dispersion property of aqueous phases of borax, zinc nitrate and zinc borate emulsions. For these purposes, the transfer of inorganic salt and borax in inverse emulsions were examined and the optical microphotographs of the borax, zinc nitrate and zinc borate emulsions were taken (Figures 7.15 and 7.16). Figure 7.15 shows two inverse emulsions and the obtained zinc borate emulsion. In this figure, these emulsions were produced by mixing via magnetic stirrer and ultrasonic bath. The ultrasonic bath helped to reduce the air bubbles by means of ultrasonic waves and this disruption destroyed the bubbles. The droplet diameter is around 50 μm. The obtained emulsions were waited for 24 h, and it was observed that these emulsions were unstable. Rotor-stator homogenizer is used not

only to form stable system but also to produce ultrafine particles. The emulsions prepared by homogenizer for 10 min are presented in Figure 7.16. Unlike the optical microscopy study of the emulsion prepared by ultrasonic bath, the optical microscopy study of the prepared inverse emulsions formed by homogenizer was achieved by a more developed optical microscope, and the diameters of the droplets were measured. The average diameters of the droplets for borax decahydrate and zinc nitrate inverse emulsions were found as 2.12 and 10 μm, respectively. The average diameter of the droplets for the zinc borate emulsion was calculated as 1.40. It was revealed that when these two inverse emulsions, zinc nitrate and borax decahydrate were mixed to form zinc borate emulsion, the diameter of the droplets which acted as reactors for the production of zinc borate decreased. Besides them, it was observed that the droplets were slightly polydisperse for all inverse emulsion samples (Figure 7.16).

(a)

(b)

(c)
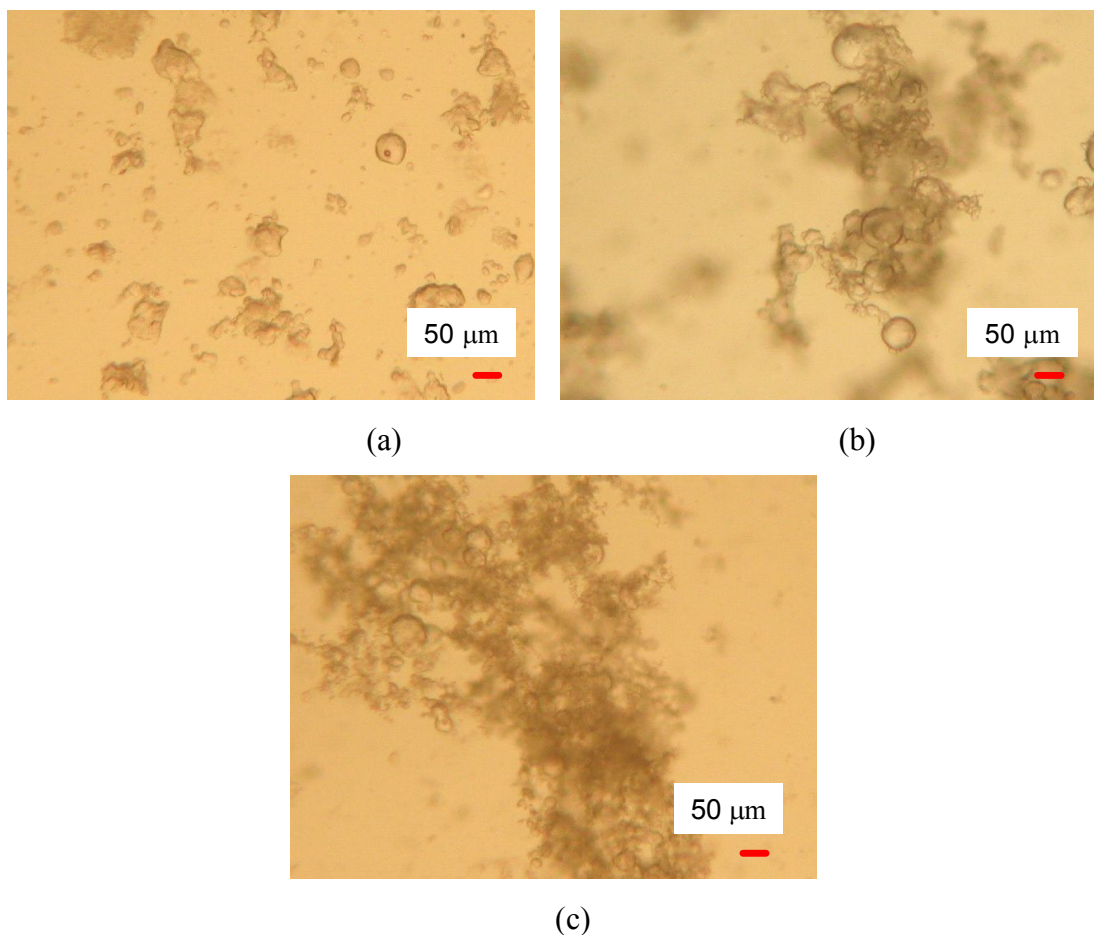
Figure 7.15. The microphotograph taken at 25 °C of a) borax emulsion b) zinc nitrate emulsion c) emulsion containing borax and zinc nitrate and mixed at 70 °C for 2h (SU-1) by magnetic stirrer and ultrasonic bath. (The microphotographs were taken by Olympus CH40 microscope).

(a)

(b)

(c)
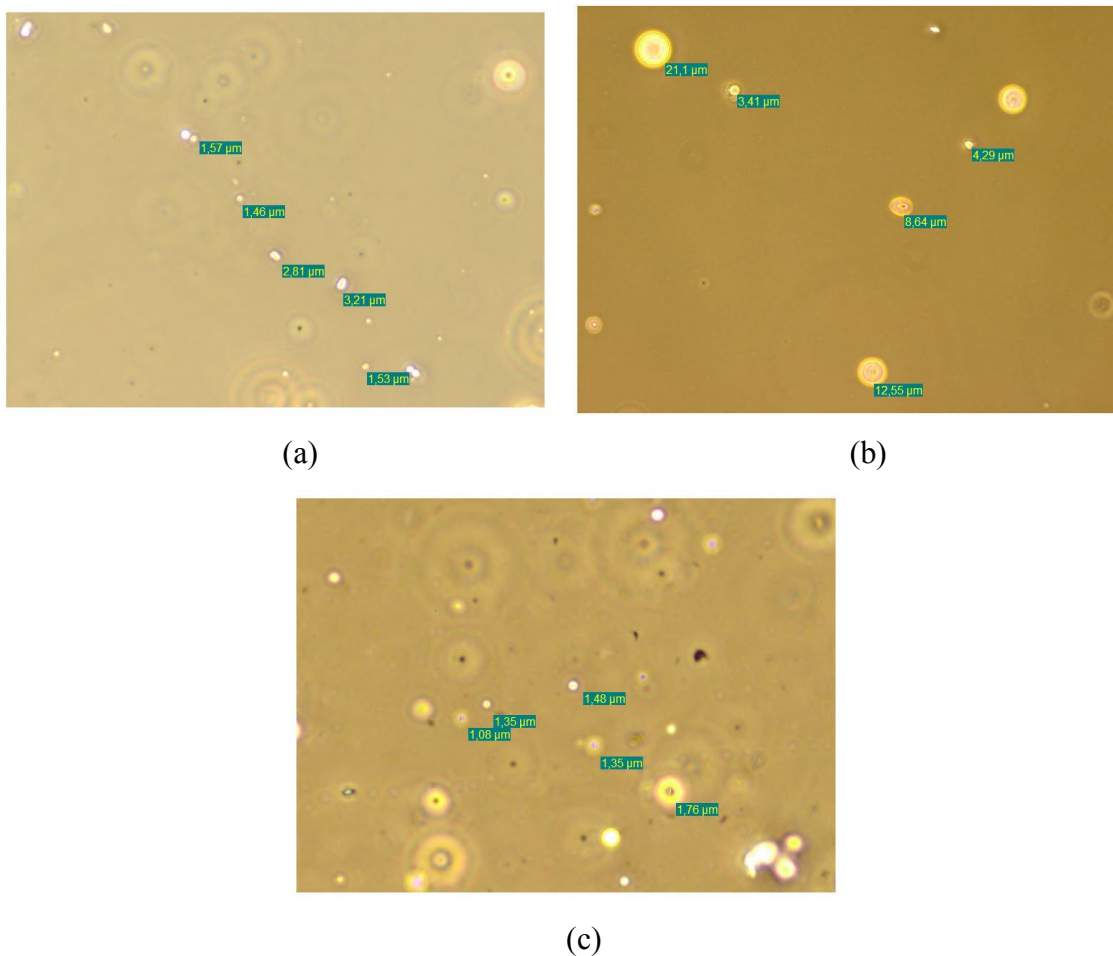
Figure 7.16. The microphotographs of a) borax emulsion b) zinc nitrate emulsion c) zinc borate emulsion (SH-1) (The microphotographs were taken by Olympus BX60M microscope).

The temperature effect on the morphology of the inverse emulsions containing inorganic particles were investigated by heating them up to 160 °C, and the microphotographs of them were taken at different temperatures as seen in Figure 7.17. It was observed that the air bubbles disappeared when the temperature was increased and transparent droplets formed. The increase in the temperature caused the decrease in the size of the droplets since surfactant particles were not dissolved in the emulsion due to low temperature.
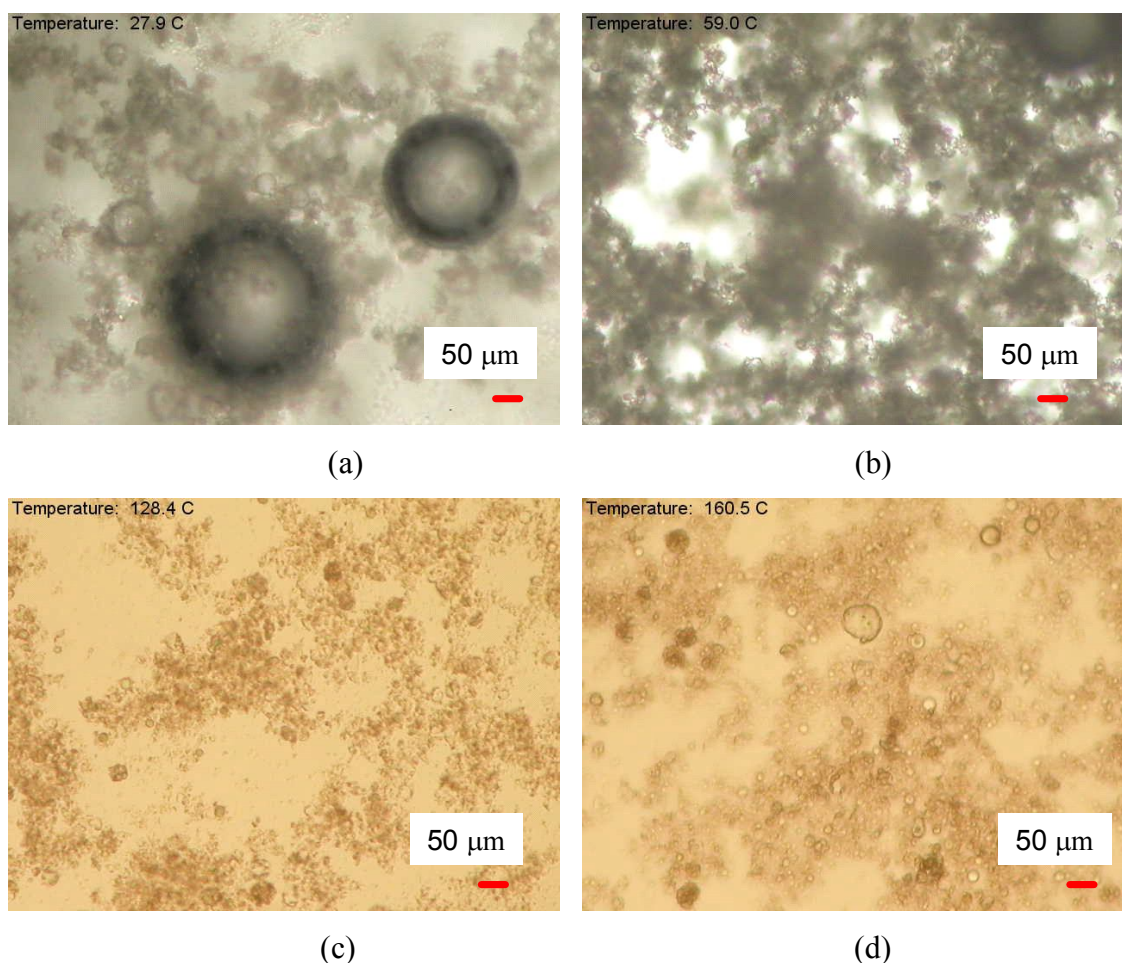
Figure 7.17. The microphotographs of emulsions containing borax and zinc nitrate (E4) and mixed at 70 °C for 2h than at a) 27.9°C, b) 59°C, c) 126.4°C, d) 160.5°C on hot plate (The microphotographs were taken by Olympus CH40 microscope).

Emulsion Stability

The prediction of emulsion stability is of great importance since it effects the formulation, quality control and the technical service of the products (metal working fluids, lubricants etc.). Unfortunately, the inverse emulsions prepared in this study are unstable. The photograph of unstable emulsion containing borax, zinc nitrate and mixed at 70 °C for 2h (SU-1) by magnetic stirrer and ultrasonic bath is shown in Figure 7.18. The particles settled down at the bottom after 1 day. Moreover, the stability of the emulsions mixed by homogenizer and magnetic stirrer were investigated and the stability of the emulsions was quantified by measuring the thickness of the precipitate layer as a function of time. Figure 7.19 presents the zinc nitrate, control and borax decahydrate inverse emulsions after the complete precipitation was achieved (after 1 day). By using data of precipitation experiment, Figure 7.20 was plotted. In this graph,

h_o indicates the initial height when time is zero. According to stability curves, zinc borate emulsion has the highest stability, whereas, instability is observed for the others in initial five minutes.
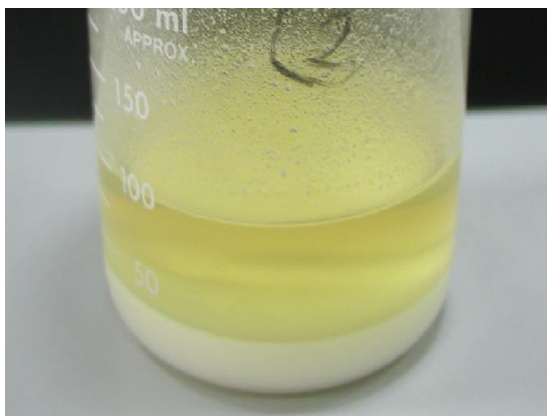
Figure 7.18. The photograph of the unstable zinc borate inverse emulsion prepared by magnetic stirrer and ultrasonic bath (SU-1).
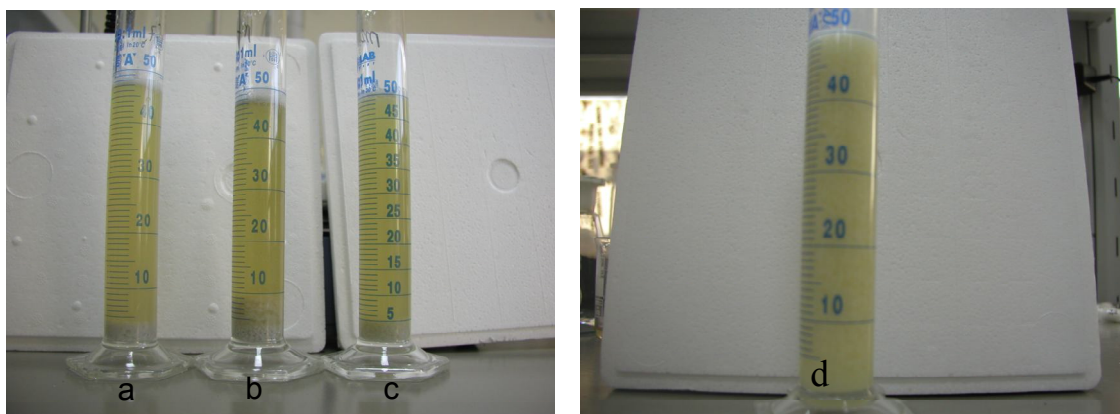
Figure 7.19. The photographs of the unstable a) zinc nitrate b) control c) borax decahydrate and d) zinc borate inverse emulsions prepared by magnetic stirrer and homogenizer.
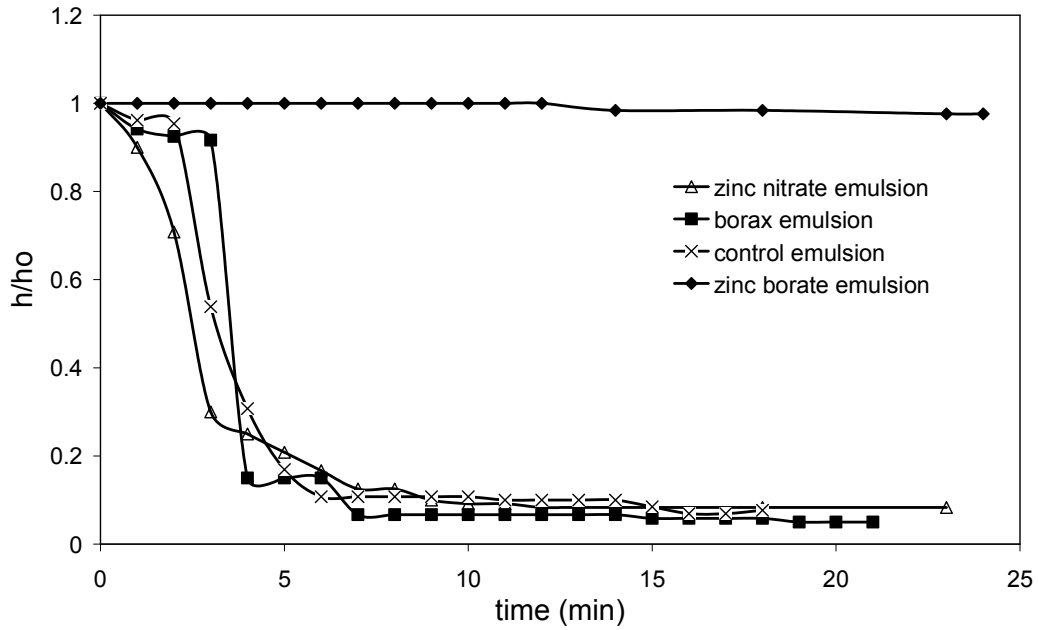
Figure 7.20. Relative height of the precipitate layer of inverse emulsions prepared by two microemulsion technique and mixed with homogenizer and magnetic stirrer versus time.
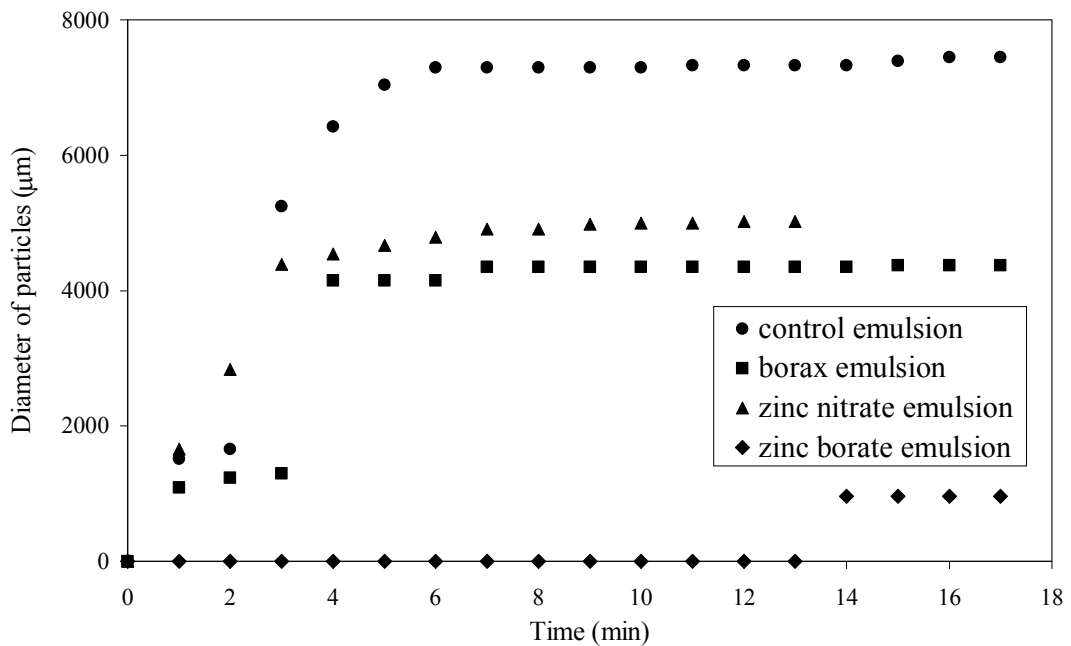
Figure 7.21. Diameter of particles prepared by inverse emulsion with respect to time

In literature it is implied that the settling velocity is directly proportional to the diameter of the particle as shown in the formula below (Alberty, 1997);

$$\frac{dx}{dt} = \frac{2r^2(\rho - \rho_o)g}{9\eta} \qquad (7.1)$$

where;

$\frac{dx}{dt}$ = rate of settling (cm/s)

ρ_o = density of medium (g/cm^3)

ρ = density of particle (g/cm^3)

η = viscosity of medium (g/cm.s)

r = radius of particle (cm)

g = 981 cm/s^2

The diameters of particles in the inverse emulsions were calculated using Equation 7.1. The results shown in Figure 7.21 were evaluated for the settling of particles within 18 minutes. The oil density and viscosity used for the calculations are 0.86 g/cm^3, and 0.35 Poise (Tüpraş, 2010). The densities of zinc nitrate and borax decahydrate and zinc borate aqueous solutions are 1.14, 1.24, and 1.00 g/cm^3 (Wikipedia, 2010 and Chemyq, 2010). The density of zinc borate is 2.85 g /cm^3 (Gönen, 2009). The diameters of the particles calculated from the settling kinetics are not consistent with those found by optical microscopy. The diameters presented in Table 7.3. are enormously larger than the particles observed by optical microscopy. This result might be due to fast sedimentation of the particles and the particles became agglomerated. Therefore the larger particles settled down in a short time. So data derived from the kinetics of settling did not reflect the actual diameter of the particles in inverse emulsions. Moreover, the stability of the droplets was examined and the pressure difference was calculated considering Young-Laplace Equation as shown below;

$$\Delta P = \frac{2\gamma}{r} \qquad (7.2)$$

where;

ΔP: Pressure difference (N/cm^2)

γ: Surface tension of the surfactant (N/cm)

r: Radius of droplet (cm)

The normal stress σ, is related to the pressure difference across the boundary and the thickness of monolayer of droplet as indicated in Equation 7.3.

$$\sigma = \frac{\Delta P.r}{2t} \qquad (7.3)$$

where;

ΔP: Pressure difference (N/cm^2)

t: Thickness of monolayer of droplet (cm)

The interfacial tension of water and mineral oil having sorbitan monostearate is 0.00019 N/cm at concentrations higher than critical micelle content (Peltonen, et al., 2001) and the thickness of monolayer of sorbitan monostearate at the interface between water and mineral oil is 2.5×10^{-7} cm. The calculated pressure difference and normal stress values for the droplets are listed in Table 7.3. For different pressure difference values, normal stresses of the samples are constant since the normal stress acting on the droplet is related to monolayer thickness and the interfacial tension. Therefore it is revealed that the pressure difference values greater than 760 N/cm^2 the droplets will not be stable, they will explode due to the high stresses acting on the walls of the droplets.

Table 7.3. The diameters of the particles and the pressure difference of the micelles.

Sample	Density (g/cm^3)	Settling between 0-2 min				Settling between 2-18 min			
		Settling velocity (cm/s)	Particle diameter (μm)	ΔP (N/cm^2)	σ (N/cm^2)	Settling velocity (cm/s)	Particle diameter (μm)	ΔP (N/cm^2)	σ (N/cm^2)
Control	1	0.3	1174	0.006	760	0.575	1809	0.004	760
Zinc nitrate	1.14	1.75	1856	0.004	760	0.5	1037	0.007	760
Borax	1.24	0.45	873	0.009	760	0.57	1049	0.007	760
Zinc borate	1	5×10^{-5}	15	0.502	760	0.06	240	0.032	760

7.2.3. Inverse Emulsion with Co-surfactant

In addition to inverse emulsions, the morphology of the microemulsions prepared by addition of propanol-2 as a co-surfactant was examined by optical microscopy. The optical microphotographs of borax, zinc nitrate and zinc borate emulsions are shown in Figure 7.22, Figure 7.23 and Figure 7.24, respectively. According to these microphotographs, five different droplets for each microemulsion were fixed and their diameters were measured by Olympus DP2-BSW program. The average values of five droplets are tabulated in Table 7.4.

(a)   (b)

(c)   (d)
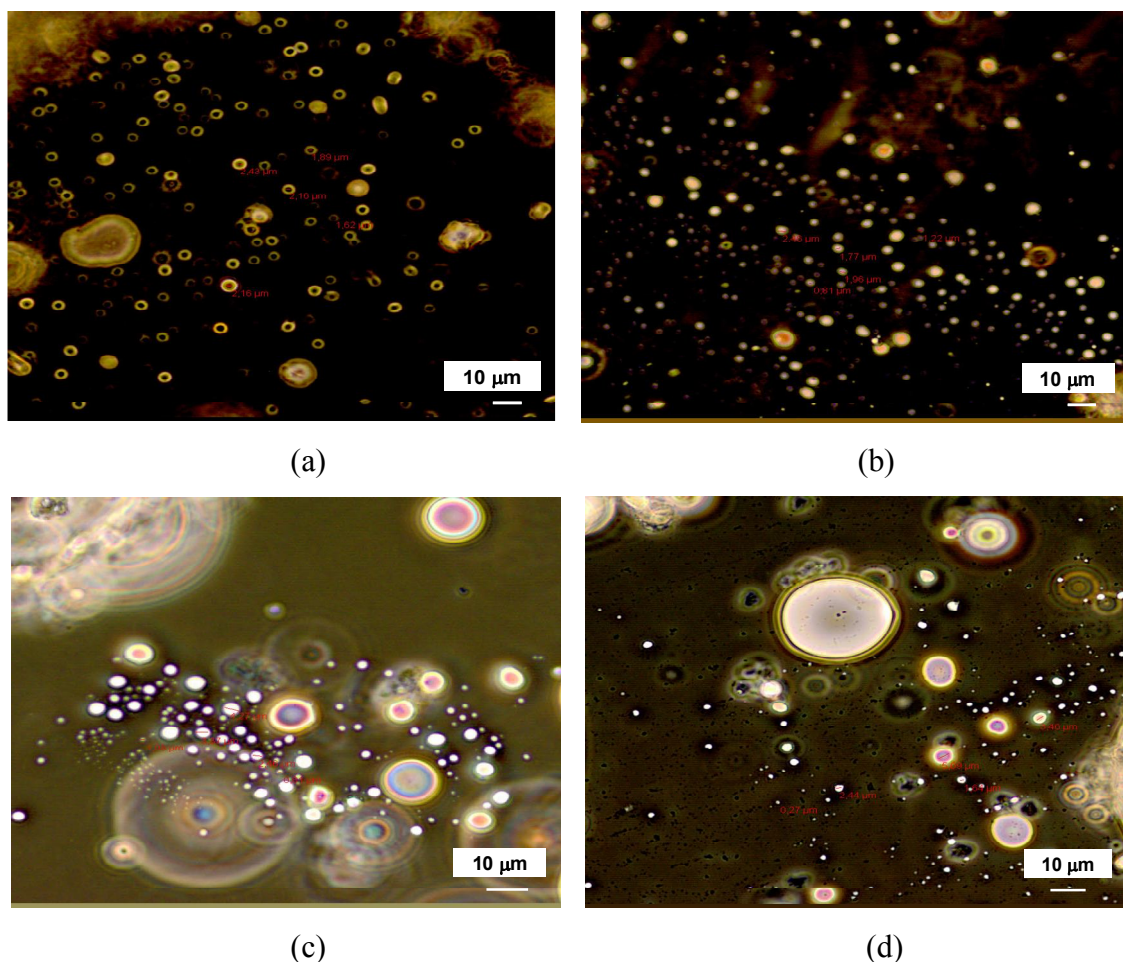
Figure 7.22. The microphotographs of borax microemulsion including a) 30.0, b) 51.5, c) 80.0 and d) 102.2 cm^3 propanol-2. (The microphotographs were taken by Olympus BX60M microscope).
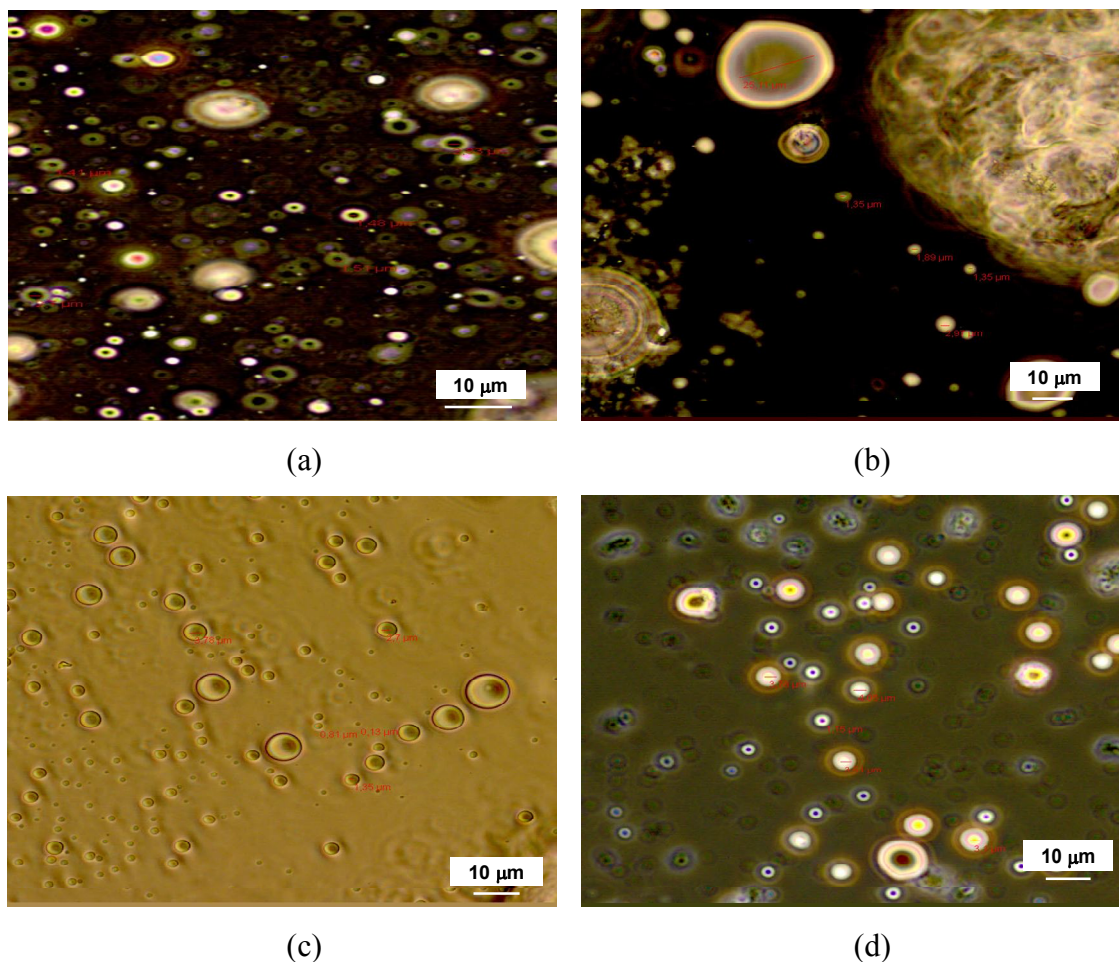
Figure 7.23. The microphotographs of zinc nitrate microemulsion including a) 30.0, b) 51.5, c) 80.0 and d) 102.2 cm^3 propanol-2. (The microphotographs were taken by Olympus BX60M microscope).

Moreover the morphology of zinc borate emulsions containing different amount of co-surfactant was examined and the diameter of droplets were determined by Olympus DP2-BSW program. The average values of five different droplets are shown in Table 7.5. It was observed that there was a tendency in the increment of droplet diameter by increasing the concentration of co-surfactant for borax and zinc nitrate microemulsions. These results were consistent with literature (Lin et al., 1997). However the droplets disappear when the propanol-2 concentration is increased to 80 and 102 cm^3 for zinc borate emulsion as seen from Figures 7.24c and 7.25d. Instead of the droplets, lamellar structures appear.
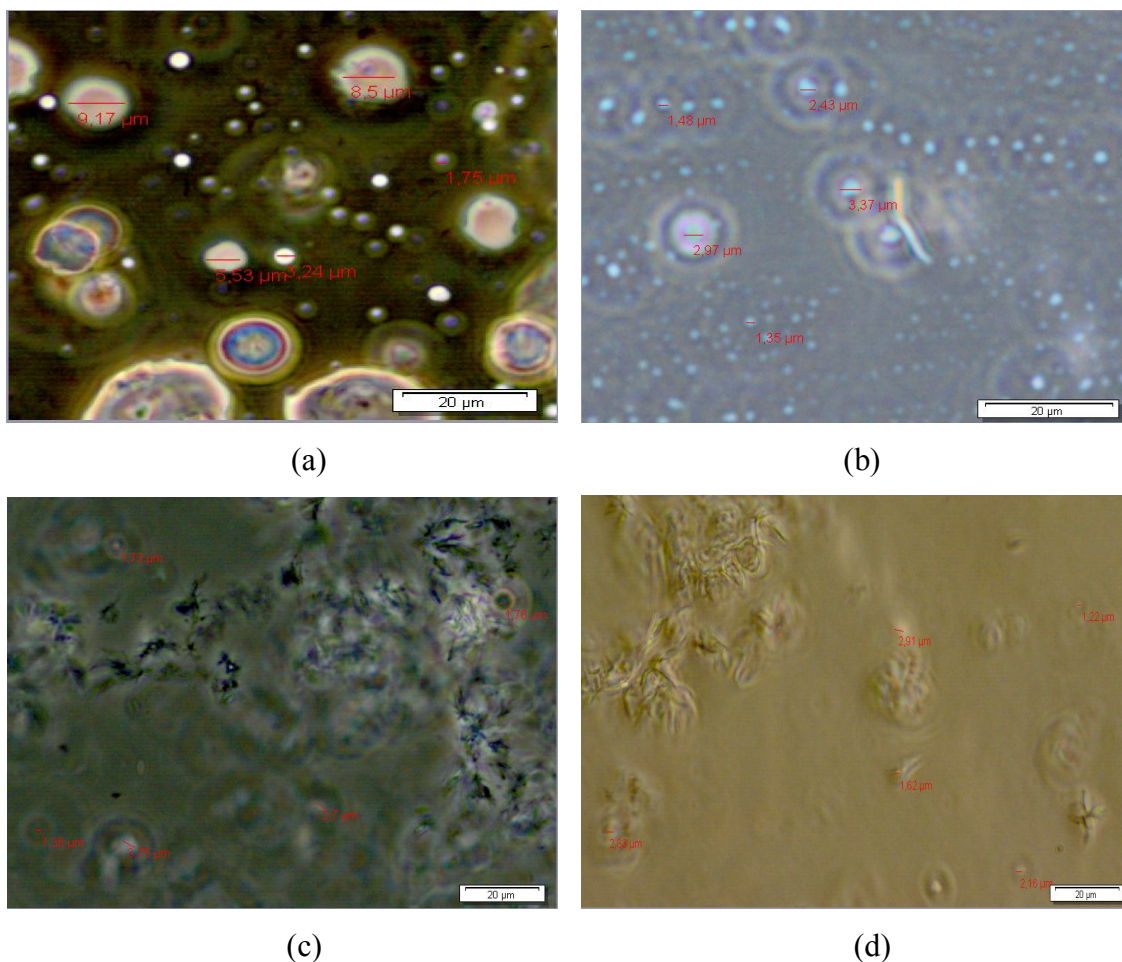
Figure 7.24. The microphotographs of zinc borate microemulsion including a) 30.0, b) 51.5, c) 80.0 and d) 102.2 cm^3 propanol-2. (The microphotographs were taken by Olympus BX60M microscope).

Table 7.4. The average droplet diameter of borax and zinc nitrate microemulsions having 10 cm^3 aqueous phase, 100 cm^3 continuous phase and 0.1 M solution.

Sample	Aqueous Phase	Co-Surfactant (cm^3)	Average droplet diameter (μm)
SC-1-B	Borax	30.0	2.05
SC-2-B		51.5	1.60
SC-3-B		80.0	2.34
SC-4-B		102.2	2.58
SC-1-Z	Zinc Nitrate	30.0	1.99
SC-2-Z		51.5	1.89
SC-3-Z		80.0	1.75
SC-4-Z		102.2	2.73

Table 7.5. The average droplet diameter of zinc borate microemulsions prepared by 10 cm^3 aqueous phase, 100 cm^3 continuous phase, 0.1 M borax and 0.1 M zinc nitrate solutions.

Sample	Aqueous Phase	Co-Surfactant (cm^3)	Average droplet diameter (μm)
SC-1		30.0	5.64
SC-2	Zinc Borate	51.5	2.32
SC-3		80.0	2.26
SC-4		102.2	2.15

7.3. Characterization of Precipitates Produced by Microemulsion

The precipitates obtained by inverse emulsion and microemulsion techniques were characterized. Additionally, the effects of emulsion preparation technique, aqueous phase amount dispersed in the continuous oil phase, emulsification technique and the employment of co-surfactant into the oil phase on the morphology and the structure of the final product were examined. Water-oil separation tube was used to remove water by heating the emulsions up to 160 °C. The reason for the removal of water is to separate the zinc borate particles synthesized in the reverse micelles. After water removal, oil removal was achieved via microfiltration process. This process is of importance in several industries for the separation of water from water-in-oil emulsions and the researchers argue that this process is feasible for the removal of oily waste from the emulsions (Hu and Scott, 2008). After microfiltration process, the samples were washed with methyl ethyl ketone, water and ethanol and dried at 110 °C for 2h.

7.3.1. Effect of Inverse Emulsion Preparation Technique on The Properties of Zinc Borates

Both size and shape of particles are of great importance to apply them in nanotechnological products. Regarding this, the morphology of the particles prepared in inverse emulsion systems was explored. SEM microphotographs of zinc borates produced by inverse emulsion at 70°C by one and two microemulsions techniques are

presented in Figure 7.25. SEM analysis showed that the particles obtained by one-microemulsion technique had small layers having nearly 1 µm thickness, whereas the crystals were in the agglomerated form when two-microemulsion technique was used.

(a)   (b)
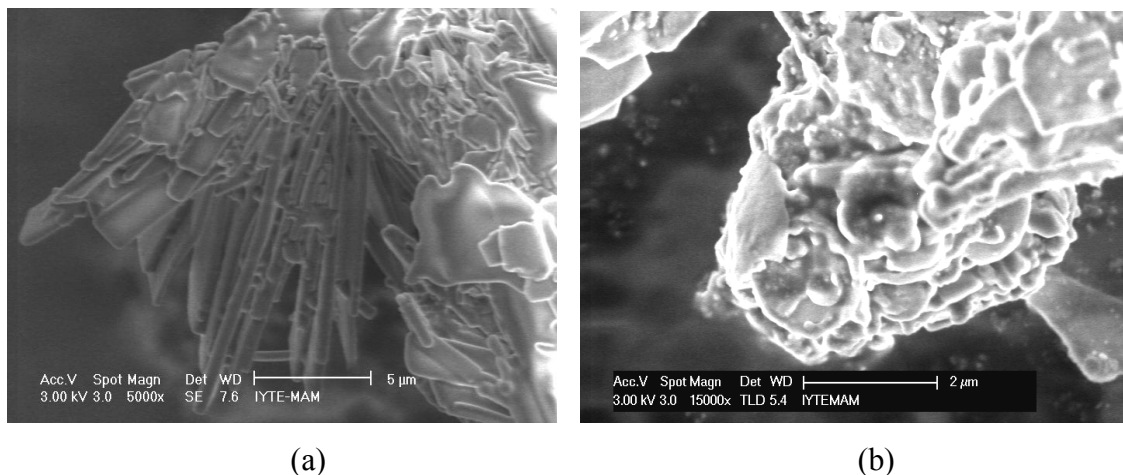
Figure 7.25. SEM images of zinc borate produced by a) one-microemulsion b) two-microemulsion techniques at 70°C.

The difference in the structure of these particles was investigated by FTIR. Figure 7.26 demonstrates FTIR spectra of zinc borate produced by one-microemulsion and two-microemulsion techniques. The spectra include not only the characteristic peaks of trihedral borate and tetrahedral borate groups but also the specific peaks of the sorbitan monostearate (at 2850, 2920, 1730, 1467 and 721 cm^{-1}). The bands at 3500 cm^{-1} are the stretching of O-H, whereas, the bands at 2920 and 2852 cm^{-1} are the characteristics peaks of the sorbitan monostearate. The band at 1047 cm^{-1} is the stretching of B(4)-O, and the peaks between 745-658 cm^{-1} are belonging to out-of-plane bending mode of B(3)-O (Gao et al., 2009c). Although the samples exhibit similar spectrum, there are many differences such as the presence of the bands at 1384 cm^{-1} and 1640 cm^{-1} for the sample obtained by two-microemulsion technique. The asymmetric stretching of O-NO$_2$ is observed at 1390 cm^{-1} proving that the sample contains nitrate ion due to the insufficient washing with water. The peak at 1640 cm^{-1} points out that the sample contains crystal water. Besides SEM and FTIR analysis, thermal behavior of the synthesized products was determined. Figure 7.27 indicates the TGA thermograms of the samples prepared by one-microemulsion and two-microemulsion techniques. Both types of zinc borate started loose its crystal water at 100 °C. The mass loss of the

sample prepared by one-microemulsion technique at 600 °C was found as 36.52%, while the mass loss for the sample prepared by two-microemulsion technique was 30.42% at the same temperature. Additionally the chemical compositions of zinc borate particles synthesized by one and two microemulsion technique were determined. The elemental compositions of these samples are similar with each other as seen in Table 7.6.
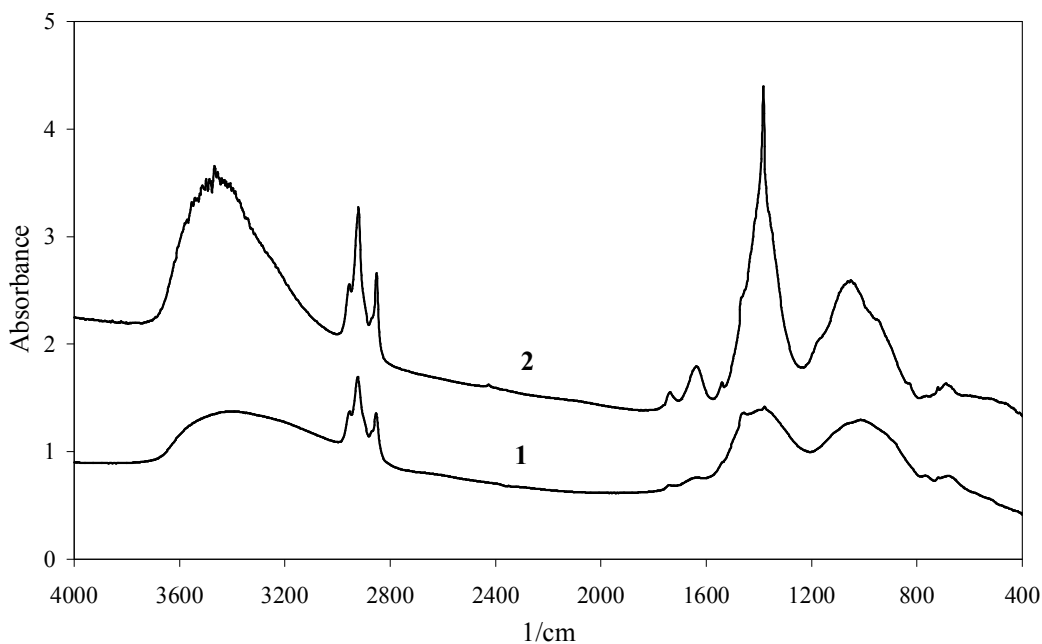
Figure 7.26. FTIR spectra of zinc borate produced by 1) one-microemulsion 2) two-microemulsion techniques at 70°C.

7.3.2. Effect of Aqueous Phase Amount on the Properties of Zinc Borates on the Properties of Zinc Borates

The amount of aqueous phase concentration for inverse emulsions is generally 5-10 wt % of the continuous phase. In order to understand the effect of starting material amount on the morphology of the final products, SEM images of the samples prepared by one-microemulsion technique having different amount of aqueous phase were obtained (Figure 7.28). Zinc nitrate and borax solution had same concentration as 1 M, however the first sample contained 10 cm^3 aqueous phase, whereas, the second sample contained 5 cm^3 aqueous phase. According to SEM images, the decrease in the amount

of aqueous phase in the mineral oil caused the change in morphology and crystal size. So 100-200 nm crystals were observed for lower amount of aqueous phase.
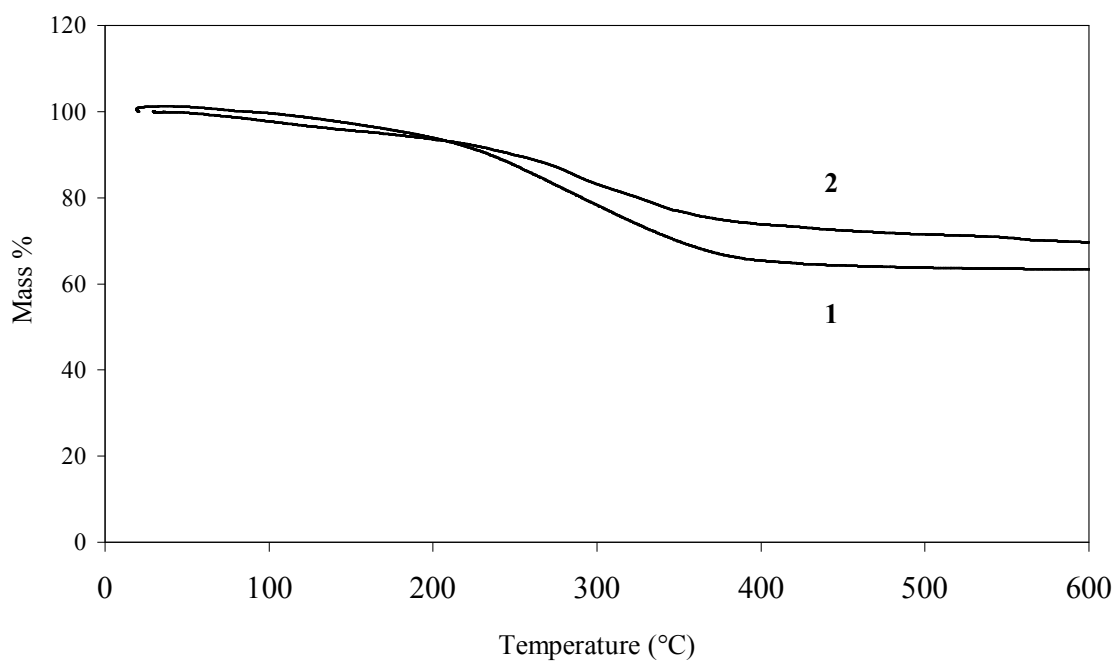
Figure 7.27. TGA thermogram of zinc borate produced by 1) one-microemulsion 2) two-microemulsion techniques at 70°C.

Table 7.6. Chemical composition of zinc borate produced one and two inverse emulsion technique.

Element	wt%	
	One-Microemulsion	Two-Microemulsion
B	26.28	22.14
C	49.57	54.77
O	13.27	10.81
N	1.02	1.13
Zn	9.86	11.16

FTIR spectra of these samples are shown in Figure 7.29. The precipitates had identical functional groups which were belonging to sorbitan monostearate and zinc borate. However, the characteristic peaks of triborate and tetraborate ion between 1200 and 600 cm^{-1} were more distinctive for the precipitate formed by 5 wt % aqueous phase.

(a)   (b)
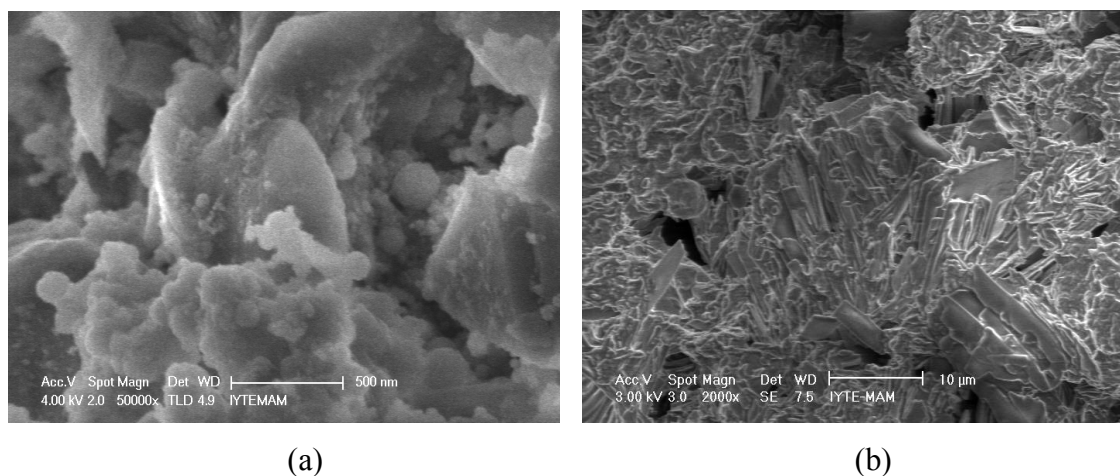
Figure 7.28. SEM images of the precipitates produced by one-microemulsion technique and containing a) 5 wt % b) 10 wt % aqueous phases.

Figure 7.30 indicates the TGA thermograms of the samples prepared by using different amounts of raw materials. The mass loss of the sample prepared by 10 wt% aqueous phase at 600 °C was determined as 36.52%, while the mass loss for the sample prepared 5 wt % aqueous phase was 28.67 % at the same temperature.
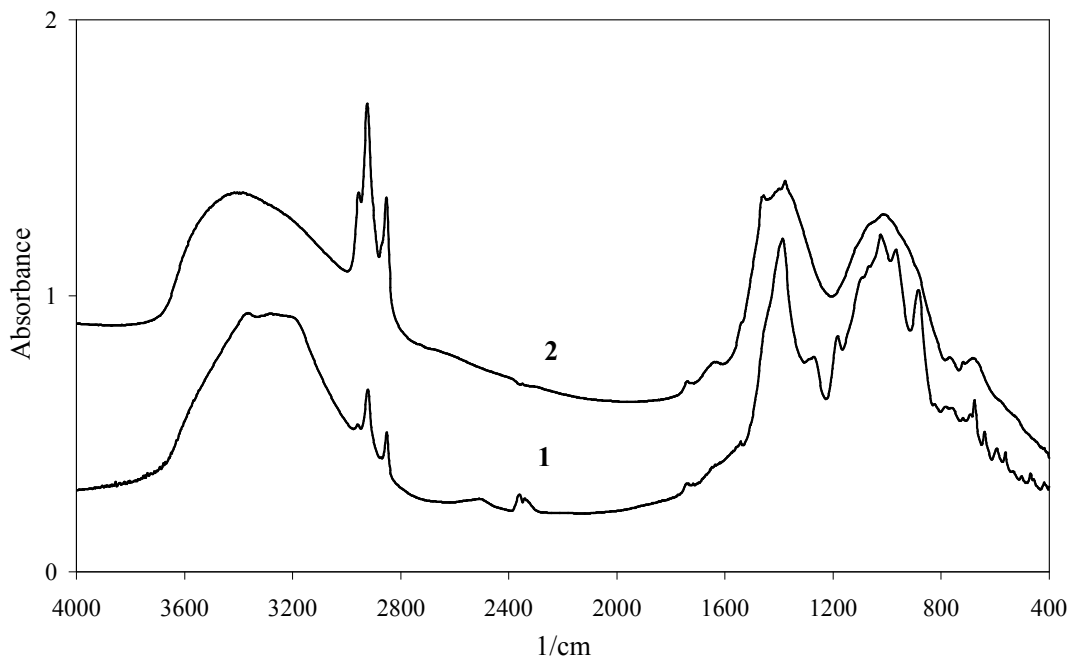
Figure 7.29. FTIR spectra of the precipitates produced by one-microemulsion technique and containing 1) 5 wt % 2) 10 wt % aqueous phases.
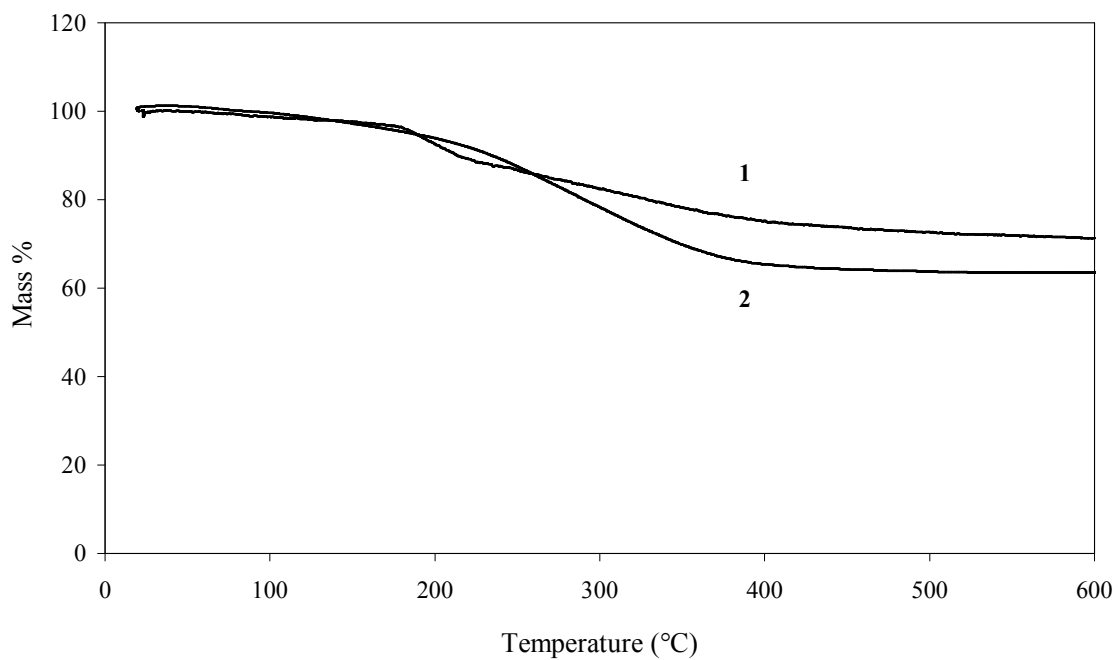
Figure 7.30. TGA thermograms of the precipitates produced by one-microemulsion technique and containing 1) 5 wt % 2) 10 wt % aqueous phases.

7.3.3. Effect of Emulsification Technique on the Properties of Zinc Borates

The energy needed to produce the droplets play an essential role in the formation of emulsion. High-speed stirrers and high-pressure homogenizers are preferred to prepare the stable emulsions containing small droplets. The researchers claim that the dispersed droplets should be as small as possible not only to obtain stable systems but also to synthesize nano-sized particles (Porras et al., 2008). In order to disclose the effect of emulsification mixing technique, the morphologies of the sample prepared via magnetic stirrer and ultrasonic bath and the sample formed by homogenizer and magnetic stirrer were compared (Figure 7.31). Both these precipitates were obtained by two-microemulsion technique. Although, the particles were washed with ethanol, the oily waste phase could not be taken away as shown in Figure 7.31a and the particles embedded in this oily phase. Nevertheless, the particles agglomerated due to the insufficient mixing of magnetic stirrer. When the homogenizer was used to mix the inverse emulsions both rod-like, and spherical crystals were formed. The diameters of spherical particles are changing between 20-30 nm as shown in Figure 7.30b.

Figure 7.32 demonstrates FTIR spectra of zinc borate produced by two-microemulsion technique and mixed via a ultrasonic bath and a homogenizer besides a magnetic stirrer. In this graph, the bands at 3500 cm^{-1} is the stretching of O-H, whereas, the bands at 2920 and 2852 cm^{-1} are the characteristics peaks of the sorbitan monostearate. The asymmetric stretching of O-NO$_2$ is observed at 1384 cm^{-1}, proving that these samples contain zinc nitrate. The peaks related to zinc borate are also observed. The band at 1047 cm^{-1} is the stretching of B(4)-O, and the peaks between 745-658 cm^{-1} are belonging to out-of-plane bending mode of B(3)-O (Gao et al., 2009c).
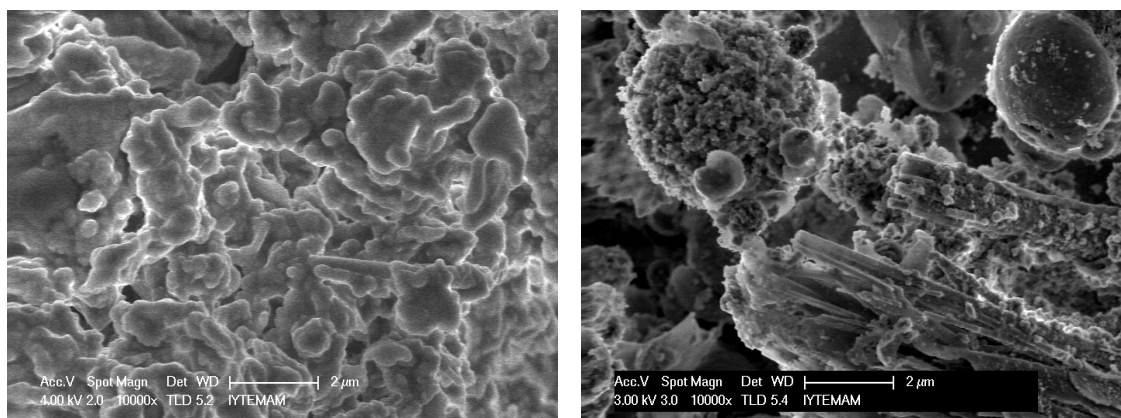
<p align="center">(a)   (b)</p>

Figure 7.31. SEM images of zinc borate produced by two-microemulsion technique and mixed via a) magnetic stirrer and ultrasonic bath b) magnetic stirrer and homogenizer.

7.3.4. Effect of Co-Surfactant on the Properties of Zinc Borates

In addition to the surfactant Span 60 in water-in-oil inverse systems, a fourth compound, propanol-2 was introduced to water-in-oil emulsions and the microemulsions were formed. Microemulsions are also used as chemical reactors and they are one of the most important features, which has to be taken into account for a comprehensive study of chemical reactions carried out in this media. In the scope of this work, different microemulsions were prepared by changing the concentration of propanol-2 while concentration of the oil, surfactant and aqueous phase were kept constant.
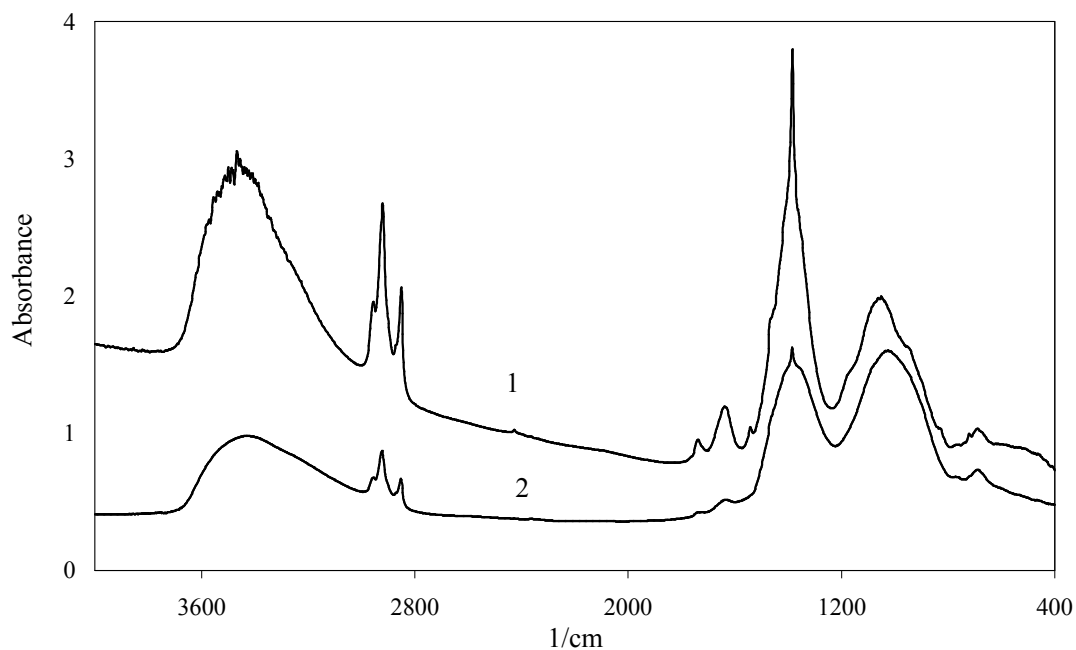
Figure 7.32. FTIR spectra of zinc borate produced by two-microemulsion technique and mixed via 1) magnetic stirrer and ultrasonic bath 2) magnetic stirrer and homogenizer.

The ternary diagram illustrating the phases of the microemulsion system is shown in Figure 7.33. The microemulsions contained 10 g surfactant and 10 cm^3 aqueous phase solutions for 100 cm^3 light neutral oil and the co-surfactant concentration was changing from 30, 51.5, 80, and 102.2 cm^3 propanol-2. The red lines and the blue point indicate the composition of the ternary system, which is used for this part of the study. According to literature the place where the blue point is located allows to be formed inverse micelles with a water core containing the polar head groups and the hydrocarbon tails have contact with the oil phase (Adityawarman, 2007). In order to understand the co-surfactant effect of the zinc borate properties, the precipitates of the microemulsions were characterized. Before the characterization, the particles were separated by centrifugation at 9000 rpm for 10 minutes. Figure 7.34 illustrates the phase separation after centrifugation process. The microemulsion was separated into three phases which are the oil, propanol-2 and the precipitate. The properties of the prepared emulsions and the phases appeared after centrifugation processes are indicated in Table 7.7. It was observed that the separated oil and alcohol phases included colloidal particles which were synthesized by microemulsion. Even though the volumes of precipitates are high, the obtained dried precipitate amount is very low since the wet precipitate contains huge amount of alcohol and water. The expected amount of zinc

borate ($2ZnO \cdot 3B_2O_3 \cdot 3H_2O$) was also evaluated in Table 7.7 considering the reaction between borax decahydrate and zinc nitrate expressed in Equation 5.5.
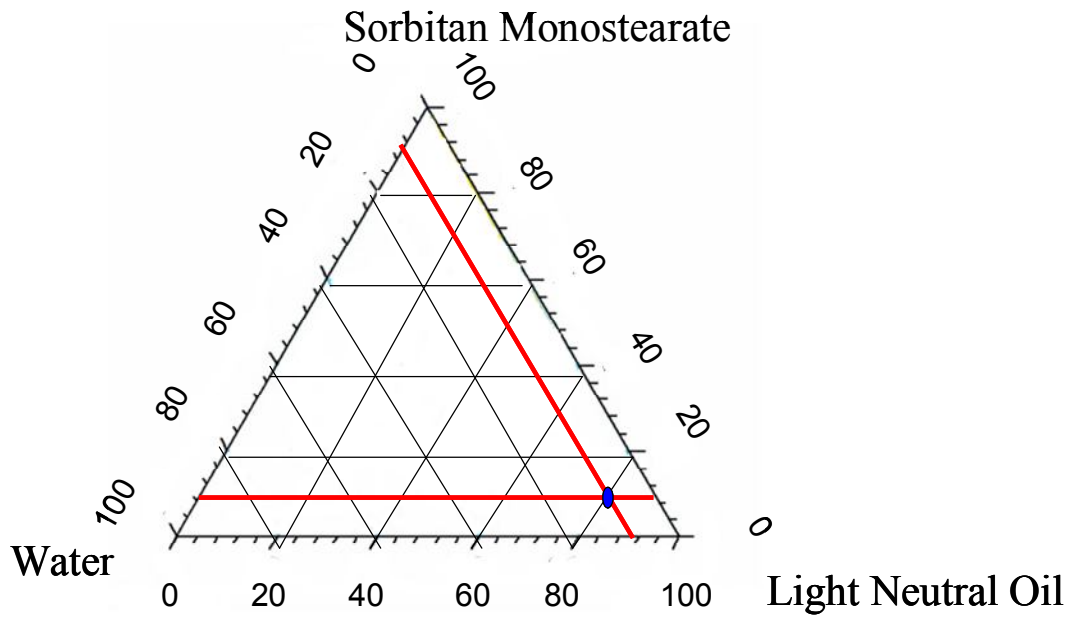
Figure 7.33. Schematic diagram illustrating the composition of oil/water/surfactant system.
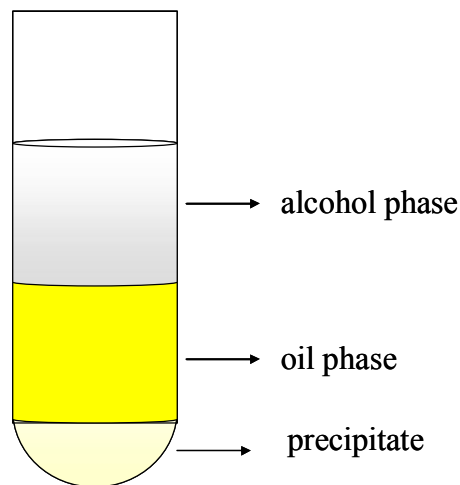
Figure 7.34. Schematic illustration of phase separation after centrifugation of the microemulsions.

Table 7.7. The volume of phases obtained by centrifugation and the amount of produced samples

Microemulsion code	Co-surfactant volume (cm^3)	Total volume (cm^3)	Phase volumes after centrifugation (cm^3)			Wet Sample (g)	Dry Sample (g)	Expected Amount of Zinc Borate (g)
			Oil	Alcohol	Precipitate			
SC-1	30.0	150.0	105.00	37.30	7.70	1.24	1.09	0.178
SC-2	51.5	181.5	96.00	51.50	33.67	1.46	0.14	0.178
SC-3	80.0	200.0	88.78	76.59	34.63	1.29	0.08	0.178
SC-4	102.2	222.2	54.31	114.80	53.09	1.43	0.06	0.178

Morphology of Precipitates

SEM images of the precipitates prepared by two-microemulsion method are given in Figure 7.35. The morphology of the crystals including 30 cm^3 propanol-2 is constructed from layers and the disk-like crystals having nano-sized thickness (Figure 7.35a). However, the spherical crystals are formed by increasing the co-surfactant amount in the emulsion (Figure 7.35b). Mean particle sizes of the fully crystallized powders could be estimated as; 50–100 nm in diameter, Plate like shapes and layers are observed when the co-surfactant amount is increased to 51.50 and 102 cm^3 (Figure 7.35c and 7.35d).

(a) (b)

(c) (d)
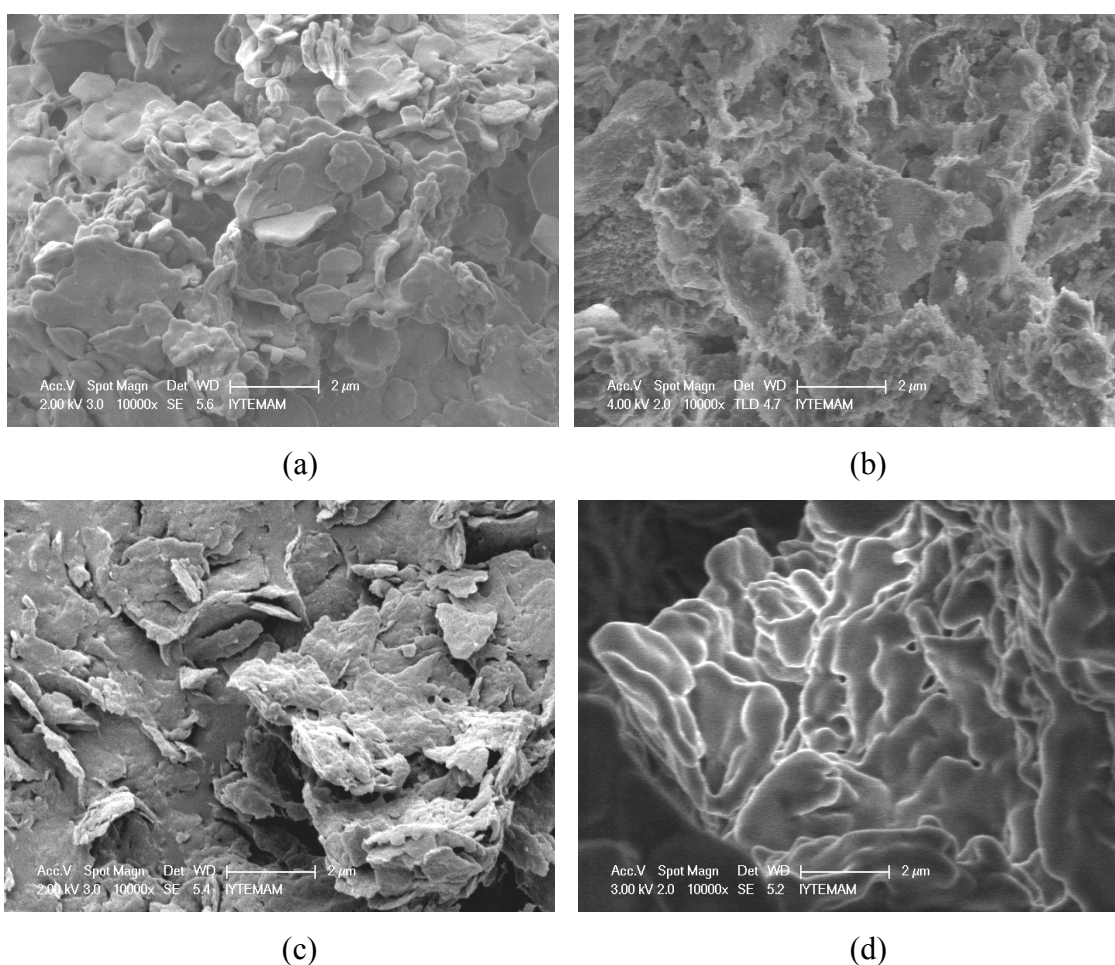
Figure 7.35. SEM images of precipitates obtained in micromemulsions including a) 30.0, b) 51.50 c) 80.0 and d) 102.2 cm^3 propanol-2.

Functional Groups of Precipitate, Oil and Alcohol Phases

FTIR spectra of the obtained precipitates are indicated in Figure 7.36. The peak at 1740 cm^{-1} is due to C=O stretching, the peaks at 1540 and 1398 cm^{-1} are assigned to

antisymmetric and symmetric carboxylate groups (v_aCOO^- and v_aCOO^-), respectively. The presence of specific peaks of the carboxylate groups revealed that the surfactant in the process was saponified. The functional groups of zinc borate and by product sodium nitrate were not observed in FTIR spectra of the precipitate, due to zinc borate's low concentration. The ratio of the absorbance difference at 1745 cm^{-1} to the absorbance difference at 1540 cm^{-1} were calculated and the lowest value was obtained for the precipitate including 80.0 cm^3 co-surfactant per 10 g surfactant which demonstrated that this sample showed the highest saponification. Further the propanol-2 and oil phases of the microemulsions which were obtained after the centrifugation process was investigated by FTIR analysis and FTIR spectra of the oil and propanol-2 phases of the samples are shown in Figures 7.37 and 7.38, respectively. The FTIR spectra of paraffin and propanol-2 phases showed the presence of unchanged surfactant in the phases. FTIR spectra of the propanol-2 phases of the samples indicate the characteristic peaks of propanol-2. The band between 3500-3000 cm^{-1} and the band at 3000-2800 cm^{-1} are attributed to –OH and C-H bonding vibrations. Similar to propanol-2 phase, the oil phase shows the typical peaks of light neutral oil. The bands at 2930 and 2860 cm^{-1} are related to C-H stretching vibrations. However any characteristic peaks of boron based materials can not be detected in these two phases.
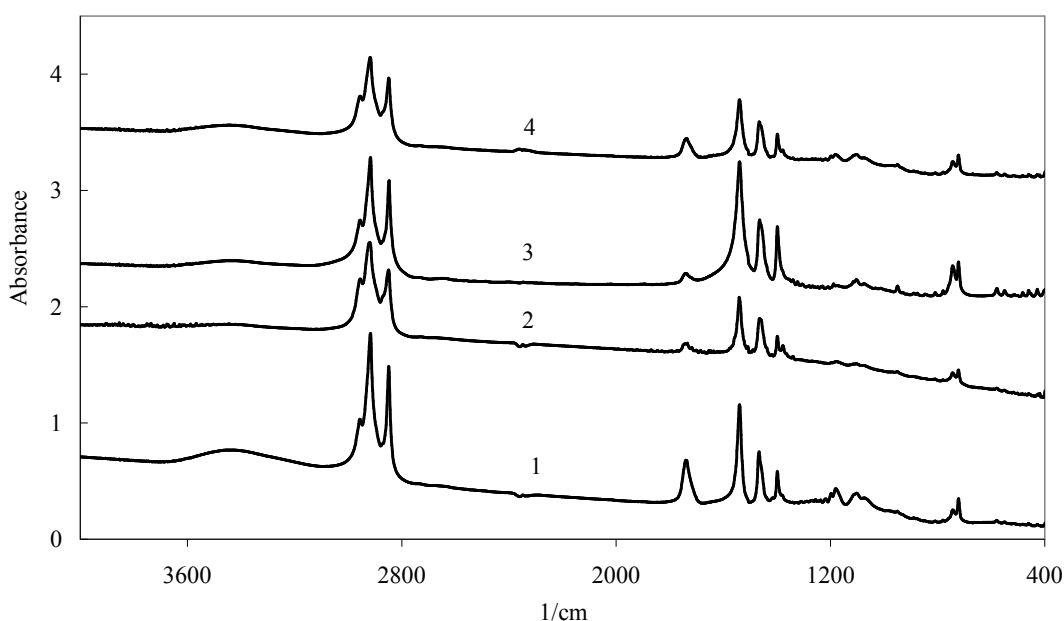
Figure 7.36. FTIR spectra of the precipitates obtained by microemulsions including 1) 30.0, 2) 51.50, 3) 80.0 and 4) 102.20 cm^3 propanol-2.
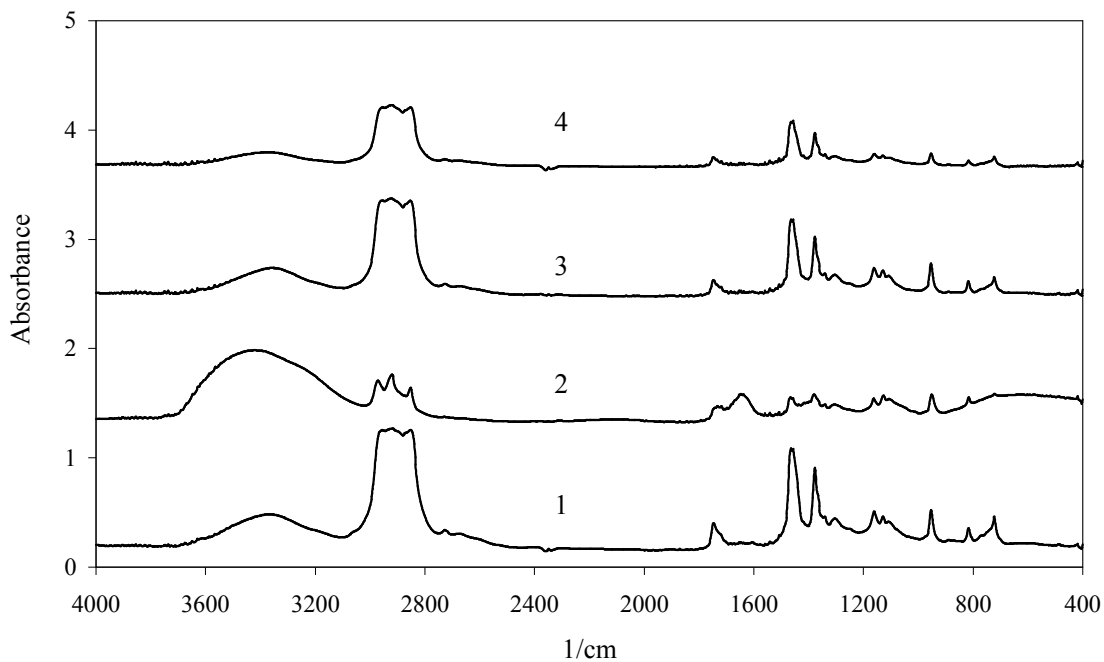
Figure 7.37. FTIR spectra of the oil phase of microemulsions including 1) 30.0, 2) 51.50, 3) 80.0 and 4) 102.20 cm^3 propanol-2.
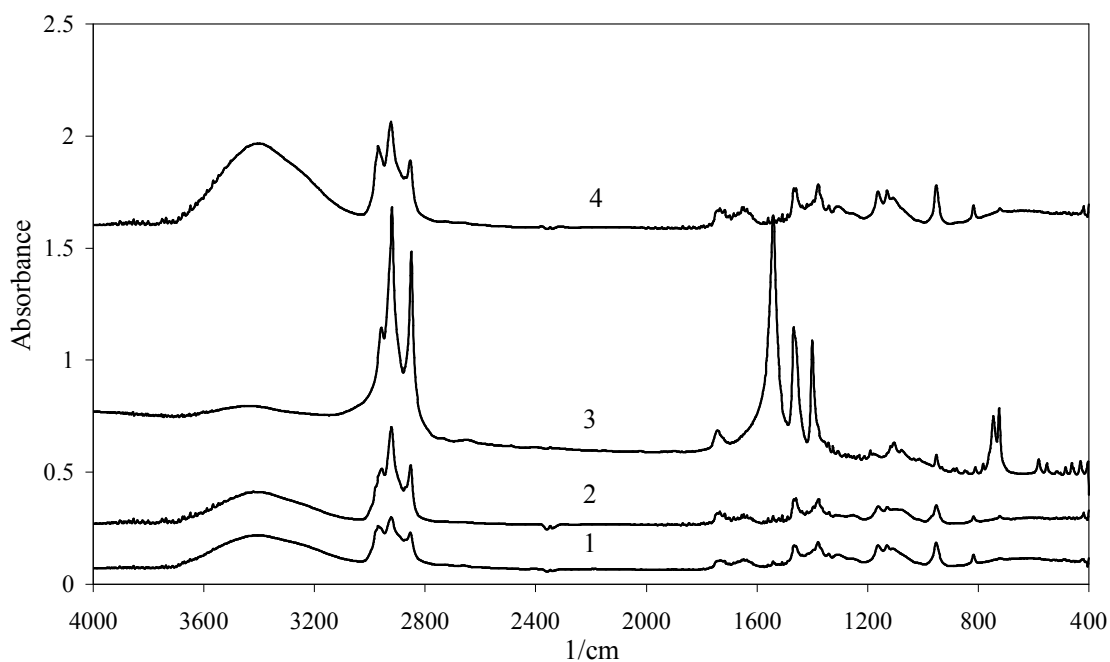
Figure 7.38. FTIR spectra of the prapanol-2 phase of microemulsions including 1) 30.0, 2) 51.50, 3) 80.0 and 4) 102.20 cm^3 propanol-2.

Thermal Behavior of Precipitates

Thermal behavior of the precipitates obtained in microemulsions was determined by both thermogravimetric analysis and differential scanning calorimeter. According to TGA analysis result, the samples had only one degradation step as shown in Figure 7.39. The onset temperature of mass loss and residual mass % at 600 °C are reported in Table 7.8. Unlike Span 60, the onset temperatures of the precipitates are changing from 217 to 273 °C. Moreover the residual mass % values of the precipitates at 600 °C are quite different than the value of Span 60. DSC endotherms of the samples are shown in Figure 7.40 and 7.41. It is more clearly observed that the precipitates have different structure than the surfactant since the surfactant shows endothermic degradation after 300 °C whereas the precipitates indicate exothermic degradation after this temperature which demonstrates a degradation belonging to a compound including oxygen. In order to expose the dehydration behavior of the precipitates the temperatures where endothermic peaks are observed are determined and the results are listed in Table 7.9. Among the samples, the precipitate which includes 40% propanol-2 shows only one endothermic peak before 300 °C. However the other products have two different melting peaks. The endothermic peak at 67 °C might be the melting point of stearic acid (Gönen, 2003), whereas the peak at 124 °C implies the melting of zinc stearate. It may be due to absence of organic acid in this sample and the saponification ratio of this sample is higher than the others.

Elemental compositions of the precipitates were determined by EDX analysis. A typical EDX spectrum of the precipitate prepared by microemulsion containing 80 cm^3 propanol-2 is indicated in Figure 7.42. The boron content of the samples is between 10.81% -15.64% by weight, whereas zinc content of the samples is changing from 2.81% to 6.48% by weight as shown in Table 7.10. The zinc content of the precipitate including 40% propanol-2 has higher than the other samples. Also the detected zinc amounts of the samples are consistent with the zinc content of the precipitates. However, the boron content of the samples was not detected correctly since boron and carbon elements overlapped in EDX spectrum. Therefore the samples might have the chemical composition of zinc stearate and this result was consistent with the FTIR and DSC results.
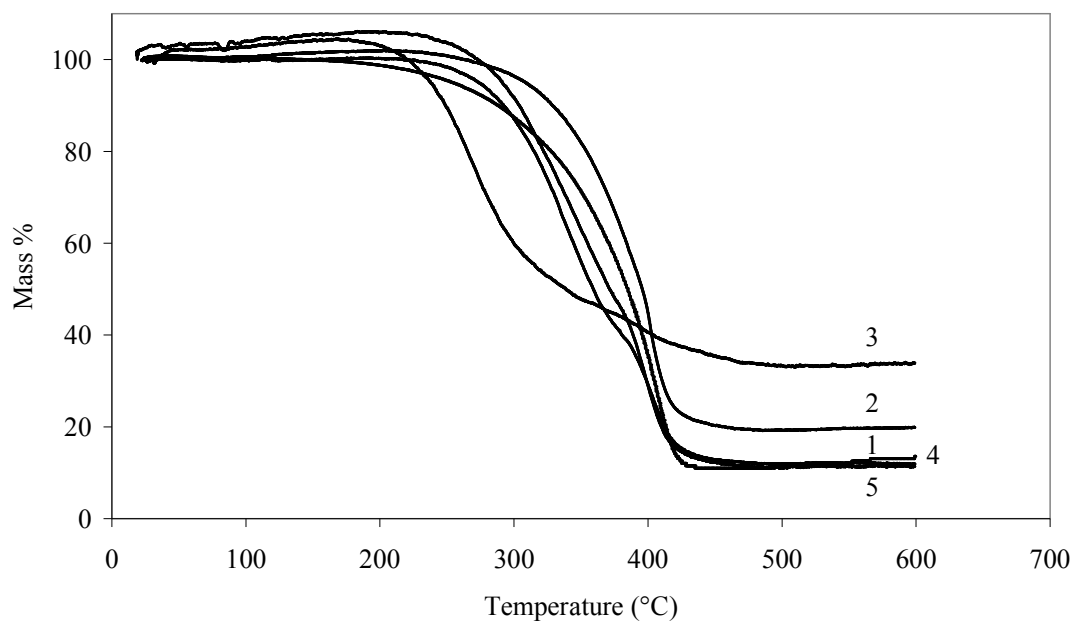
Figure 7.39. TGA thermogram of 1) Span 60, and the precipitates obtained by microemulsions including 2) 30.0, 3) 51.50, 4) 80.0 and 5) 102.20 cm^3 propanol-2.

Table 7.8. Onset temperature and residual mass percentages at 600 °C for Span 60 and the precipitates obtained in microemulsion.

Sample	Onset temperature (°C)	Residual Mass % at 600°C
Span-60	148	13.61
SC-1	263	19.88
SC-2	220	33.94
SC-3	217	11.93
SC-4	273	11.37
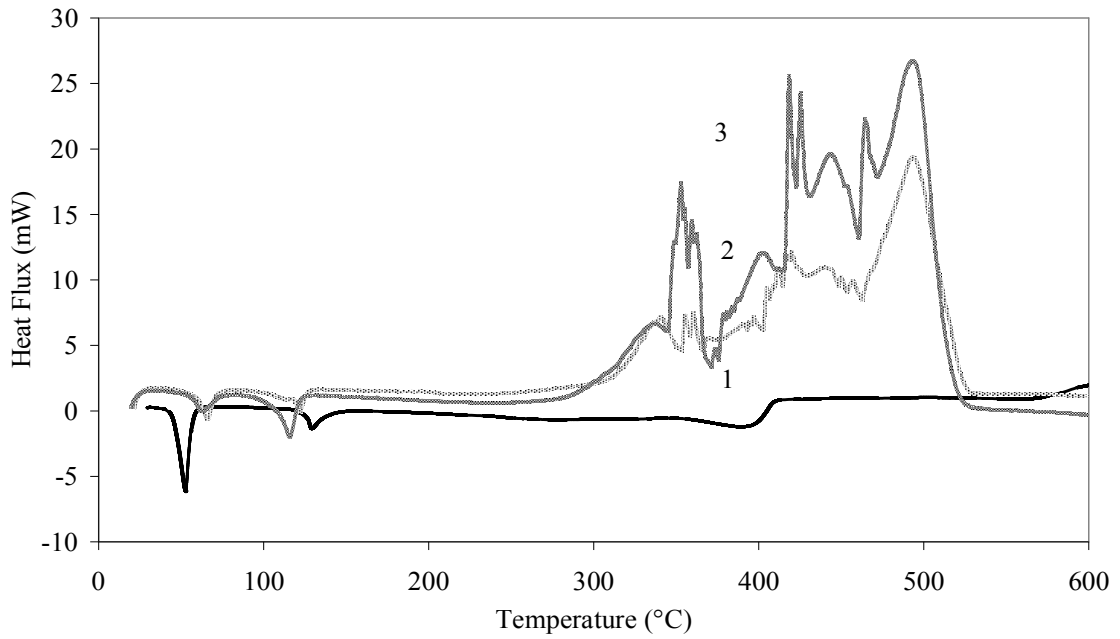
Figure 7.40. DSC curves of 1) Span 60 and precipitates obtained by microemulsions including 2) 30.0, 3) 51.5 cm^3 propanol-2.
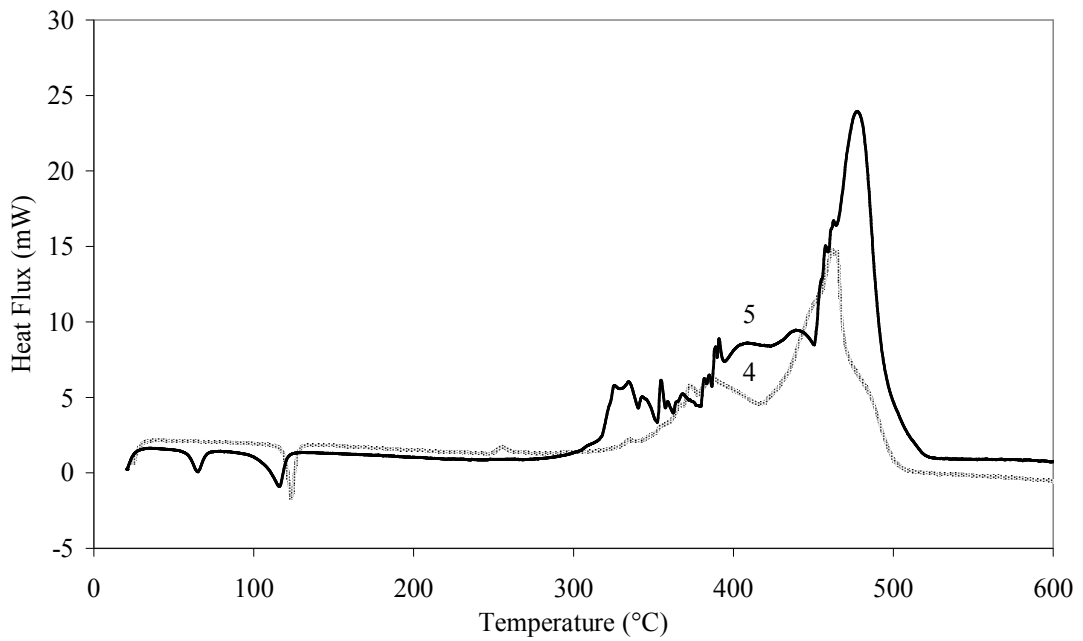
Figure 7.41. DSC curves of the precipitates obtained by microemulsions including 4) 80.0, 5) 102.2 cm^3 propanol-2.

Table 7.9. Dehydration behavior of the precipitates obtained in microemulsion.

Sample	First Peak				Second Peak			
	Onset (°C)	Endset (°C)	Maximum (°C)	ΔH (J/g)	Onset (°C)	Endset (°C)	Maximum (°C)	ΔH (J/g)
SC-1	58.02	71.96	65.98	-53.89	100.20	126.91	121.83	-50.65
SC-2	52.62	75.05	62.63	-29.38	104.34	122.19	115.77	-62.24
SC-3	-	-	-	-	118.41	128.34	123.45	-129.91
SC-4	54.05	74.28	65.14	-28.31	100.62	121.89	115.91	-50.65
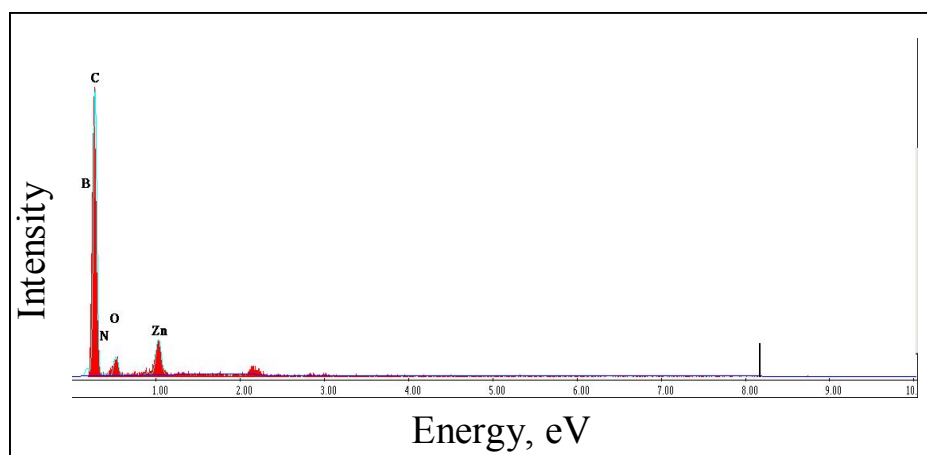
Figure 7.42. EDX spectrum of the precipitate obtained by microemulsion including 80 cm^3 propanol-2.

Table 7.10. Elemental composition of the precipitates produced in microemulsion

Element	Average Weight %		
	SC-1	SC-3	SC-4
B	15.64	10.81	13.42
C	76.46	77.58	79.38
N	1.16	0.65	1.11
O	3.41	4.49	3.03
Zn	3.34	6.48	2.81

The characterization results of the precipitates obtained by microemulsion revealed that zinc stearate or stearic acid were formed instead of zinc borate. The

microemulsions pH values were measured to explain why zinc borate could not be synthesized. The pH values of zinc nitrate, borax decahydrate and zinc borate emulsions were found as 4.68, 8.20 and 7.74, respectively. It was understood that the surfactant might undergo a change due to the acidic medium and form organic compounds. The suggested reaction of the formation of stearic acid after hydrolysis is demonstrated in Equation 7.4.

$$H_2O \; + \; \text{—R—}\overset{\displaystyle O}{\overset{\|}{C}}\text{—O—R'} \; \xrightarrow{\; OH^- \;} \; R\text{—}\overset{\displaystyle O}{\overset{\|}{C}}\text{—OH} \; + \; R'\text{—OH} \tag{7.4}$$
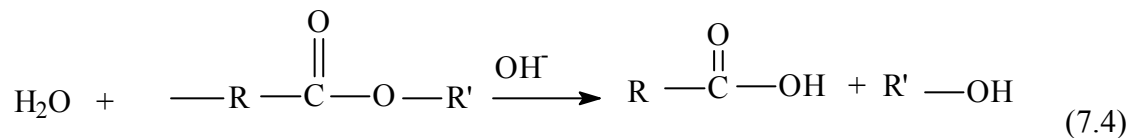
where R denotes the stearyl group. The ester group of sorbitan monostearate reacted with water and formed stearic acid and alcohol. The stearic acid might react with hydroxyl and zinc ions to give zinc stearate as shown in Equation 7.5.

$$R\text{—}\overset{\displaystyle O}{\overset{\|}{C}}\text{—OH} \; + \; OH^- \; + \; Zn^{2+} \; \longrightarrow \; \left(R\text{—}\overset{\displaystyle O}{\overset{\|}{C}}\text{—O}^- \right) Zn^{2+} \tag{7.5}$$
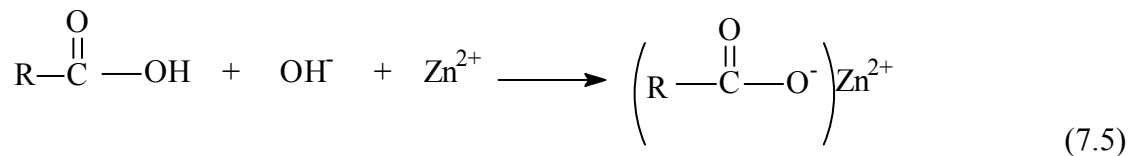
7.4. Characterization of PVC-Zinc Borate Films

PVC films are generally formed by using a plasticizer or this polymer can be dissolved in any polar ethers. Tetrahydrofurane is one of the solvents capable of dissolving PVC as well, and is the main ingredient in PVC adhesives. PVC films including zinc borate have potential use in flame retardancy application and heat stabilization of PVC (Pi et al., 2002; Erdoğdu et al., 2009). In this study, zinc borate inverse emulsion was added to PVC-THF solution to determine the particle size of the zinc borate particles and to obtain a uniform dispersion in the composite film. The optical microphotographs of these films are presented in Figure 7.43. It is observed that two phases are obtained in control PVC film and when oil is added to the film quadrilateral structure is formed. Besides them, the addition of zinc borate emulsion produces spherical droplets having diameters between 1-10μm. These might be the

micelles that contain zinc borate. In order to get a better visualization, scanning electron microscopy was used and the images in Figure 7.44 were taken. It was observed that PVC control film had some particles on the surface due to some impurities of PVC (Figure 7.44a). When the bottom precipitate of zinc borate emulsion was added to PVC-THF solution, the obtained film had more particulate structure because of the dispersion of zinc borate particles (Figure 7.44b). The particle size of the zinc borate particles was found as 100-200 nm. In Figure 7.44c, spherical droplets having diameters lower than 1 µm were observed on the surface of PVC film. It was thought that these droplets might be the micelles that contain zinc borate.

PVC control film (F1), PVC film contains the bottom precipitate of zinc borate inverse emulsion prepared by magnetic stirrer (F4), PVC film contains zinc borate emulsion prepared by homogenizer (F5) were used for elemental analysis. In order to find the elemental composition of the control film, the whole area was scanned, while the surfaces of particles were scanned for the composite films. The obtained results are presented in Table 7.11. Due to the absence of zinc borate in the control film, B, N, Zn elements were not detected, but the composite films including zinc borate emulsion precipitate and zinc borate emulsion had 22.87% and 21.83% boron element, respectively.

(a)

(b)

(c)

(d)

(e)
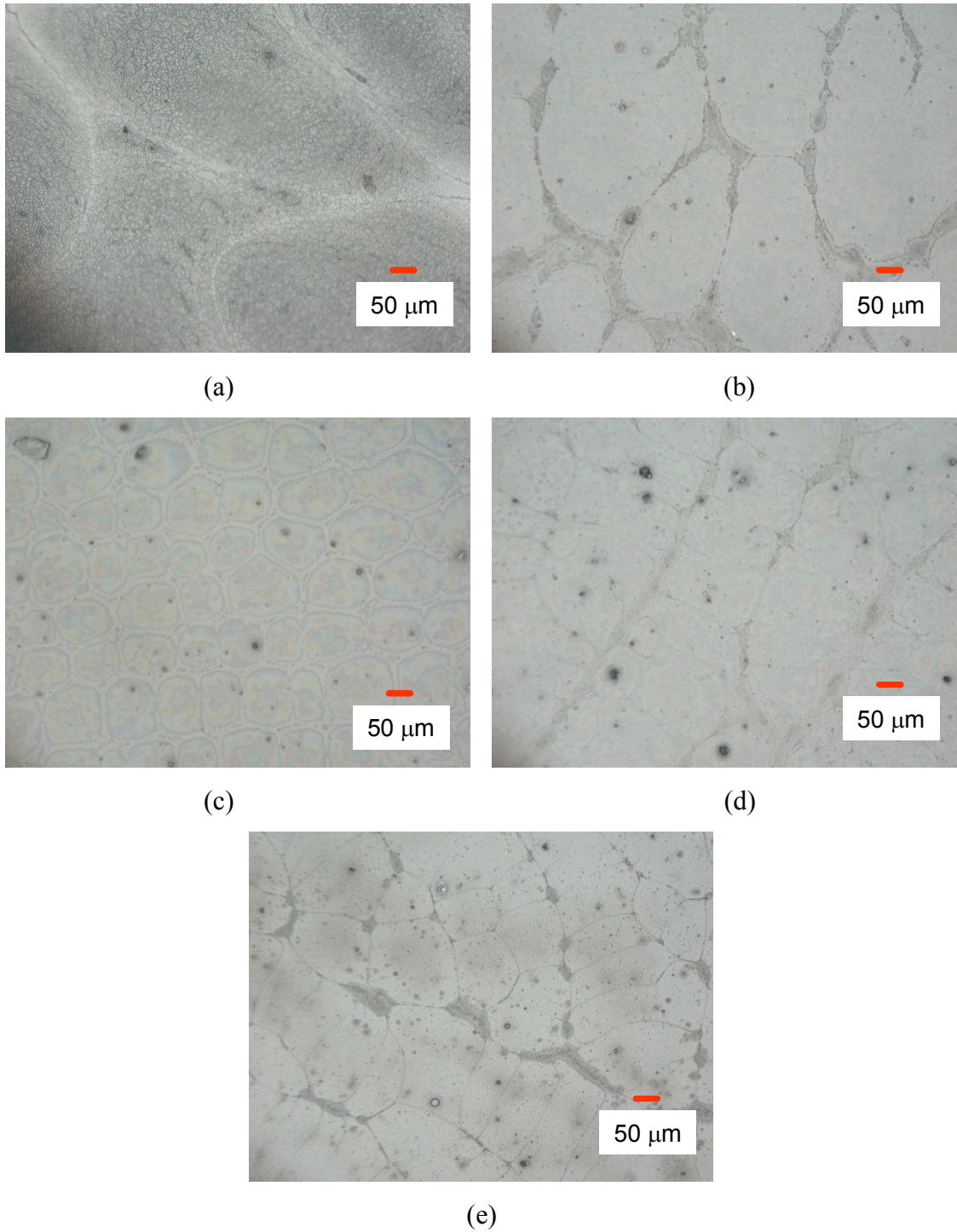
Figure 7.43. The microphotographs of a) PVC film (F1) b) PVC film includes light neutral oil containing 1 wt % surfactant (F2) c) PVC film contains zinc borate inverse emulsion prepared by magnetic stirrer and heated up to 160 °C (F3) d) PVC film contains the bottom precipitate of zinc borate inverse emulsion prepared by magnetic stirrer (F4) e) PVC film contains zinc borate emulsion prepared by homogenizer (F5).

(a)   (b)

(c)
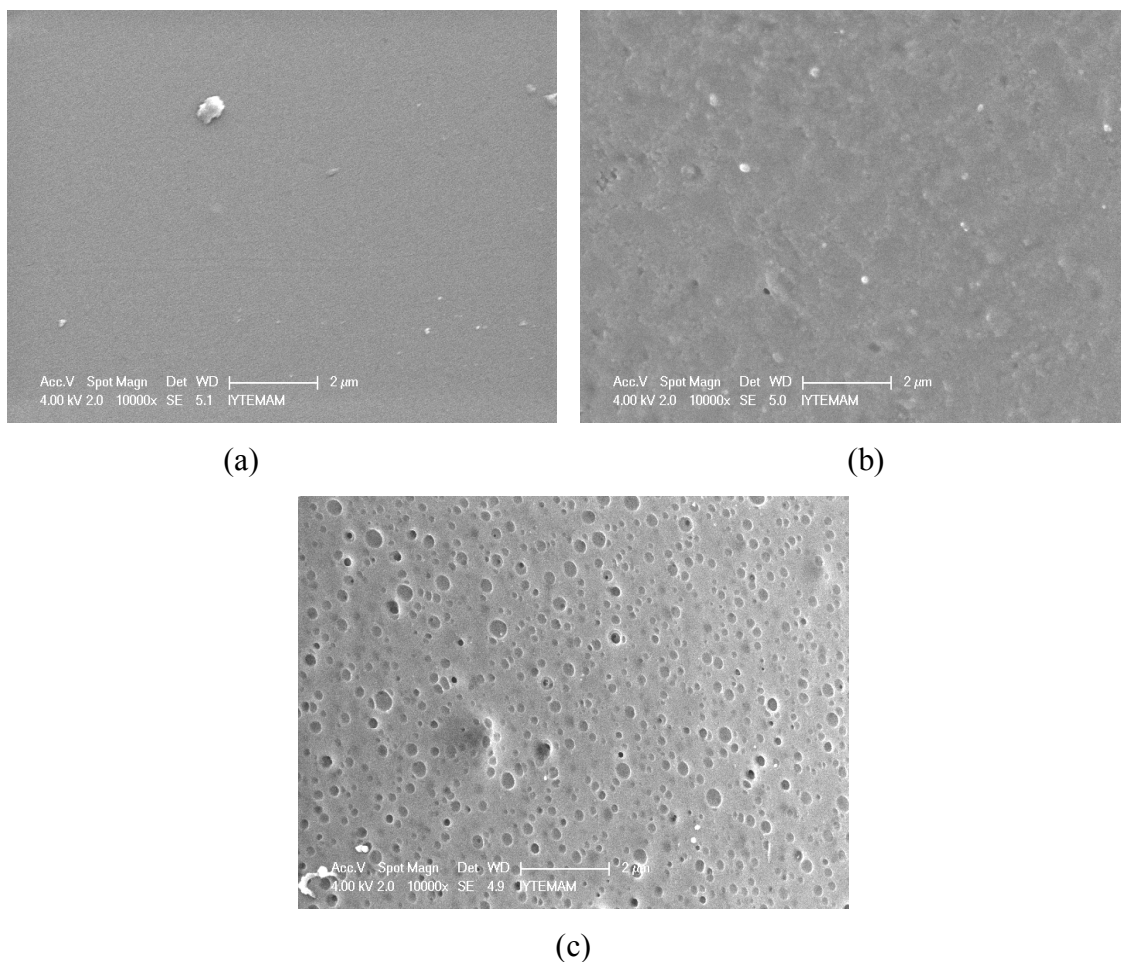
Figure 7.44. The SEM images of a) PVC film (F1) b) PVC film contains the bottom
precipitate of zinc borate inverse emulsion prepared by magnetic stirrer
(F4) c) PVC film contains zinc borate emulsion prepared by homogenizer
(F5).

Table 7.11. The chemical composition of PVC-zinc borate composite films

Element	Samples		
	PVC control film	**PVC film contains the bottom precipitate of zinc borate emulsion (F4)**	**PVC film contains zinc borate emulsion prepared by homogenizer (F5)**
	Wt%	Wt%	Wt%
C	58.93	60.37	67.57
O	1.03	4.22	1.48
Cl	40.04	8.49	6.55
B	0	22.87	21.83
N	0	1.81	1.53
Zn	0	2.25	1.06

In order to understand whether the dispersed particles on the PVC-zinc borate composite films were zinc borate or not, boron, zinc and carbon elements mappings were achieved by energy dispersion of X-ray (EDX). The mapping results of these elements are shown in Figures 7.45, 7.46 and 7.47. From Figures 7.45a, 7.46a and 7.47a, it can be seen that elements boron, zinc and carbon are well dispersed on the surface of the films including zinc borate inverse emulsion, but their contents are different. The existence of the elements boron and zinc indicates that the dispersed particles on the PVC films might be zinc borate. When the precipitated part of the emulsion was added to PVC suspension, it was expected that this film would present high concentration of zinc borate compared to the one including the emulsion. However, the number of green shiny spots which demonstrate the concentration of zinc element (Figure 7.46b) is lower than the one in Figure 7.46a. Also this unexpected result might be due to the film sample placed on the sample holder. The sample could not reflect the whole film since there might be a heterogeneous dispersion of the particles on the film surface. The map of carbon element is presented in Figure 7.47 and it implies that the films have high concentration of carbon element which exactly corresponds with PVC, sorbitan monostearate and mineral oil.

(a)   (b)
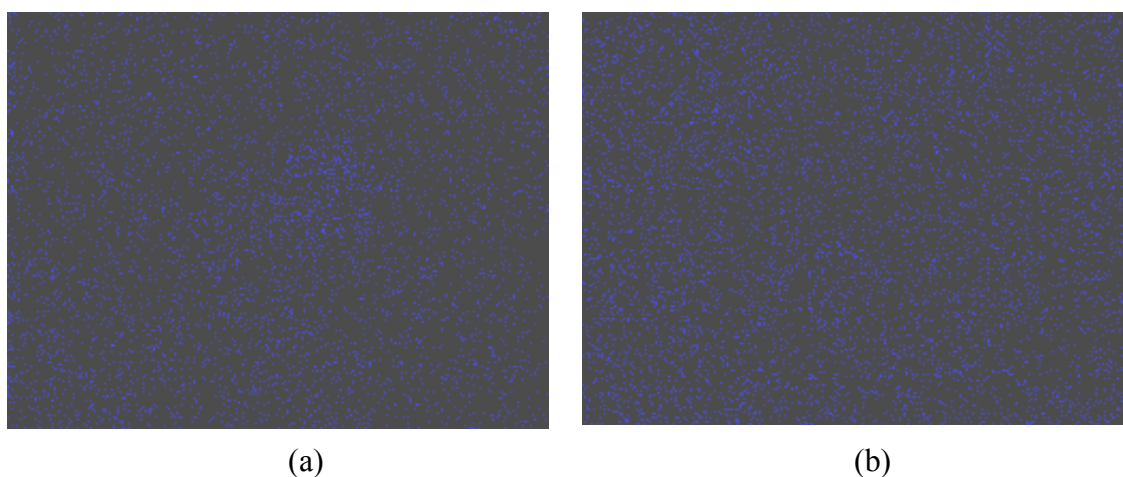
Figure 7.45. Boron mapping of a) PVC film contains zinc borate inverse emulsion prepared by magnetic stirrer and heated up to 160 °C (F3) and b) PVC film contains the bottom precipitate of zinc borate inverse emulsion prepared by magnetic stirrer (F4).

<center>(a)   (b)</center>
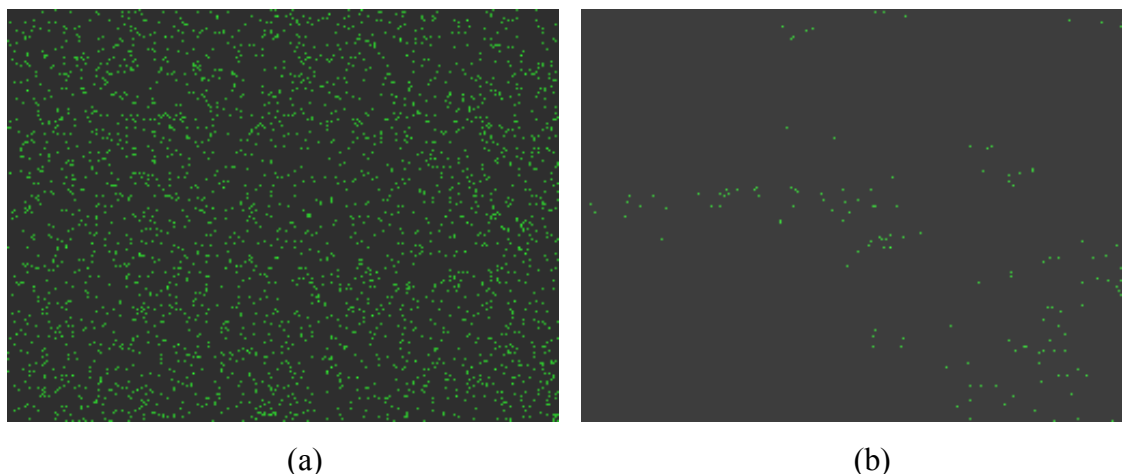
Figure 7.46. Zinc mapping of a) PVC film contains zinc borate inverse emulsion prepared by magnetic stirrer and heated up to 160 °C (F3) and b) PVC film contains the bottom precipitate of zinc borate inverse emulsion prepared by magnetic stirrer (F4).

<center>(a)   (b)</center>
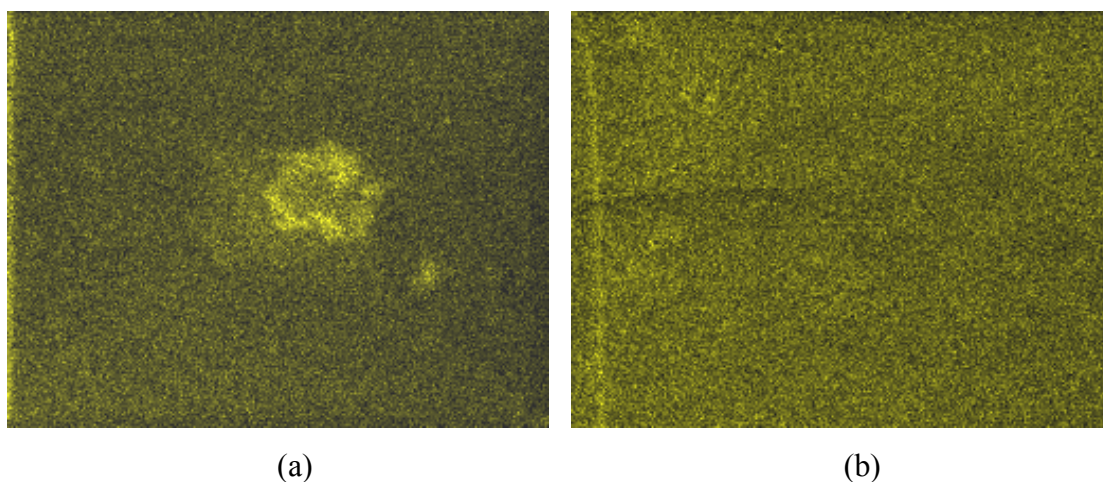
Figure 7.47. Carbon mapping of a) PVC film contains zinc borate inverse emulsion prepared by magnetic stirrer and heated up to 160 °C (F3) and b) PVC film contains the bottom precipitate of zinc borate inverse emulsion prepared by magnetic stirrer (F4).

7.5. Zinc Borate Synthesis in Aqueous Phase

The dispersion stability of lubricating oil additives play a major role in the preparation of lubricants. In literature it is implied that the dispersion property of nanoparticles in base oil is superior to micron particles in lubrication systems (Hu et al., 1999). Therefore, it is important to study lubricating oil additives of nanoparticles considering low cost in the production method. The preparation methods generally can

be classified as solid, gas, and liquid methods. Liquid methods, including the precipitation method, hydrothermal treatment, spray drying, spray thermal decomposition, freeze drying, the microemulsion method, the phase transfer technique, and supercritical fluid drying, were widely used. In this part of the study, conventional precipitation technique and coordination homogeneous technique were used to synthesize zinc borate in aqueous phase. Surface modifier, Span 60 was used with the raw materials in the conventional aqueous phase precipitation, whereas ammonia was required for the coordination homogeneous precipitation technique.

7.5.1. Zinc Borate Synthesis via Precipitation

In literature it was indicated that the transfer of the structure from a variety of organic templates (e.g. PEG, PVP, CTAB etc.) to the inorganic product allowed for the formation of otherwise unattainable inorganic structures (Shi et al., 2009). However, there is no study dealing with preparation of zinc borate in the presence of sorbitan monostearate. Therefore, in the scope of our research, it was aimed to produce zinc borate via precipitation method in the presence of a surface modifier. The zinc borate particles were characterized by FTIR, TGA, DSC, SEM and EDX analysis.

SEM images of zinc borate produced in the presence of sorbitan monostearate are shown in Figure 7.48. Micron sized prismatic crystals as well as lamellar-like crystals are observed in Figure 7.48. Closer inspection reveals that the lamellar-like crystals are the conglomeration of lots of rods having 500 nm thicknesses. According to elemental analysis of the prepared zinc borate, it contains both carbon and hydrogen elements (Table 7.12). The presence of carbon element for the sample formed by precipitation technique arises from the sorbitan monostearate and the C% (1.91%) demonstrates that this sample contains 2.85% sorbitan monostearate since 1 gram of this surfactant includes 67 %C element by weight. On the other hand, the water content of the sample is 26.02% in accordance with its hydrogen element content and this value is close to water content of $2ZnO \cdot 3B_2O_3 \cdot 7H_2O$ type zinc borate which is reported by Briggs (Briggs, 2001). Particle size distribution of zinc borate produced in the presence of sorbitan monostearate is indicated in Figure 7.49. The volume weighted mean particle diameter of the sample is 27.71 μm. The FTIR spectrum of zinc borate prepared via precipitation technique in the presence of sorbitan monostearate is shown in Figure

7.50 and it exhibits both the specific peaks of the surfactant and the zinc borate having seven moles of crystal water ($2ZnO \cdot 3B_2O_3$ $7H_2O$). The characteristic peaks of zinc borate are assigned referring the literature (Gao et al., 2009c). The band at 1047 cm^{-1} is the stretching of B(4)-O, and the peaks between 745-658 cm^{-1} are belonging to out-of-plane bending mode of B(3)-O. The decrease in the intensity of the specific peaks of the surfactant (at 2850, 2920 cm^{-1}) reveals that the sorbitan monostearate is partially removed from the samples during the washing process. Figure 7.51 shows the XRD pattern of the zinc borate produced via precipitation technique in aqueous medium. The presence of peaks with high intensity shows that product has a crystalline structure. The major peaks in XRD pattern of zinc borate are observed at 13.07°, 17.58°, 19.66°, 25.54°, 26.38°, 27.04°, 29.42° and 36.97° 2θ values. When these values were compared with those in the JPDS database, it was implied that the specific peaks were consistent with those of $Zn(B_3O_3(OH)_5) \cdot H_2O$. In literature this type of zinc borate was also defined as $2ZnO \cdot 3B_2O_3 \cdot 7H_2O$ (Eltepe et al., 2007). Moreover, no other crystalline phases can be detected, which is indicative of pure $2ZnO \cdot 3B_2O_3 \cdot 7H_2O$ obtained under the current synthetic conditions. All the diffraction peaks can be perfectly indexed to $2ZnO \cdot 3B_2O_3 \cdot 7H_2O$. (JPDS PDF File Number 721789). TGA thermogram of zinc borate indicates that mass loss of the sample is 22.08% due to the removal of water of crystallization (Figure 7.52). In accordance with the elemental analysis, the sample contained 2.85% sorbitan monostearate. The water loss of the surfactant was 53% according to its TGA thermogram. Therefore the mass loss of the surfactant for this amount was evaluated as 1.52%. The remaining mass loss (20.56%) was due to the condensation of hydroxyl groups of zinc borate sample. 20.56% is close to the value indicating the water content of the sample evaluated from elemental analysis. Therefore all the characterization results imply that $2ZnO \cdot 3B_2O_3 \cdot 7H_2O$ is formed when borax decahydrate and zinc nitrate are used at 70 °C in the presence of the surfactant. Moreover, DSC curve of the product is given in Figure 7.53. For sorbitan monostearate, the endothermic peak at 50 °C is observed due to the melting of sorbitan monostearate and the heat of melting is evaluated as 3.50 J/g. Also, the peaks between 100-200 °C are related to evaporation of free water. The endotherms of zinc borate samples show the removal of interstitial water and the dehydration energy for the zinc borate prepared by precipitation technique is 172.22 J/g. The dehydration energies for the zinc borate produced via the same technique by using zinc oxide and boric acid were between 385.7

and 457.3 J/g (Gönen, 2009). The difference in the energies was observed since the condensations of B-OH groups in zinc borate structures were different.

(a)   (b)
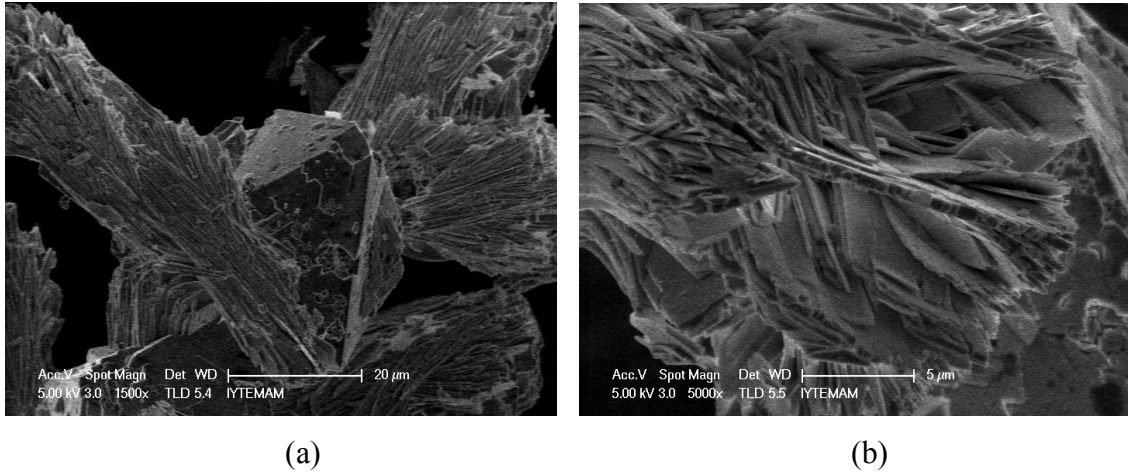
Figure 7.48. SEM images of zinc borate produced in the presence of sorbitan monostearate a) 1500x b) 5000x magnifications.

Table 7.12. Elemental composition of zinc borate

Element	Av. Wt %
C	1.91
H	2.89
N	0
S	0
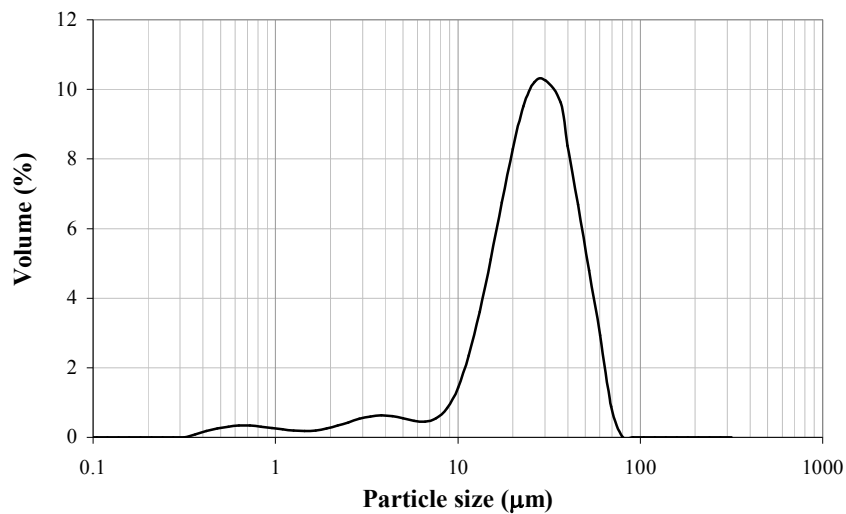
Figure 7.49. Particle size distribution of zinc borate produced in the presence of sorbitan monostearate.
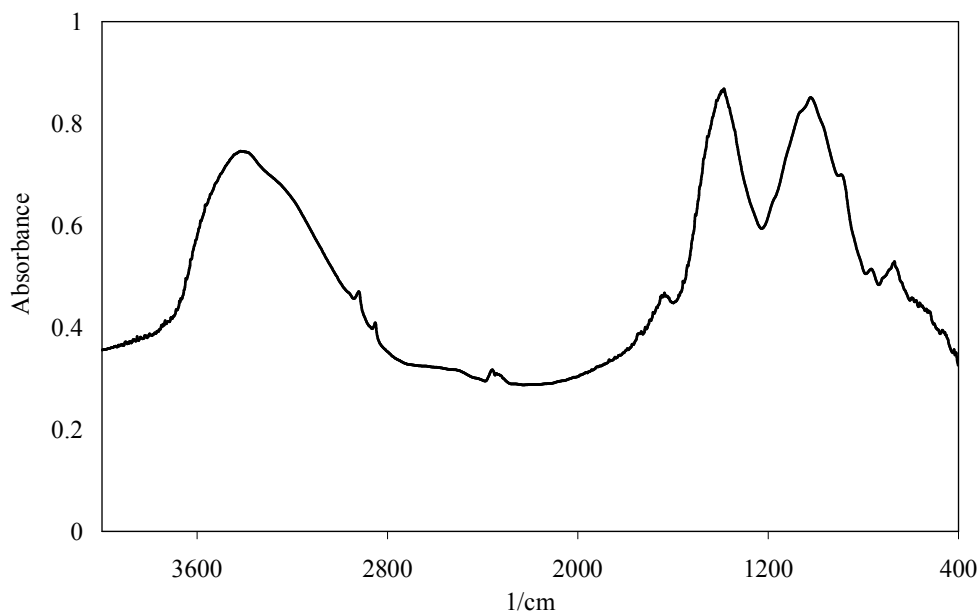
Figure 7.50. FTIR spectrum of zinc borate produced via precipitation technique in the presence of sorbitan monostearate.
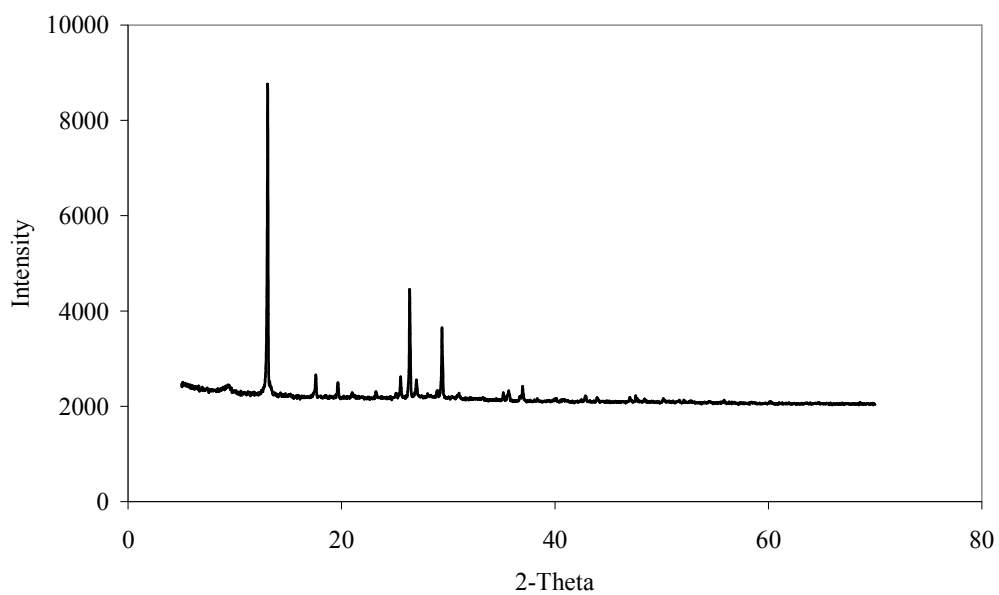
Figure 7.51. XRD pattern of zinc borate produced via precipitation technique in the presence of sorbitan monostearate.

136
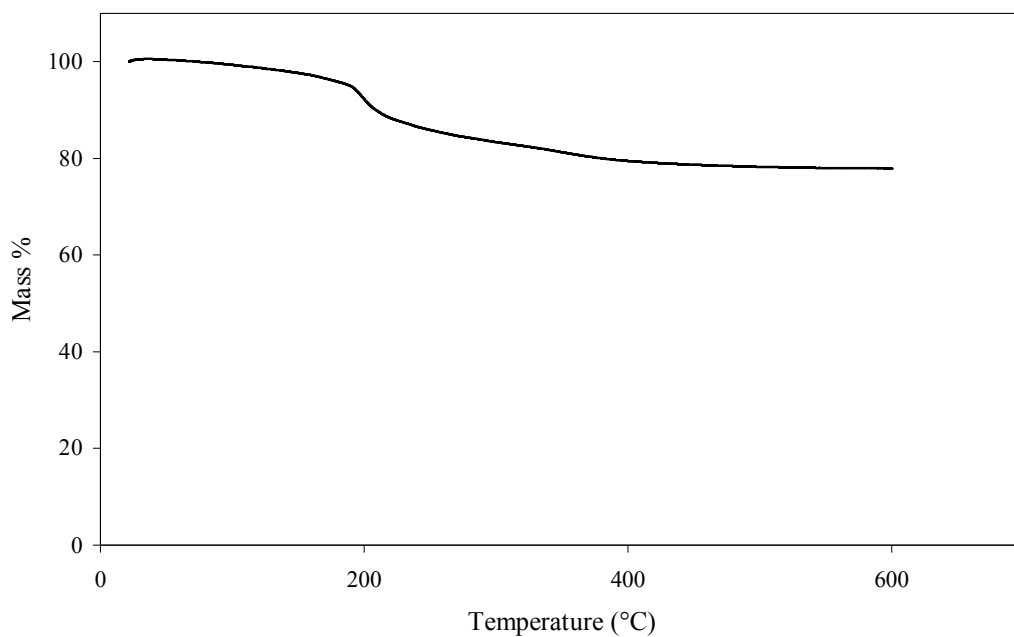
Figure 7.52. TGA thermogram of zinc borate produced via precipitation technique in the presence of sorbitan monostearate.
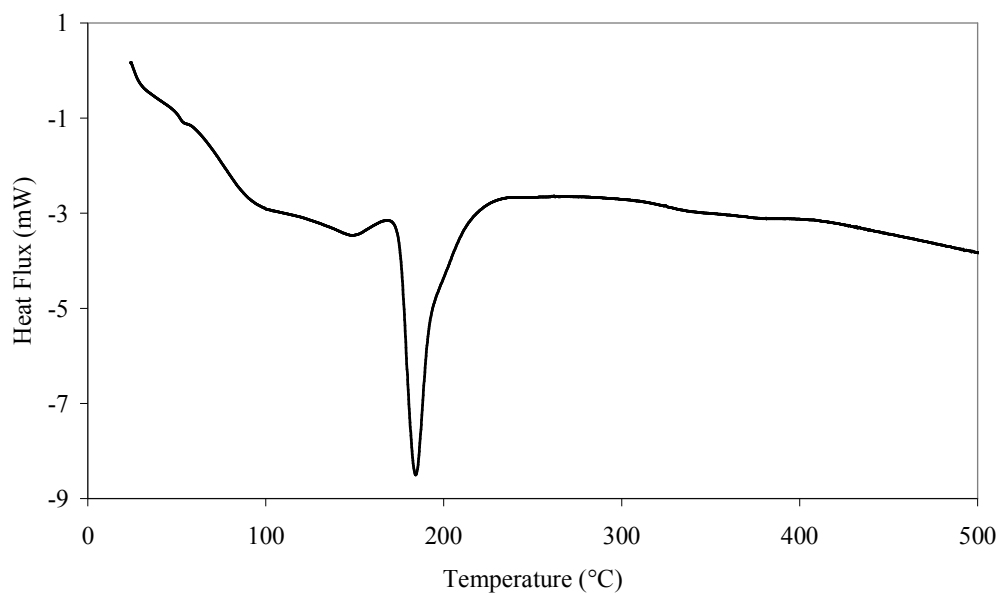
Figure 7.53. DSC curve of zinc borate produced via precipitation technique in the presence of sorbitan monostearate.

7.5.2. Synthesis of Zinc Borate via Coordination Homogeneous Precipitation Technique

Homogeneous precipitation technique was developed by Ting et al. (2009) and this method provided information to produce nano-sized zinc borate particles. The mechanism of this precipitation method is explained by the equations below; firstly, zinc nitrate and borax decahydrate dissociates to its ions in the solutions according to In Equation 7.6, borax dissolves in aqueous phase according to form tetra borate anion $[B_4O_5(OH)_4]^{2-}$ and sodium cation In Equation 7.7, zinc nitrate dissolves to produce zinc cations and nitrate anions. The formed polyborate anions and zinc cations precipitate when mixed together as shown in Equation 7.8. $Zn[B_4O_5(OH)_4]_{(s)}$ react with ammonia, forming a complex solution coexisting with precipitator borax in solution 1. Borate sediments are formed in the solution when the zinc ions reach a certain amount. Because the metal ions and the precipitator are dispersed in the solution homogeneously, thus the precipitation reaction of metal ions and precipitator can reach molecular level, which ensures the sedimentation of desired nanomaterials yielding and separating out homogeneously from the solution. The precipitation mechanism based on the formation of $Zn(NH_3)_4^{2+}{}_{(aq)}$ complex, therefore a few Zn^{2+} ions present in the solution which inhibits the enlargement of the zinc borate crystals and provides to produce nano-sized particles. However at higher pH values (10-12) Zn^{2+} ions reacts with OH^- and NO_3^- ions to form zinc hydroxyl nitrate. The possible reaction is shown in Equation 7.15.

$$Zn(NO_3)_2 \cdot 6H_2O \quad \rightarrow \quad Zn^{2+} + 2NO_3^- + 6H_2O \text{ (solution 1)} \qquad (7.6)$$

$$Na_2B_4O_7 \cdot 10H_2O \quad \rightarrow \quad 2Na^+{}_{(aq)} + B_4O_5(OH)_4{}^{2-}{}_{(aq)} + 8H_2O_{(l)} \text{ (solution 2)} \qquad (7.7)$$

$$Zn^{2+}{}_{(aq)} + B_4O_5(OH)_4{}^{2-}{}_{(aq)} \quad \rightarrow \quad Zn[B_4O_5(OH)_4]_{(s)} \qquad (7.8)$$

$$\text{Solution 1 + Solution 2} \quad \rightarrow \quad Zn[B_4O_5(OH)_4]_{(s)} + yH_2O \qquad (7.9)$$

$$Zn[B_4O_5(OH)_4]_{(s)} + 4NH_3{}_{(l)} \quad \rightarrow \quad Zn(NH_3)_4{}^{2+}{}_{(aq)} + B_4O_5(OH)_4{}^{2-}{}_{(aq)} \qquad (7.10)$$

$$Zn(NH_3)_4{}^{2+}{}_{(aq)} \quad \rightarrow \quad Zn^{2+}{}_{(aq)} \; + \; 4NH_3 \, (g) \tag{7.11}$$

$$B_4O_5(OH)_4{}^{2-}{}_{(aq)} + Zn^{2+}{}_{(aq)} + H_2O_{(l)} \longrightarrow Zn[B_4O_5(OH)_4]\cdot H_2O_{(s)} \tag{7.12}$$

$$Zn[B_4O_5(OH)_4]\cdot H_2O_{(s)} + 2H_2O_{(l)} \longrightarrow Zn[B_3O_3(OH)_5] \, H_2O_{(s)} + B(OH)_{3(s)} \tag{7.13}$$

$$Zn[B_3O_3(OH)_5] \, H_2O_{(s)} \longrightarrow Zn[B_3O_3(OH)_5]_{(s)} + H_2O_{(l)} \tag{7.14}$$

$$5Zn^{2+} + 8OH^- + 2NO_3{}^- + 2H_2O \longrightarrow Zn_5(OH)_8(NO_3)_2\cdot H_2O_{(s)} \tag{7.15}$$

The streams defined in the production of zinc borate by coordination homogeneous precipitation are shown in Figure 7.54, while the amounts of main components of the streams are indicated in Table 7.13. F1, F2, F4 and F6 streams show the amounts of main components at inlet. The predicted amounts of NH3, B and Zn element in F7 stream are also displayed. F8 stream indicates the removal of ammonia and water by heating and it is assumed that all of the ammonia is removed at the end of 15 h. The obtained dried sample after 15 h mixing is found as 2.36 g. In Table 7.13 the amounts of B and Zn in F11 stream show that this sample includes 0.31 g and 0.62 g B and Zn, respectively. The efficiency of this process is calculated as 48.94% considering the number of moles of zinc at inlet and outlet.
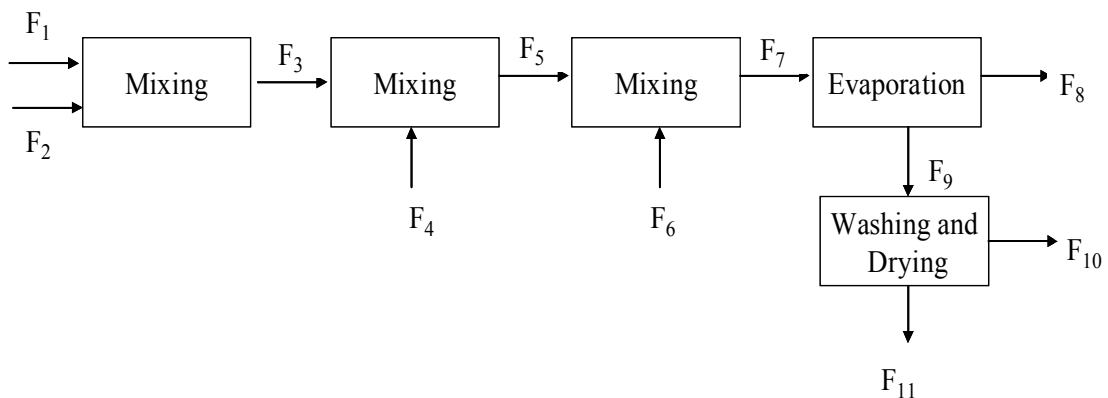
Figure 7.54. Streams in zinc borate production by coordination homogeneous precipitation.

Table 7.13. The amount of stream and the amounts of main components in the streams.

Stream Code	Stream	Amount	Amounts of main components in the streams , g		
			NH_3	B	Zn
F_1	Borax solution	30 cm^3	-	1.08	-
F_2	Zinc nitrate solution	20 cm^3	-	-	1.63
F_4	NH_3 solution (25%)	12.5 cm^3	2.85	-	-
F_6	H_2O	75 cm^3	-	-	-
F_7	$Zn(NH_3)_4^{2+}$ $B_4O_5(OH)_4^{2-}$ $2NaNO_3$ H_2O	137.5 cm^3	2.85	1.08	1.63
F_8	$H_2O + NH_3$	116 cm^3	2.85	-	-
F_{11}	Dried solid	2.36 g	-	0.23	0.80

The pH values of the aqueous solutions were recorded with respect to time for different periods. The results are shown in Figures 7.55 and 7.56. At the end of 3, 6, 12 and 15 hours pH values are 8.79, 8.22, 6.55 and 5.29, respectively. Table 7.14 demonstrates the amount of wet and dry samples at the end of 3, 6, 12 and 15 hours. When the mixing period is increased it is seen that the dry amount of the samples increases, accordingly. The difference between the amounts of wet samples washed with only ethanol and the samples washed with both ethanol and water is related to the amount of $NaNO_3$ formed in the solution. However it is removed from the solution by washing with water. The amounts of removed $NaNO_3$ are 0.4, 0.27, 0.51, and 5.85 g for the samples stirred for 3, 6, 12 and 15 hours, respectively.

In order to calculate the moles of water evaporated from the solution with respect to time, the whole amount removed from the solution was assumed as only water since ammonia had low concentration in the solution. Water removed from 8 cm diameter beakers. Figure 7.57 demonstrates the evaporation of water with respect to time. When the time was increased, the amount of water evaporated from the solution increased, accordingly.
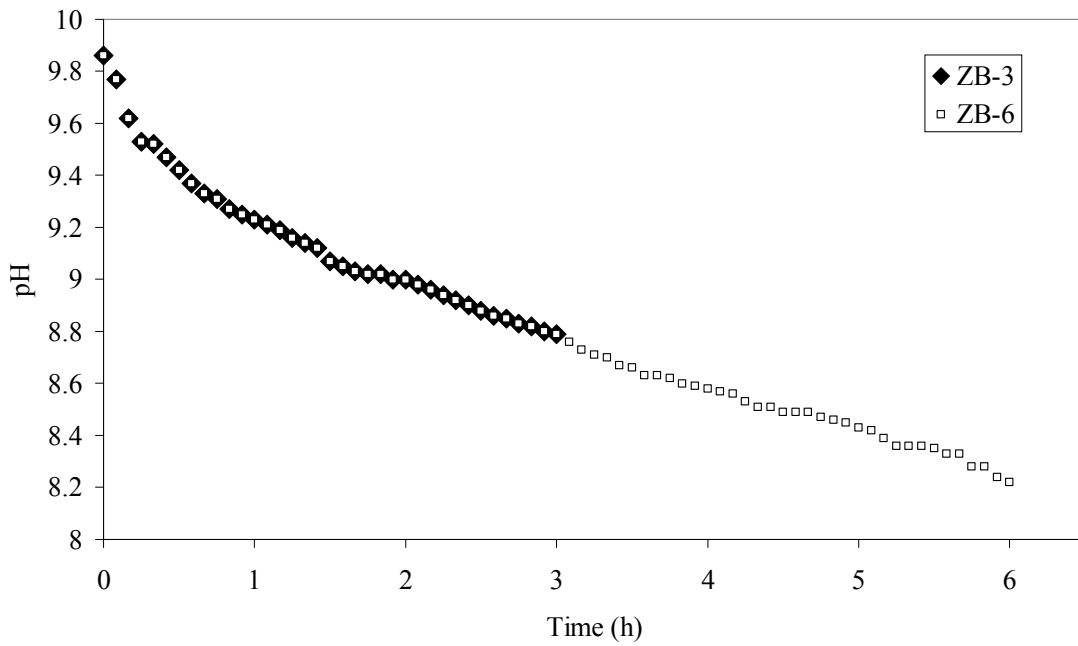
Figure 7.55. pH change of zinc borate aqueous solutions with respect to time.
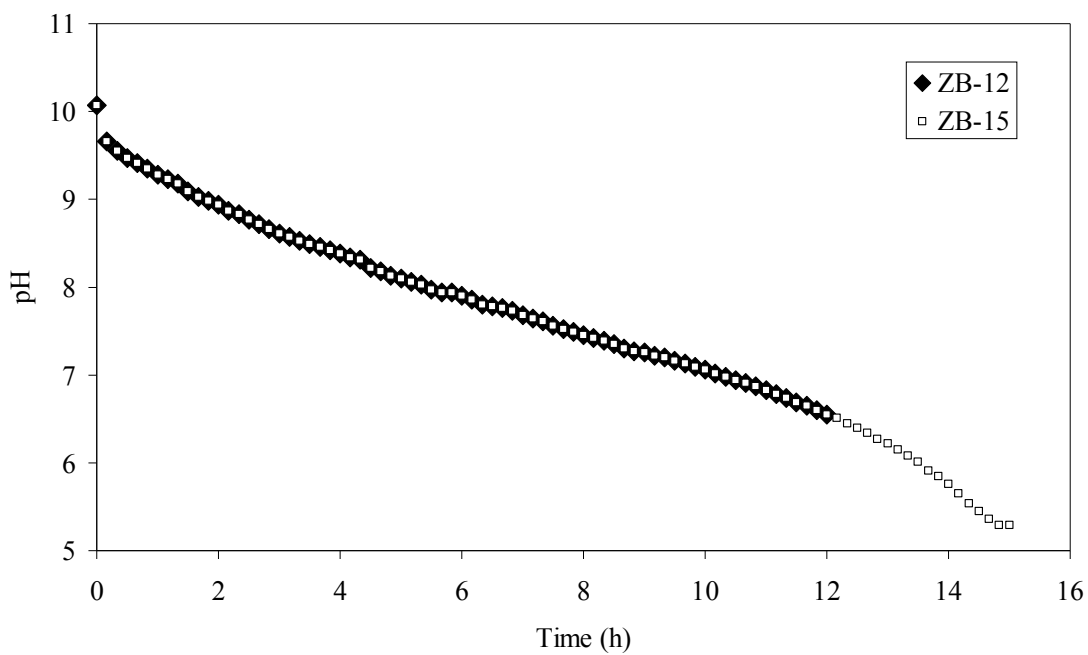
Figure 7.56. pH change of zinc borate aqueous solutions with respect to time.

Table 7.14. Amount of zinc borate produced by precipitation method

Sample	Weight (g)					Volume of ammonia and water removed from sample (cm^3)	
	Wet sample		Dry sample		Predicted amount of $2ZnO\cdot3B_2O_3\cdot7H_2O$	Run 1	Run 2
	Run 1	Run 2	Run 1	Run 2*			
ZB-3h	2.12	1.72	0.99	0.68	12.42	15	17
ZB-6h	5.26	4.99	2.52	2.20	12.42	35	36
ZB-12h	6.61	6.10	3.12	2.96	12.42	95	93
ZB-15h	10.61	4.76	4.52	2.36	12.42	107	116

* These samples were washed with both water and ethanol before drying.
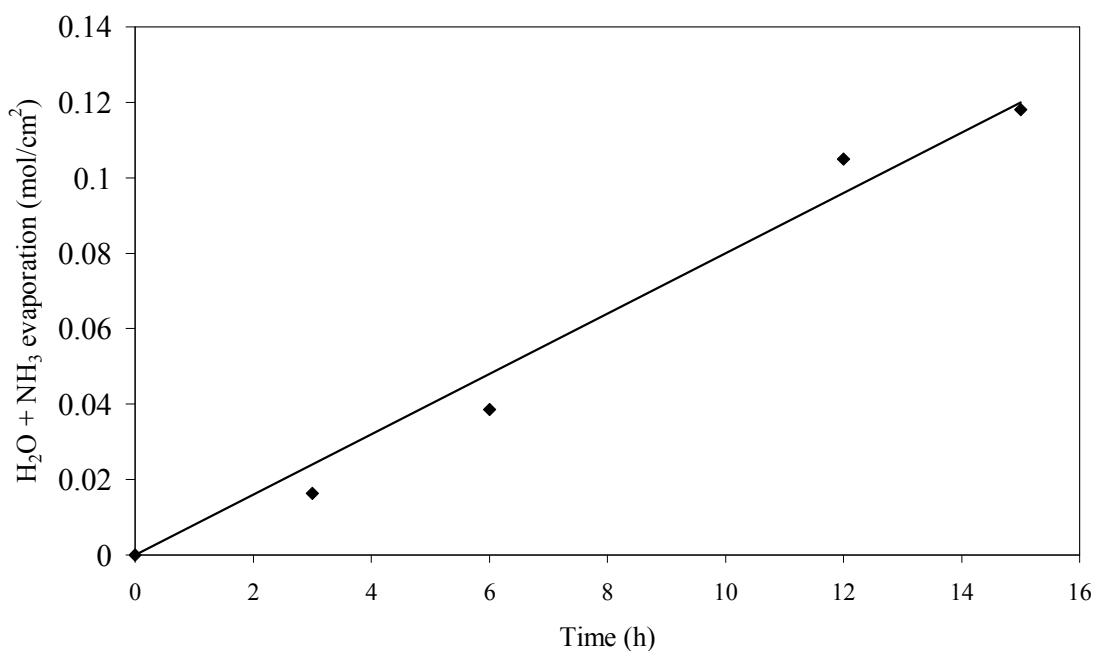
Figure 7.57. Water and ammonia evaporation with respect to time.

SEM images of zinc borate produced in the presence of ammonium in aqueous phase are shown in Figures 7.58 and 7.59. When the mixing period is low (3 and 6 h) nano-sized crystals as well as sub-micron sized spherical crystals are observed (Figure 7.58a and Figure 7.59b). It is revealed that the crystal sizes of nano-sized particles and sub-micron particles are nearly 30 nm and 400 nm, respectively. However, the crystals

become larger with the prolonged mixing time and spherical agglomerated crystals are formed as shown in Figure 7.58c. Unlike other samples, the product obtained after 15 h mixing time has rod-like crystals as indicated in Figure 7.58d. Furthermore the morphologies of the products washed with not only ethanol but also water are investigated and SEM images of the samples are given in Figure 7.59. It is observed that sub-micron sized crystals are still present in SEM images, whereas a few nano-sized crystals are observed on the surface of larger crystals. It may occur due to the washing of samples with water; hence water peels off the nano-sized crystals from the surface of the sub-micron sized crystals. Even if the samples shown in Figure 7.58d and 7.59d have same mixing periods, rod-like morphology is not obtained for the product washed with water. Spherical agglomerated crystals are formed and this result again arises from the washing effect of water. Water washing dissolves the precipitated $NaNO_3$. For 0.05 moles of zinc nitrate 0.1 mol sodium nitrate is obtained. So the amount of sodium nitrate in 100 cm^3 water is 8.5 g. The solubility of sodium nitrate at 40 ^oC is 102 g/100 cm^3 water (Wikipedia, 2010). Therefore it is understood that sodium nitrate crystals are not formed in the solution.

The particle size distributions of zinc borate samples produced by coordination homogeneous precipitation technique and washed with only ethanol are given in Figure 7.60. Both sub-micron and micron sized particles are observed from the figure. The volume-weighted mean particle diameter of zinc borate particles are found as 14.37, 18.35, 21.24 and 25.02 μm for 3, 6, 12 and 15 hours, respectively. It is inferred that the particle size of the sample increases by increasing mixing time, accordingly. Furthermore, these results are in good agreement with the results obtained from SEM. Figure 7.61 displays the particle size distributions of zinc borate samples produced by coordination homogeneous precipitation technique and washed with both ethanol and water. The volume-weighted mean particle diameter of zinc borate particles are found as 16.78, 18.93, 18.22 and 22.36 μm for 3, 6, 12 and 15 hours, respectively.

(a)

(b)

(c)

(d)
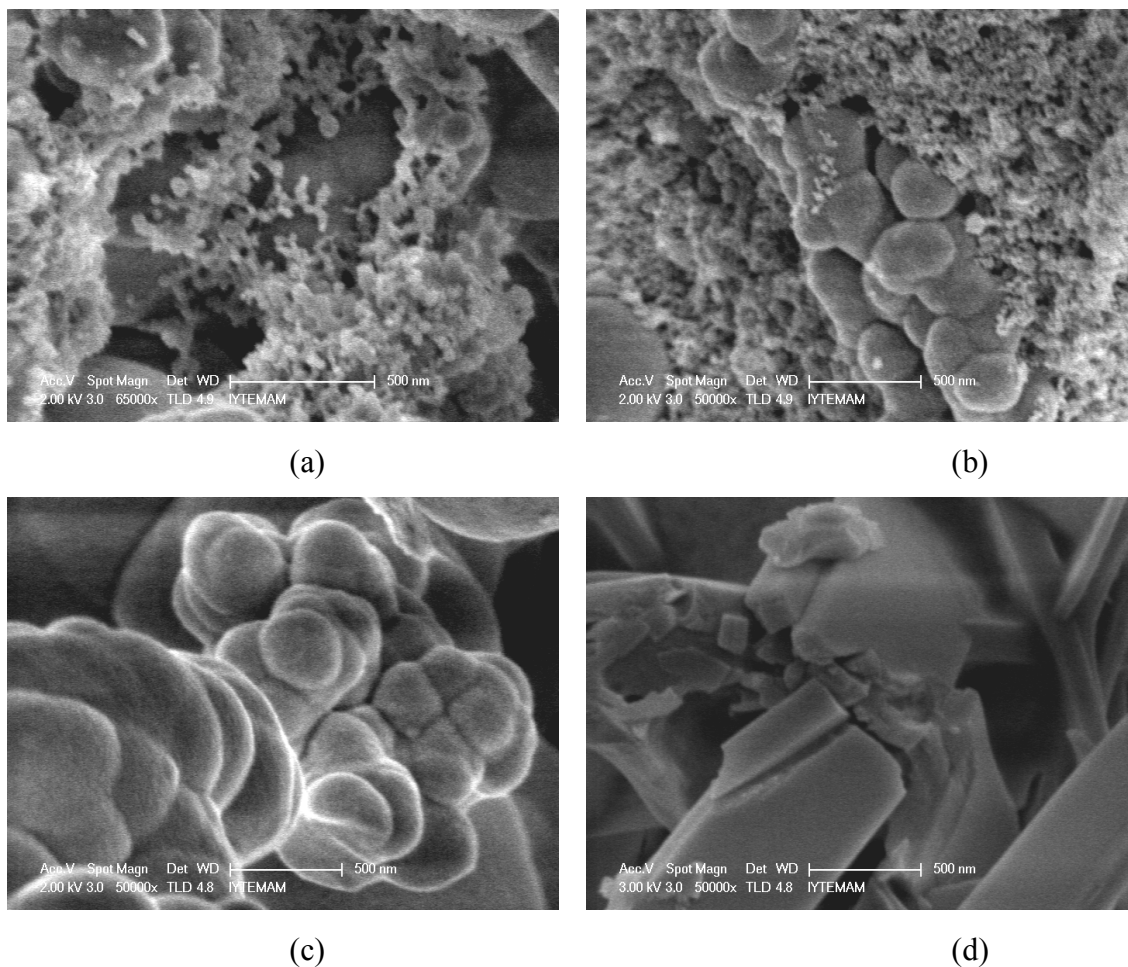
Figure 7.58. SEM images of zinc borate obtained in aqueous phase after a) 3, b) 6 c) 12 and d) 15 hours and washed with only ethanol

The FTIR spectrum of zinc borate prepared via precipitation technique in the presence of ammonium in aqueous phase is shown in Figures 7.62 and 7.63. They exhibits the specific peaks of zinc borate having seven moles of crystal water ($2ZnO \cdot 3B_2O_3 \cdot 7H_2O$). The characteristic peaks of zinc borate are assigned referring the literature (Goa et al., 2009; Ting et al., 2009). The band at 3300 cm^{-1} is attributed to O–H stretching vibration whereas the band at 1634 cm^{-1} is assigned to the H–O–H bending mode, which shows that the compound contains crystal water. All the samples exhibit the similar characteristics, but the sample having 15 h mixing period and washed by only ethanol has more clear peaks in its spectrum. The asymmetric stretching of O-NO$_2$ is observed at 1384 cm^{-1}, proving that these samples contain nitrate ion. The band at 1050 cm^{-1} is the stretching of B(4)-O, and the peaks between 745-658 cm^{-1} are belonging to out-of-plane bending mode of B(3)-O. The characteristic peaks of B(3)-O

144

are also observed at 1343 cm^{-1}. The peaks intensities also do not increase with mixing time.

(a) (b)

(c) (d)
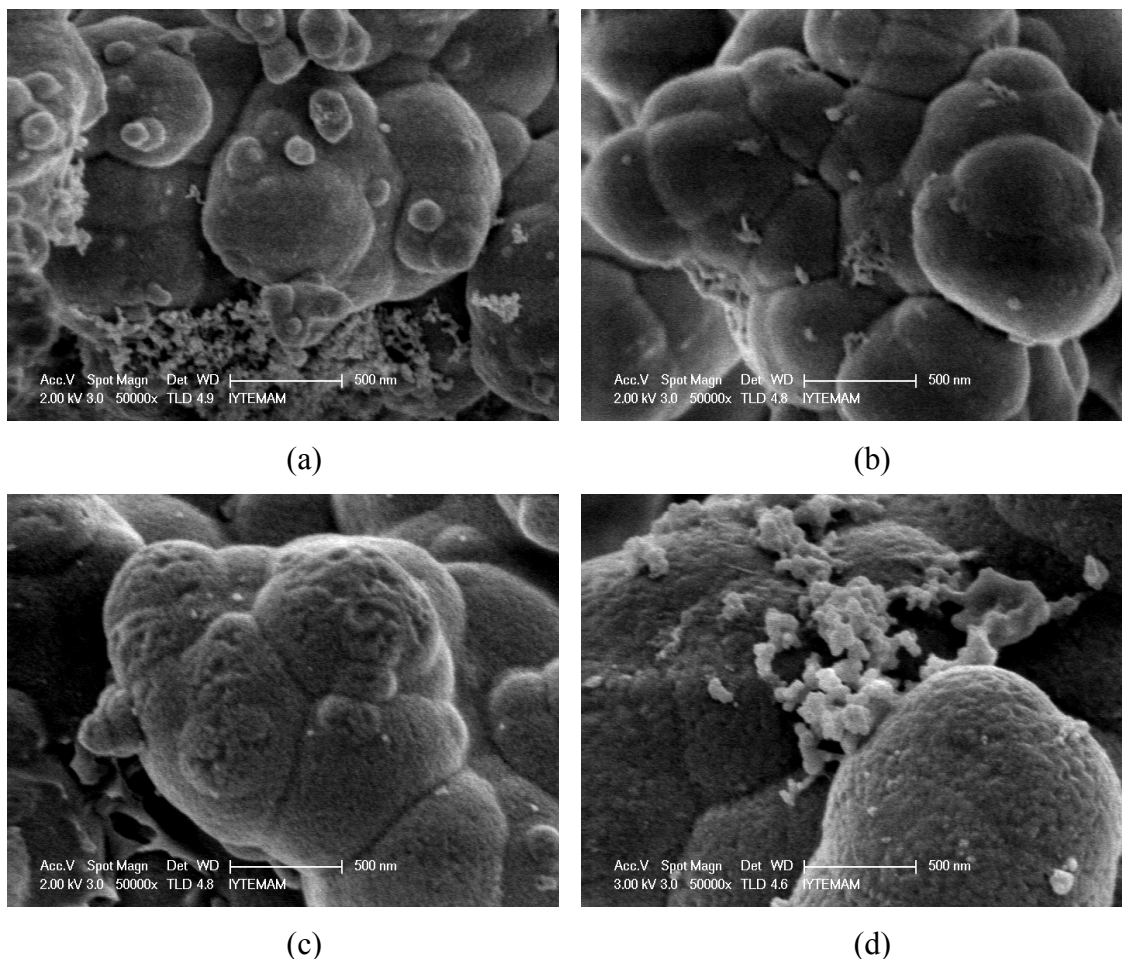
Figure 7.59. SEM images of zinc borate obtained in aqueous phase after a) 3, b) 6 c) 12 and d) 15 hours and washed with ethanol and water.

The thermal behavior of the products is investigated using TGA and DSC measurements in the temperature range of 25–600 $^{\circ}$C. It can be found that the samples start to loose their mass immediately as shown in Figures 7.64 and 7.65. Residual masses at the end of 600 $^{\circ}$C are listed in Table 7.15. Mass losses of the samples are changing from 9.48% to 13.89%. In literature it is revealed that water loss of zinc borate having formula $2ZnO{\cdot}3B_2O_3{\cdot}3H_2O$ is 12.69% which is close to the values of the samples obtained in aqueous phase (Schubert et al., 2003). DSC endotherms of the samples exhibit endothermic peaks at different temperature that may be due to different types of crystal water desorption. Also the endothermic peaks at 300 $^{\circ}$C in Figures 7.66 and 7.67 show the degradation of nitrate ion. Table 7.16 reports the dehydration

behavior of the samples and the first endothermic peaks of the samples related to removal of interstitial water from the products and the water formed from the condensation of OH groups (Figure 7.66 and Figure 7.67).
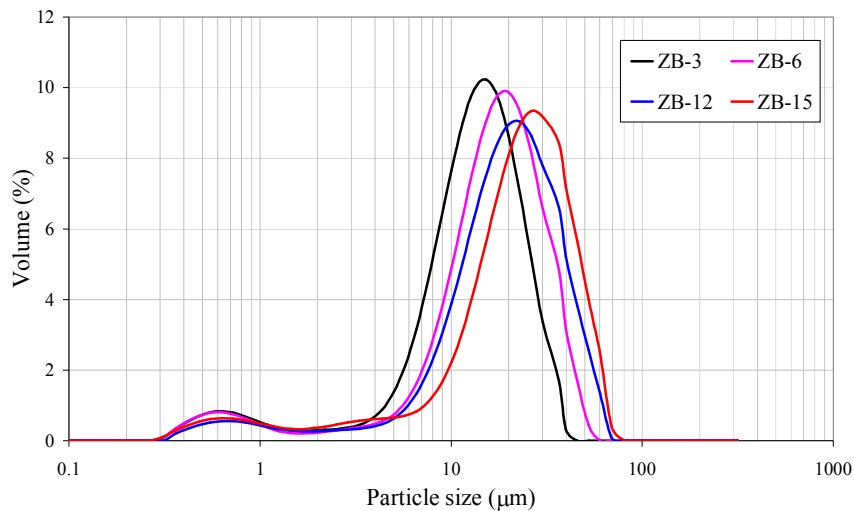
Figure 7.60. Particle size distribution of zinc borate particles prepared by homogeneous precipitation and washed with only ethanol.
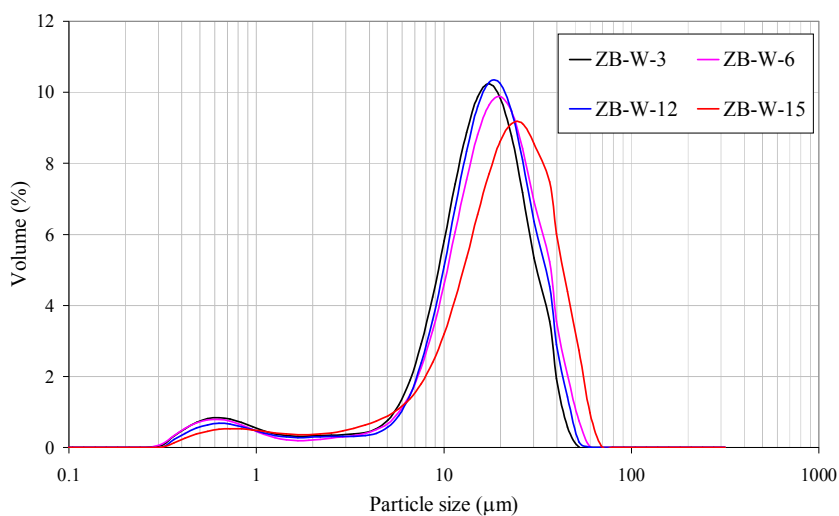
Figure 7.61. Particle size distribution of zinc borate particles prepared by homogeneous precipitation and washed with both ethanol and water.
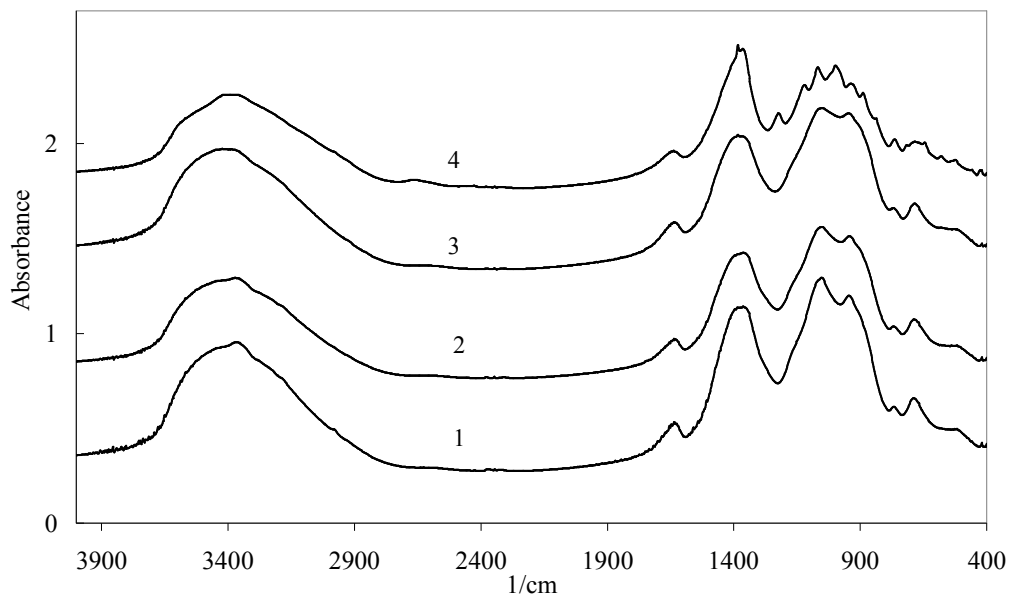
Figure 7.62. FTIR spectra of zinc borate obtained in aqueous phase after 1) 3, 2) 6 3) 12 and 4) 15 hours and washed with only ethanol.
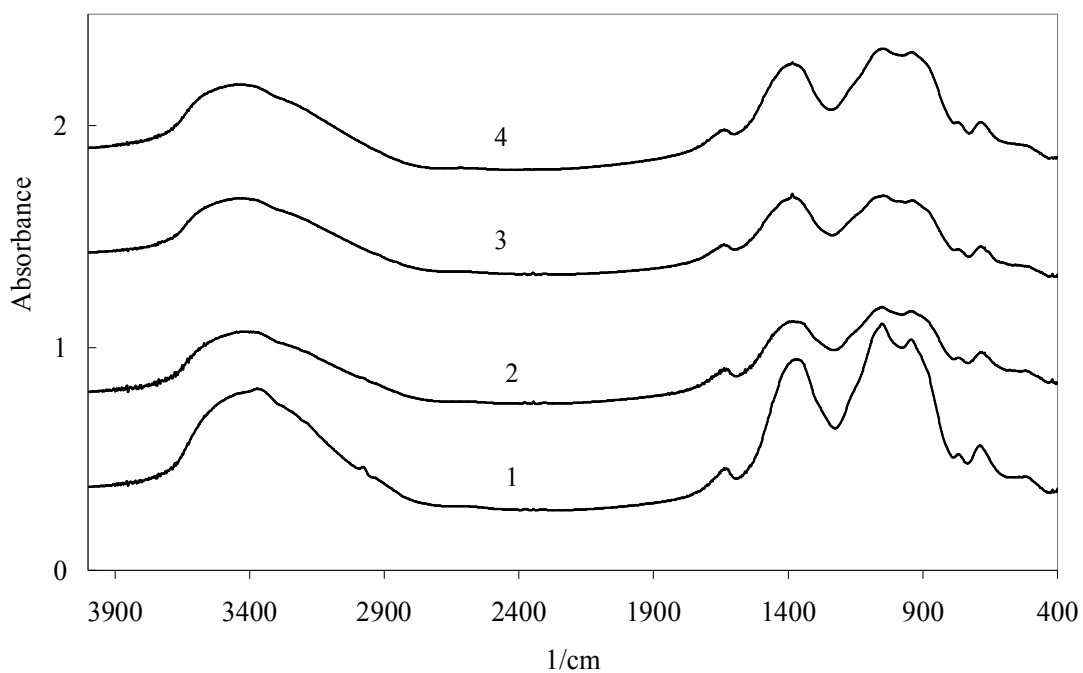
Figure 7.63. FTIR spectra of zinc borate obtained in aqueous phase after 1) 3, 2) 6 3) 12 and 4) 15 hours and washed with ethanol and water.
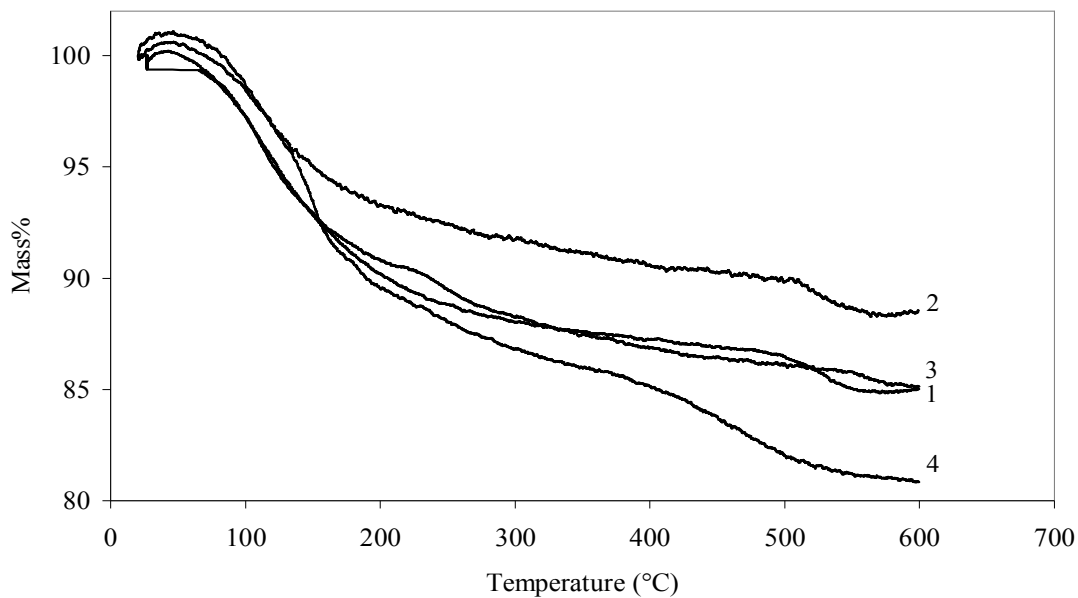
Figure 7.64. TGA thermogram of zinc borate obtained in aqueous phase after 1) 3, 2) 6 3) 12 and 4) 15 hours and washed with ethanol.
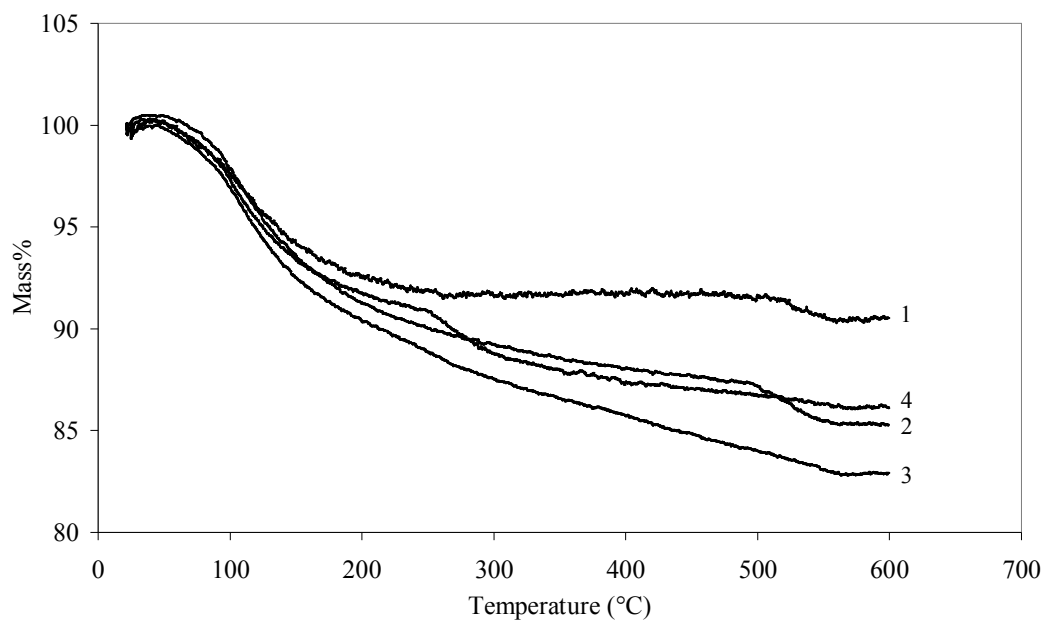
Figure 7.65. TGA thermogram of zinc borate obtained in aqueous phase after 1) 3, 2) 6 3) 12 and 4) 15 hours and washed with ethanol and water.

Table 7.15. Residual mass percentages at different temperatures for zinc borate samples prepared by precipitation in aqueous phase

Sample	Residual Mass % at temperature level			
	100 °C	200 °C	400 °C	600 °C
ZB-3	97.23	90.21	87.21	85.00
ZB-6	98.66	93.27	90.60	88.52
ZB-12	97.27	90.82	86.84	85.14
ZB-15	98.45	89.55	85.16	80.83
ZB-W-3	97.63	92.59	91.67	90.52
ZB-W-6	97.81	91.25	88.07	85.24
ZB-W-12	96.93	90.42	85.72	82.93
ZB-W-15	97.34	91.76	87.36	86.11
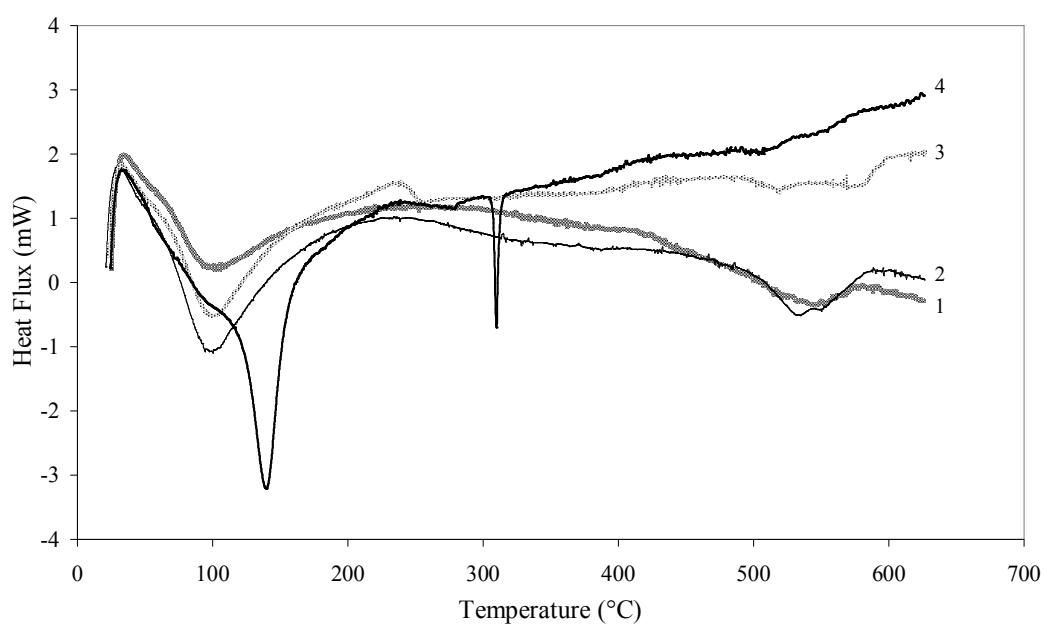
Figure 7.66. DSC curves of zinc borate obtained in aqueous phase after 1) 3, 2) 6 3) 12 and 4) 15 hours and washed with ethanol.
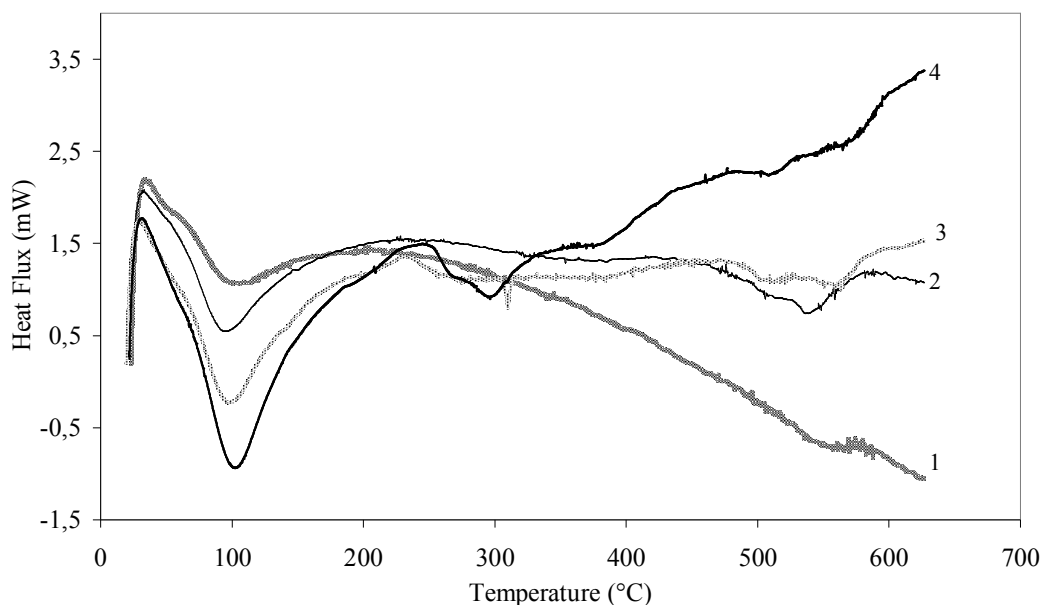
Figure 7.67. DSC curves of zinc borate obtained in aqueous phase after 1) 3, 2) 6 3) 12 and 4) 15 hours and washed with ethanol and water.

The XRD study shows that the structure of the products washed with ethanol transform from amorphous to crystal phase with increasing reaction time (Figure 7.68). The samples mixed for 3, 6 and 12 hours are amorphous and they do not indicate any tendency to be crystal. However the mixing time is increased to 15 hour, the sample becomes crystal. The XRD pattern of the crystal sample shows both the characteristic peaks of sodium nitrate and zinc borate. The XRD peaks belong to sodium nitrate are shown by star according to JCPDS data of 80-813. The presence of sodium nitrate in this sample is due to the washing of the sample only with ethanol. When these products are washed with water as well as ethanol, the crystal structure of the sample mixed for 15 h is disappeared and the product exhibits amorphous structure as shown in Figure 7.69. However the solubility of sodium nitrate at 40 °C is found as 102 g/100 cm^3 and this value is significantly higher than the amount of sodium nitrate formed in the solution. These results are not consistent with literature since Ting et al. (2009) demonstrate that zinc borate samples having 12 and 15 hours mixing time are crystalline.

Table 7.16. Thermal behavior of the zinc borates obtained in aqueous phase

Sample	First Peak				Second Peak			
	Onset (°C)	Maximum (°C)	Endset (°C)	ΔH (J/g)	Onset (°C)	Maximum (°C)	Endset (°C)	ΔH (J/g)
ZB-3	5.47	100.83	263.46	-97.14	504.43	545.69	582.27	-61.59
ZB-6	42.74	100.36	235.10	290.26	495.44	534.46	575.23	-45.61
ZB-12	5.31	99.92	236.45	-326.42	496.01	519.04	529.30	-4.90
ZB-15	106.89	139.82	166.18	-484.42	298.27	309.79	316.18	-12.67
ZB-W-3	33.05	100.59	204.70	-163.72	520.58	582.54	580.78	-10.67
ZB-W-6	10.97	94.57	230.43	-220.17	504.43	538.45	582.27	-61.59
ZB-W-12	48.91	98.21	162.34	-190.99	309.71	521.50	313.86	-1.68
ZB-W-15	40.42	102.18	233.26	-304.98	245.55	296.39	365.92	-42.98
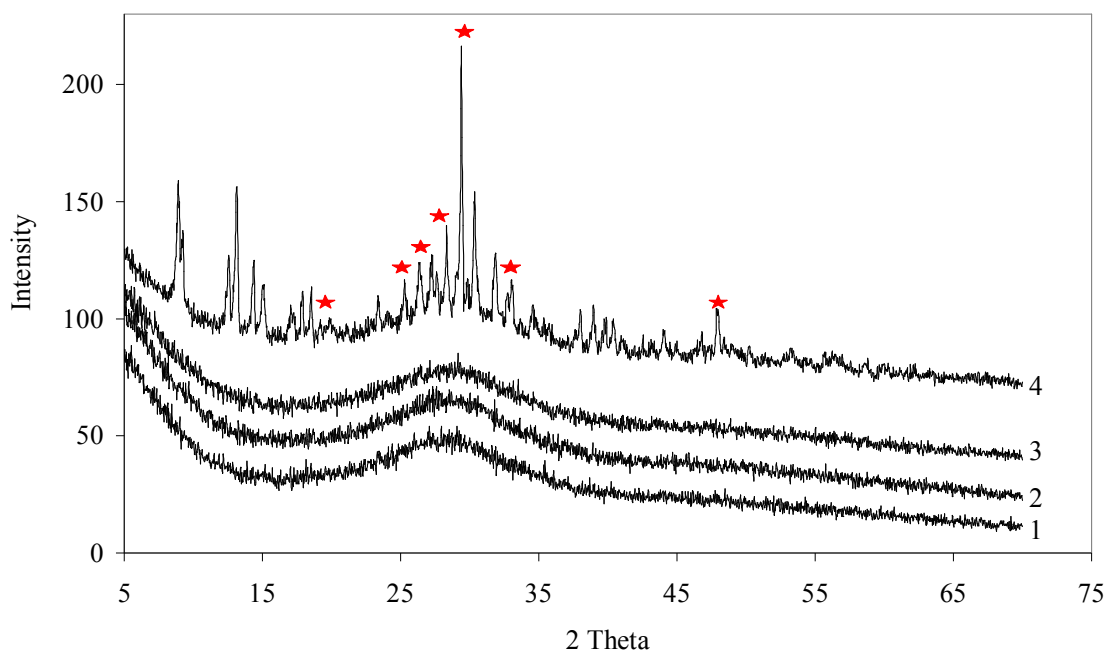
Figure 7.68. XRD pattern of zinc borate obtained in aqueous phase after 1) 3, 2) 6 3) 12 and 4) 15 hours and washed with ethanol.
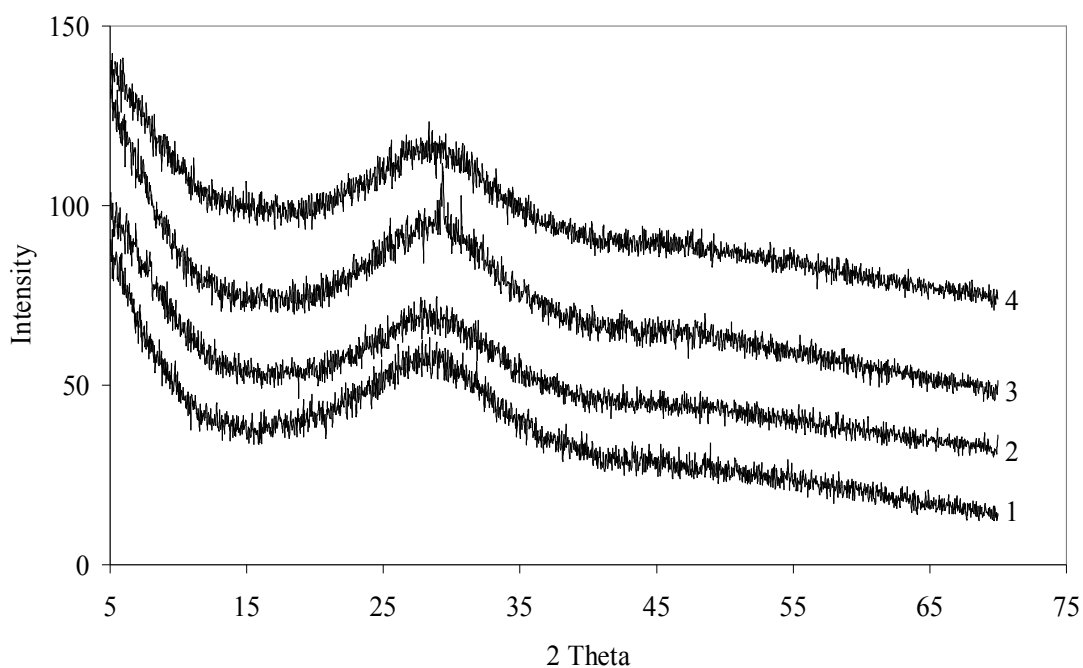
Figure 7.69. XRD pattern of zinc borate obtained in aqueous phase after 1) 3, 2) 6 3) 12 and 4) 15 hours and washed with ethanol and water.

The elemental composition of the products synthesized in aqueous phase is obtained by analytical titration technique, CHNS elemental analysis and EDX analysis.

Table 7.17. shows the ZnO % and B_2O_3 % contents of the zinc borate samples determined by conventional titration technique. B_2O_3/ZnO molar ratio of zinc borates produced in aqueous phase at different mixing periods is changing between 0.683 and 0.764, except the sample having 15 hours mixing period and washed with only ethanol. B_2O_3/ZnO molar ratio of this sample is found as 0.958. Water content of zinc borate samples was determined by subtracting the summation of B_2O_3 % and ZnO % from unity. According to their ZnO %, B_2O_3 % and H_2O % contents, the molecular formula of the products are evaluated. CHNS elemental analysis is carried out not only to expose the nitrogen content of the sample but also to understand if the nitrate ions are removed from the samples by washing of water or not. The results are tabulated in Table 7.18. It is demonstrated that the nitrogen content of the products are changing from 1.13 to 2.66 and this content slightly decreases when the products are washed with water. The presence of carbon in the samples may be due to the CO_2 adsorption of the samples from the air. Besides, analytical titration and CHNS analysis, EDX analysis is also performed to determine B, Zn, O, N contents of the samples and the results are given in Table 7.19. Boron content increases with increasing mixing period for the samples washed with only ethanol and the B% is reached its highest concentration for the sample having crystal structure (ZB-15). Nitrogen contents of the products determined by EDX analysis are greater than the values found by CHNS analysis, but it is in the range of accuracy of EDX analysis. When the B_2O_3/ZnO mol ratio values obtained from EDX analysis and analytical titration are compared with each other, it is observed that lower B_2O_3/ZnO mol ratio values are evaluated by EDX analysis results.

The H_2O weight % evaluated by different analysis are tabulated in Table 7.20. CHNS elemental analysis results show that H_2O% of the synthesized products are changing from 17.91 to 20.79 which is close to 19.25 indicating the water loss belonging to zinc borate (ZnO·B_2O_3·2H_2O) having two moles of crystal water (Briggs, 2001). However, the H_2O% content of the samples evaluated by CHNS results are moderately different than the content of H_2O % obtained by TGA analysis. The H_2O wt% of the samples found by TGA analysis reveals that H_2O % are between 9.48 and 19.17. In literature the water content of 2ZnO·3B_2O_3·3H_2O and ZnO·B_2O_3·2H_2O are indicated as 12.69% and 19.25%, respectively. Therefore, the synthesized samples having lower water content might be 2ZnO·3B_2O_3·3H_2O, whereas the samples containing higher water content might be ZnO·B_2O_3·2H_2O

Table 7.17. ZnO, B_2O_3 content, and B_2O_3/ZnO molar ratio of the products determined by chemical analysis.

Sample	Weight %		B_2O_3/ZnO mol ratio	Molecular formula
	ZnO	B_2O_3		
ZB-3	43.26	30.77	0.711	$3ZnO \cdot 2B_2O_3 \cdot 9H_2O$
ZB-6	42.99	27.73	0.692	$3ZnO \cdot 2B_2O_3 \cdot 9H_2O$
ZB-12	40.07	30.43	0.764	$3ZnO \cdot 2B_2O_3 \cdot 10H_2O$
ZB-15	32.48	30.94	0.958	$ZnO \cdot B_2O_3 \cdot 6H_2O$
ZB-W-3	44.81	31.27	0.683	$3ZnO \cdot 2B_2O_3 \cdot 9H_2O$
ZB-W-6	42.28	30.94	0.736	$3ZnO \cdot 2B_2O_3 \cdot 9H_2O$
ZB-W-12	43.78	30.95	0.734	$3ZnO \cdot 2B_2O_3 \cdot 8H_2O$
ZB-W-15	42.36	31.78	0.755	$3ZnO \cdot 2B_2O_3 \cdot 9H_2O$

Table 7.18. Elemental composition and water content of the products measured by CHNS elemental analysis.

Sample	Average wt%			
	C	H	N	H_2O
ZB-3	0.56	2.22	2.22	19.98
ZB-6	0.24	2.31	2.18	20.79
ZB-12	0.31	2.14	1.13	19.26
ZB-15	0.25	2.18	2.66	19.62
ZB-W-3	0.43	1.99	1.19	17.91
ZB-W-6	0.44	2.15	2.13	19.35
ZB-W-12	0.39	1.99	1.77	17.91
ZB-W-15	1.51	2.30	2.02	20.70

The zinc borate precipitation techniques used in this study were compared with each other by considering their efficiencies. The efficiencies of the techniques were calculated using the produced amount of zinc content of the samples. Table 7.21 presents the input moles of zinc and output moles of zinc. The efficiency of the precipitation technique in the presence of surfactant is found as 30.14%, whereas the efficiencies of the samples prepared by coordination homogeneous precipitation are changing between 14.97% and 63.67%. However the efficiency of the precipitation

technique carried out by boric acid and zinc oxide was close to 100% in literature (Eltepe et al., 2007).

Table 7.19. Elemental composition, and B_2O_3/ZnO molar ratio of the products determined by EDX analysis.

Sample	Average wt%				
	B	N	O	Zn	B_2O_3/ZnO mol ratio
ZB-3	2.77	5.30	41.09	50.84	0.16
ZB-6	3.94	5.25	41.57	49.24	0.24
ZB-12	6.82	3.72	40.65	48.81	0.42
ZB-15	15.29	5.14	48.61	30.96	1.01
ZB-W-3	8.10	5.08	38.81	48.00	0.55
ZB-W-6	7.05	4.54	39.19	49.22	0.44
ZB-W-12	8.84	4.13	41.35	45.67	0.54
ZB-W-15	7.61	4.21	43.29	44.90	0.47

Table 7.20. H_2O weight percentages evaluated by TGA and CHNS elemental analysis.

Sample	H_2O weight %	
	TGA analysis	CHNS analysis
ZB-3	15.00	19.98
ZB-6	11.48	20.79
ZB-12	14.86	19.26
ZB-15	19.17	19.62
ZB-W-3	9.48	17.91
ZB-W-6	14.76	19.35
ZB-W-12	17.07	17.91
ZB-W-15	13.89	20.70

Table 7.21. Efficiencies of zinc borate production techniques.

Sample	Production Technique	Output moles of zinc in zinc borate	Efficiency %
ZBS-1	Precipitation in the presence of Span 60	30.14	30.14
ZB-W-3	Homogeneous precipitation	14.97	14.97
ZB-W-6	Homogeneous precipitation	45.70	45.70
ZB-W-12	Homogeneous precipitation	63.67	63.67
ZB-W-15	Homogeneous precipitation	49.12	49.12

7.6. Lubricants

Lubricants are essentially composed of one or more base oils representing at least 85% of the formulation. The most commonly used base stocks are mineral oils, complex mixtures of hydrocarbons that are produced from petroleum crude by various processing steps and involve three main chemical families, i.e. paraffins, naphthenes and aromatics (Haus et al., 2004). It is well established that pure petroleum base oil does not meet all the requirements of the mother engines and equipments. The usual solution of this problem is the addition of certain compounds which are capable of improving the properties of base oil. Especially, antiwear and extreme pressure additives are essential for lubricants to protect the equipment from wear and enable it to operate successfully under heavy loads.

In this study, light oil belonging to mineral oils family was used as the base oil and its tribological properties were tried to enhance by mainly boron-based additives. Another inorganic material, clinoptilolite rich mineral was tested to understand if it had antiwear property or not. An organic material sorbitan monostearate was also employed in the lubricants to obtain a better dispersion of inorganic particles. In the scope of the project, the effects of dispersing agent, zinc borate type, surfactant concentration on the tribological properties of the mineral oil were investigated. The lubricants containing zinc borate particles were compared with a commercial product called as BOR POWER. BOR POWER is one of the lubricants in the market that can be used in all

156

transport vehicles with 4-stroke engines. The characterization of this lubricant was performed since it was claimed that it contained boron material so what kind of boron source it included became the important question for our work considering the parallelism between this commercial product and ours. Therefore both BOR POWER oil and the particles obtained by separating the oily phase were identified.

In literature, there is no study related to the employment of water-in-oil emulsions in lubrication processes according to our knowledge. However, oil-in-water emulsions are widely used in metal forming applications to provide lubrication and cooling when high temperature prevent use of neat oil products or the high speed operation necessitate an efficient removal of heat (Lu and Guo, 2009; Januszkiewicz et al., 2004). Therefore, it was aimed to examine the inverse emulsions containing zinc borate particles whether they could be used directly as lubricants or not. Consequently, the prepared inverse emulsion (E3) was also tested to present a new lubrication preparation technique in the field of both colloidal systems and nano-size particle preparation.

Although there are many studies related to the utilization of clinoptilolite rich mineral in separation processes or the thermal stability of polymers (Tıhmınlıoğlu and Ülkü, 1996; Atakul et al., 2005) there is no research about the employment of zeolites in mineral oil to enhance the tribological behavior of base oil. This lack of literature motivated us to prepare lubricants containing clinoptilolite rich mineral. The tribological property of this lubricant was also analyzed. Moreover, clinoptilolite particles having 2-3 mm diameter was used as water adsorber in inverse emulsion which was tested as a lubricant.

In addition the tribological behavior of the lubricants, their morphology, functional groups, and viscosities were also investigated.

7.6.1. Optical Microscopy Study of Lubricants

Inorganic materials possess many special physical and chemical properties, and it is anticipated that these materials as oil or grease additives will provide a well bonded boundary film to the steel surfaces which will enable it to work at high temperature and extremely high load. The dispersion of the inorganic particles is of great importance in order to be used as lubricating oil additives. For this reason, the surfaces of the additives

are generally modified or surface active agents are used in mineral oil (Huang et al., 2006; Xue et al., 1997). So as to demonstrate the dispersion properties of the additives, the optical microphotographs of the prepared lubricants were taken.

Effect of dispersing agent on the morphology of the lubricants

The inorganic additives were not used alone to form lubricants. The surfactant, sorbitan monostearate was employed to cover the surfaces of inorganic additives and to provide a better dispersion of the particles in the mineral oil. Additionally, BYK products are examined to understand if they play a significant role in the dispersion of the particles or not. Figure 7.70 indicates the optical microphotographs of the base oil, base oil with surfactant and the lubricants prepared by commercial zinc borate (Firebrake 2335). The average diameters of the particles listed in Table 7.22 were measured by Olympus DP2-BSW program considering five different particles or droplets. The microphotograph of the mineral oil without any additive (Figure 7.69a) shows only an air bubble, whereas, the microphotographs of the oil with additives exhibit the particles are polydisperse in the mineral oil. Unlikely, the spherical morphology of sorbitan monostearate obtained by SEM (Figure 7.6), the microphotograph of the mineral oil including sorbitan monostearate shows that the particles of this surfactant are rod-like shape. The average length of these rod-like particles was calculated as 5.55 µm (Figure 7.70b). The microphotograph of the lubricant with commercial zinc borate particles shows the particles having 5.55 µm average diameter. When Viscobyk 5025 and Disperbyk 1161 are added to mineral oil with commercial zinc borate, the average diameters of the particles are found as 5.44 and 1.80 µm, respectively. The addition of Disperbyk into the base oil results a low degree of smaller particles, but they tend to agglomerate Viscobyk enhances the colloidal stability of the system compared to Disperbyk chemical as shown in Figure 7.70d and 7.70e.

(a)   (b)

(c)   (d)

(e)
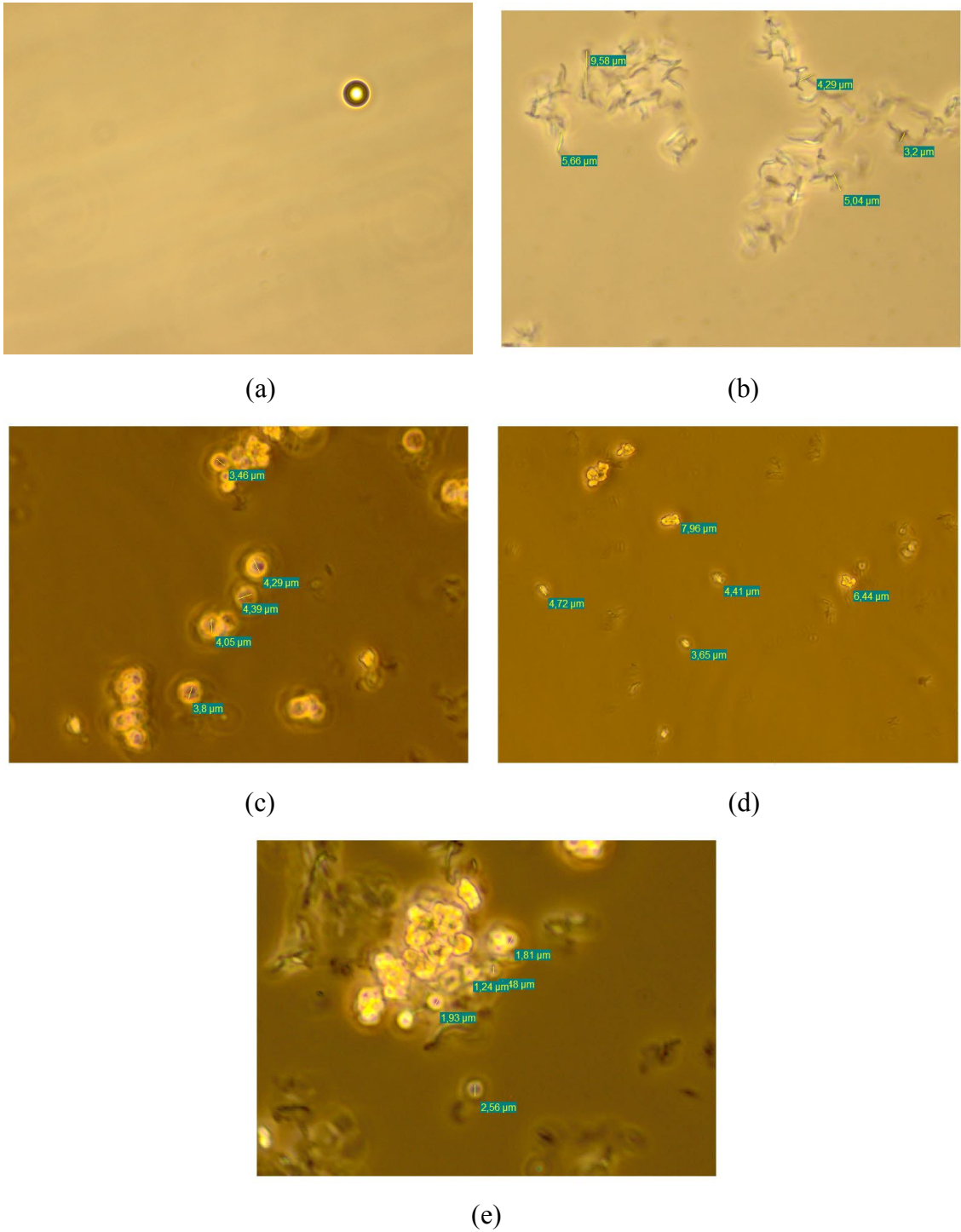
Figure 7.70. The microphotographs of a) base oil (L1), b) base oil with sorbitan monostearate (L2) and the lubricants containing c) commercial zinc borate and sorbitan monostearate (L5) d) commercial zinc borate, sorbitan monostearate and Viscobyk e) commercial zinc borate, sorbitan monostearate and Disperbyk. (The microphotographs were taken by Olympus BX60M microscope).

Table 7.22. Average particle diameters of dispersed phase containing commercial zinc borate in mineral oil.

Sample Code	Base Oil (cm^3)	Additives			Average diameter of particles (μm)
		Span 60 (g)	Zinc Borate (g) 2ZnO·3B$_2$O$_3$·3.5H$_2$O	Dispersing agent	
L1	100	-	-	-	-
L2	100	1	-	-	5.55
L5	100	1	1	-	4.00
L7	100	1	1	Viscobyk (0.05 cm^3)	5.44
L8	100	1	1	Disperbyk (0.05 cm^3)	1.80

Effect of zinc borate type on the morphology of the lubricants

In the scope of this study, different types of zinc borate species were synthesized by different techniques and raw materials. These zinc borate particles were dispersed into the mineral oil and their morphology was analyzed by optical microscopy as shown in Figure 7.71. By taking the average diameter of five different particles displayed on the microphotographs, the average particle diameters were determined. Table 7.23 indicates the types of inorganic additives and their average diameters within the oil. When the zinc borate species produced from boric acid and zinc oxide and dried conventionally was used as an additive for oil, it was observed that the particles agglomerate and form larger particles (Figure 7.71a). The average diameter of the particles is 2.84 μm and this value is in good agreement with particle size of the zinc borate species as shown in Figure 7.8. On the other hand, the microphotograph of the lubricant including zinc borate particles prepared by supercritical drying is cloudy and the observation of the particles is very difficult since it has nano-sized crystals and the microscope allows displaying particles in micron-sized (Figure 7.71b). The shape of the zinc borate particles prepared in the presence of the surfactant totally differs from the others except the shape of sorbitan monostearate. The morphology of these particles also shows rod-like structure (Figure 7.71c). When the zinc borates synthesized with coordination homogeneous precipitation method in the presence of ammonia and mixed

for 6, 15 and 12 hours were added into the mineral oil, average diameters were found as 0.95, 3.06 and 1.67 µm. It was revealed that the particle size was increased by increasing mixing time as shown in Figures 7.71d, 7.71e, and 7.71f. This is consistent with the results of SEM analysis of the zinc borates produced in the presence of ammonia.

Effect of surfactant concentration on the morphology of the lubricants

The surfactant concentration in the mineral oil was examined by decreasing the amount of sorbitan monostearate from 1g to 0.00005 g which was below its critical micelle concentration. The microphotographs of these samples are demonstrated in Figure 7.72 and the average diameters of the droplets are listed in Table 7.24. The average diameters of the particles are increased with the increasing surfactant concentration, accordingly.

Clinoptilolite rich mineral as lubricant additive

In this part of the study, clinoptilolite rich mineral having 5 µm particle size was used as a lubricating oil additive and the lubricant morphology was also investigated by optical microscopy. Figure 7.73 indicates the microphotograph of the lubricant containing clinoptilolite rich mineral. From this microphotograph, the average diameter of the particles was found as 1.19 µm.

(a)   (b)

(c)   (d)

(e)   (f)
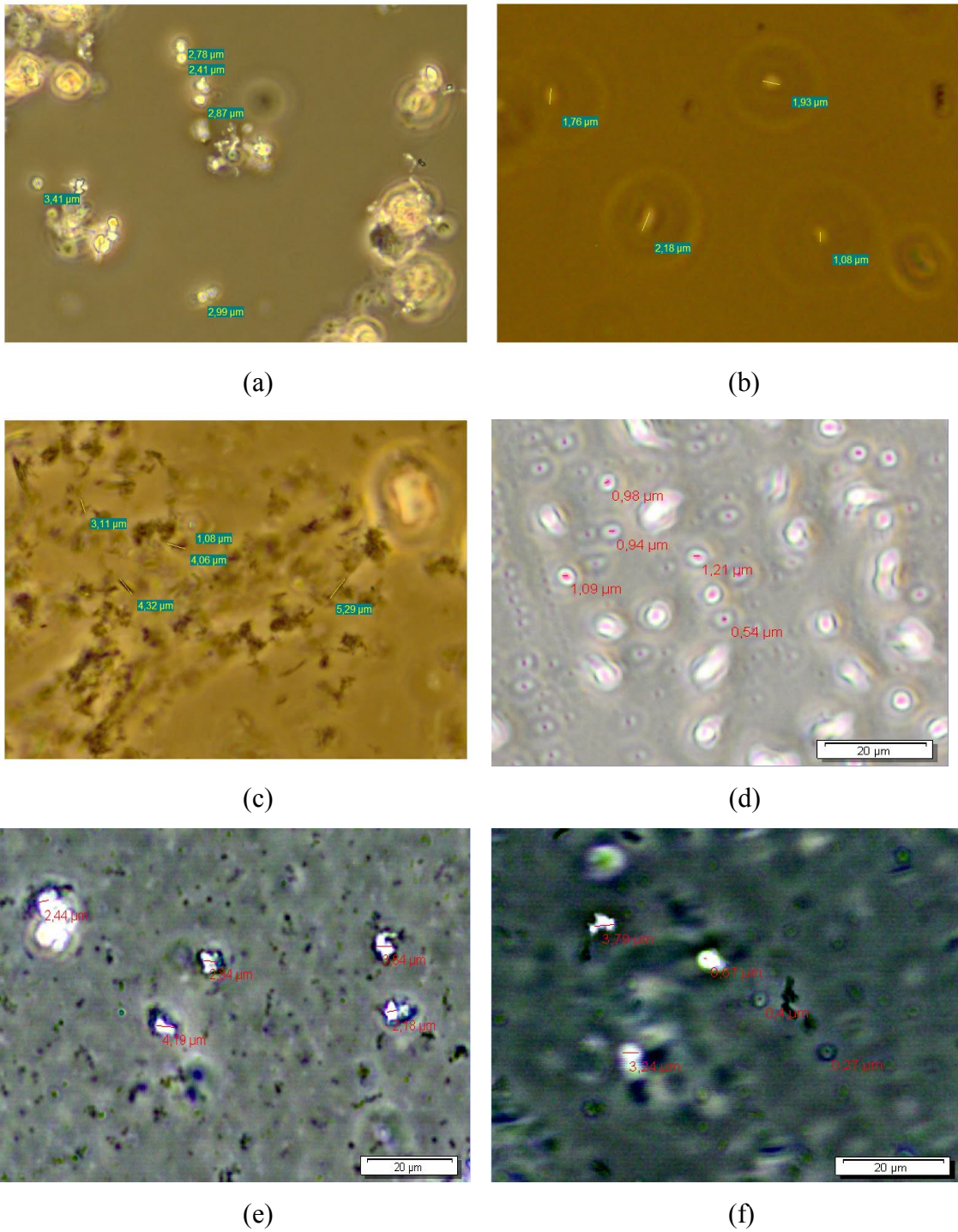
Figure 7.71. The microphotographs of the lubricants containing surfactant and zinc
borate produced by a) zinc oxide and boric acid and dried by
conventionally (ZBC) b) zinc oxide and boric acid and dried by
supercritical ethanol (ZBE) c) borax decahydrate, zinc nitrate and Span
60 (ZBS-1) d) borax decahydrate, zinc nitrate and ammonia mixed for 6h
dried washed by water and ethanol e) borax decahydrate, zinc nitrate and
ammonia mixed for 15 h washed by only ethanol f) borax decahydrate,
zinc nitrate and ammonia mixed for 12 h washed by water and ethanol.
(The microphotographs were taken by Olympus BX60M microscope).

162

Table 7.23. Average particle diameters of dispersed phase containing different types of zinc borate in mineral oil.

Sample Code	Type of Zinc Borate	Average diameter of particles (μm)
L3	ZBC	2.89
L4	ZBE	1.61
L6	ZBS-1	3.57
L9	ZB-W-6	0.95
L10	ZB-15	3.06
L11	ZB-W-12	1.67

Inverse emulsions as lubricant

Even though the lubricant preparation in industry consists of the addition of organic or inorganic materials into the base oil, this study aims to use the inorganic boron based particles synthesized in the inverse micelles without separating them from the continuous phase. As a result, the inverse emulsion was heated up to 160 °C to remove water from the emulsion. Figure 7.74 presents the microphotograph of the inverse emulsion prepared by one-microemulsion technique (E3). It is observed that the droplets have tendency to agglomerate and this explains why the stable inverse emulsions can not be obtained. The average diameter of the droplets is 1.81 μm.

(a)

(b)

(c)
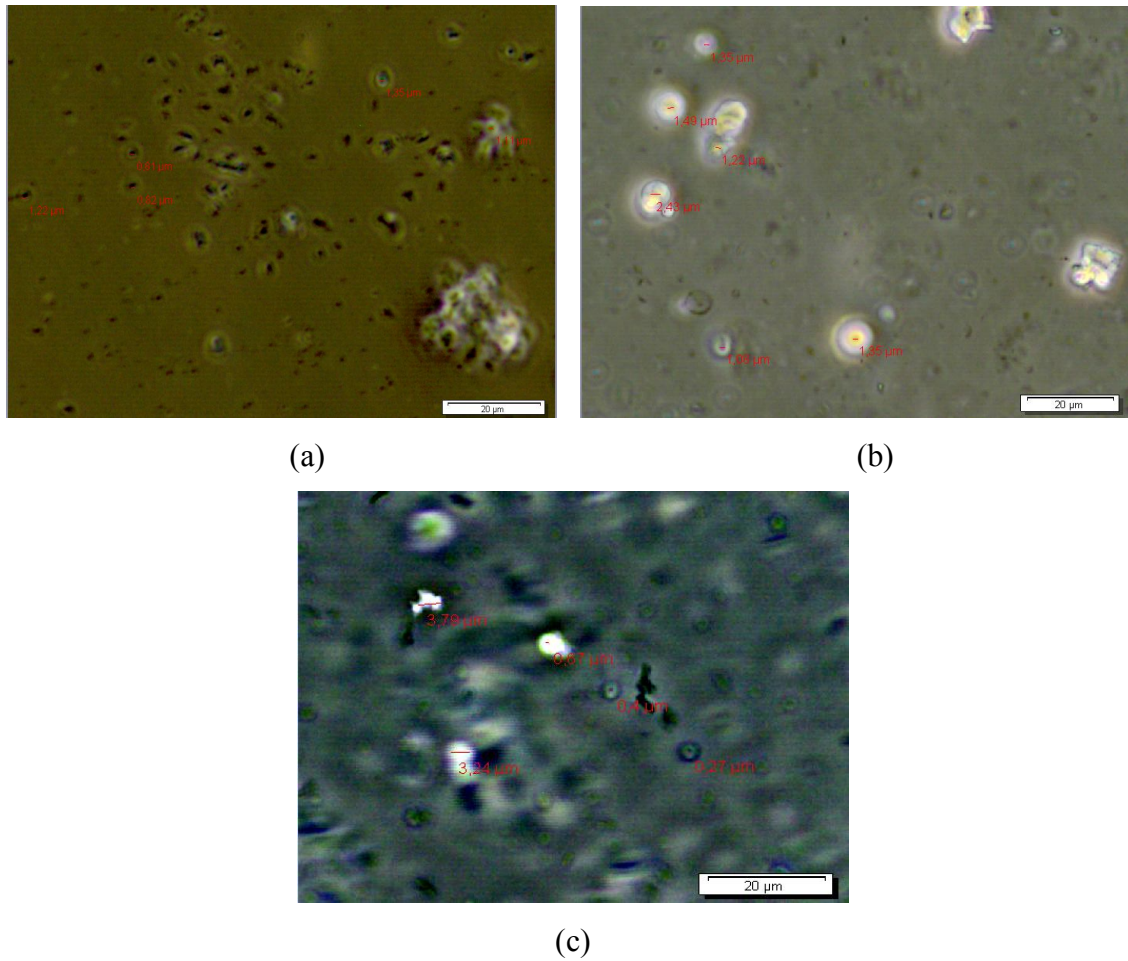
Figure 7.72. The microphotographs of the lubricants containing zinc borate produced by borax decahydrate, zinc nitrate and ammonia mixed for 12 h and a) 0.00005 g, b) 0.1 g, c)1 g surfactant (The microphotographs were taken by Olympus BX60M microscope).

Table 7.24. Average particle diameters of dispersed phase containing different amount of surfactant in mineral oil.

Sample Code	Base Oil (cm^3)	Additives		Average diameter of particles (µm)
		Span 60 (g)	Zinc Borate	
L12	100	0.00005	ZB-W-12	1.06
L13	100	0.1	ZB-W-12	1.49
L11	100	1	ZB-W-12	1.67

164

Figure 7.73. The microphotograph of the lubricant containing surfactant and clinoptilolite rich mineral (The microphotograph was taken by Olympus BX60M microscope).
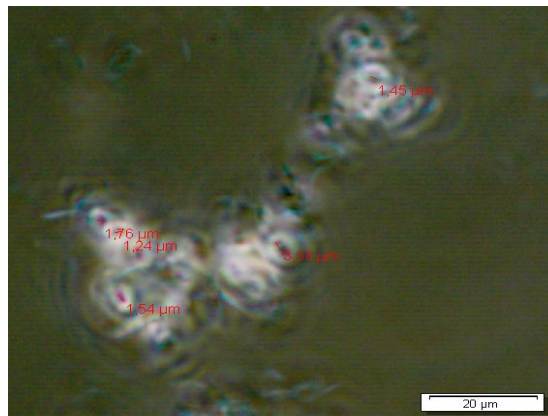
Figure 7.74. The microphotograph of the inverse emulsion (E3) heated up to 160 °C (The microphotograph was taken by Olympus BX60M microscope)

7.6.2. Surface Tension and Viscosities of Lubricants

Surface Tension

Liquid properties, such as surface tension, hydrophile–lipophile-balance (HLB), viscosity, and density, are known to affect the ability of a liquid to wet a solid (Kim et al., 2000). However, systematic research on this subject has been limited to adsorption of surfactants on inorganic surfaces. Surface tension is a phenomenon caused by the cohesive forces between liquid molecules. It is an effect within the surface film of a liquid that causes the film to behave like an elastic sheet. Commonly it is measured in mN/m or mJ/m^2 depending on how it is defined. The knowledge of surface tension is useful for many applications and processes as the surface tension governs the chemical

165

and physical behavior of liquids. It can be used to determine the quality of numerous industrial products such as paints, ink jet products, detergents, cosmetics, pharmaceuticals, lubricants, pesticides and food products (Lee et al., 2009). In this part of the study, how the surface tension of the mineral oil was affected with the addition of the surfactant was examined. The average value of the mineral oil (L1) surface tension was found as 31.7 mN/m at 25 °C, this value decreased to 31.0 mN/m by adding the sorbitan monostearate in the base oil (L2) at the same temperature. Furthermore, the surface tension of the mineral oil was 31.6 mN/m at 70 °C, whereas, the oil including sorbitan monostearate was evaluated as 26.8 mN/m at the same temperature. Consequently, it was understood that the surfactant used for the preparation of the inverse emulsions and the lubricants rarely decreased the surface tension of the mineral oil. This result was consistent with literature (Peltonen and Yliruusi, 2000). The addition of the surfactant into the water decreased the surface tension of the water from 70.1 mN/m to 68.9 mN/m.

Viscosity

Viscosity is defined as a measurement of resistance to flow and is a key physical property of lubricants. It must be high enough to provide proper lubricating films while avoiding excessive friction losses. The viscosity of complex organic mixtures such as oils and fuels is strongly dependent on the size (Wakabayashi, 1997), shape and chemical composition of their different constituents, and on the molecular interactions (Burg et al., 1997). Industrial lubricating oils are generally measured at 40° C and results are reported as centiStokes (cSt) or centiPoise (cP).

Effect of dispersing agent on the viscosity of the lubricants

The viscosities of the lubricants containing commercial zinc borate were measured at 40 °C and the results are shown in Figure 7.75. The viscosity of the mineral oil was measured as 29.50 cP (33.52 cSt) and this value was consistent with the literature value of light neutral SN-150 mineral oil which is 35 cSt. When the sorbitan monostearate and zinc borate additive were added to mineral oil, the viscosities of these lubricants significantly increase. However a slight decrease is observed for the viscosities of lubricants containing Viscobyk 5025 and Disperbyk 1161 since they include viscosity depressants. Moreover, the shear rate-shear stress characteristics of the lubricants are shown in Figures 7.76. Even though these curves indicate that the

rheologies of the lubricants have some deviations from the linearity, the viscosity values are constant and these fluids can be accepted as Newtonian fluids. Considerable decreases in the viscosities of all the lubricants between 60-70 1/sec are observed as shown in Figures 7.76. This means that apparent viscosity falls over shear rate and the original viscosity is restored.

Effect of zinc borate type on the viscosity of the lubricants

The lubricants having different types of zinc borate species have similar viscosity values in the range of 32.00-32.74 cP as shown in Figure 7.77. The lubricants containing zinc borate produced from zinc oxide and boric acid and dried conventionally and the zinc borate synthesized in the presence of surfactant decreases the viscosity when compared with the mineral oil with surfactant. Also, the shear rate-shear stress characteristics of the lubricants are shown in 7.78. Similar to previous samples, the viscosity values are constant and these fluids can be accepted as Newtonian fluids.
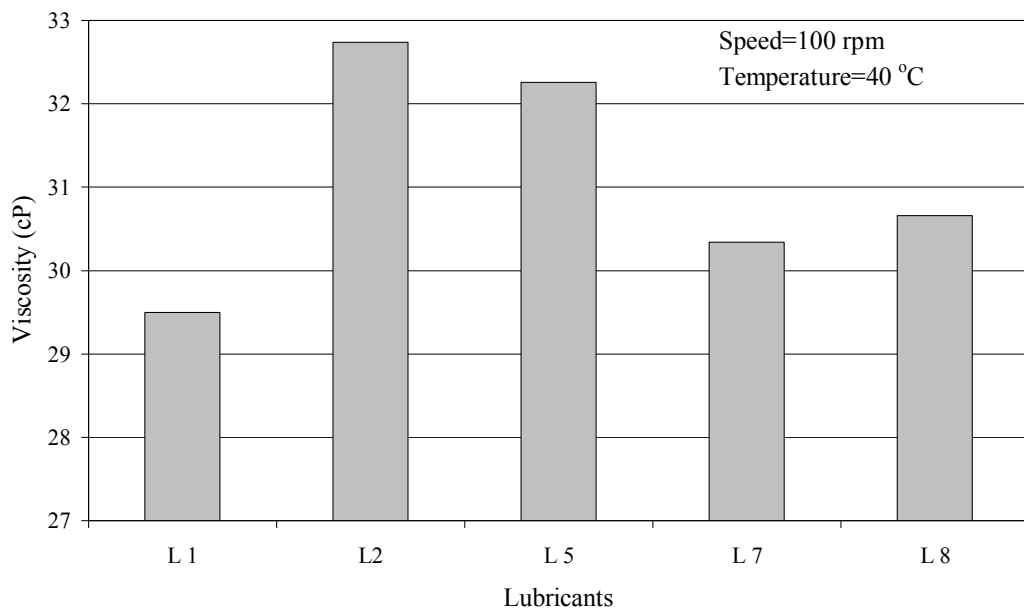
Figure 7.75. Viscosity of the mineral oil and the lubricants containing commercial zinc borate. L1: mineral oil; mineral oil with L2: sorbitan monostearate, L5: sorbitan monostearate and commercial zinc borate, L7: sorbitan monostearate, commercial zinc borate and Viscobyk 5025, L8: sorbitan monostearate, commercial zinc borate and Disperbyk 1161.

Volume fractions of the suspended particles were also calculated in this study considering Einstein's viscosity theory. The volume fraction of the suspended particles ϕ in the oil was found by using Equation 7.16.

$$\eta_r = 1 + 2.5\phi \qquad\qquad (7.16)$$

where;

η_r is relative viscosity and it is the ratio of dispersion viscosity to the viscosity of liquid dispersant. The calculated relative viscosities and the volume fractions of the suspended particles for the lubricants are listed in Table 7.25. When sorbitan monostearate and zinc borate prepared by supercritical ethanol was added to mineral oil, highest volume fraction was obtained since this type of zinc borate had the lowest particle size, hence the particles suspended in the mineral oil.
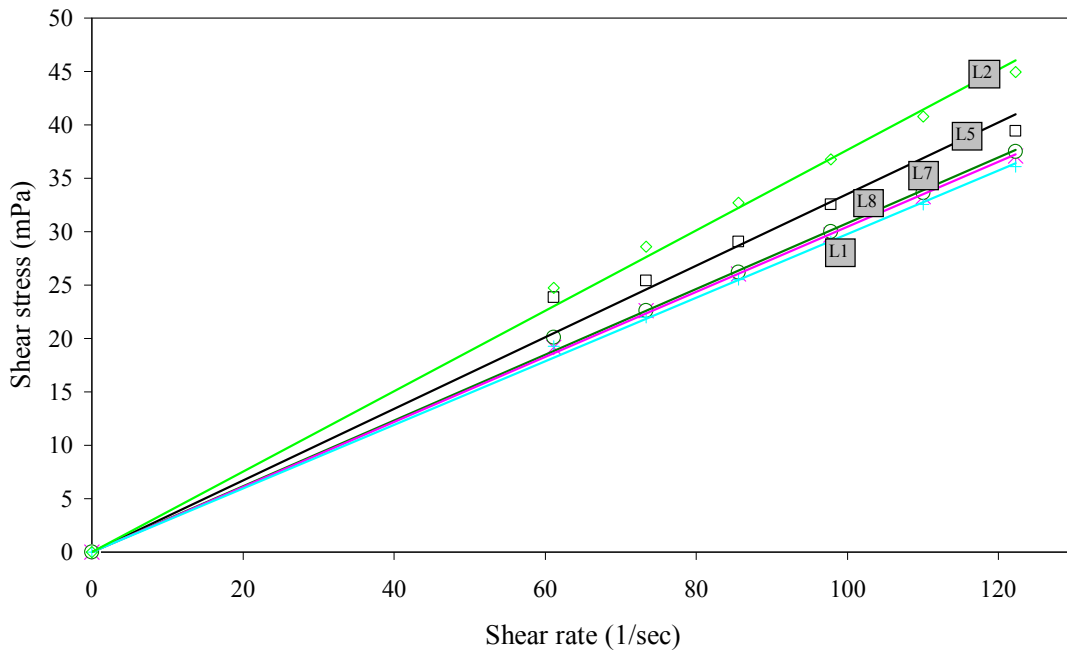
Figure 7.76. Shear rate-shear stress characteristics of the mineral oil, the mineral oil with surfactant and the lubricants prepared by commercial zinc borate. L1: mineral oil; mineral oil with L2: sorbitan monostearate, L5: sorbitan monostearate and commercial zinc borate, L7: sorbitan monostearate, commercial zinc borate and Viscobyk 5025, L8: sorbitan monostearate, commercial zinc borate and Disperbyk 1161.

168
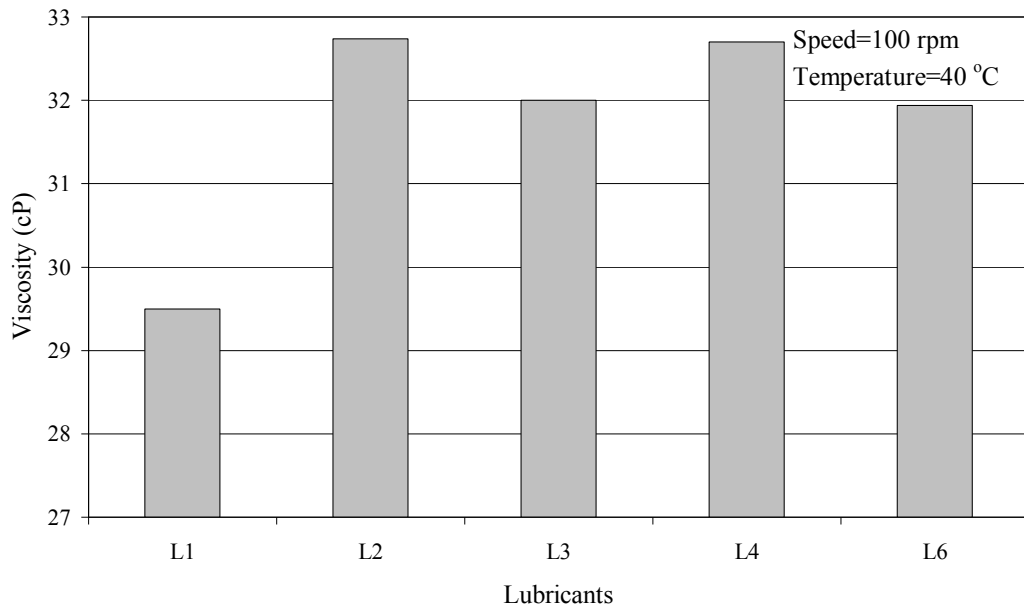
Figure 7.77. Viscosity of the mineral oil, mineral oil with surfactant, and the lubricants prepared by different zinc borate additives. Mineral oils with sorbitan monostearate and zinc borate L3: produced from boric acid and zinc oxide, dried by conventionally, L4: produced from boric acid and zinc oxide, dried by supercritical ethanol, L6: produced in the presence of sorbitan monostearate.
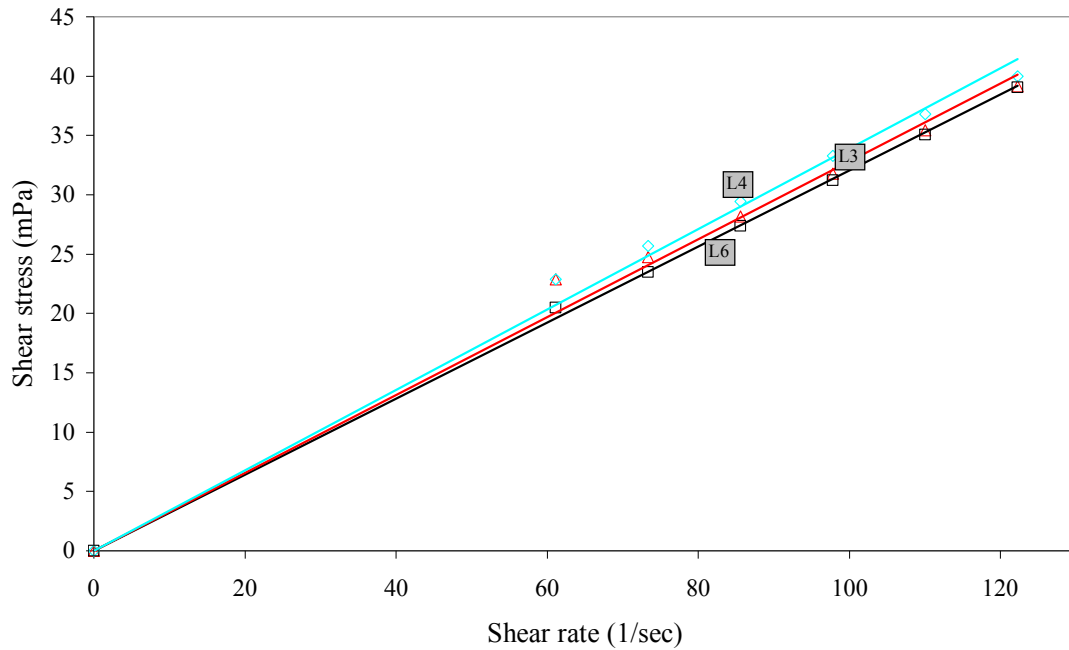
Figure 7.78. Shear rate-shear stress characteristics of the lubricants prepared by different zinc borate additives. Mineral oils with sorbitan monostearate and zinc borate L3: produced from boric acid and zinc oxide, dried by conventionally, L4: produced from boric acid and zinc oxide, dried by supercritical ethanol, L6: produced in the presence of sorbitan monostearate.

Table 7.25. Volume fractions of the suspended particles in the mineral oil

Lubricant Code	η (Pa.s)	η_o (Pa.s)	ηr	ϕ
L1	0.030	0.030	1	0
L2	0.033	0.030	1.110	0.042
L3	0.032	0.030	1.085	0.034
L4	0.033	0.030	1.108	0.043
L5	0.032	0.030	1.094	0.037
L6	0.032	0.030	1.083	0.033
L7	0.030	0.030	1.028	0.011
L8	0.031	0.030	1.039	0.016

7.6.3. Functional Groups of Lubricants

FTIR spectrometry is a fast nondestructive analytical method used for the assessment of physical and chemical properties of the lubricants and base oils. It is suitable not only for detection of the additives but also determination of degradation and oxidation. The FTIR spectra of all the lubricants before the utilization of them in the tribological test were obtained. The FTIR spectra of the mineral oil and the oil heated up to 160 °C for the preparation of L1 lubricant is given in Figure 7.79. The spectra of these products exhibit the specific peaks of mineral oil. The band at 2928 cm^{-1} is the stretching vibrations of hydrocarbons, whereas the band at 2854 cm^{-1} is related to the asymmetric stretching of –C-H. Besides them, the peak at 1464 cm^{-1} and 1377 cm^{-1} are attributed to the –CH$_2$ and –C-H symmetric vibrations of hydrocarbons. When the oil was heated the spectrum of the mineral oil did not change, which indicated that no degradation occurred after the heating of the oil. Furthermore, oxidation peaks (1715-1719 cm-1) are not observed when the oil is exposed to four ball wear test.
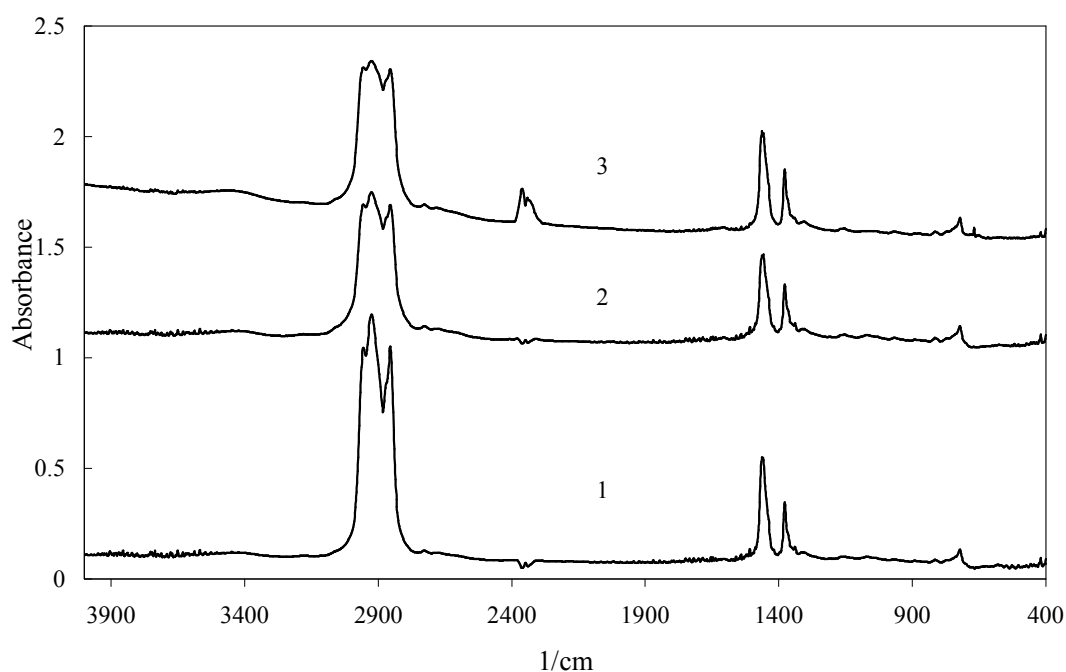
Figure 7.79. FTIR spectra of 1) mineral oil and 2) mineral oil heated up to 160°C 3) mineral oil after four ball wear test.

The samples having sorbitan monostearate and zinc borate additives are displayed through Figures A.1-A.6 in Appendix A. In these spectra the band at 1700

cm^{-1} is one of the characteristic peak of sorbitan monostearate and it shows the presence of carbon oxygen double bond. Furthermore, the specific bands for CH bends appear at approximately 1000 cm^{-1} for the in-plane bends and at about 675 cm^{-1} for the out-of-plane bend. For all of the lubricants except L1 and L2 lubricants, the characteristic peaks of zinc borate are detected and they are assigned referring to the literature (Goa et al., 2009c). The band at 1047 cm^{-1} is the stretching of B(4)-O, and the peaks between 745-658 cm^{-1} are belonging to out-of-plane bending mode of B(3)-O. In addition to zinc borate and the surfactant characteristic peaks, the peak at 2350 cm^{-1} is assigned to the carbon dioxide and nitrogen in the air and this band can be seen either a positive or a negative peak for all the samples. All these spectra revealed that the structure of the lubricants did not change when they were exposed to four ball wear test.
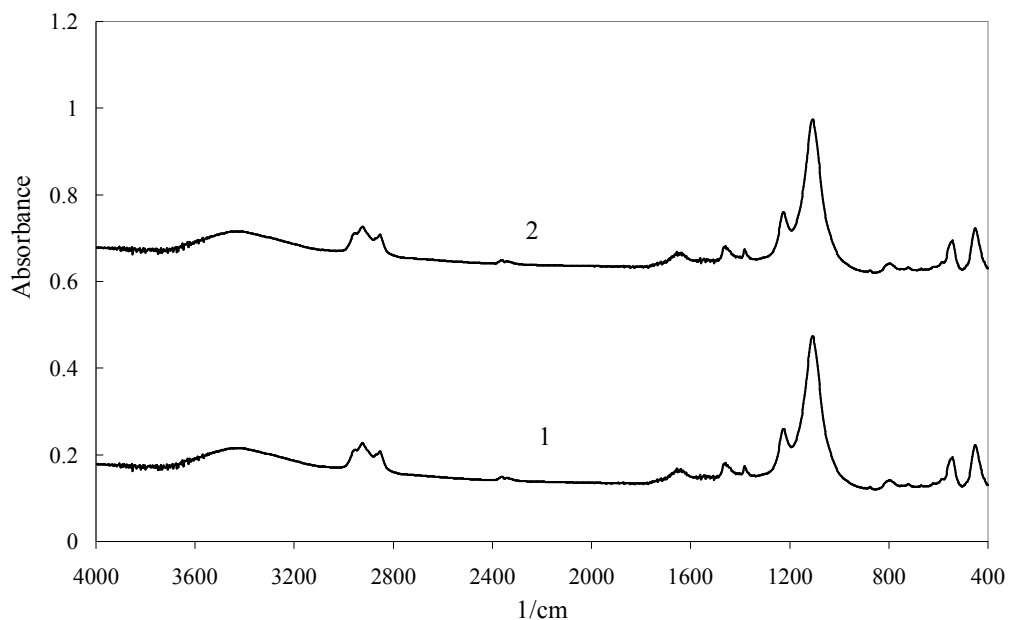
Figure 7.80. FTIR spectra of L15 lubricant containing sorbitan monostearate and clinoptilolite rich mineral 1) before and 2) after four ball wear test.

Unlike the lubricants including zinc borate, L15 lubricant prepared by the addition of clinoptilolite rich mineral in the mineral oil exhibits the characteristics peaks of natural zeolite. The peaks at 450 and 609 cm^{-1} are assigned to the internal and external Si(Al)-O double ring, respectively. H$_2$O bending vibration is detected at 1627 cm^{-1}, whereas the peak related to the H-bonded O-H stretching are observed at 3400 cm^{-1} as shown in Figure 7.80 (Breck, 1974). The presence of the characteristic peaks of natural zeolite indicates that clinoptilolite rich mineral oil suspends in the mineral oil.

7.6.4. Color Change of Lubricants

In this part of the study, the colors of the lubricants before and after four ball wear tests were determined by UV spectroscopy in the visible region. As shown from Figure 7.81, the lubricants prepared by the addition of sorbitan monostearate and zinc borate are yellow color, whereas the lubricant (L15) containing zeolite is grey. The lubricants prepared by the removing of water content from the inverse emulsions are orange.

Figure 7.81. The photographs of the prepared lubricants. Mineral oils with sorbitan monostearate and L9: zinc borate produced by coordination homogeneous precipitation, mixed for 6 h. L10: zinc borate produced by coordination homogeneous precipitation, mixed for 15 h, L11: zinc borate produced by coordination homogeneous precipitation, mixed for 12 h., L12:, 0.00005 g sorbitan monostearate and zinc borate mixed for 12 h. L13: mineral oil, 0.1 g sorbitan monostearate and zinc borate, L14: precipitate obtained by inverse emulsion having 30% propanol-2, L15: clinoptilolite rich mineral, L16: inverse emulsion of which water was removed by water, L17: inverse emulsion of which water was removed by clinoptilolite rich mineral.

UV spectrum of mineral oil is shown in Figure 7.82 and it is observed that there is an increase in the absorbance at 400-450 nm. The UV spectra of the lubricants containing only sorbitan monostearate and, sorbitan monostearate and zinc borate

prepared by coordination homogeneous technique, mixed for 15 h are indicated in Figure 7.83 and 7.84, respectively. The UV spectra of the other lubricants are displayed in Figure B.1-B.6 in Appendix B. The differences in the absorbances at 450 nm for all the lubricants are exhibited in Figure 7.85. It was revealed that the absorbances of the lubricants which were exposed to four ball wear test increased since the additive particles were crushed into the small pieces as a result of the high load during the test and accordingly, they suspended in the oil.
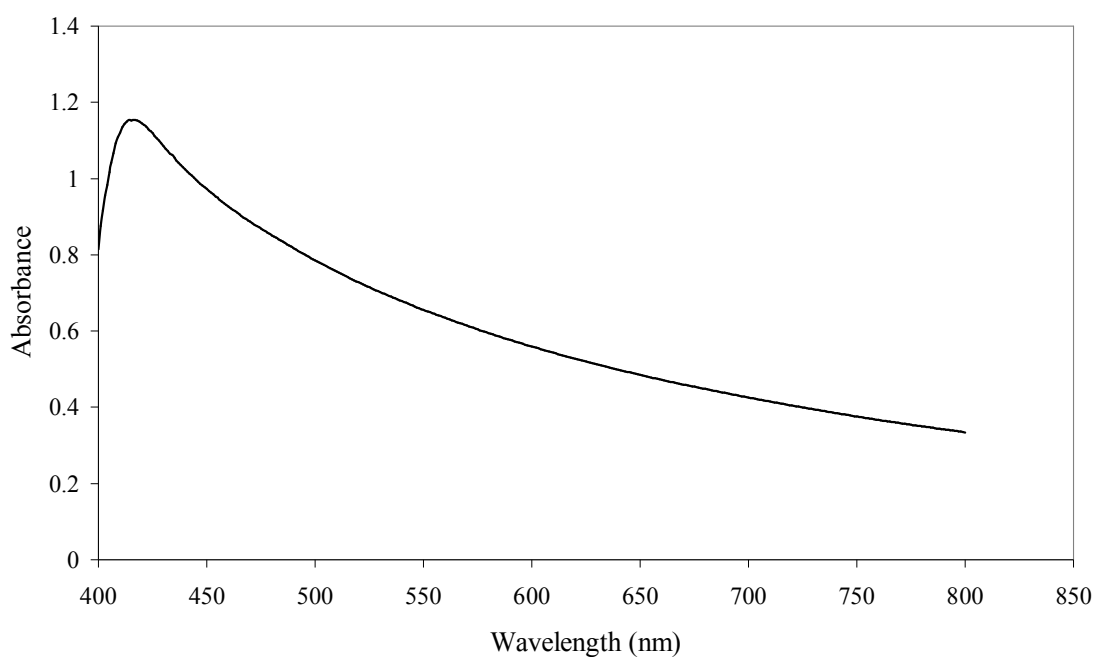
Figure 7.82. UV spectrum of mineral oil (L1) after four ball wear test.
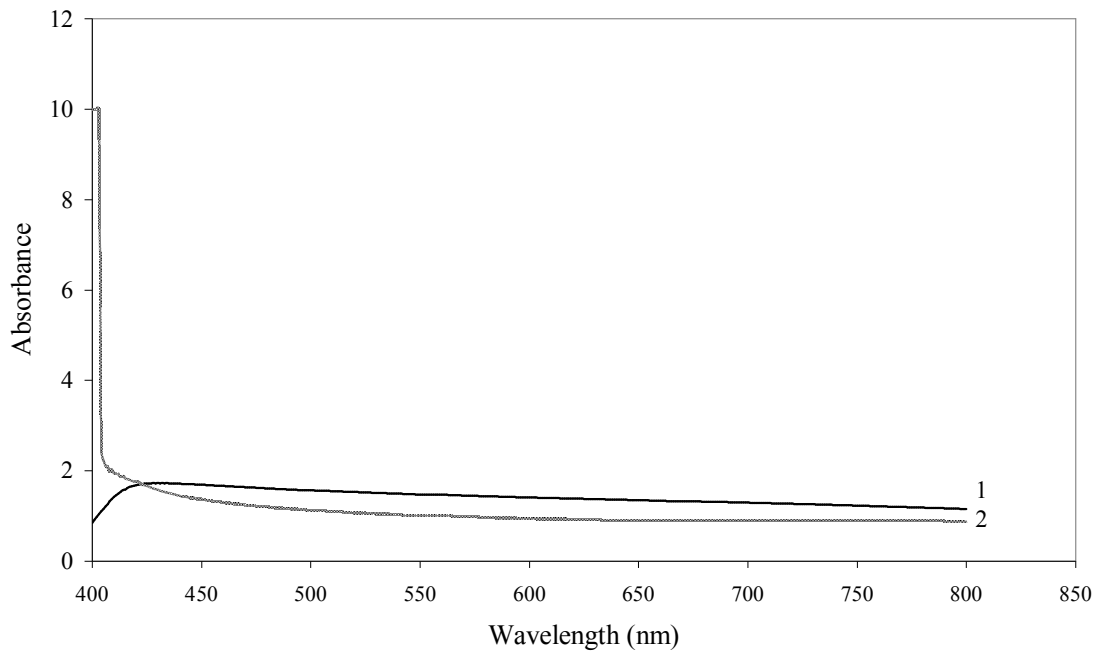
Figure 7.83. UV spectrum of L2 lubricant containing only sorbitan monostearate 1) before and 2) after four ball wear test.
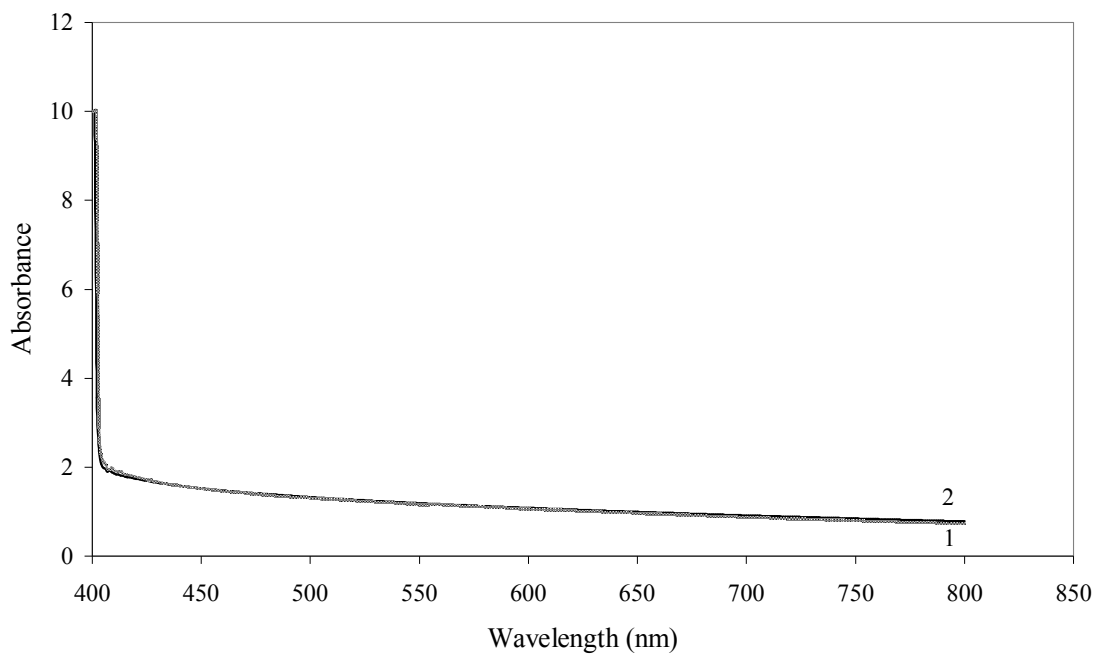
Figure 7.84. UV spectrum of L10 lubricant containing sorbitan monostearate and zinc borate prepared by coordination homogeneous technique and mixed for 15 h 1) before and 2) after four ball wear test.
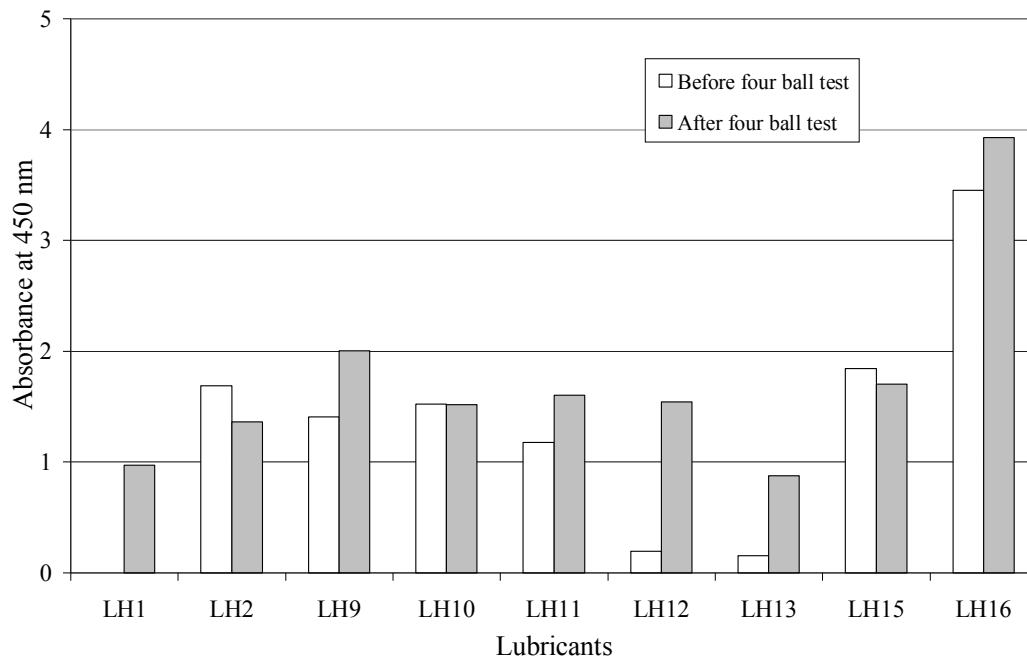
Figure 7.85. Absorbance differences of the lubricants at 450 nm. L1: mineral oil, mineral oil with L2: sorbitan monostearate, L9: zinc borate produced by coordination homogeneous precipitation, mixed for 6 h. L10: zinc borate produced by coordination homogeneous precipitation, mixed for 15 h, L11: zinc borate produced by coordination homogeneous precipitation, mixed for 12 h., L12: 0.00005 g sorbitan monostearate and zinc borate mixed for 12 h. L13: 0.1 g sorbitan monostearate and zinc borate, L14: precipitate obtained by inverse emulsion having 30% propanol-2, L15: clinoptilolite rich mineral, L16: inverse emulsion of which water was removed by water, L17: inverse emulsion of which water was removed by clinoptilolite rich mineral.

7.6.5. Tribological Properties of Lubricants

There have been many investigations on the tribological properties of lubricants with different inorganic particles added (Dong and Hu, 1998; Hu and Dong, 1998; Battez et al., 2006; Yu et al., 2010). A large number of papers have reported that the addition of particles to base oil is effective in reducing wear and friction. This part of the study attempts to explore the tribological behavior of synthesized boron based particles, clinoptilolite rich mineral in the mineral oil. The tribological property of the inverse emulsion is examined, as well. The results are given in order considering the effects of dispersing agent, zinc borate type, as well as surfactant concentration on the tribological properties of the lubricants. Among the tribotesters used for the

determination of wear and friction properties of the lubricants, a four ball wear test machine was used in order to reveal the effect of inorganic particles in the anti-wear and friction-reduction abilities. The outputs of the four ball tester indicated the optical microscopy microphotographs and the friction and the wear test results conducted at 1200±60 rpm and under a constant load of 392 N. A computer connected to the four ball tribometer provided the visualization and evaluation of the friction coefficient and wear scar diameter of the fixed balls used in the four ball tribometer. The special software evaluated the mean scar diameter for the three fixed balls and mean friction coefficient value considering one hour rotating period.

Effect of dispersing agent on the tribological properties of the lubricants

Since stabilization of commercial zinc borate particles in the mineral oil was resolved by the addition of a dispersing agent or the use of a surface modification preparation technique, their effect on the tribological property of the mineral oil was obtained by a four ball tribometer. Figures 7.86 and 7.87 exhibit typical output of the results measured by four ball tribometer and evaluated by lubricant diagnostics program. The left side of the figures shows the friction coefficient of the samples with respect to time, whereas, the right side displays the optical microphotograph of one of the fixed balls used in the four-ball wear tester. As seen in Figure 7.86, the friction coefficient of the mineral oil without any additive fluctuates with time and the mean friction coefficient of the base oil is 0.099. The wear scar of the ball rotated in mineral oil is extremely large and the average wear diameter of the sample is 1.402 mm. When the sorbitan monostearate was introduced into the oil as a dispersing agent, the friction coefficient became more stable than the mineral oil and it decreased with increasing time. The tests of other lubricants have similar outputs indicated in Figures 7.86 and 7.87. The measured friction coefficient and wear scar diameter values of the lubricants are shown in Figure 7.88 and 7.89, respectively. According to friction coefficient values in Figure 7.88, the employment of zinc borate, sorbitan monostearate and other additives has scarce effect on the reduction of friction coefficient. However, it can be seen that the lubricating oils with additives give a smaller and more stable friction coefficient than pure mineral oil. Stable friction coefficient of the oil with additive can be explained in that at a given concentration, the particles more easily will penetrate into the interface with mineral oil and form continuous film in concave of rubbing face which can decrease shearing stress, therefore, give low friction coefficient. The wear

scar diameters on the surfaces of the balls, running in the mineral oil with additives are smaller than that running in the mineral oil. For the anti-wear test, when sorbitan monostearate is added to the mineral oil the worn scar diameter is decreased by 53.21% as compared to the mineral oil without any additives. The anti-wear mechanism of the surfactant is attributed to its strong interaction with surfaces and formation of ordered structures (Wasilewski and Sulek, 2006). On the other hand, the lubricants containing zinc borate species have improving effect on the anti-wear ability of the mineral oil. However the friction could not be enhanced by these additives. Among these lubricants, the best result for anti-wear ability is obtained for the lubricant containing commercial zinc borate and Viscobyk (L7). The wear scar diameter is reduced by 54.92% for L7 lubricant as compared to the mineral oil (L1) (Figure 7.89).
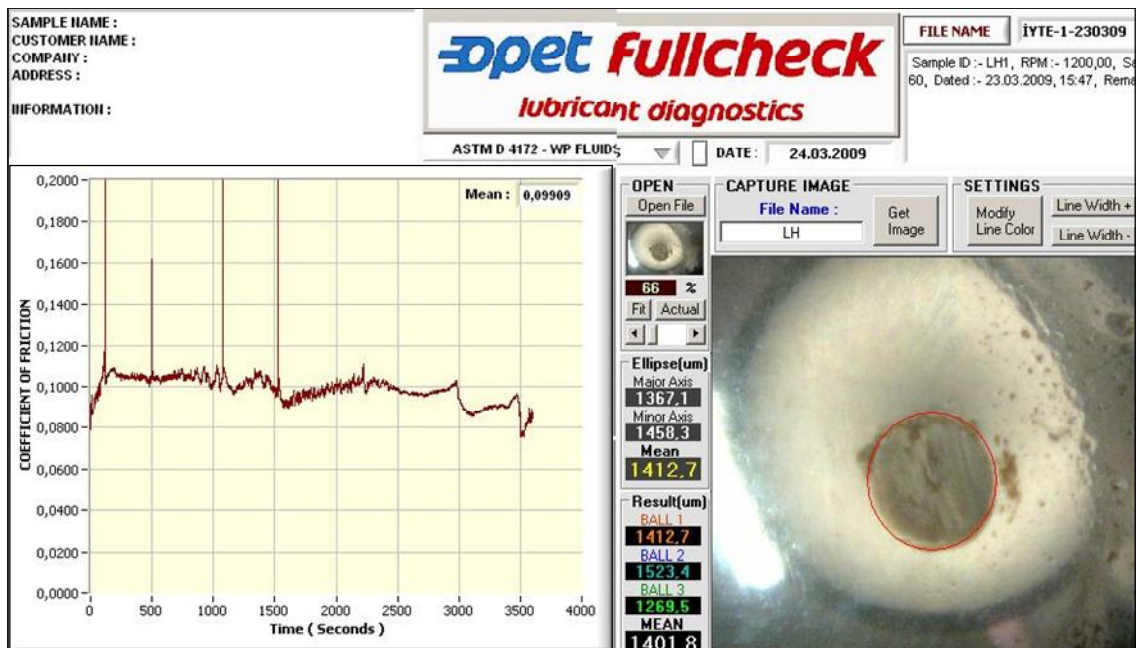
Figure 7.86. The wear and friction behavior of the mineral oil (L1).
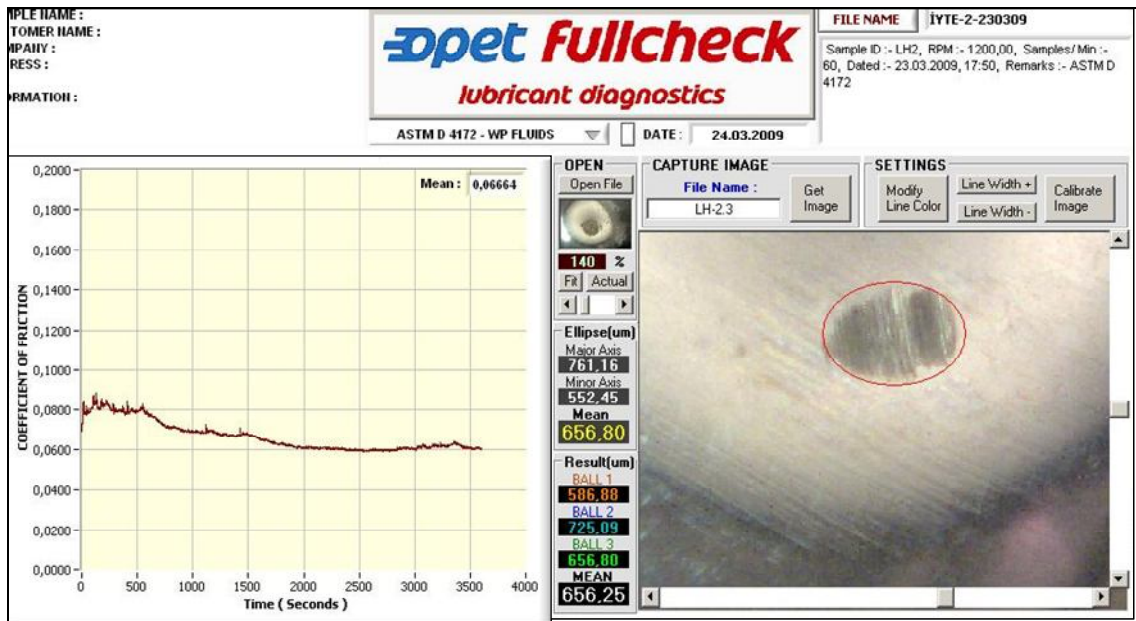
Figure 7.87. The wear and friction behavior of the mineral oil having sorbitan monostearate (L2).

Figure 7.88. Friction coefficient of the mineral oil, mineral oil with surfactant and the lubricants containing commercial zinc borate. L1: mineral oil, mineral oil with L2: sorbitan monostearate, L5: sorbitan monostearate and commercial zinc borate, L7: sorbitan monostearate, commercial zinc borate and Viscobyk 5025, L8: sorbitan monostearate, commercial zinc borate and Disperbyk 1161.

The wear resistance mechanism of the lubricant including additives is due to the deposition of particles on the worn surface which may decrease the shearing stress and strong attachment of the tribofilms to the steel surfaces, thus improving the tribological properties.

Effect of zinc borate type on the tribological properties of the lubricants

Boron compounds have been reported to be effective extreme pressure and anti wear additives (Zheng et al., 1998; Dong and Hu, 1998; Hu and Dong, 1998; Erdemir, 1995). Especially metal borates are often used as lubricating oil additives. In order to explore the antiwear efficiency of the synthesized zinc borates the lubricants prepared by using different types of zinc borate species were tested in the four ball machine. Figure 7.90 shows the wear and friction behavior of mineral oil having sorbitan monostearate and zinc borate synthesized by coordination homogeneous precipitation technique, mixed for 15 h and washed by water and ethanol. It was observed that the wear scar diameter was lower than the diameter of the ball lubricated with pure mineral oil.

Figure 7.89. Wear scar diameter of the mineral oil, mineral oil with surfactant and the lubricants containing commercial zinc borate.L1: mineral oil, mineral oil with L2: sorbitan monostearate, L5: sorbitan monostearate and commercial zinc borate, L7: sorbitan monostearate, commercial zinc borate and Viscobyk 5025, L8: sorbitan monostearate, commercial zinc borate and Disperbyk 1161.
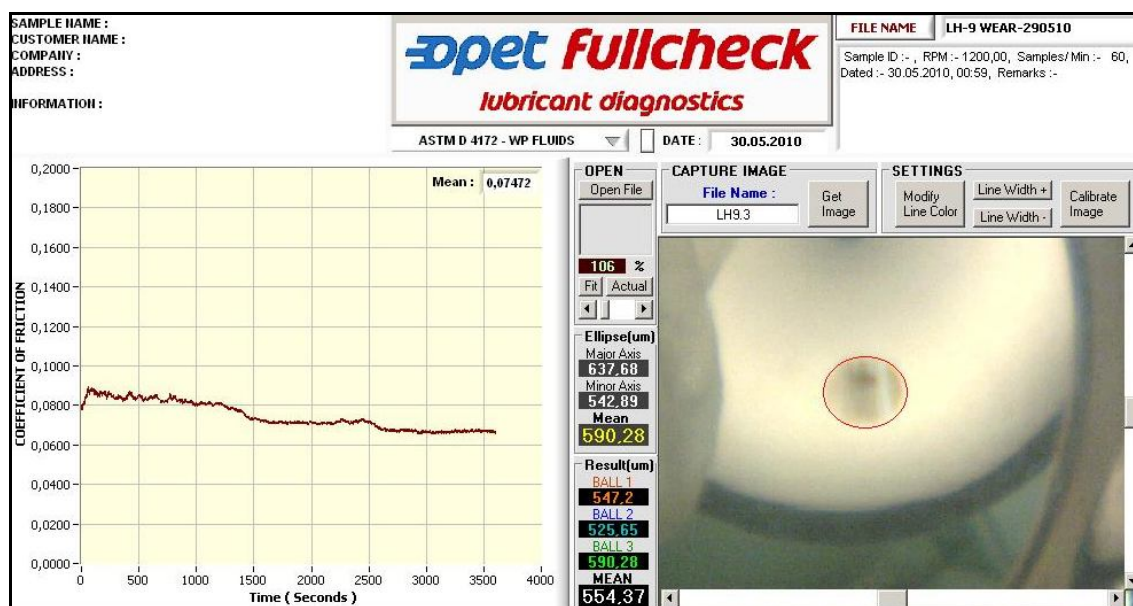
Figure 7.90. The wear and friction behavior of the mineral oil having sorbitan monostearate and zinc borate synthesized by coordination homogeneous precipitation technique, mixed for 15 h and washed by water and ethanol.

Figures C.1, and C.2 exhibit typical output of the friction and wear analysis results in Appendix C. The friction coefficient and the wear scar diameter of the samples are shown in Figure 7.91 and Figure 7.92, respectively. Zinc borate species produced by coordination homogeneous precipitation and mixed for 6, 12 and 15 hours displayed an insufficient effect to decrease the friction coefficient. However, the friction coefficient of the lubricant contained the zinc borate (ZB-15) decreased with increasing time. This type of zinc borate exhibited crystal structure and unlike the other samples (ZB-W-6 and ZB-W-12) the morphology of this type of zinc borate showed rod-like crystals. As a consequence, the mechanism of the apparent anti wear action of this zinc borate could be explained by the crystals of the sample. The crystals might have layered structure with interlayer bonds. Such a structure caused the formation of tribofilm on the metal surface. The lowest wear scar diameters were obtained when zinc borate obtained by homogeneous precipitation (ZB-W-12) was introduced into the base oil. The wear resistance mechanism of the lubricants including additives is due to the deposition of zinc borate particles on the worn surface which may decrease the shearing stress, and strong attachment of the tribofilms to the steel surfaces, thus improving the tribological properties. The scar diameter was reduced by 60.77% for lubricant containing zinc borate obtained by homogeneous precipitation and mixed for 12 h as compared to the mineral oil (L1). The other types of zinc borate did not have any

significant effect to reduce the wear when compared with the mineral oil having surfactant (L2).

Figure 7.91. Friction coefficient of the mineral oil, mineral oil with surfactant and the lubricants containing different types of zinc borate. L1: mineral oil,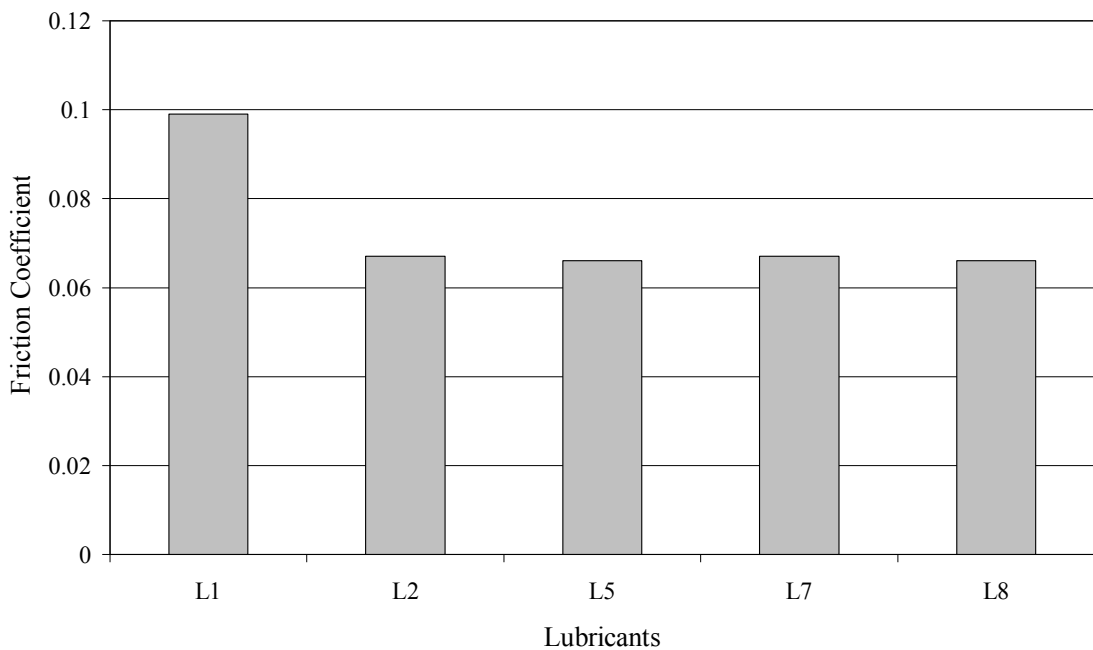 mineral oil with L2: sorbitan monostearate and L3: zinc borate produced from boric acid and zinc oxide, dried by conventionally, L4: zinc borate produced from boric acid and zinc oxide, dried by supercritical ethanol L6 zinc borate produced in the presence of sorbitan monostearate, L9: zinc borate produced by coordination homogeneous precipitation, mixed for 6 h. L10: zinc borate produced by coordination homogeneous precipitation, mixed for 15 h, L11: zinc borate produced by coordination homogeneous precipitation, mixed for 12 h

Effect of surfactant concentration on the tribological properties of the lubricants

By so far the tribological test of the lubricants revealed that the surfactant played a major role in the enhancement of the antiwear and friction reducing properties. The amounts of the surfactant in the previous samples were constant as 1 g which was significantly larger than the critical micelle concentration. So as to understand the effect of surfactant concentration on the tribological properties of the mineral oil, the lubricants were formed by changing the surfactant amount, while the same type zinc borate (ZB-W-12) were dispersed in the oil. The friction and behavior of the lubricants having 0.00005 g, 0.1 g and 1 g surfactant are shown in Figures C.3, C.4, and C.2 in

Appendix C, respectively. It was observed that the friction coefficient became stable by increasing the amount of surfactant. The wear scar diameters of the lubricants increased when the surfactant concentration was decreased. The results are explicitly shown in Figures 7.93 and 7.94. When the lubricants having only surfactant (L2) and the one containing same amount of surfactant (1 g) and also zinc borate particles (L11) were compared with each other, it was revealed that the lubricant containing also zinc borate (ZB-W-12) had the ability to decrease the wear scar diameter as seen in Figure 7.94.
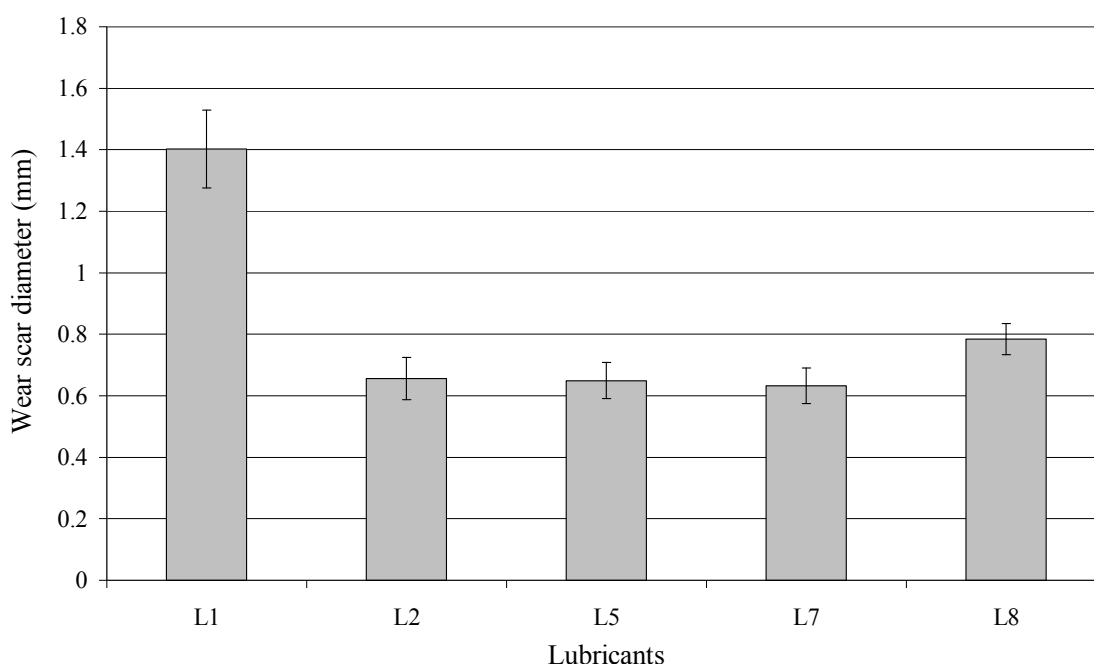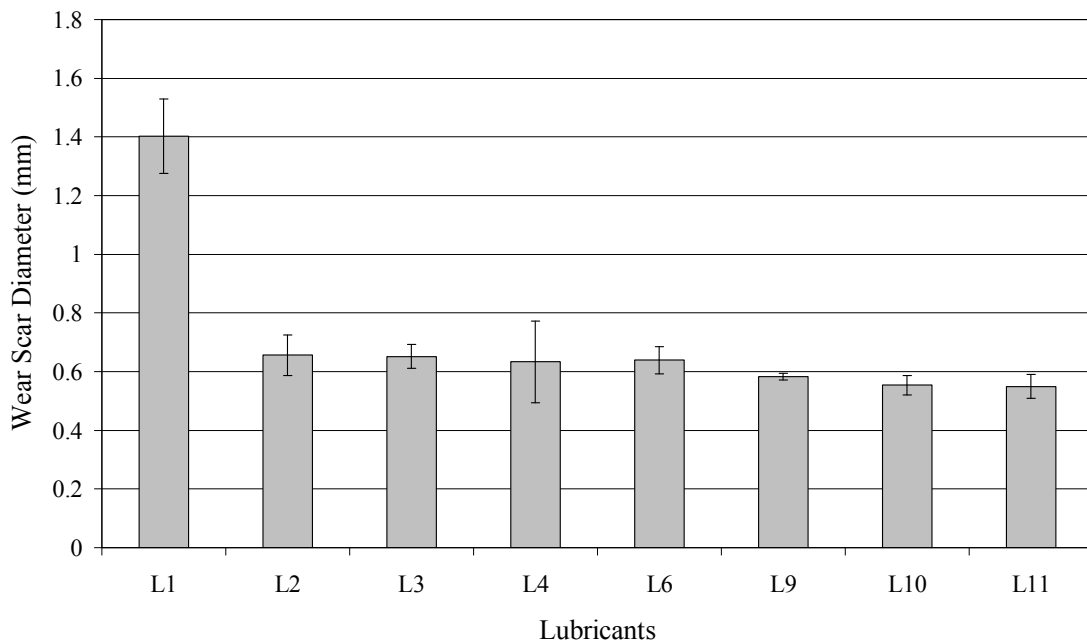

Figure 7.92. Wear scar diameter of the mineral oil, mineral oil with surfactant and the lubricants containing different types of zinc borates. L1: mineral oil, mineral oil with L2: sorbitan monostearate and L3: zinc borate produced from boric acid and zinc oxide, dried by conventionally, L4: zinc borate produced from boric acid and zinc oxide, dried by supercritical ethanol L6 zinc borate produced in the presence of sorbitan monostearate, L9: zinc borate produced by coordination homogeneous precipitation, mixed for 6 h. L10: zinc borate produced by coordination homogeneous precipitation, mixed for 15 h, L11: zinc borate produced by coordination homogeneous precipitation, mixed for 12 h

It was understood that zinc borate particles caused the decrease in the wear scar diameter. The highlighted part of the tribological results is the exposure of the surfactant effect in the enhancement of anti-wear ability of the mineral oil. In literature studies related to the employment of metal borate particles with a surfactant claim that

zinc borate develops the tribological properties of the mineral oil. However, the researchers do not notice or consider the effect of the surfactant on the tribological results (Dong and Hu, 1998 and Hu and Dong, 1998). But in this study it was explored that the introduction of the mixture containing ester the base oil shows stable friction coefficient with increasing time. This might be due to the strong interaction of surfactants with surfaces, formation of ordered structures (Wasilewski and Sulek, 2006). Besides them, when the surfactant concentration was used higher than the critical micelle concentration, the surfactant covers the surfaces and enables to improve the tribological characteristic of the base oil.
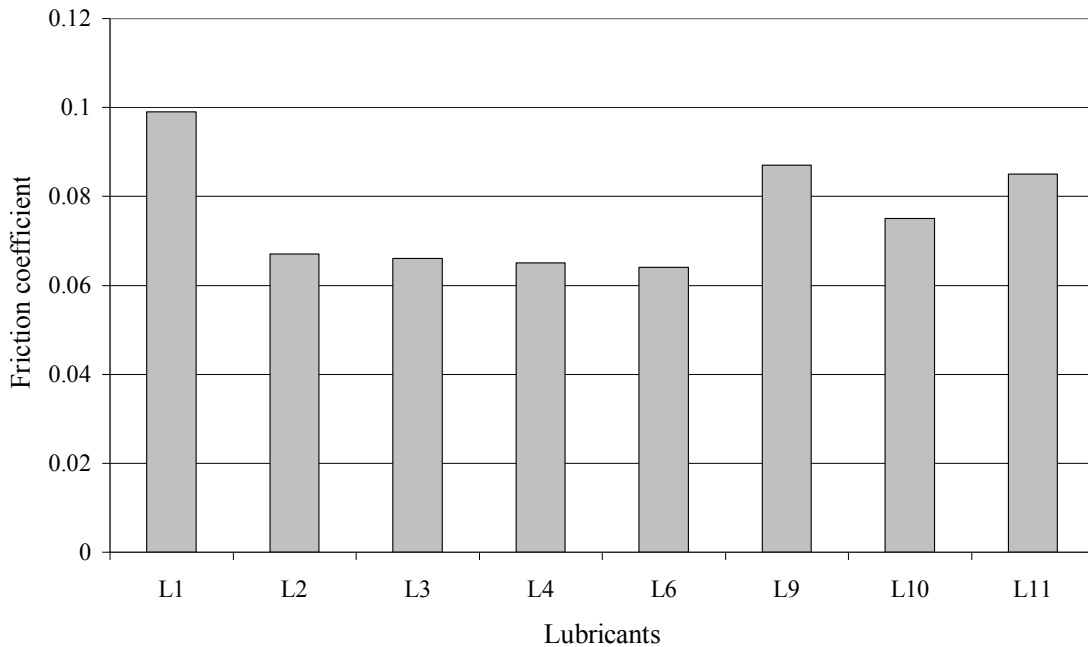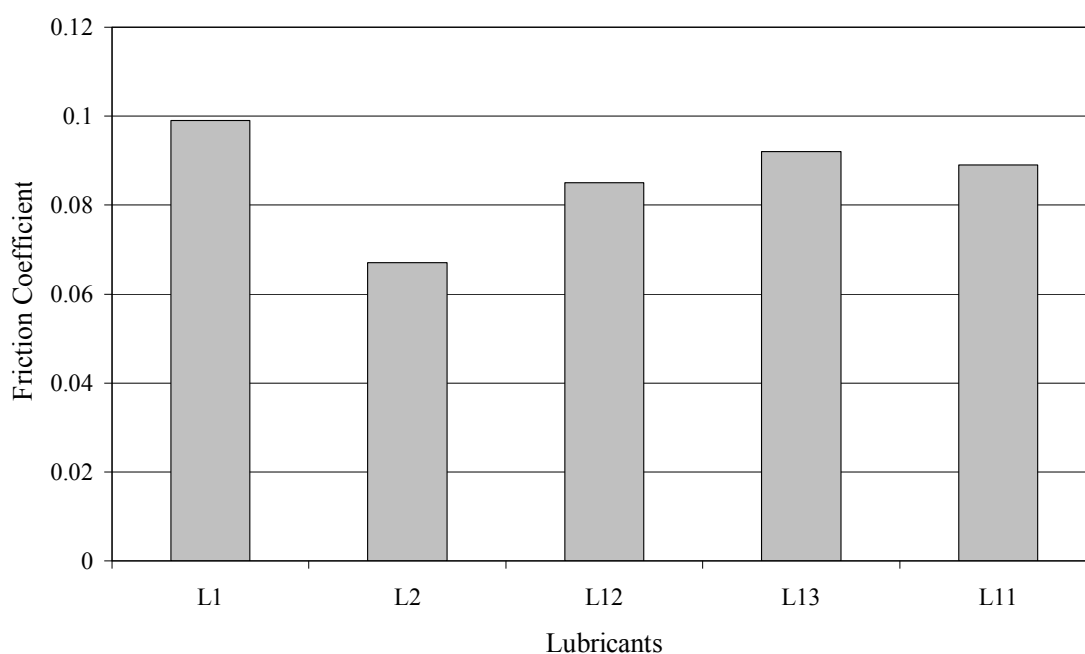

Figure 7.93. Friction coefficient of the mineral oil, mineral oil with surfactant and the lubricants containing zinc borate synthesized by homogeneous precipitation and mixed for 12 h and different amount of surfactant. L12: 0.00005 g sorbitan monostearate, L13: 0.1 g sorbitan monostearate, L11: 1g sorbitan monostearate.
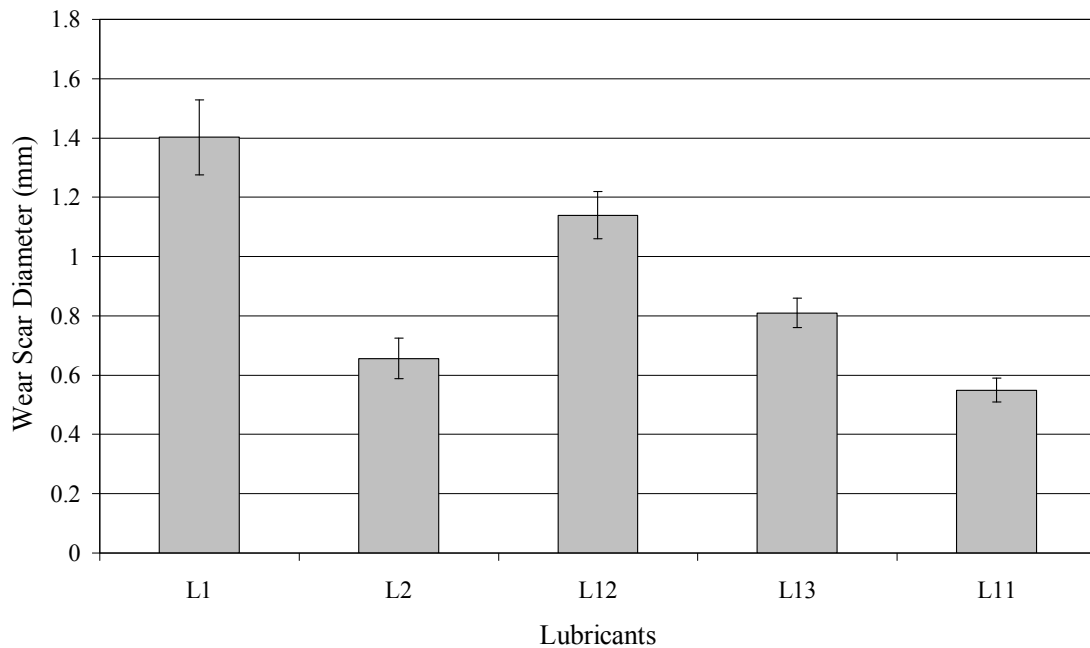
Figure 7.94. Wear scar diameter of mineral oil, mineral oil with surfactant and the lubricants containing zinc borate synthesized by homogeneous precipitation and mixed for 12 h and different amount of surfactant. L12: 0.00005 g sorbitan monostearate, L13: 0.1 g sorbitan monostearate, L11: 1g sorbitan monostearate.

Clinoptilolite rich mineral as lubricant additive and water adsorber in inverse emulsion

Among the inorganic materials used as antiwear additives, clinoptilolite rich mineral was tested in two ways. Firstly, clinoptilolite with 5 μm particle size was dispersed in the mineral oil and it was investigated whether it had antiwear ability or not. The test result is indicated in Figure C.7 in Appendix C. The friction coefficient value of the sample is almost stable and the average friction coefficient is 0.080, whereas the average wear scar diameter is 0.613 mm. Therefore the wear scar diameter is reduced by 6.70% for this lubricant as compared to the mineral oil containing surfactant. This result proved that clinoptilolite rich minerals could also be used as antiwear additives in the base oils. In literature, the mechanism responsible for the improvement of tribological properties of base oil by inorganic mineral is explained by the formation of a protective layer with smoother and harder surface on rubbed metal surface. These super lubricious oxide layers on the worn ferrous surfaces enhanced the tribological properties of the mineral oil (Yu et al., 2010).

Secondly, the water adsorber property of clinoptilolite rich mineral was examined by adding clinoptilolite rich minerals having 2-3 mm particle size in the in the inverse emulsion. The inverse emulsion containing clinoptilolite particles were kept for two days for the adsorption of water from the inverse emulsion .The lubricant obtained after the separation of clinoptilolite particles (L15) was tested by the four ball tribometer. Figure C.8 in Appendix C shows the friction and wear behavior of this sample. The friction coefficient value of the sample is almost stable and the average friction coefficient is 0.080, whereas the wear scar diameter is 0.565.

7.6.6. Characterization of the Worn Surfaces

The wear scar surfaces of the balls after the tests with lubricants were characterized by optical microscope, and SEM. The surface roughnesses of the scars were measured and the elemental analysis was also carried out by EDX in order to understand the lubrication mechanism.

Effect of dispersing agent on the worn surfaces

The optical microscope microphotographs of worn surfaces of both rotating and fixed balls were obtained for all the lubricants. The microphotographs of the balls lubricated with pure mineral oil, oil with surfactant and the lubricants containing commercial zinc borate are shown in Figures between 7.95 and 7.99. The worn surfaces of the rotating balls show continuous scars around the balls while the worn surfaces of the fixed balls exhibit circular and ellipsoid structures. Since the anti-wear performance of the pure mineral oil is very poor, the wear scar area of the balls lubricated with mineral oil are larger than the others. The addition of dispersing agent in the mineral oil enhances the worn surfaces since the trace of the worn surfaces of the fixed balls lubricated with Disperbyk displays circular scar, whereas the others show ellipsoid shape scars.
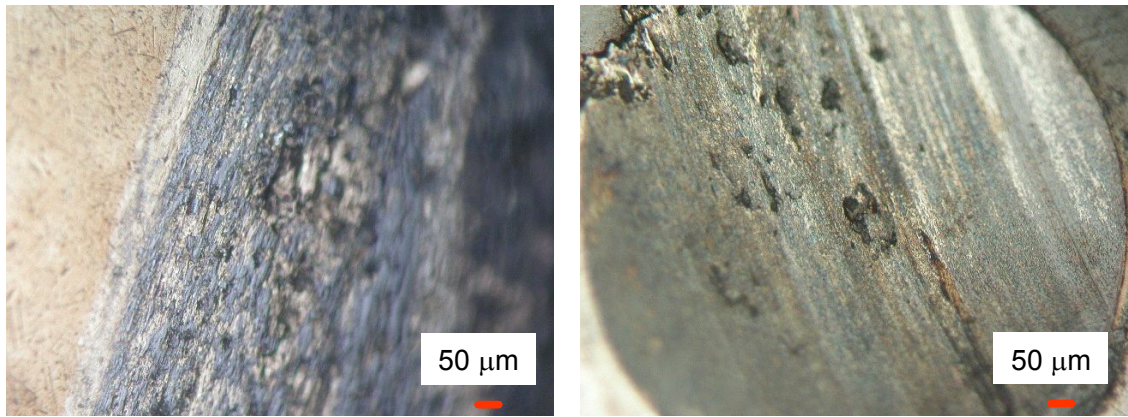
(a)   (b)

Figure 7.95. The optical microphotographs of the worn surfaces of a) rotating ball b) fixed ball lubricated with mineral oil without any additive (L1).
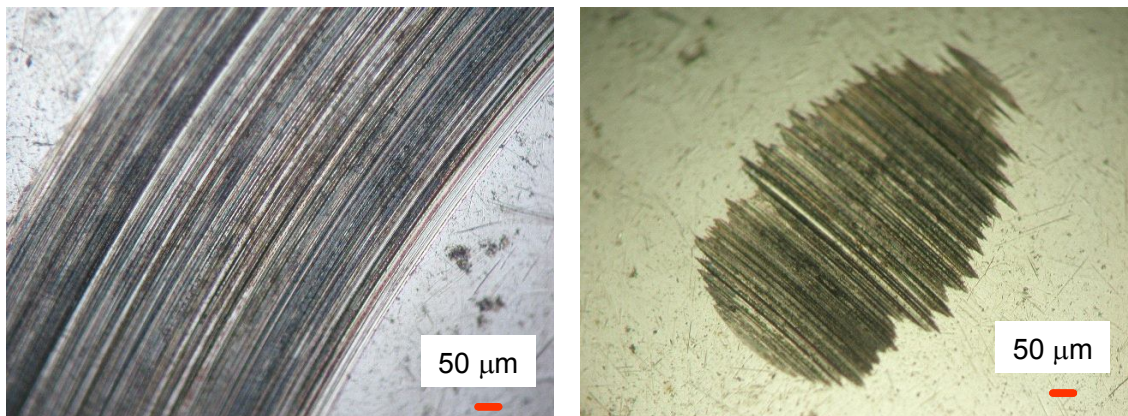
(a)   (b)

Figure 7.96. The optical microphotographs of the worn surfaces of a) rotating ball b) fixed ball lubricated with mineral oil including sorbitan monostearate (L2).

In order to obtain more detailed information of the worn surfaces of the steel balls, the morphology of the surfaces of the fixed balls were examined by SEM. The SEM images of the fixed ball surfaces are shown in Figure 7.100-Figure 7.104. Even though these SEM images are similar to those obtained by optical microscopy, more particular visualization can be obtained by SEM. As shown in Figure 7.100, severe wear is observed for the ball lubricated with mineral oil without any additives and small hollows take place due to the poor lubrication property of the mineral oil and protective film can not be produced on the rubbing surfaces. The worn scar depths decrease by the addition of sorbitan monostearate into the mineral oil (Figure 7.101). It verified the anti-wear action of the surfactant and its enhancement of the load carrying capacity. As

esters are polar molecules, they tend to migrate to metal surfaces and form physical bonds with surfaces. This result is in agreement with literature which indicates the anti-wear action of sorbitan ester surfactants (Wasilewski et al., 2006).

| (a) | (b) |
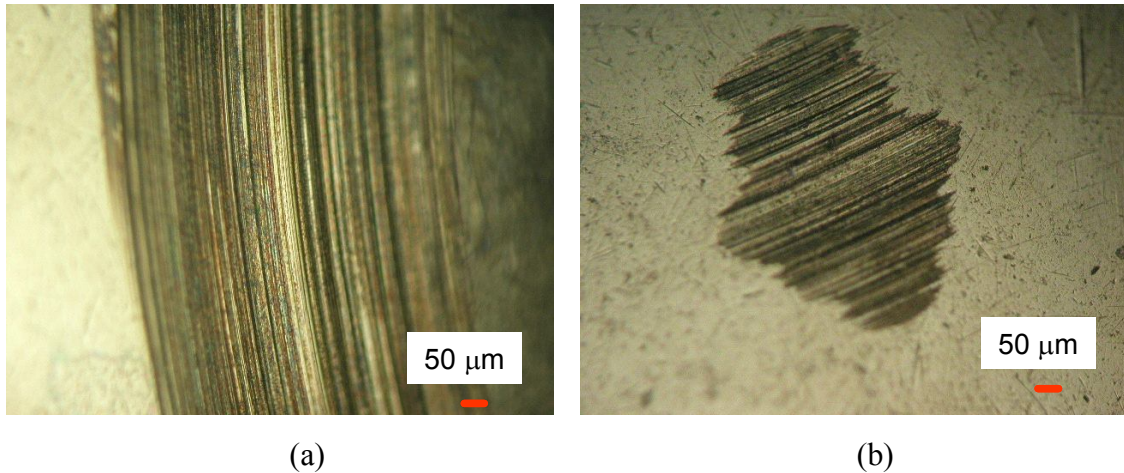
Figure 7.97. The optical microphotographs of the worn surfaces of a) rotating ball b) fixed ball lubricated with mineral oil including sorbitan monostearate and commercial zinc borate (L5).

| (a) | (b) |
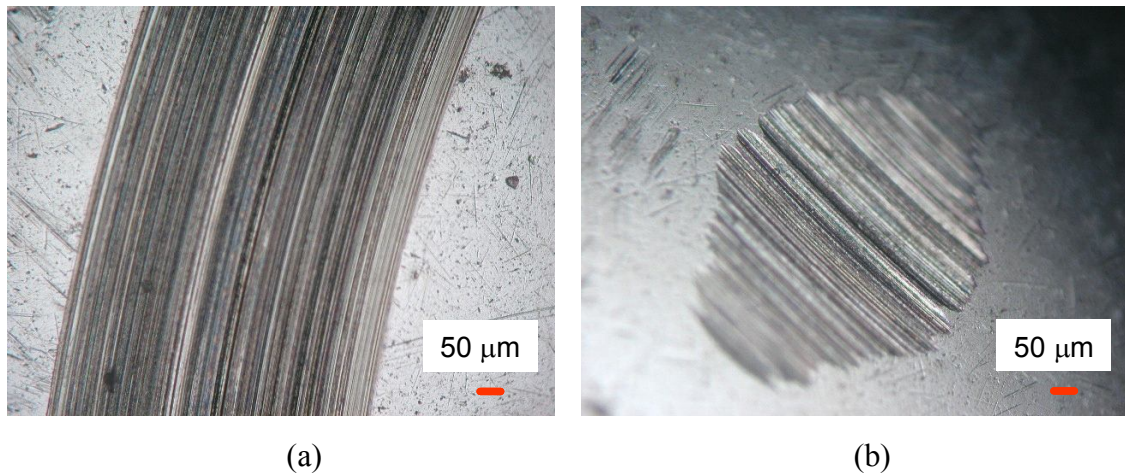
Figure 7.98. The optical microphotographs of the worn surfaces of a) rotating ball b) fixed ball lubricated with mineral oil including sorbitan monostearate, commercial zinc borate and Viscobyk (L7).

When the balls lubricated with commercial zinc borate, few scratches on the steel surface was observed (Figure 7.102). Less worn and much smoother surface was obtained by using Viscobyk 5025 than that lubricated with mineral oil including Disperbyk 1161 (Figures 7.103 and 7.104). It is revealed that Viscobyk has a potential

use as an anti-wear agent, while Disperbyk has friction-reducing property since they are the carboxylic acid esters. In literature it is stated that organic acid may react with metal surface to form chemical adsorbed or reacted boundary film which improves the tribological characteristic of the oil (Xue et al., 1997).
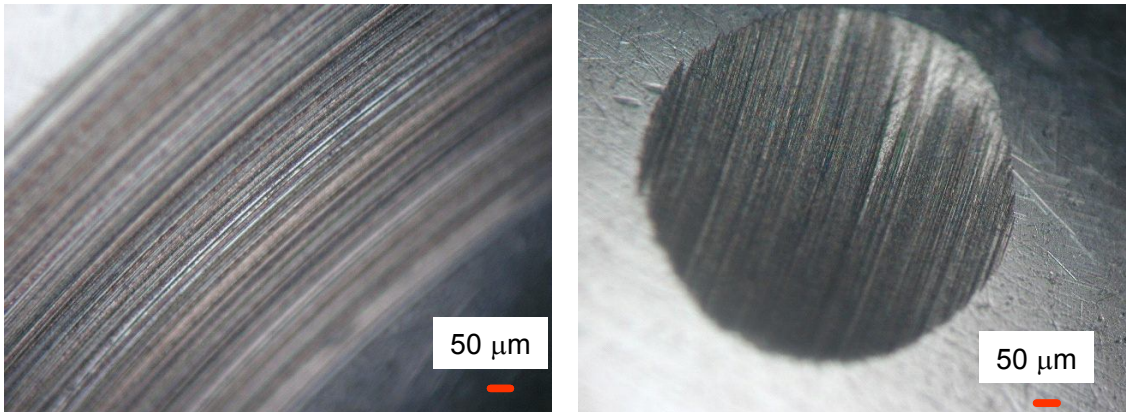
Figure 7.99. The optical microphotographs of the worn surfaces of a) rotating ball b) fixed ball lubricated with mineral oil including sorbitan monostearate, commercial zinc borate and Disperbyk (L8).

(a)   (b)
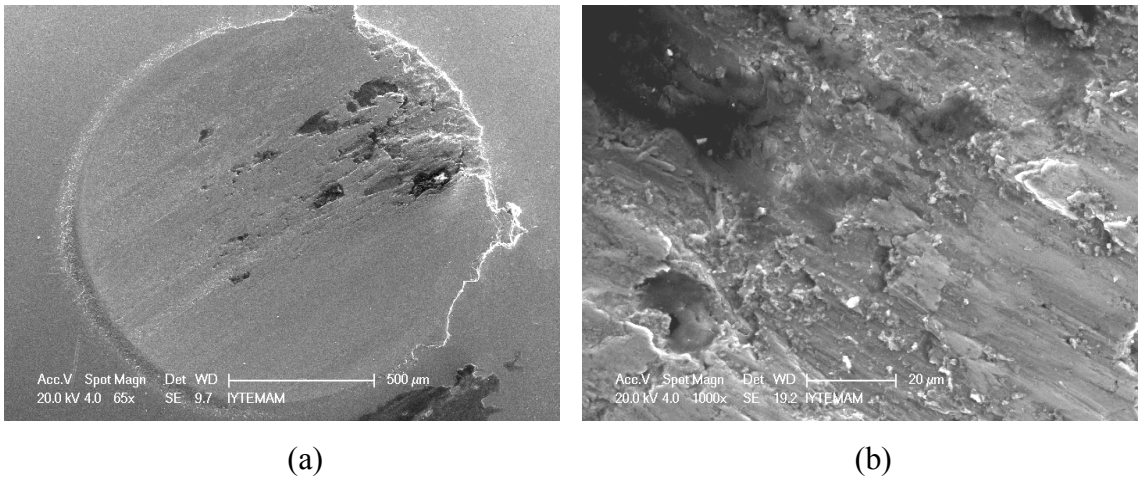
Figure 7.100. SEM images of the worn surface of the steel ball lubricated with mineral oil (L1) a) 65x and b) 1000x magnification.
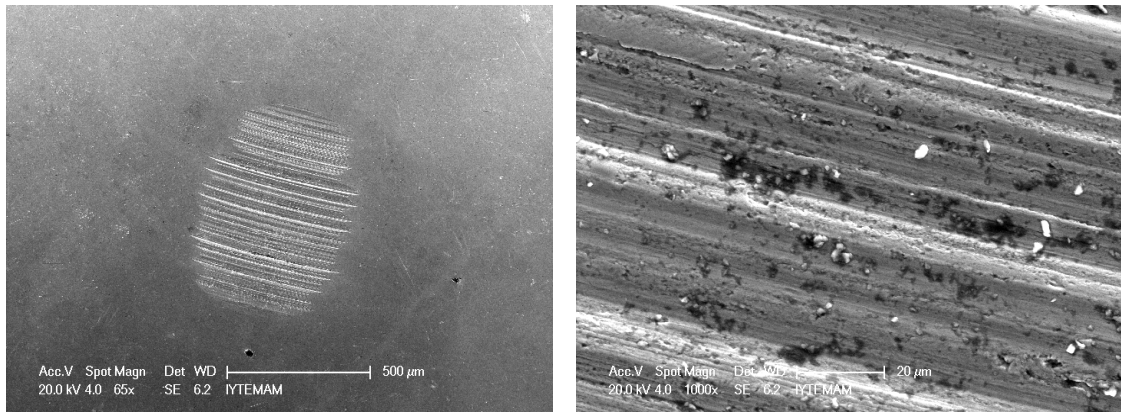
Figure 7.101 SEM images of the worn surface of the steel ball lubricated with mineral oil including sorbitan monostearate (L2) a) 65x and b) 1000x magnification.
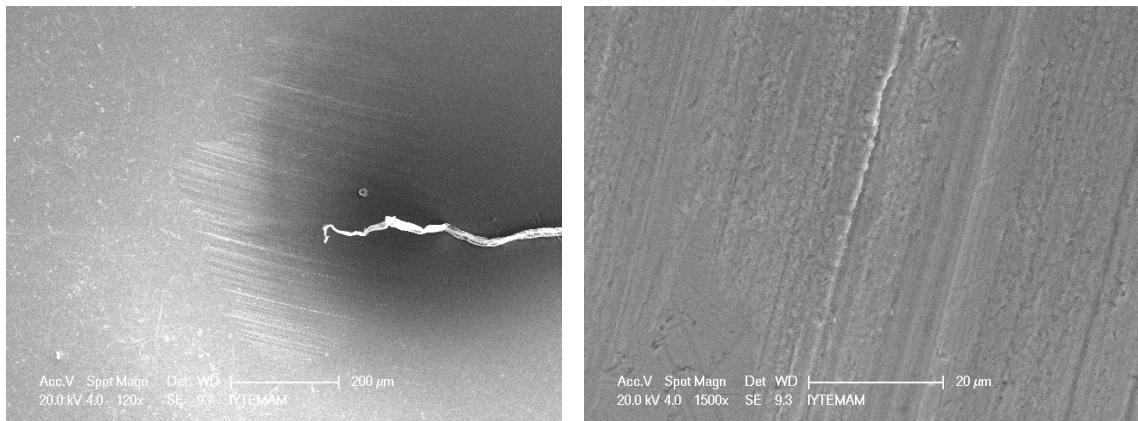
Figure 7.102. SEM images of the worn surface of the steel ball lubricated with mineral oil including sorbitan monostearate and commercial zinc borate (L5) a) 120x and b) 1500x magnification.

The chemical composition of the worn surfaces formed between two rubbing bodies in the presence of the lubricants were determined since it was the first key area to look at in searching for factors that affected the lubricants' anti-wear performance. However, these kinds of analysis were extensively carried out by X-ray photoelectron spectroscopy (XPS), and Auger electron spectroscopy (AES) in literature (Nicholls et al., 2005; Xue et al., 1997). However, only EDX analysis was used to determine the composition of the worn surfaces in this study. After wear tests, the steel balls were rinsed with ethanol and the chemical composition of the worn surfaces were analyzed. The results are listed in Table 7.25. The balls used for the wear experiments are chrome

steel balls including chromium, phosphate, manganese, silicon and sulphur. The carbon, chromium and silicon weight percent of these balls in literature (Leśniewski and Krawiec, 2008) are 1.10%, 1.30% and 0.35%, respectively. The EDX spectra of the unworn and worn surfaces of the balls are displayed in Figure 7.105. When the ball lubricated with zinc borate a small peak related to boron element appeared in EDX spectrum as shown in Figure 7.105b.

(a)   (b)
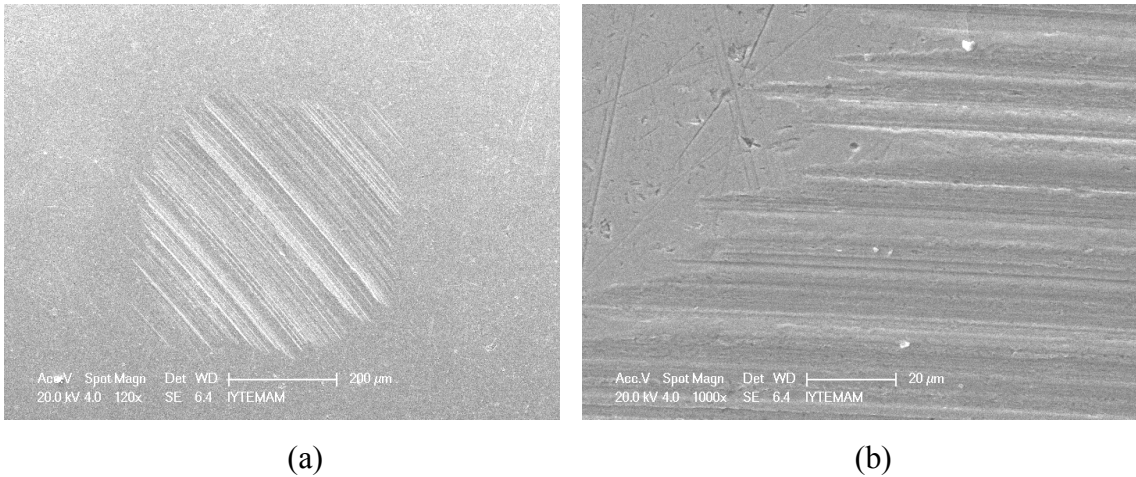
Figure 7.103. SEM images of the worn surface of the steel ball lubricated with mineral oil including sorbitan monostearate, Viscobyk 5025 and commercial zinc borate (L7) a) 120x and b) 1000x magnification.

(a)   (b)
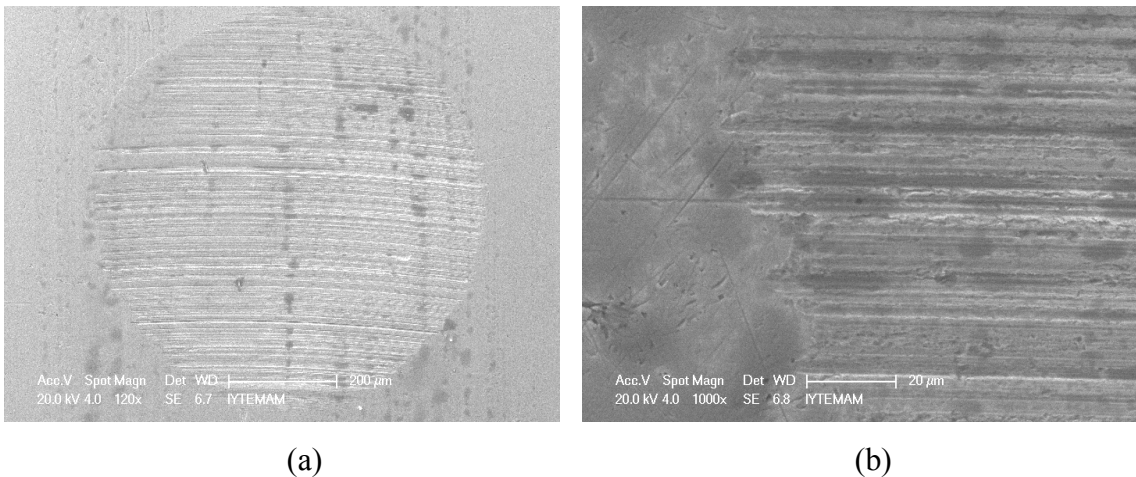
Figure 7.104. SEM images of the worn surface of the steel ball lubricated with mineral oil including sorbitan monostearate, Disperbyk 1161 and commercial zinc borate (L8) a) 120x and b) 1000x magnification.

According to the results in Table 7.26, the carbon weight percentage of the samples are significantly higher than the balls indicated the presence of mineral oil and /or the surfactant deposit on the worn surface. The oxygen weight percentages of the samples are between 2.62-8.00% and these high values arise from the mineral oil and sorbitan monostearate. Besides them, this analysis reveals that the boron and zinc elements are also adsorbed by the surfaces; therefore, the tribological properties of the mineral oil can be improved.
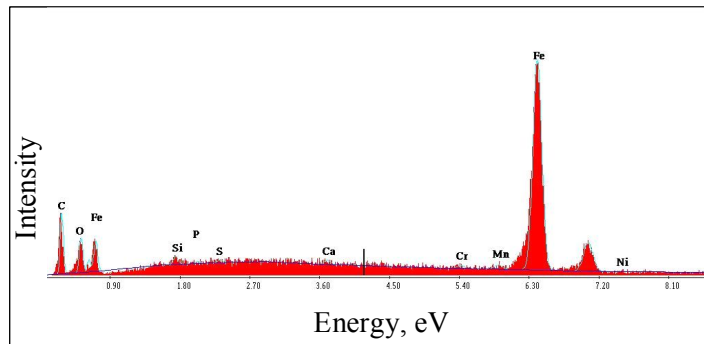
(a)
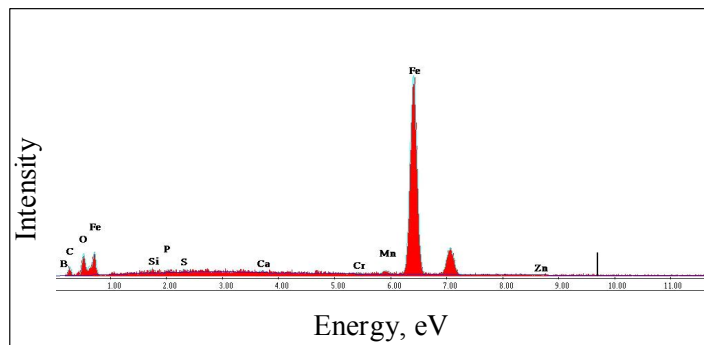
(b)

Figure 7.105. EDX spectra of a) unworn surface of the ball b) worn surface of the ball lubricated with mineral oil having commercial zinc borate (L5).

In this part of the study, the roughness values of the worn surfaces of the test balls are measured to investigate the correlation between roughness parameters and wear. Average surface roughness (Ra) gives very good overall description of height variations but it is not sensitive on small changes in profile. The measured roughness values of the fixed balls (Ra) lubricated with mineral oil, mineral oil with surfactant and the lubricants containing commercial zinc borate are given in Figure 7.106 whereas, the

measured roughness values of the rotating balls are indicated in Figure 7.107. According to these three fixed balls, minimum surface roughness is obtained when the balls lubricated with the lubricant (L7) including commercial zinc borate and Viscobyk. Besides them, the maximum roughness depth which refers to Ry is measured both for the fixed and rotating balls. Maximum roughness depth values indicate the peak to valley distance for each sample. Similar to the average surface roughness results, the minimum peak to valley distances are measured for the fixed and rotating balls when they are lubricated with the lubricant (L7) including commercial zinc borate and Viscobyk and the lubricant (L6) including zinc borate produced in the presence of the surfactant, respectively as shown in Figure 7.108 and 7.109.

Table 7.26. Elemental composition of the worn surfaces lubricated mineral oil, mineral oil with surfactant and the lubricants containing commercial zinc borate.

Element	Av.wt.%					
	Unworn	L1	L2	L5	L7	L8
C	5.09	16.47	14.73	14.48	7.96	10.65
O	0.87	7.13	8.00	5.16	7.81	12.2
Fe	90.50	75.77	74.31	68.48	72.26	63.74
Si	0.32	0.40	0.66	0.41	0.40	0.53
Cr	0.50	0.06	0.16	0.30	0.24	0.28
Mn	1.49	0.00	0.00	0.69	0.91	0.95
S	0.19	0.00	0.43	0.44	0.38	0.39
P	0.17	0.00	0.00	0.21	0.22	0.37
Ni	0.63	0.17	0.24	0.00	0.00	0.00
Ca	0.47	0.00	1.49	0.16	4.72	5.36
B	0	0.00	0.00	7.48	3.45	4.93
Zn	0	0.00	0.00	0.97	0.64	0.60
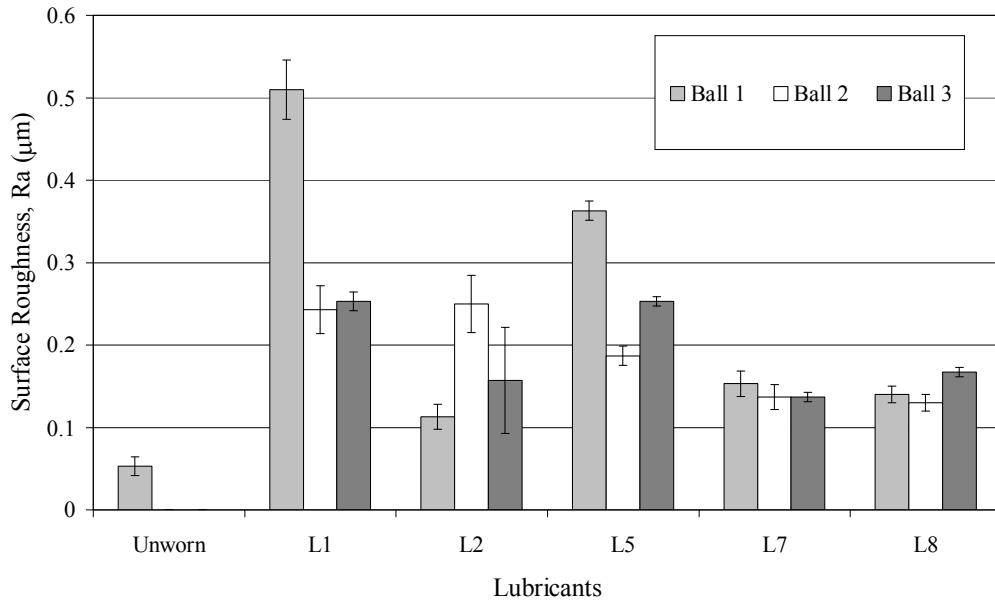
Figure 7.106. The surface roughness of the fixed balls lubricated with mineral oil, mineral oil with surfactant and the lubricants containing commercial zinc borate. L1: mineral oil; mineral oil with L2: sorbitan monostearate, L5: sorbitan monostearate and commercial zinc borate, L7: sorbitan monostearate, commercial zinc borate and Viscobyk 5025, L8: sorbitan monostearate, commercial zinc borate and Disperbyk 1161.
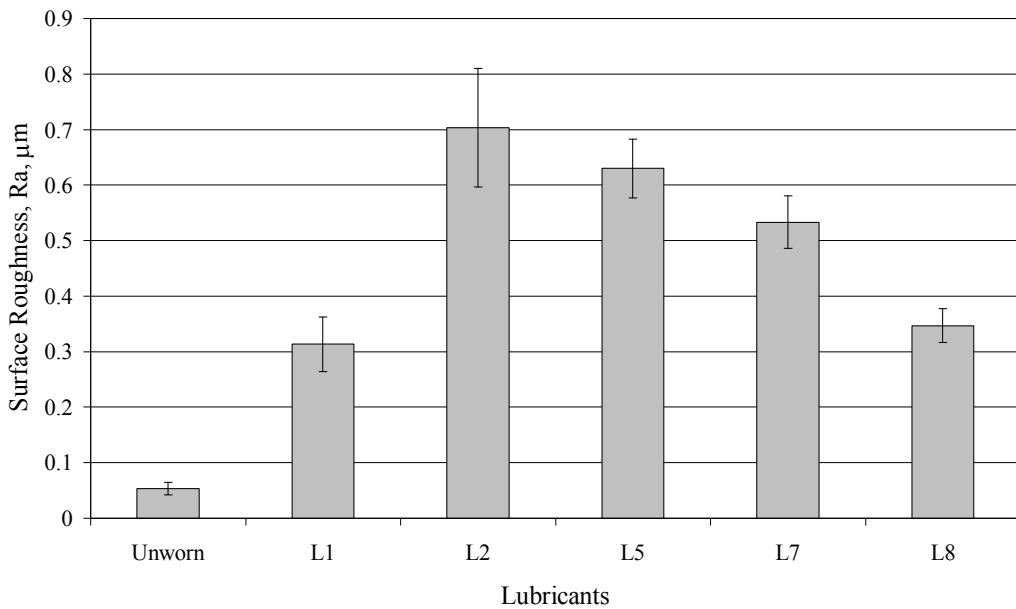
Figure 7.107. The surface roughness of the rotating balls lubricated with mineral oil, mineral oil with surfactant and the lubricants containing commercial zinc borate. L1: mineral oil; mineral oil with L2: sorbitan monostearate, L5: sorbitan monostearate and commercial zinc borate, L7: sorbitan monostearate, commercial zinc borate and Viscobyk 5025, L8: sorbitan monostearate, commercial zinc borate and Disperbyk 1161.

194
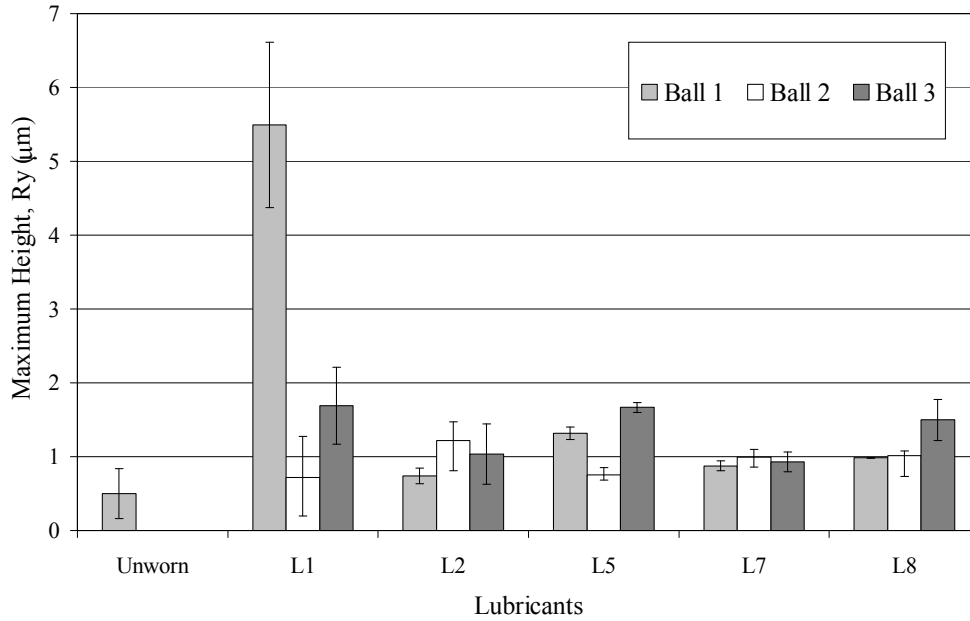
Figure 7.108. Maximum height of the fixed balls lubricated with mineral oil, mineral oil zinc borate with surfactant and the lubricants containing commercial zinc borate. L1: mineral oil; mineral oil with L2: sorbitan monostearate, L5: sorbitan monostearate and commercial zinc borate, L7: sorbitan monostearate, commercial zinc borate and Viscobyk 5025, L8: sorbitan monostearate, commercial and Disperbyk 1161.
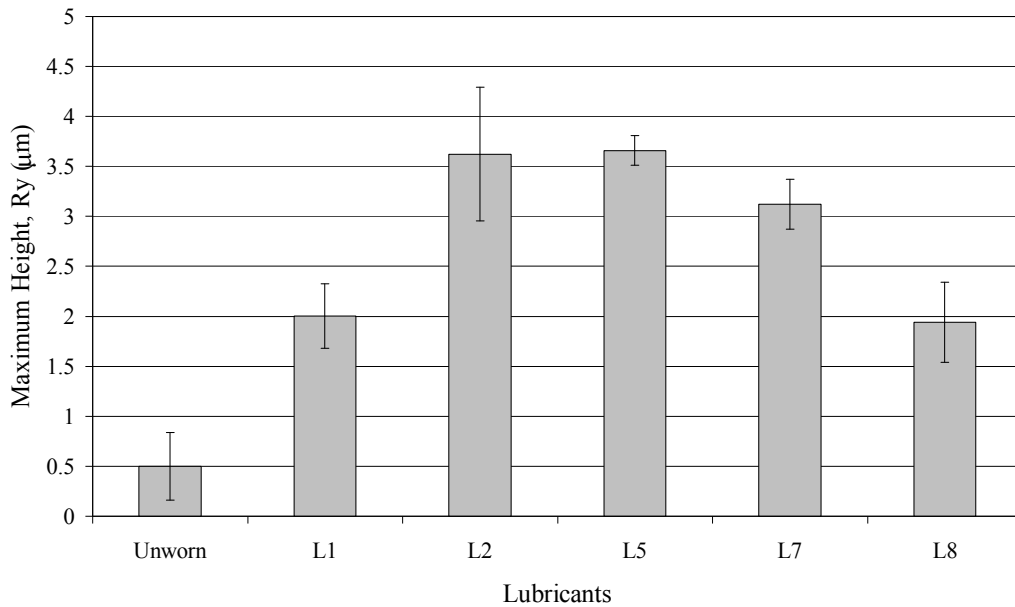
Figure 7.109. Maximum height of the rotating balls lubricated with mineral oil, mineral oil with surfactant and the lubricants containing commercial zinc borate. L1: mineral oil; mineral oil with L2: sorbitan monostearate, L5: sorbitan monostearate and commercial zinc borate, L7: sorbitan monostearate, commercial zinc borate and Viscobyk 5025, L8: sorbitan monostearate, commercial zinc borate and Disperbyk 1161.

Effect of zinc borate type on the worn surfaces

In order to characterize the worn surfaces of the balls run in the lubricants having different types of zinc borate in the four ball machine, the optical microphotographs of the worn surfaces of both fixed and rotating balls were obtained as shown in Figures 7.110, 7.111 and 7.112. The worn surfaces of the rotating balls show continuous scars around the balls while the worn surfaces of the fixed balls exhibit circular and ellipsoid structures. Among these samples, the worn scar diameter of the fixed ball lubricated with the lubricants containing zinc borate synthesized in the presence of surfactant is lower than the others. Furthermore the continuous scars around the rotating ball of this sample are not as severe as the others.

(a) (b)
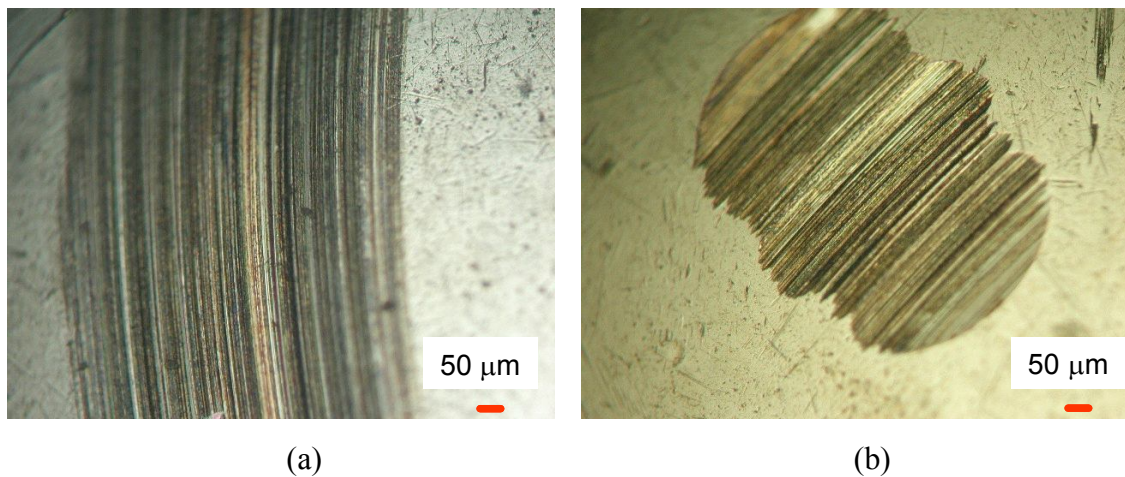
Figure 7.110. The optical microphotographs of the worn surfaces of a) rotating ball b) fixed ball lubricated with mineral oil including sorbitan monostearate and zinc borate dried by conventionally (L3).
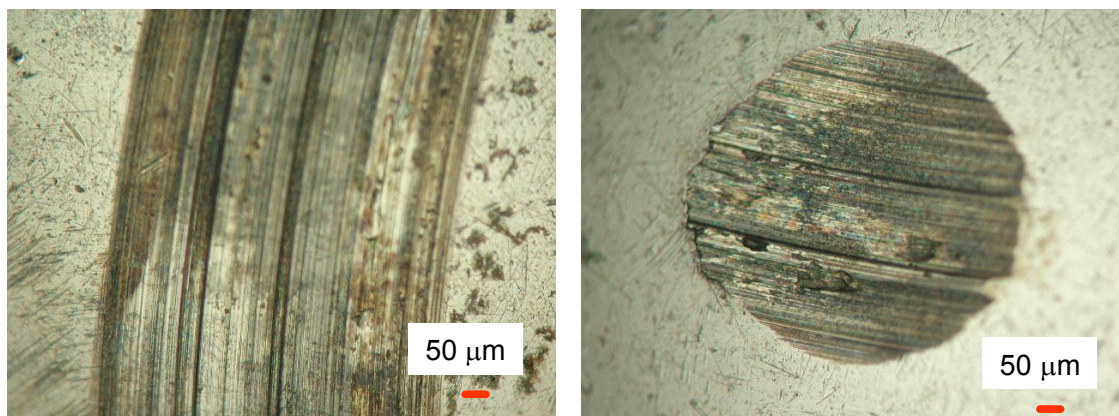
(a)	(b)

Figure 7.111. The optical microphotographs of the worn surfaces of a) rotating ball b) fixed ball lubricated with mineral oil including sorbitan monostearate and zinc borate dried by supercritical ethanol (L4).
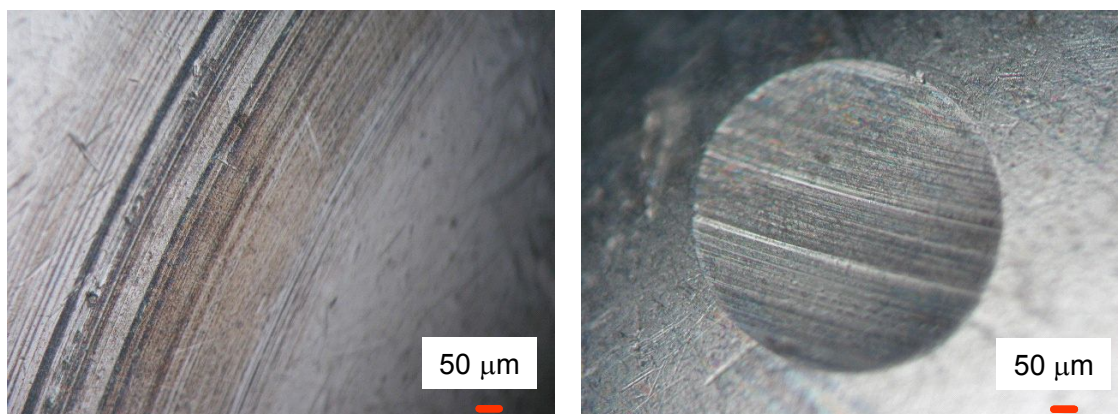
(a)	(b)

Figure 7.112. The optical microphotographs of the worn surfaces of a) rotating ball b) fixed ball lubricated with mineral oil including sorbitan monostearate and zinc borate produced in the presence of sorbitan monostearate (L6).

The detailed investigations of the worn surfaces of the balls are given in Figures 7.113- 7.118. Even if the wear scar diameter of the worn surface lubricated with zinc borate conventionally dried is larger than the value of surface lubricated with zinc borate dried by supercritical ethanol, the deeper worn scars are observed as shown in Figures 7.113 and 7.114. This may be explained by not all nanoparticles prepared by supercritical fluid drying being coated by the surfactant and therefore colliding and sticking can be taken place to form larger particles, which act as abrasive bodies. The zinc borate prepared in the presence of the surfactant also enhances the anti-wear property of the mineral oil and lower scar depth might be due to the rolling effect of the

zinc borate particles which has lamellar-like morphology (Figure 7.115). Moreover, the lubricant (L6) including zinc borate produced in the presence of the surfactant shows a considerable decrease when compared with balls lubricated only with light neutral oil. When the balls are lubricated with lubricants containing zinc borate particles synthesized by coordination homogeneous precipitation technique, wear scars exhibit circular structure and the existence of these zinc borate particles in the mineral oil make the wear scar smoother than the pure mineral oil does as shown in Figures 7.116, 7.117 and 7.118. In literature, it is suggested that the antiwear ability of metal nanoparticles at a low applied load is attributed to the formation of deposition films on the worn surface, which can reduce the adhesive wear during the tribological process (Sun et al., 2010).

(a)   (b)
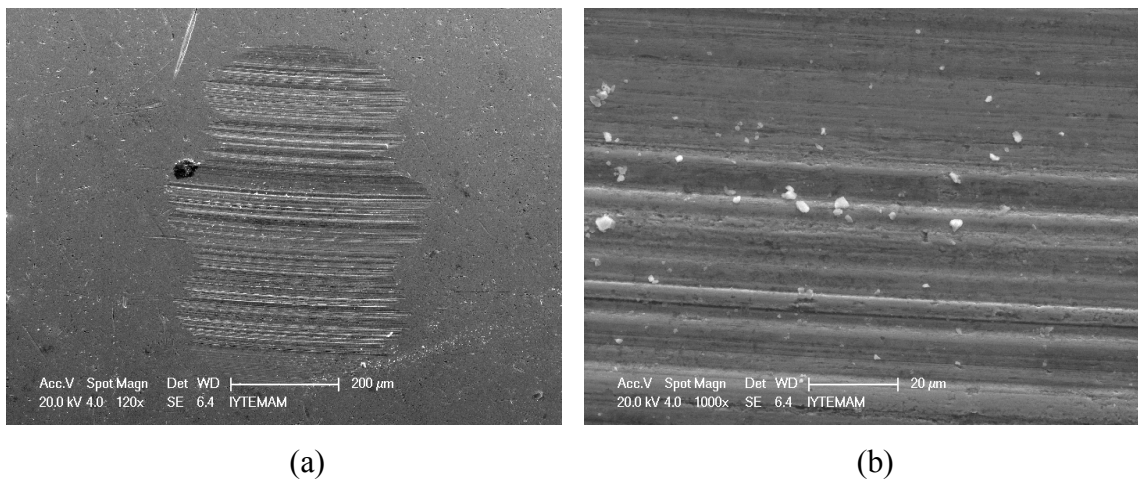
Figure 7.113. SEM images of the worn surface of the steel ball lubricated with mineral oil including sorbitan monostearate and zinc borate dried by conventionally (L3) a) 120x and b) 1000x magnification.
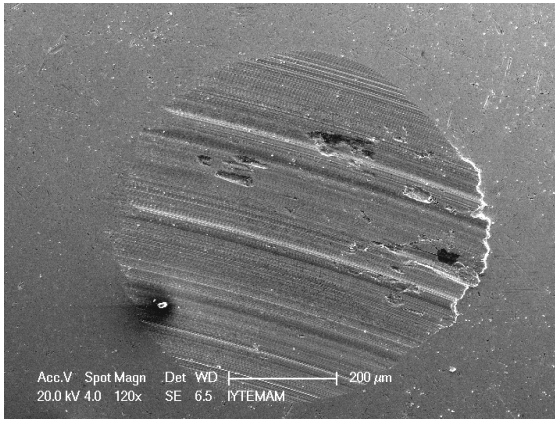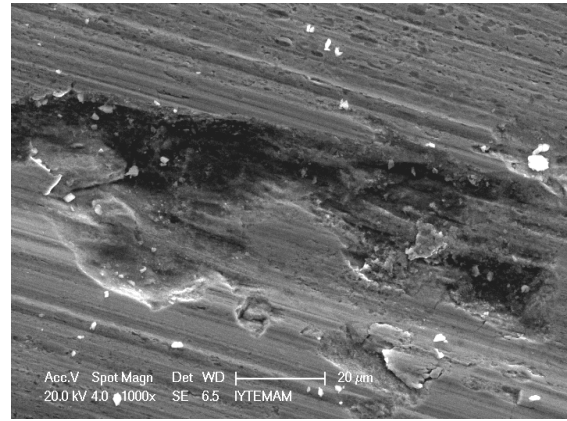
(a)   (b)

Figure 7.114. SEM images of the worn surface of the steel ball lubricated with mineral oil including sorbitan monostearate and zinc borate dried by supercritical ethanol (L4) a) 120x and b) 1000x magnification.
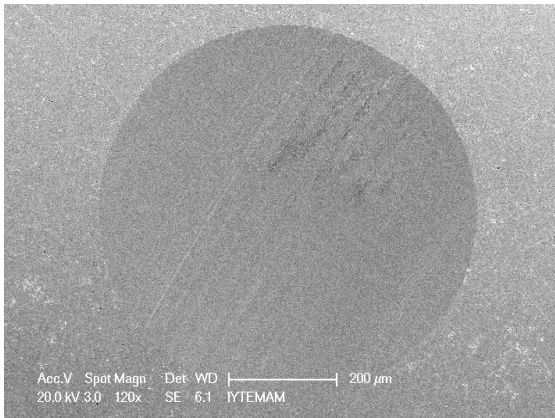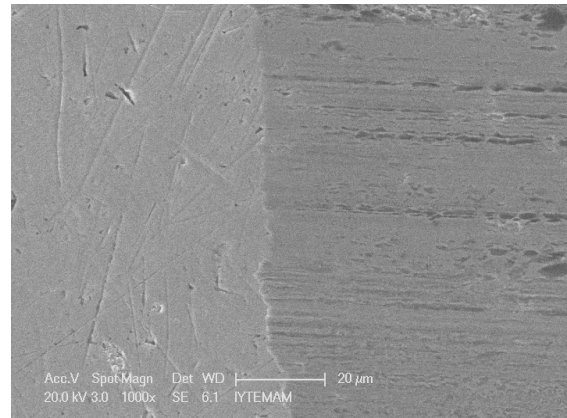
(a)   (b)

Figure 7.115. SEM images of the worn surface of the steel ball lubricated with mineral oil including sorbitan monostearate and zinc borate produced in the presence of sorbitan monostearate (L6) a) 120x and b) 1000x magnification.

(a)	(b)
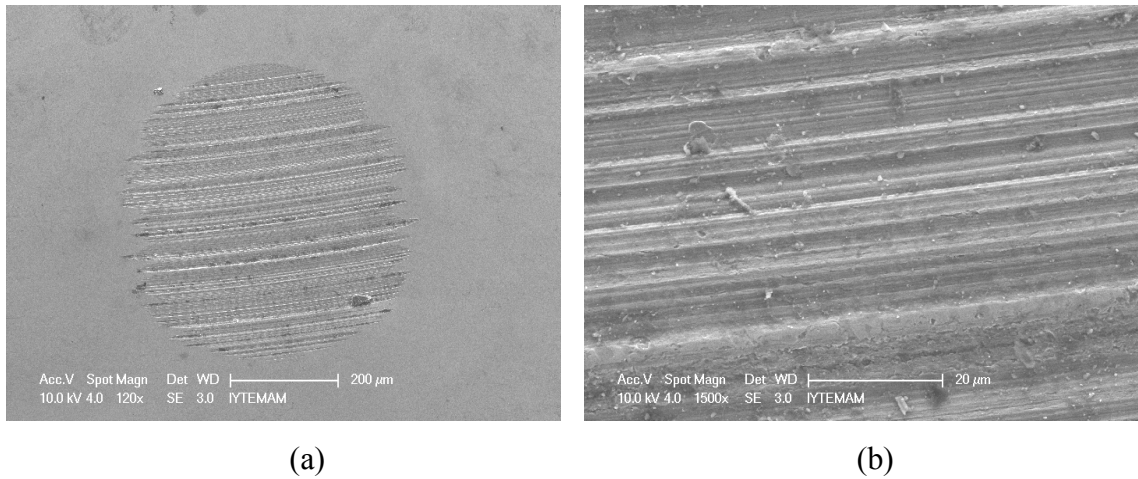
Figure 7.116. SEM images of the worn surface of the steel ball lubricated with mineral oil including sorbitan monostearate and zinc borate produced by homogeneous precipitation and mixed for 6 h (L9) a) 120x and b) 1500x magnification.

(a)	(b)
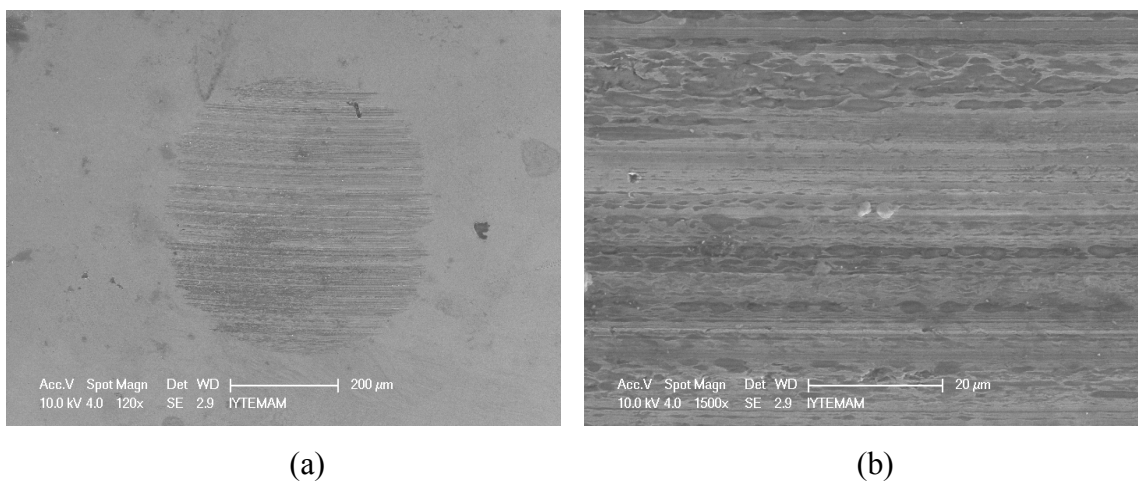
Figure 7.117. SEM images of the worn surface of the steel ball lubricated with mineral oil including sorbitan monostearate and zinc borate produced by homogeneous precipitation and mixed for 15 h (L10) a) 120x and b) 1500x magnification.

<div align="center">(a)   (b)</div>
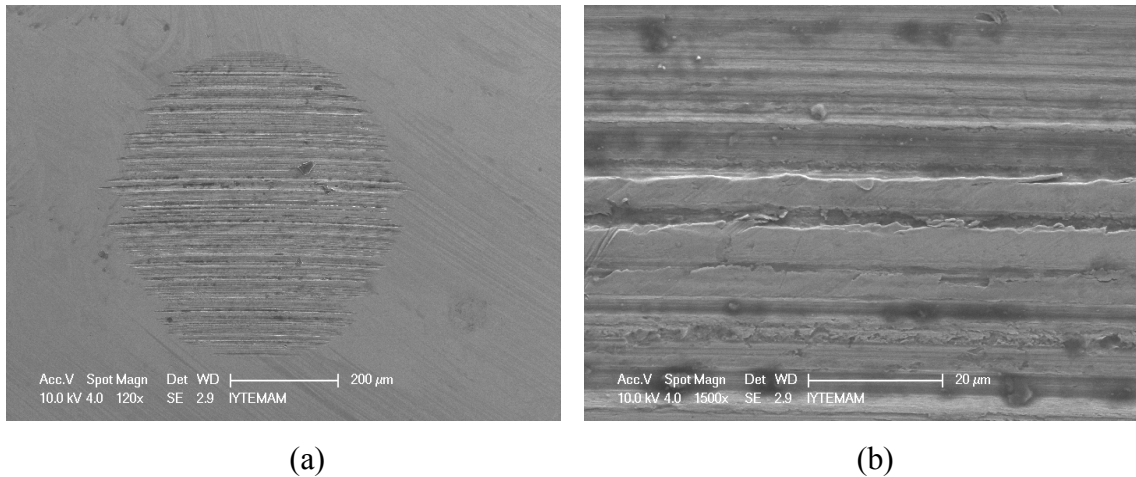
Figure 7.118. SEM images of the worn surface of the steel ball lubricated with mineral oil including sorbitan monostearate and zinc borate produced by homogeneous precipitation and mixed for 12 h (L11) a) 120x and b) 1500x magnification.

The chemical composition of the worn surfaces formed between two rubbing bodies in the presence of the lubricants were obtained, as well. The results are listed in Table 7.27. The balls used for the wear experiments are chrome steel balls including chromium, phosphate, manganese, silicon and sulphur. When the balls lubricated with the lubricants with zinc borate, the boron weight percentages of the samples are between 0.51-14.84%. This might be the reason of the enhancement of wear surfaces by these lubricants. It was suggested that boron elements were adsorbed by the surfaces and therefore the tribological properties of the mineral oil could be improved.

Table 7.27. Elemental composition of the worn surfaces lubricated mineral oil, mineral oil with surfactant and the lubricants containing different types of zinc borate

Element	Mass %								
	Unworn	L1	L2	L3	L4	L6	L9	L10	L11
C	5.09	16.47	14.73	3.95	7.44	3.86	10.63	7.95	12.41
O	0.87	7.13	8.00	3.25	4.00	2.62	21.24	6.07	5.20
Fe	90.50	75.77	74.31	90.08	85.89	82.98	41.92	59.96	58.93
Si	0.32	0.40	0.66	0.57	0.35	0.67	1.88	0.74	0.87
Cr	0.50	0.06	0.16	0.25	0.25	0.31	1.33	1.70	2.07
Mn	1.49	0.00	0.00	0.00	0.00	1.06	1.44	1.24	1.50
S	0.19	0.00	0.43	0.51	0.50	0.37	0.67	0.69	0.76
P	0.17	0.00	0.00	0.00	0.00	0.40	0.68	0.48	0.48
Ni	0.63	0.17	0.24	0.20	0.16	0.00	4.37	4.47	3.90
Ca	0.47	0.00	1.49	0.42	0.29	2.86	0.49	0.55	0.53
B	0	0.00	0.00	0.00	0.51	4.14	13.85	14.84	12.14
Zn	0	0.00	0.00	0.78	0.60	0.73	1.49	1.42	1.21

The measured roughness values of the fixed balls (Ra) lubricated with mineral oil, mineral oil with surfactant and the lubricants containing different types of zinc borate species are given in Figure 7.119 whereas, the measured roughness values of the rotating balls are indicated in Figure 7.120. The lubricant (L9) including zinc borate produced by coordination homogeneous precipitation shows a considerable decrease when compared with balls lubricated only with light neutral oil. Besides them, the maximum roughness depth which refers to Ry is measured both the fixed and rotating balls as seen Figures 7.121 and 7.122. The minimum peak to valley distances are measured for the fixed and rotating balls when they are lubricated by the lubricant (L9) and the lubricant (L6), respectively.
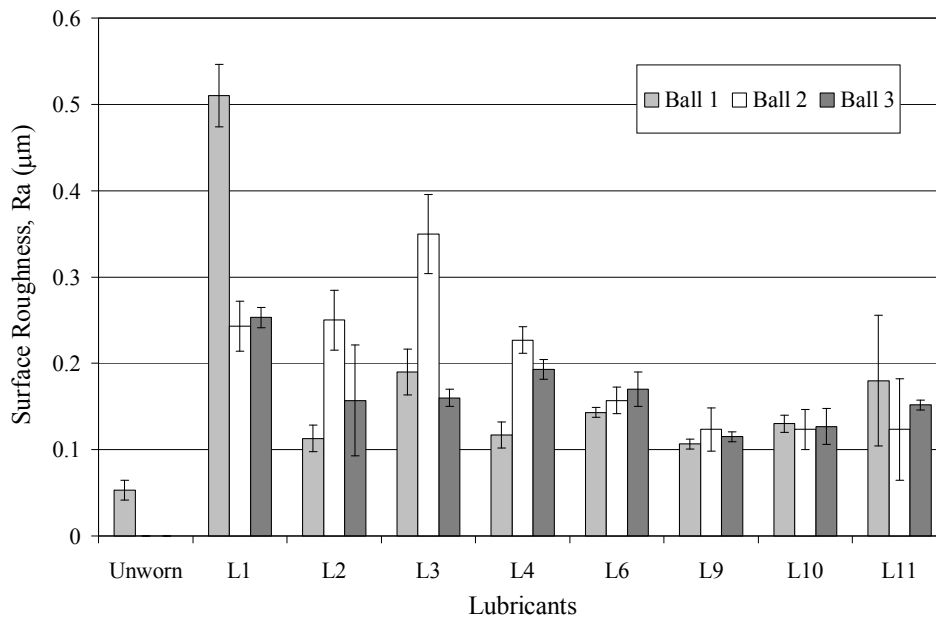
Figure 7.119. The surface roughness of the fixed balls lubricated with mineral oil, mineral oil with surfactant and the lubricants containing commercial zinc borate. L1: mineral oil, mineral oil with L2: sorbitan monostearate and L3: zinc borate produced from boric acid and zinc oxide, dried by conventionally, L4: zinc borate produced from boric acid and zinc oxide, dried by supercritical ethanol L6 zinc borate produced in the presence of sorbitan monostearate, L9: zinc borate produced by coordination homogeneous precipitation, mixed for 6 h. L10: zinc borate produced by coordination homogeneous precipitation, mixed for 15 h, L11: zinc borate produced by coordination homogeneous precipitation, mixed for 12 h.

Figure 7.120. Surface roughness of the rotating balls lubricated with mineral oil, mineral oil with surfactant and the lubricants containing different types of zinc borate. L1: mineral oil, mineral oil with L2: sorbitan monostearate and L3: zinc borate produced from boric acid and zinc oxide, dried by conventionally, L4: zinc borate produced from boric acid and zinc oxide, dried by supercritical ethanol L6 zinc borate produced in the presence of sorbitan monostearate, L9: zinc borate produced by coordination homogeneous precipitation, mixed for 6 h. L10: zinc borate produced by coordination homogeneous precipitation, mixed for 15 h, L11: zinc borate produced by coordination homogeneous precipitation, mixed for 12 h.

Effect of surfactant concentration on the tribological properties of the lubricants

The wear-scar morphology of the balls running in the lubricant (L12) including zinc borate and 0.000005 g sorbitan monostearate and in the lubricant (L13) with 0.1 g sorbitan monostearate are given in Figures 7.123 and 7.124, respectively. The magnification of the image shown in Figure 7.123a is higher than the magnification of Figure 7.124a since the wear scar diameter of the ball lubricated with the lubricant (L12) is larger than the diameter of the ball lubricated with the lubricant (L13). These figures inferred that the amount of surfactant in light neutral oil could not form a deposition film on the friction contacting region when its concentration was too low. On the contrary, when the surfactant concentration was high, the particles might form abrasive grain wear.
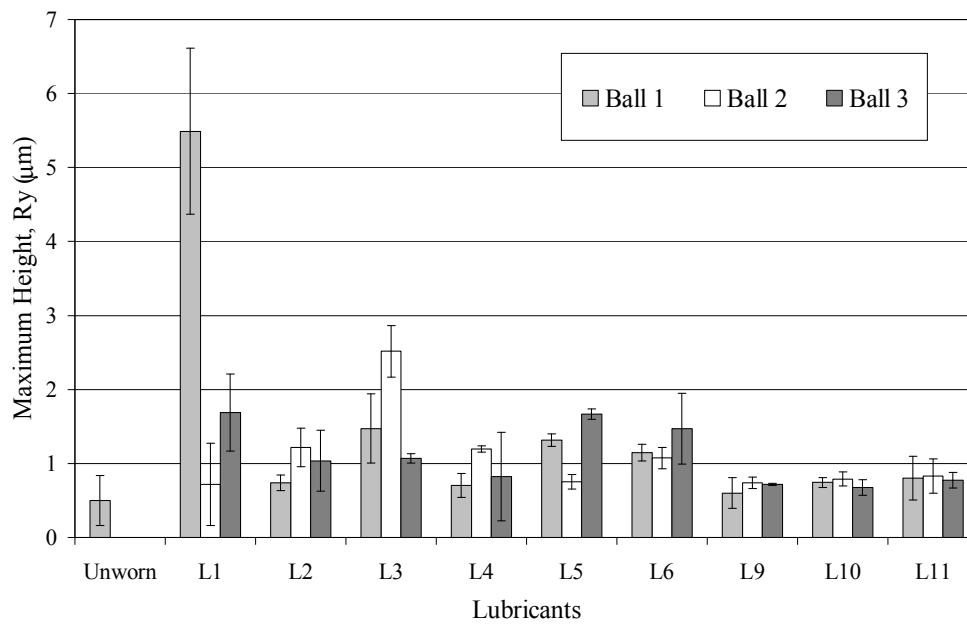
Figure 7.121. Maximum height of the fixed balls lubricated with mineral oil, mineral oil with surfactant and the lubricants containing different types of zinc borate. L1: mineral oil, mineral oil with L2: sorbitan monostearate and L3: zinc borate produced from boric acid and zinc oxide, dried by conventionally, L4: zinc borate produced from boric acid and zinc oxide, dried by supercritical ethanol L6 zinc borate produced in the presence of sorbitan monostearate, L9: zinc borate produced by coordination homogeneous precipitation, mixed for 6 h. L10: zinc borate produced by coordination homogeneous precipitation, mixed for 15 h, L11: zinc borate produced by coordination homogeneous precipitation, mixed for 12 h.

The measured roughness values of the fixed balls (Ra) lubricated with the lubricants containing different amount of surfactant concentration are given in Figure 7.125 whereas, the measured roughness values of the rotating balls are indicated in Figure 7.126. It was observed that the surface roughness increased when the concentration of sorbitan monostearate in the mineral oil was decreased. The maximum height which refers to Ry is measured both the fixed and rotating balls as seen Figures 7.127 and 7.128. In the case of rotating balls, the highest surface roughness and depth values were obtained for the ball lubricated with L11 lubricant containing zinc borate synthesized homogeneous precipitation technique and 1 g surfactant.
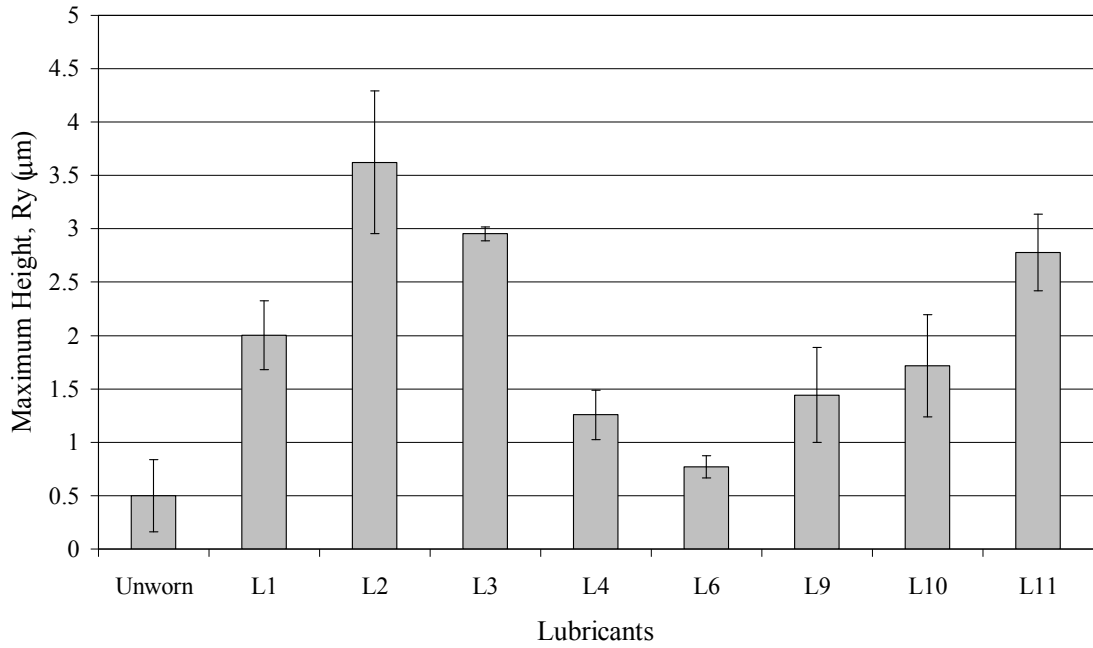
Figure 7.122. Maximum height of the rotating balls lubricated with mineral oil, mineral oil with surfactant and the lubricants containing different types of zinc borate. L1: mineral oil, mineral oil with L2: sorbitan monostearate and L3: zinc borate produced from boric acid and zinc oxide, dried by conventionally, L4: zinc borate produced from boric acid and zinc oxide, dried by supercritical ethanol L6 zinc borate produced in the presence of sorbitan monostearate, L9: zinc borate produced by coordination homogeneous precipitation, mixed for 6 h. L10: zinc borate produced by coordination homogeneous precipitation, mixed for 15 h, L11: zinc borate produced by coordination homogeneous precipitation, mixed for 12 h
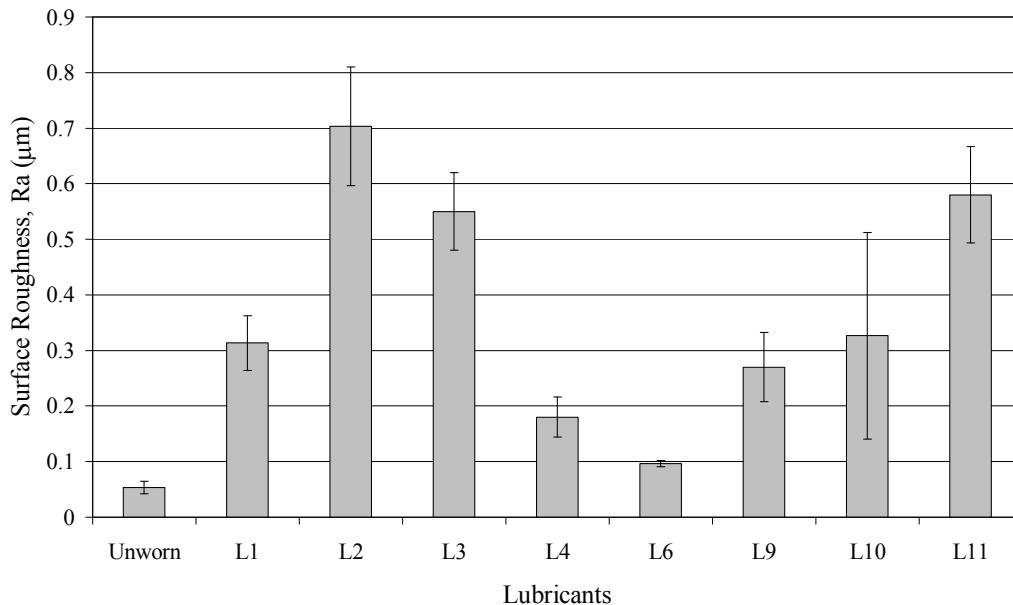

(a)   (b)

Figure 7.123. SEM images of the worn surface of the steel ball lubricated with mineral oil including 0.000005 g g sorbitan monostearate and zinc borate produced by homogeneous precipitation and mixed for 12 h (L12) a) 65x and b) 1500x magnification.

(a)   (b)
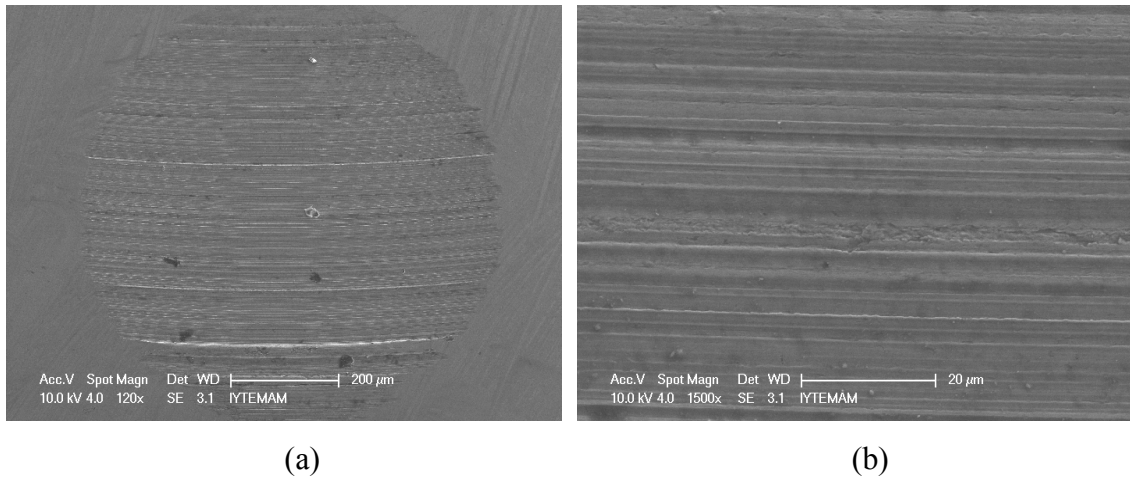
Figure 7.124. SEM images of the worn surface of the steel ball lubricated with mineral oil including 0.1 g sorbitan monostearate and zinc borate produced by homogeneous precipitation and mixed for 12 h (L13) a) 120x and b) 1500x magnification.
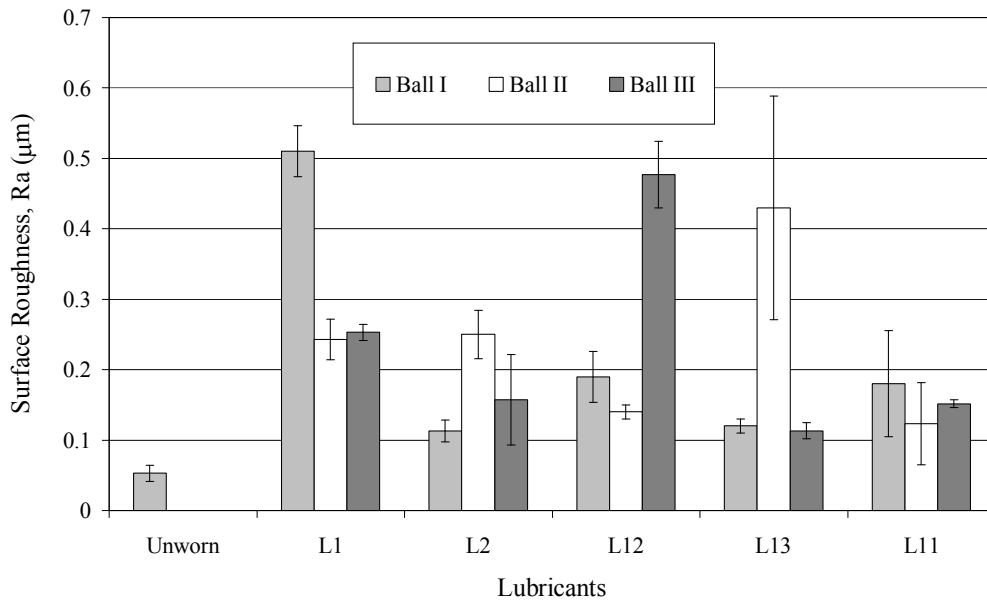
Figure 7.125. The surface roughness of the fixed balls lubricated with mineral oil containing zinc borate prepared by coordination homogeneous technique, mixed for 12 h and different amount of surfactant. L12: 0.00005 g sorbitan monostearate L13: 0.1 g sorbitan monostearate and, L11: 1g sorbitan monostearate.
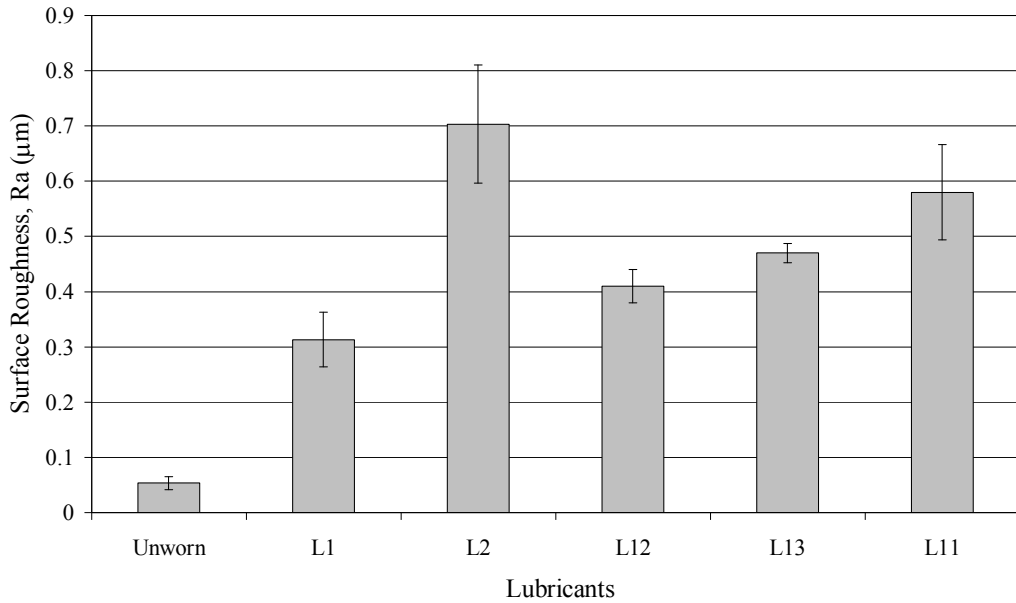
Figure 7.126. Surface roughness of the rotating balls lubricated with mineral oil containing zinc borate prepared by coordination homogeneous technique, mixed for 12 h and different amount of surfactant. L12: 0.00005 g sorbitan monostearate, L13: 0.1 g sorbitan monostearate, L11: 1g sorbitan monostearate.
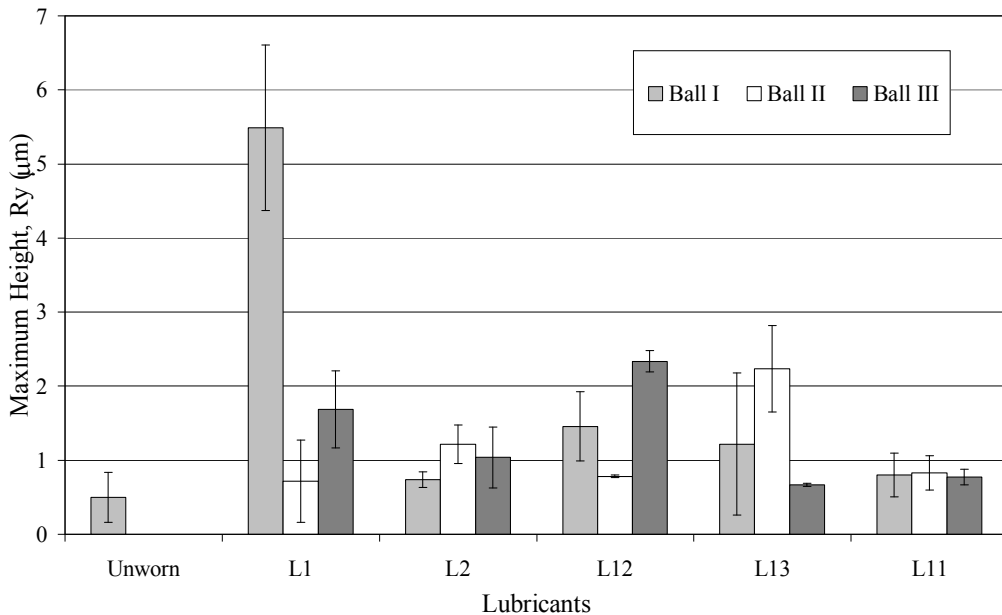
Figure 7.127. Maximum height of the fixed balls lubricated with mineral oil containing zinc borate prepared by coordination homogeneous technique, mixed for 12 h and different amount of surfactant. L12: 0.00005 g sorbitan monostearate, L13: 0.1 g sorbitan monostearate, L11: 1g sorbitan monostearate.

208
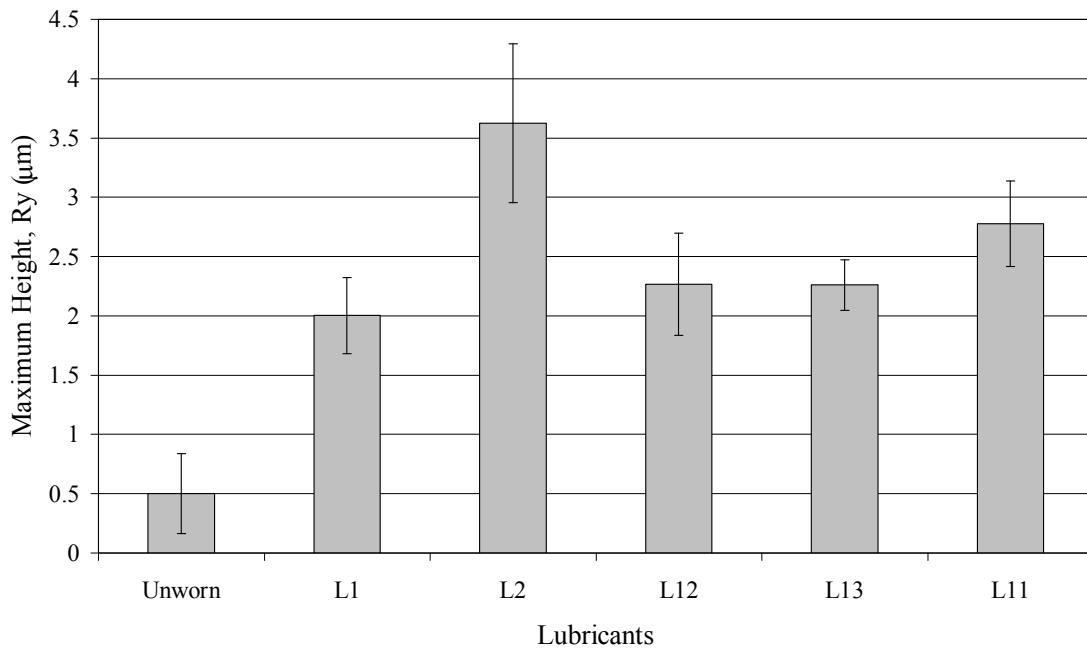
Figure 7.128. Maximum height of the rotating balls lubricated with mineral oil, containing zinc borate prepared by coordination homogeneous technique, mixed for 12 h and different amount of surfactant. L12: 0.00005 g sorbitan monostearate, L13: 0.1 g sorbitan monostearate, L11: 1g sorbitan monostearate.

Lubricants from precipitate of inverse emulsion and inverse emulsions as lubricants

The wear scar morphologies of the steel balls after running in the lubricants L14 and L16 are given in Figures 7.129 and 7.130, respectively. The grooves indicated that the wear scar did not result from plastic deformation but from evident wear. The worn surface of the ball lubricated with inverse emulsion is smoother of the surface lubricated with the lubricant (L14) indicating that inverse emulsion had anti-wear ability. Furthermore the surface roughness and the maximum height values of the balls were measured. The average surface roughness of the ball lubricated with the precipitate of the inverse emulsion having 30% propanol-2 was found as 0.129 μm, whereas the average surface roughness of the ball running in the inverse emulsion heated up to 160 °C was measured as 0.110 μm. The maximum height values of the balls lubricated with the lubricant containing the precipitate prepared by inverse emulsion and the inverse emulsion were found as 0.584 and 0.654 μm, respectively. The smaller surface roughness indicated lower friction between contact balls. The ball running in the inverse

emulsion had lower surface roughness value than the other, revealing that inverse emulsion could influence reduction of friction.
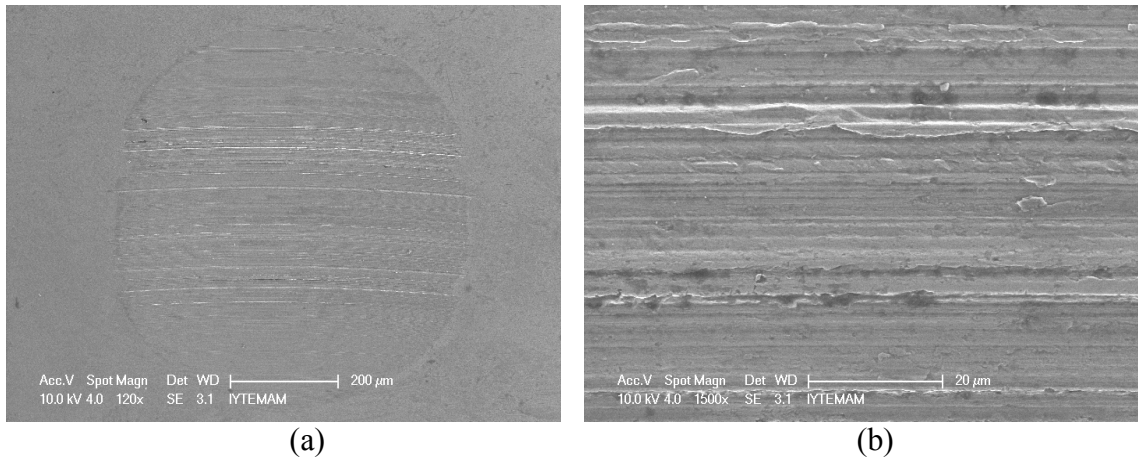
Figure 7.129. SEM images of the worn surface of the steel ball lubricated with mineral oil including the precipitate of the inverse emulsion having 30% propanol-2 (L14) a) 65x and b) 1500x magnification.

Figure 7.130. SEM images of the worn surface of the steel ball lubricated with inverse emulsion of which water content was removed by heating up to 160 °C (L16) a) 302x and b) 3726x magnification.

Clinoptilolite rich mineral as lubricant additive and water adsorber in inverse emulsion

SEM image of the worn surface of the balls lubricated with the lubricant containing clinoptilolite rich mineral is indicated in Figure 7.131. Even if the wear scar of the sample exhibits circular structure, severe grooves are obtained on the surface. Figure 7.132 displays the worn surface of the ball lubricated with the inverse emulsion

of which water content was removed by clinoptilolite rich mineral. When this sample was compared with the inverse emulsion of which water content was removed by heating, it was observed that the scar transformed to circular structure from the ellipsoid structure indicating the decrease in the wear scar diameter.

Furthermore the surface roughness and the maximum height values of the balls were measured. The average surface roughness of the ball lubricated with the lubricant containing clinoptilolite rich mineral was found as 0.114 μm, whereas the average surface roughness of the ball running in the inverse emulsion of which water content was removed by clinoptilolite rich mineral was measured as 0.140 μm. The maximum height values of the balls lubricated with the lubricant containing clinoptilolite rich mineral and inverse emulsion of which water content was removed by clinoptilolite rich mineral were 0.606 and 0.384, respectively.

(a)   (b)
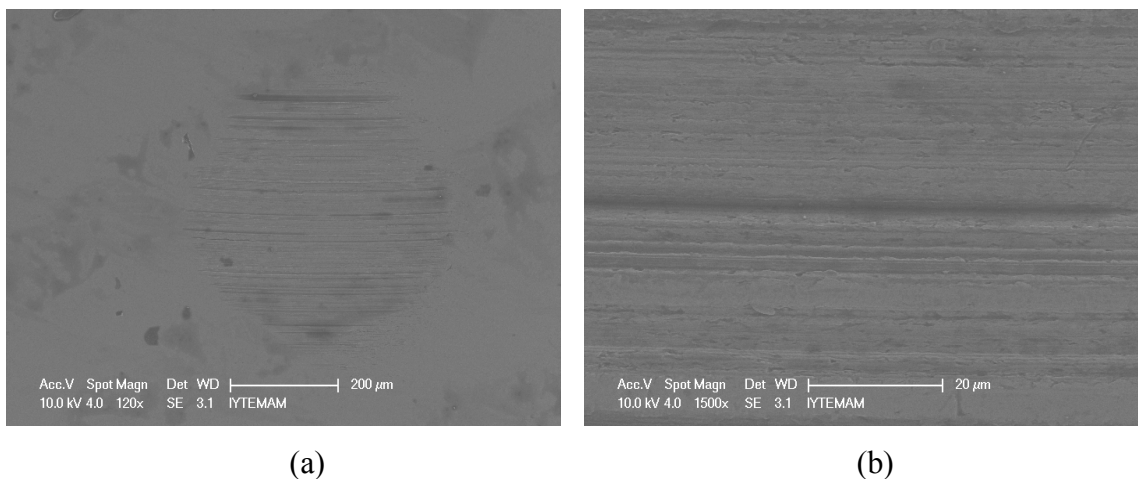
Figure 7.131. SEM images of the worn surface of the steel ball lubricated with the lubricant containing clinoptilolite rich mineral (L15) a) 120x b)1500x.

(a)   (b)
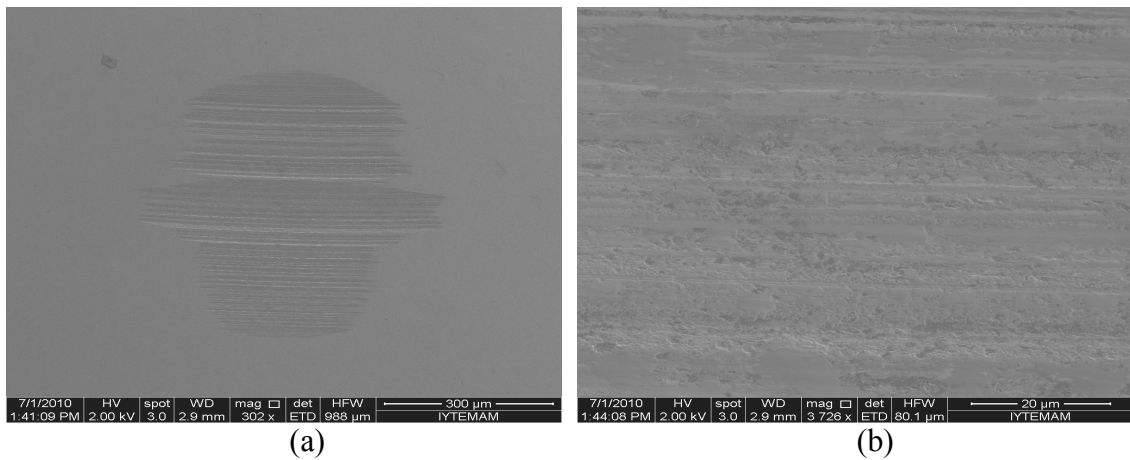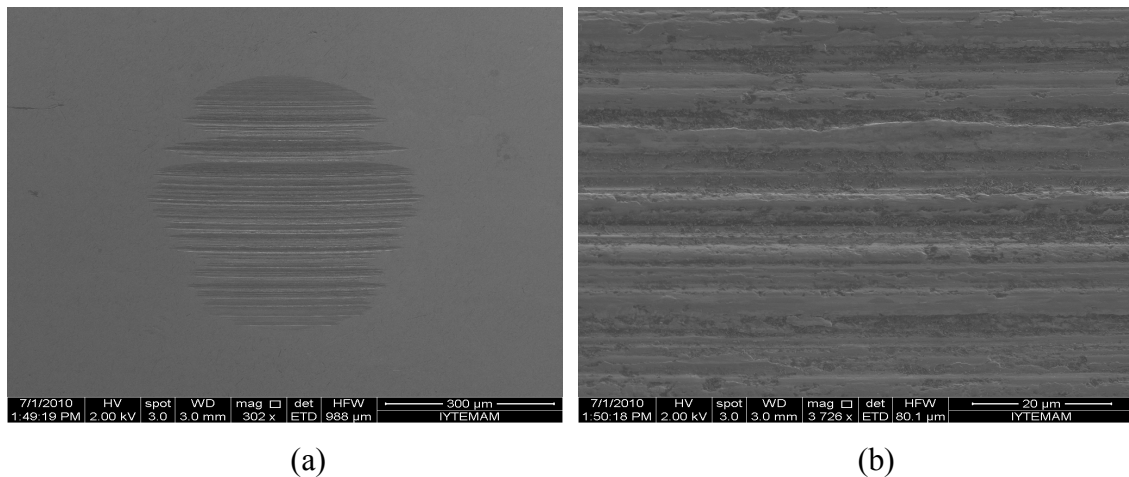
Figure 7.132. SEM images of the worn surface of the steel ball lubricated with inverse emulsion of which water content was removed by clinoptilolite rich mineral a) 302x and b) 3726x.

Surface Hardness

The hardness of worn surfaces is an important component of friction and wear and has a significant influence on the magnitude of the friction and on the wear of the surfaces. Besides SEM and roughness analysis, indentation test was carried out to obtain the hardness of the worn surfaces of the steel balls. The average Vickers hardness value of the unworn surface was found as 709 Hv (equivalent to 61 HRC). This value is consistent with literature value of 52100 steel which is 59-61 HRC. The average Vickers hardness values of the balls lubricated with mineral oil (L1), mineral oil with surfactant (L2) and the lubricant including zinc borate synthesized by homogeneous precipitation and mixed for 15 h (L10) were 677, 688 and 618 Hv as shown in Figure 7.133. The hardness of the worn surface lubricated with mineral oil containing surfactant is larger than that of the worn surface lubricated with pure oil. This result might be due to the migration of polar groups to the metal surface and formation of physical bonds with surfaces. However, the addition of zinc borate particles in the mineral oil decreases the hardness of the worn surface, considerbly. It might be due to the formation of a soft thin layer on the surface and this layer can deform easily. Therefore the load applied per unit area is decreased by increasing the contact area between the moving bodies. Hence the wear of the surfaces can be decreased (Yu et al., 2008).
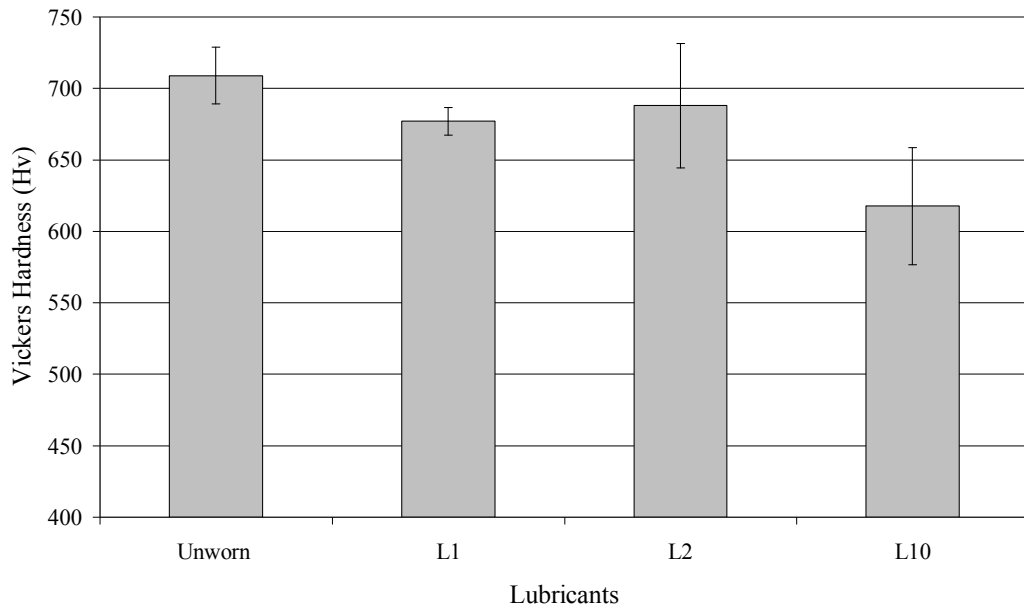
Figure 7.133. The hardness of the worn surfaces of the steel ball lubricated with mineral oil (L1), mineral oil with surfactant (L2) and the lubricant (L10) containing zinc borate prepared by homogeneous precipitation and mixed for 15 h.

Surface Topography

The morphology of unworn and worn surfaces were examined by AFM. The topographical images of the samples are shown in Figures 7.134, 7.135, 7.136. The corresponding average surface roughness were determined by two dimensional images and the results are tabulated in Table 7.28. The images inferred that a new phase was not obtained on the rubbed surfaces. The obtained scars and pits are visible on the surfaces as shown in Figures 7.134, 7.135 and 7.136. The agglomeration of particles on the pit in Figure 7.134 might be the deposition film on the friction contacting area. Figure 7.135 exhibits much smoother surface and this subtle difference in the morphology can enhance the wear property. The corresponding average surface roughness of the samples for 5x5 μm^2 are lower than the values obtained by the profilometry since the the areas scanned by AFM are significantly smaller than the area scanned by profilometer.
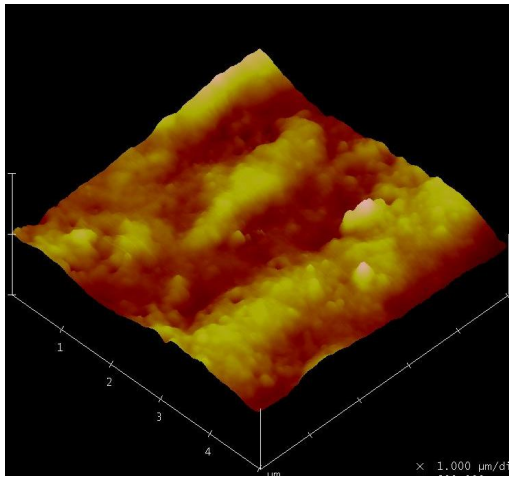
(a)
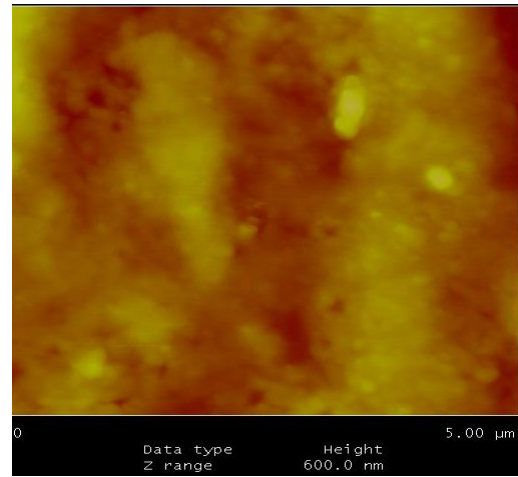
(b)

Figure 7.134. AFM a) three dimensional b) two dimensional images of the worn surface lubricated with mineral oil (L1). Image size: 5x5 μm^2.
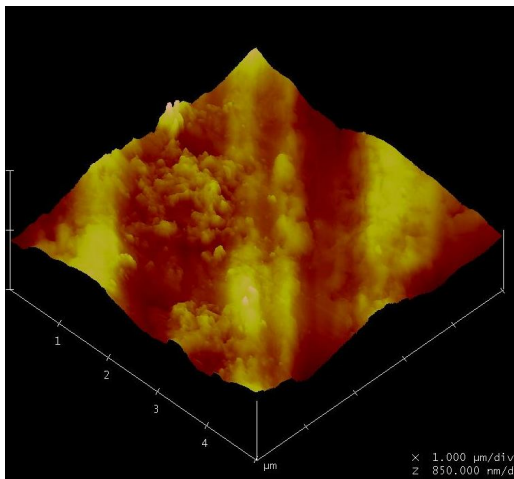
(a)
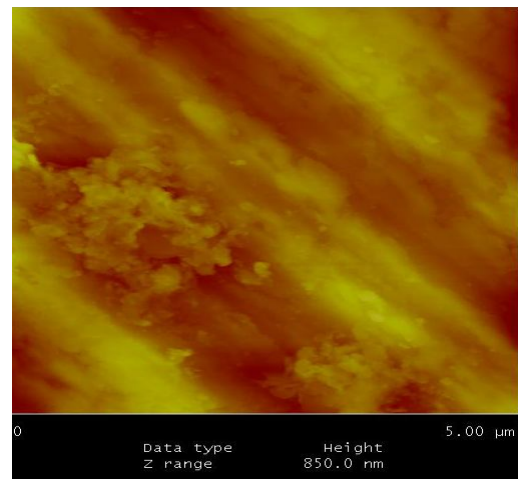
(b)

Figure 7.135. AFM a) three dimensional b) two dimensional images of the worn surface lubricated with mineral oil with sorbitan monostearate (L2). Image size: 5x5 μm^2.

<center>(a)</center>

<center>(b)</center>
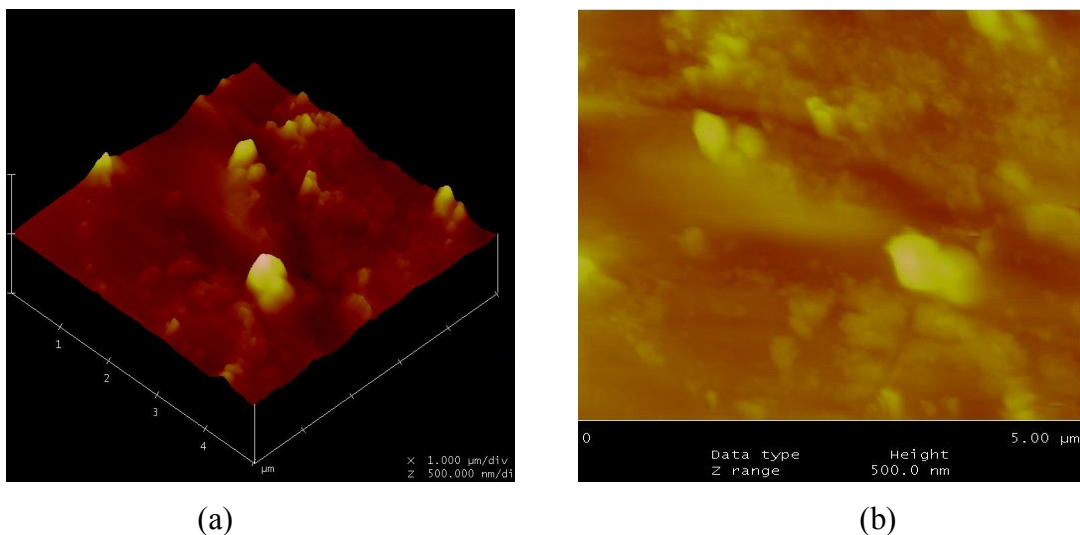
Figure 7.136. AFM a) three dimensional b) two dimensional images of the worn surface lubricated with mineral oil with sorbitan monostearate and zinc borate prepared by coordination homogeneous precipitation, mixed for 15 h (L10). Image size: 5x5 μm^2.

Table 7.28. Average surface roughness of the surfaces measured from AFM topographic images.

Sample	Average surface roughness, Ra (nm)
Unworn	35.37
L1	27.10
L2	35.63
L10	27.60

The fixed balls lubricated with mineral oil (L1), mineral oil and sorbitan monostearate (L2), the lubricant containing sorbitan monostearate and zinc borate prepared by homogeneous precipitation, mixed for 15 h (L10) were cut with a microcutter for closer examination of worn surfaces by SEM. The morphologies of the worn surfaces are shown in Figure 7.137. When the rubbed surfaces lubricated with L2 and L10 lubricants were compared with the samples which were not exposed to cutting process (presented in Figures 7.01a nd 7.117a), some deformation on the surface of the fixed balls were observed. Therefore, a detailed EDX analysis was carried out analysis to explore the differences of the elemental composition of unworn, worn and deformed surfaces. For the fixed ball lubricated with the lubricant including both sorbitan monostearate and zinc borate particles (Figure 7.137c), the areas corresponded to the

<center>215</center>

unworn, worn and deformed surfaces were pointed out by white, red and green frames, respectively. The chemical composition of these surfaces was investigated and the results were tabulated in Table 7.29. It was observed that the mass percentage of oxygen element was higher for the deformed surface indicating the oxidation of the surface. This might be due to the cutting process since water was used to cool the system. Moreover, the mass percent of iron decreased for the worn and deformed surfaces. When the boron mass percentages of the worn and unworn surfaces were compared, it was revealed that the boron mass percentage was higher for the worn surface. It might be due to the presence of embedded zinc borate additive on the worn surface.

(a)　　　　　　　　　　　　　　　　　　(b)

(c)
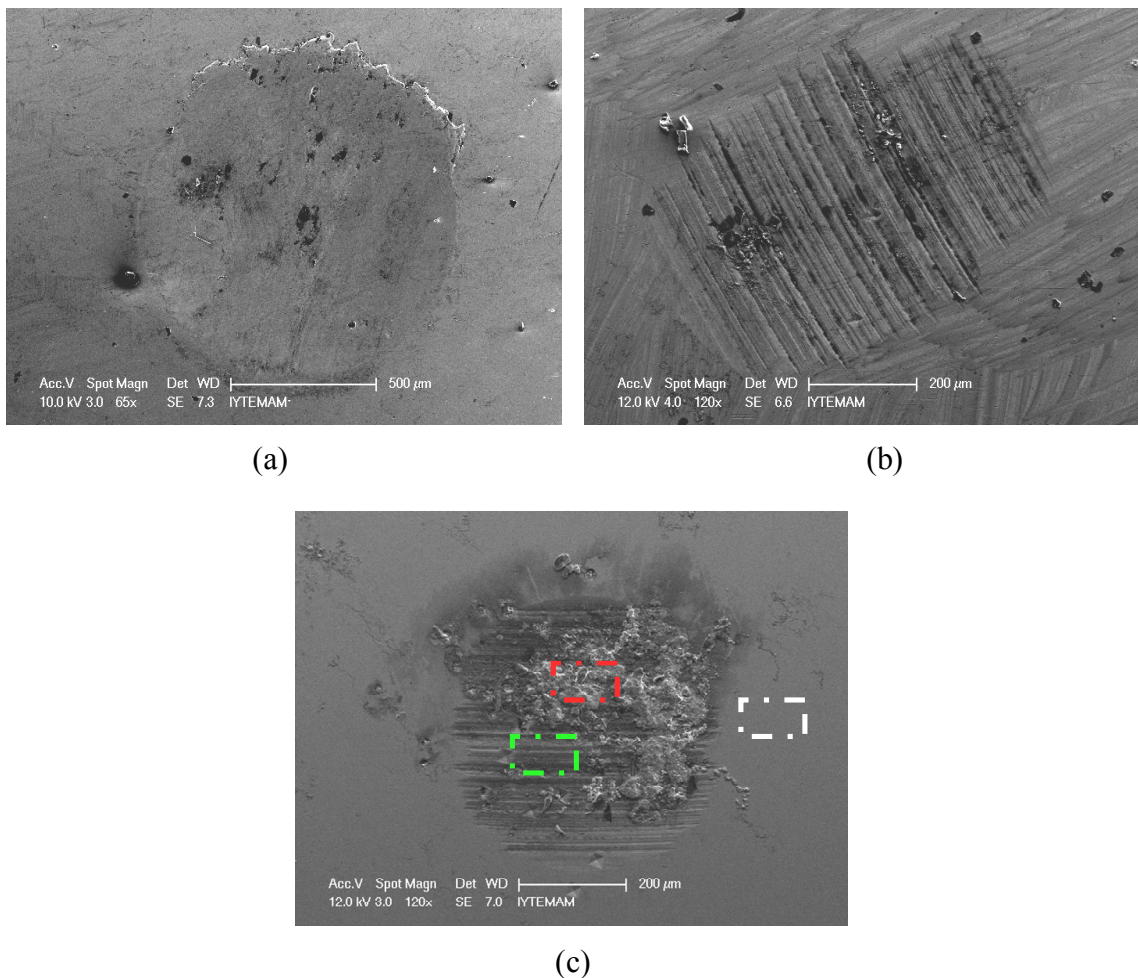
Figure 7.137. SEM images of the worn surface after cutting of the steel ball a) lubricated with mineral b) oil with sorbitan monostearate and c) lubricant containg sorbitan monostearate and zinc borate produced by homogeneous precipitation and mixed for 15 h

Table 7.29. Elemental composition of the worn surfaces lubricated with the lubricant including both sorbitan monostearate and zinc borate particles

Element	Mass%		
	Unworn surface	Worn surface	Deformed surface
C	4.75	18.48	38.42
O	1.68	8.43	13.48
Fe	80.26	56.17	21.03
Si	0.80	0.43	0.75
Cr	1.40	1.31	0.64
Mn	2.01	0.71	0.64
S	0.35	0.24	0.36
P	0.62	0.14	0.19
Ni	2.59	1.05	0.89
Ca	0.17	0.24	0.55
B	5.39	10.76	21.42
Zn	0.00	2.25	1.63

7.7. BOR POWER Characterization

BOR POWER is one of the lubricants in the market that can be used in all transport vehicles with 4-stroke engines. Among the other lubricants, the characterization of this lubricant was performed since it is claimed that it contains boron material so what kind of boron source it includes becomes the important question for our work considering the parallelism between this commercial product and ours. Therefore both BOR POWER oil and the particles obtained by separating the oily phase were identified. The morphology of the particles is constructed from layers and the disk-like crystals have nano-sized thickness as shown in Figure 7.138. The elemental analysis of this sample reveals that this material includes boron, nitrogen and carbon elements as shown in Table 7.30 and Figure 7.139. The average weight % values of boron and nitrogen elements were found as 26.72 and 42.75, respectively. When these values were used to calculate the moles of boron and nitrogen elements, it was indicated that the sample contained 2.47 moles of boron and 3.05 moles nitrogen. This result

implied that one mole of boron corresponded to practically one mole nitrogen which was consistent with the elemental composition of boron nitride. Before separating the particles from this commercial product, its FTIR spectrum was obtained as indicated in Figure 7.140. The spectrum exhibits the specific peaks of mineral oil. The peak at 1464 cm^{-1} and 1377 cm^{-1} are attributed to the $-CH_2$ and $-C-H$ symmetric vibrations of hydrocarbons. The band at 2928 cm^{-1} is the stretching vibrations of hydrocarbons, whereas, the band at 2854 cm^{-1} is related to the asymmetric stretching of $-C-H$. Even though the mineral oil does not consist a proper peak at 729 cm^{-1}, a band is observed in FTIR spectrum of BOR POWER oil. This extra peak is compared with the FTIR spectrum of BOR POWER particles. In Figure 7.41, two strong characteristic absorption bands near 1375 and 819 cm^{-1} are observed, which are close to the reported specific peaks of hexagonal boron nitride. The peak around 1380 cm^{-1} results from the in-plane TO models of the sp^2-bonded BN, while the peak centered at 819 cm^{-1} can be attributed to the B–N–B bonding vibrations (Shi et al., 2008). The XRD pattern implies that this sample has high crystallinity and the major peak is observed at 2θ 26° (Figure 7.142). The other peaks of this sample are observed at 43, 50, 55, 71 and 75°. According to this XRD diagram is basically in agreement with the reported values of hexagonal boron nitride. The characterization of BOR POWER shows that the additive used in the mineral oil is hexagonal boron nitride which has captured attention as a solid lubricant for general use due to its easy shearing along the basal plane of the hexagonal crystalline structure.

(a)   (b)
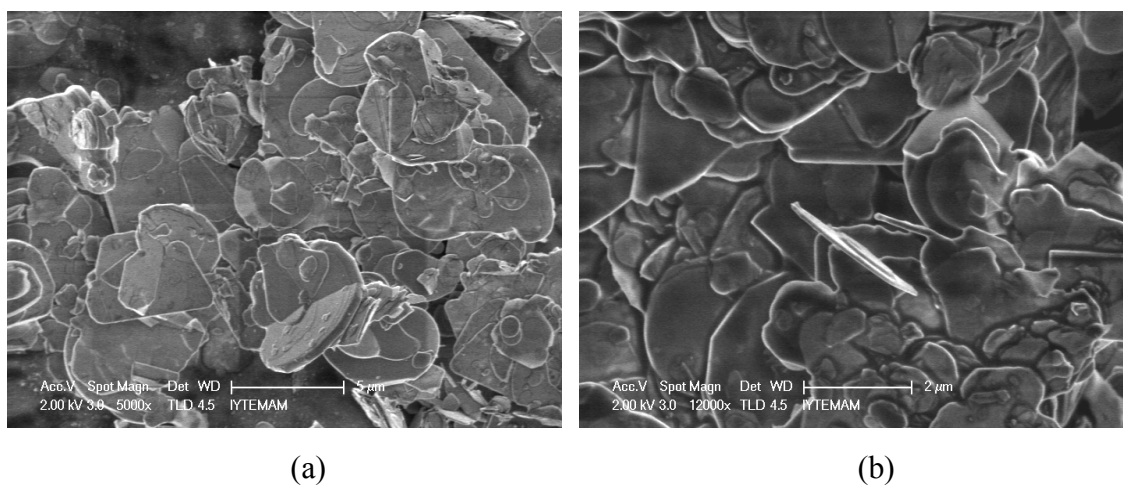
Figure 7.138. SEM images of BOR POWER particles a) 5000x and b) 12000x magnification.

Table 7.30. Elemental composition of BOR POWER analysis.

Element	Mass %
B	26.72
C	33.87
N	42.75
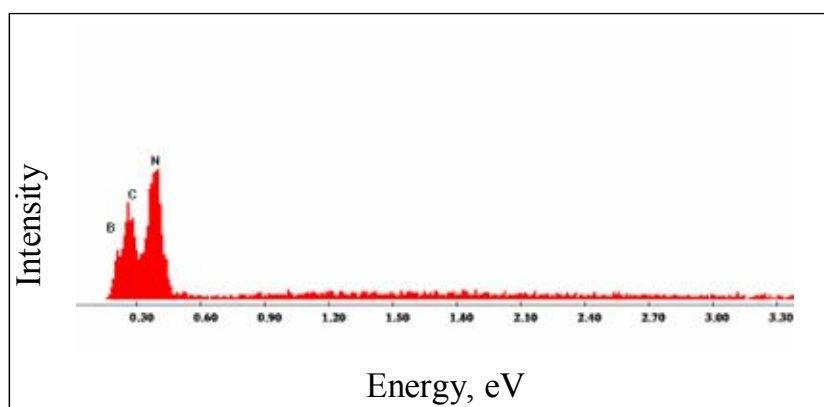
Figure 7.139. EDX spectrum of BOR POWER particles.
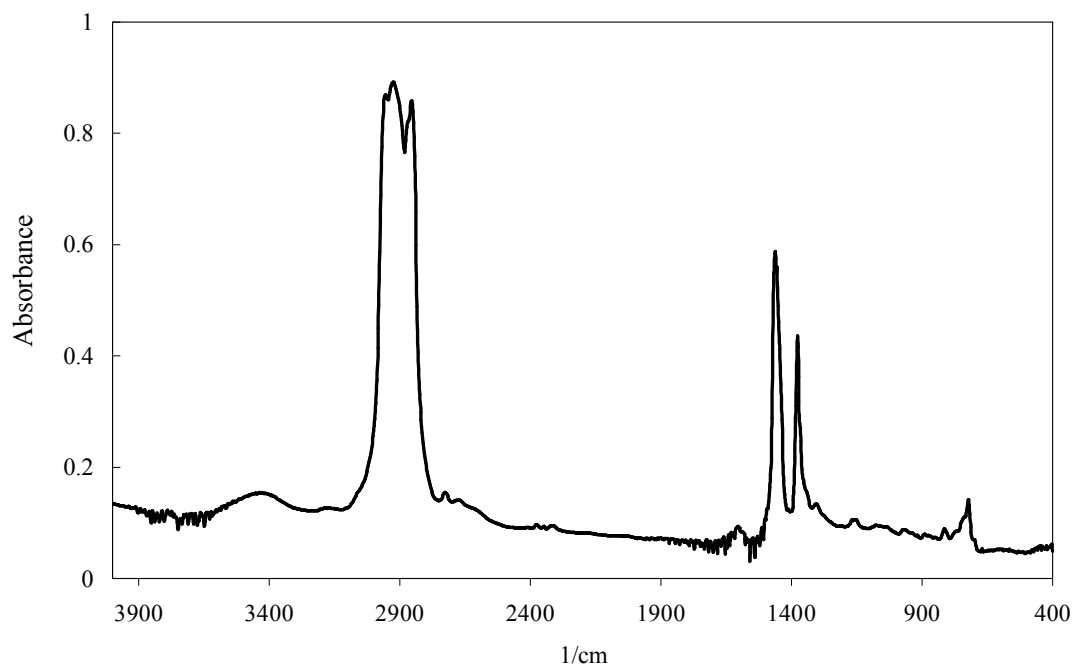
Figure 7.140. FTIR spectrum of BOR POWER lubricant.
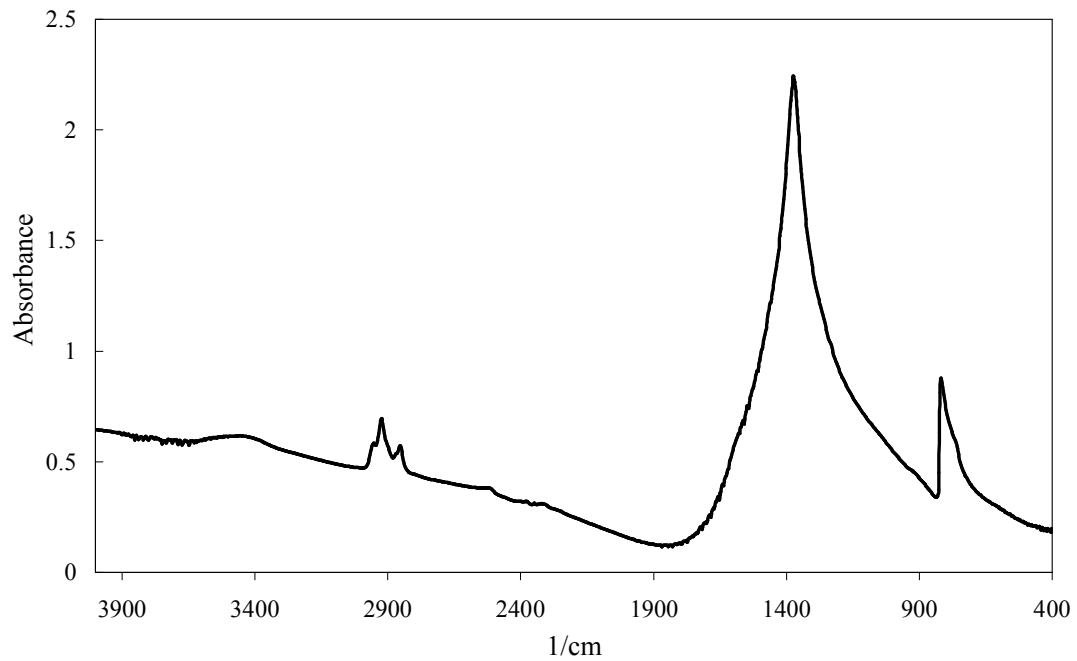
Figure 7.141. FTIR spectrum of particles separated from BOR POWER lubricant.
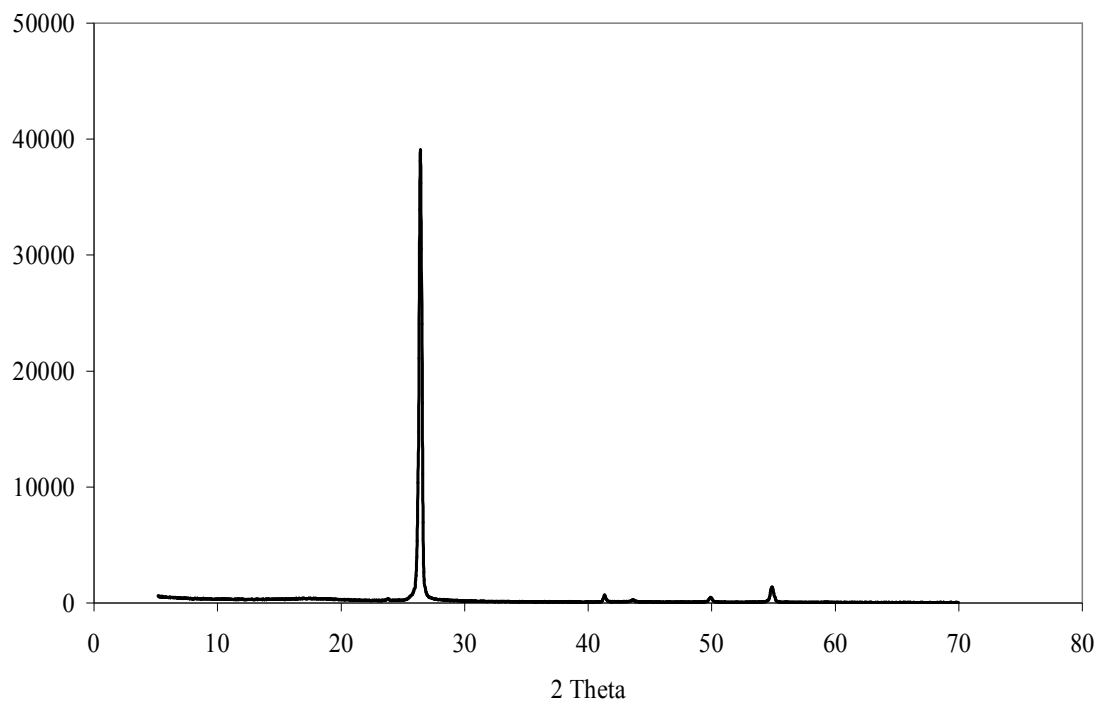
Figure 7.142. XRD pattern of particles separated from BOR POWER lubricant.

The result of four ball test of BOR POWER is shown in Figure 7.143. The friction coefficient is not stable during the wear test. At the end of fifteen minutes, the friction coefficient reaches to 0.12. The average wear scar diameter is measured as 0.645.
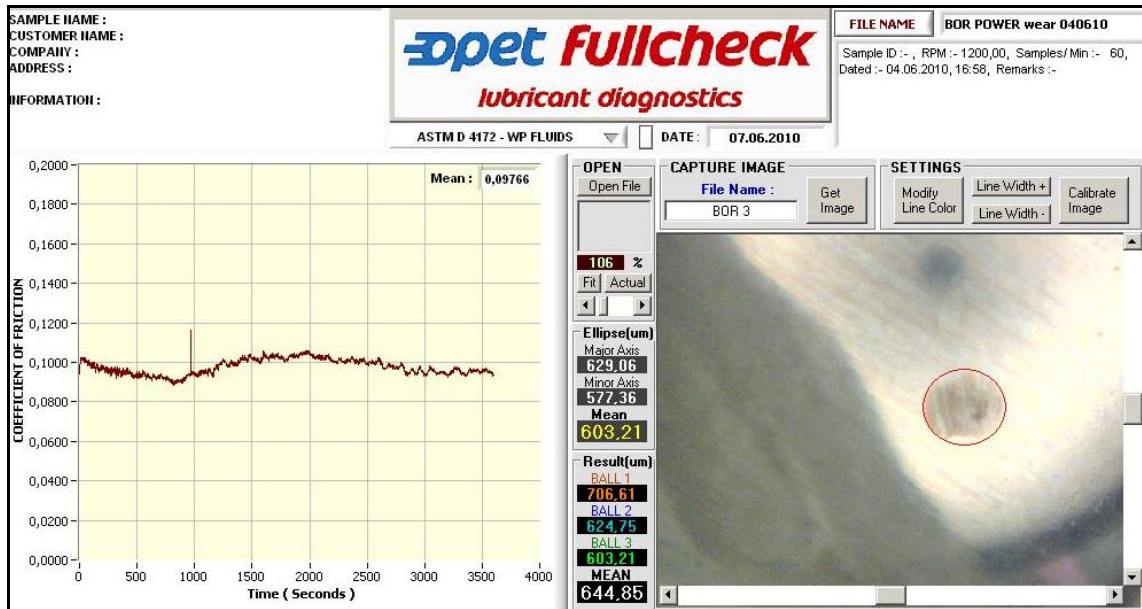
Figure 7.143. The wear and friction behavior of BOR POWER lubricant.

When the tribological behavior of BOR POWER is compared with the lubricants prepared in the scope of this study, it was obtained that the mean friction coefficient values of all the lubricants except pure mineral oil (L1) are smaller than the value of BOR POWER. Even though when the balls lubricated with BOR POWER, it decreased the wear of the balls as compared to pure mineral oil, this lubricant was not as effective as the lubricants containing 1 g surfactant and zinc borate particles. It was concluded that especially the lubricants containing zinc borates synthesized by coordination homogeneous precipitation were superior to BOR POWER by means of antiwear ability.

CHAPTER 8

CONCLUSIONS

The increasing interest of petrochemical industries on improving the performance of their products (lubricants, greases, gasoline, among others) has been simultaneously generating great incentives to develop additives that are able to supply the commercial demand of the competitive industrial markets. For tribology applications, particles as additives in base oil have been investigated widespreadly. Among these additives, nano-sized particles are promising materials for lubrication since they offer a better understanding of the interfacial properties of fluid-solid interfaces and the dispersion stability of nanoparticles in base oil is superior to micron sized particles. The tribological behavior of light neutral oil was tried to enhance by zinc borate additives and the focus of this work arised from the production of zinc borate particles as small as possible for lubrication.

Precipitation reactions are widely used in particle technology, however this technique usually leads to particles on micrometer scale. A number of process conditions and physical mechanisms such as mixing effects, particle agglomeration limit and the nanomaterial production. In this study, these problems in the production technology were tried to overcome with the investigated inverse emulsion technique. The effects of inverse emulsion preparation technique, initial aqueous phase concentration in emulsions, mixing rate, co-surfactant addition on the morphology and the structure of the precipitates were examined. The crystal size of the precipitate was found as 100-200 nm when the initial amount of aqueous phase was 5 wt% for one-microemulsion technique. The employment of a rotor-stator homogenizer for emulsion mixing reduced the diameters of the droplets since rotor knife spinned within the tube and created a pumping action. Therefore, both rod-like and spherical crystals having 20-30 nm were obtained by two-microemulsion technique with the help of homogenizer. However, the use of a fourth component, a co-surfactant, did not prove to be a useful technique for nanomaterial production. Moreover, it increased the cost and the complexity of the production technique and instead of zinc borate, only zinc sterate and stearic acid were formed as the precipitate.

Two type of precipitation techniques were developed in aqueous medium to prepare zinc borate particles for lubrication. The first one is related to the employment of a surface modifier (sorbitan monostearate) in the reaction medium. All the characterization results implied that $2ZnO \cdot 3B_2O_3 \cdot 7H_2O$ was formed when borax decahydrate and zinc nitrate are used at 70 °C in the presence of the surfactant. The morphology of the zinc borate presented micron sized cubic and prismatic crystals as well as lamellar-like crystals. The second one was coordination homogeneous technique which was carried out in the presence of ammonia. It was revealed that the crystal sizes of nano-sized particles and sub-micron particles are nearly 30 nm and 400 nm, respectively. Contrary, the crystals became larger with the prolonged mixing time and spherical agglomerated crystals were formed. FTIR spectra verified the specific peaks of zinc borate having seven moles of crystal water ($2ZnO \cdot 3B_2O_3 \cdot 7H_2O$). The XRD study showed that the structure of the products washed with ethanol transformed from amorphous to crystal phase with increasing reaction time. The samples mixed for 3, 6 and 12 hours were amorphous and they did not indicate any tendency to be crystal. However when the mixing time was increased to 15 hour, the sample became crystal. The XRD pattern of the crystal sample displayed both the characteristic peaks of sodium nitrate and zinc borate. When these two precipitation techniques were compared with each other considering the efficiencies, the efficiency of the precipitation in the presence of the surfactant (32%) was higher than the efficiency (2.16%) of homogeneous precipitation.

The focus of this study is the applicability of the produced zinc borate particles and inverse emulsions serving to lubrication purposes. The lubricants prepared by the addition of synthesized particles were tested in a four-ball wear test machine. Effects of dispersing agent, zinc borate type, surfactant concentration on the friction reduction and antiwear behavior of mineral oil were investigated. It was revealed that sorbitan monostearate not only outperformed as a dispersing agent of inorganic particles, but also it proved to be an antiwear agent. Viscobyk 5025 also had a positive effect on the reduction of wear scar diameter. The wear scar diameter was decreased by 54.92% for the lubricant containing Viscobyk 5025 as compared to pure mineral oil. Zinc borates produced by coordination homogeneous precipitation displayed an insufficient effect to decrease the friction coefficient, but they decreased the wear scar diameter. The friction coefficient of pure mineral oil was found as 0.099, whereas the value for the lubricant containing zinc borate particles synthesized by homogeneous precipitation and mixed

for 12 h was 0.085. This sample decreased the wear scar diameter from 1.402 mm to 0.550 mm. The highlighted part of the study is the exposure of the employment of inverse emulsions as lubricants. When the water content of inverse system was removed (by heating or adsorption of water by clinoptilolite rich mineral), they could be used as lubricants and they decreased the wear scar diameter from 1.402 mm to 0.596 mm. This production process required the synthesis of particles within the continuous phase, hence the problems related to nanoparticle production such as separation of particles from the solution, dispersion of the particles in the oil were overcome.

Another inorganic material, clinoptilolite rich mineral was also used as a lubricant additive and tribological test of this lubricant showed that clinoptilolite based lubricant was as effective as boron-based lubricants in the enhancement of wear.

The characterization of worn surfaces of the balls lubricated with different lubricants were carried out by SEM and it was verified the antiwear action of surfactant. The polar molecules tended to migrate the metal surfaces and formed physical bonds with surfaces. Minimum surface roughness value was observed by the lubricant containing zinc borate in the presence of surfactant. The antiwear mechanism of zinc borate particles might be due to the deposition of particles on the worn surface. The tribological properties of the lubricants prepared in the scope of this study were compared with a commercial product named BOR POWER. The characterization of the additive dispersed in this lubricant indicated that, it was hexagonal boron nitride. This lubricant could not sustain a stable friction coefficient.

This study presents extensive laboratory techniques to characterize the synthesized anti-wear additives and prepared lubricants. It also forwards the potential employment of inverse emulsions as lubricants which are important for cost saving and environmental purposes. A novel application area of clinoptilolite rich mineral for lubrication application is proposed, as well.

REFERENCES

Adityawarman, D. Precipitation of Barium Sulphate Nanoparticles in Microemulsion: Experiments and Modelling. Ph.D. Thesis, Otto-von-Guericke-University, Magdeburg, April, 2007

Adityawarman, D.; Voigt, A.; Veit, P.; Sundmacher, K. Precipitation of $Baso_4$ Nanoparticles in a Non-Ionic Microemulsion: Identification of Suitable Control Parameters. *Che. Eng. Sci.* **2005,** 60. 3373-3381.

Alberty, R.A. *Physical Chemistry*; John Wiley and Son: New York, 1997**.**

Atakul, S.; Balköse, D.; Ülkü, S. Synergistic Effect of Metal Soaps and Natural Zeolites on Poly (Vinyl Chloride) Thermal Stability. *J. Vinyl Addit. Technol.* **2005,** 11, 47-56.

Barton, T.; Steffens, J.; Sawyer, W.G.; Schmitz, T.L.; Ziegent, J.C.; Lovell, M.R.S. *In Situ Solid Lubricant Deposition for Environmentally Benign Forming,* STLE Annual Meeting Proceedings, Toronto, Italy, 2004.

Battez, A.H.; González, R.; Viesca, J.L.; Fernández, J.E.; Díaz, Fernández, J.M.; Machado, A.; Chou, R., Riba, J. CuO, ZrO_2 and ZnO Nanoparticles as Antiwear Additive in Oil Lubricants. *Wear.* **2008,** 265, 422-428.

Battez, A.H.; Rico, J.E.F.; Arias, A. N.; Rodriguez, J.L.V.; Rodriguez, R.C.; Díaz Fernández, J.M. The Tribological Behaviour of Zno Nanoparticles as an Additive to PAO6. *Wear.* **2006,** 261, 256-263.

Bayrak, Y. Interficial Composition and Formation of W/O Microemulsion with Different Amphiphiles and Oils. *Colloids Surf. A*. **2004,** 247, 99-103.

Bhushan, B. Nanoscale Tribophysics and Tribomechanics. *Wear.* **1999,** 225, 465-492.

Bhushan, B. Nanotribology and Nanomechanics. *Wear.* **2005,** 259, 1507-1531.

Biswick, T.; Jones, W.; Pacula, A.; Serwicka, E.; Podobinski, J. The Role of Anhydrous Zinc Nitrate in the Thermal Decomposition of the Zinc Hydroxy Nitrates $Zn_5(OH)_8(NO_3)_2 \cdot 2H_2O$ and $ZnOHNO_3 \cdot H_2O$. *J. Solid State Chem.* **2007,** 180, 1171–1179.

Breck D, W. *Zeolite Molecular Sieve; Structure; Chemistry and Use*; John Wiley and Son: New York, **1974.**

Briggs, M. Boron Oxides, Boric Acid, and Borates, *Kirk-Othmer Encyclopedia of Chemical Technology;* Wiley & Sons: New York, 2001**.**

Burg, P.; Selves J.L.; Colin J.P. Prediction of Kinematic Viscosity of Crude Oil from Chromatographic Data. *Fuel.* **1997,** 76, 1005-1011.

Cambiella, A.; Benito, J.M.; Pazos, C.; Coca, J.; Ratoi, M.; Spikes, H.A. The Effect of Emulsifier Concentration on the Lubricating Properties of Oil-In-Water Emulsions. *Tribol. Lett.* **2006,** 22, 53-65.

Capek, I. Preparation of Metal Nanoparticles in Water-in-Oil (W/O) Microemulsions. J. *Colloid Interface Sci.* **2004**, 110, 49-74.

Chandradass, J.; Bae, D.S.; Kim, K.H. Synthesis of Calcium Hexaaluminate ($CaAl_{12}O_{19}$) via Reverse Micelle Process. *J. Non-Cryst. Solids.* **2009,** 355, 2429-2432.

Charinpanitkul, T.; Chanagul, A.; Dutta, J.; Rungsardthong, U.; Tanthapanichakoon, W. Effect of Cosurfactant on ZnS Nanoparticle Synthesis in Microemulsion. *Sci. Technol. Adv. Mater.* **2005,** 6, 266-271.

Chemyq, Span 60, http://www.chemyq.com/En/xz/xz1/1550dnbdj.htm (Accessed June 5, 2010).

Chen, B.; Fang, J.; Wang, J.; Li, J.; Lou, F. Friction and Wear Performances of Borates and Lanthanum Chloride in Water. *J. Rare Earths.* **2008,** 26, 590-593.

Choundary, R.B.; Pande, P.P. Lubrication Potential of Boron Compounds: An Overview. *Lubr. Sci.* **2006,** 14, 211-222.

Damera, N.R.; Pasam, V.K. Performance Profiling of Boric Acid as Lubricant in Machining. *J. of the Braz. Soc. of Mech. Sci. & Eng.* **2008**, 30, 239-244.

Deshmukh, P.; Lovell, M.; Sawyer, W.G.; Mobley, A. On the Friction and Wear Performance of Boric Acid Lubricant Combinations in Extended Duration Operations. *Wear.* **2006**, 260, 1295-1304.

Dong, J.X.; Hu, Z.S. A Study of the Anti-Wear and Friction-Reducing Properties of the Lubricant Additive, Nanometer Zinc Borate. *Tribol. Int.* **1998**, 31, 219-223.

Donnet,C.; Erdemir, A. Historical Developments and New Trends in Tribological and Solid Lubricant Coatings. *Surf. Coat. Technol.* **2004,** 180-181, 76,84.

Eltepe, E.H.; Balköse, D.; Ülkü, S. Effect of Temperature and Time on Zinc Borate Species Formed from Zinc Oxide and Boric Acid in Aqueous Medium. *Ind. Eng. Chem. Res.* **2007,** 46, 2367 -2371.

Elwell, M. W.; Roberts, R.F.; Coupland, J.N. Effect of Homogenization and Surfactant Type on the Exchange of Oil between Emulsion Droplets. *Food Hydrocolloids*. **2008,** 18, 413-418.

Erdemir, A. Synergistic Effects of Liquid and Boric Acid Solid Lubricant Films on Friction and Wear of Sliding Steel Surfaces, Tribology Section, Materials and Components Technology Division, **2008,** Argonne National Lab. In: http://www.luboron.com/pdf/SynergisticEffects.pdf (Accessed 14 May, 2010)

Erdemir, A. Lubrication with Boric Acid Additives. U.S. Patent 6,025,306, 2000.

Erdemir, A. Lubrication from Mixture of Boric Acid with Oils and Greases. U.S. Patent 5,431,830, 1995.

Erdoğdu, C.A.; Atakul, S.; Balköse, D.; Ülkü, S. Development of Synergistic Heat Stabilizers for PVC from Zinc Borate-Zinc Phosphate. *Chem. Eng. Commun.* **2009,** 196, 148-160.

Fukishima, J.; Tatsuta, H.; Ishii, N.; Chen, J.; Nishiumi, T.; Aoki, K. Possibility of Coalescence of Water Droplets in W/O Emulsions by Means of Surface Processes. *Colloids Surf., A*. **2009**, 33, 53-58.

Gadelmawla, E.S.; Koura, M.M.; Maksoud, T.M.A.; Elewa, I.M.; Soliman, H.H. Roughness Parameters. *J. Mater. Process. Technol.* **2002,** 123, 133-145.

Gao, Y.H.; Liu, Z.H. Synthesis and Thermochemistry of Two Zinc Borates, $Zn_2B_6O_{11} \cdot 7H_2O$ and $Zn_3B_{10}O_{18} \cdot 14H_2O$. *Thermochim. Acta*. **2009a,** 484, 27-31.

Gao, Y.H.; Liu, Z.H. Hydrothermal Synthesis and Standard Molar Enthalpy of Formation of Zinc Borate of $4ZnO \cdot B_2O_3 \cdot H_2O$. *J. Chem. Eng. Data*. **2009b,** 54, 2789-2790.

Gao, Y.H.; Liu, Z.H.; Wang, X.L. Hydrothermal Synthesis and Thermodynamic properties of $2ZnO \cdot 3B_2O_3 \cdot 3H_2O$. *J. Chem. Thermodyn*. **2009c,** 41, 775-778**.**

Gönen, M.; Balköse, D. Gupta, R.B.; Ülkü, S. Supercritical Carbon Dioxide of Methanol-Zinc Borate Mixtures. *Ind. Eng. Chem. Res.* **2009,** 48, 6869-6876.

Gönen, M. Nanosized Zinc Borate Production. Ph.D. Thesis, İzmir Institute of Technology, June 2009.

Gönen, M. Process Development of Metal Soaps. MSc Thesis, İzmir Institute of Technology, January, 2003.

Guan, X. Y.; Deng, J.C. Preparation and Electrochemical Performance of Nano-Scale Nickel Hydroxide with Different Shapes. *Mater. Lett.* **2007,** 61, 621-625.

Gürhan, D.; Çakal, G.Ö.; Eroğlu, İ.; Özkar, S. Improved Synthesis of Fine Zinc Borate Particles using Seed Crystal. *J. Cryst. Growth.* **2009,** 311, 1545-1552.

Haus, F.; Boissel, O.; Junter, G.A. Primary and Ultimate Biodegradabilities of Mineral Base Oils and Their Relationships with Oil Viscosity. *Int. Biodeterior. Biodegrad.* **2004,** 54, 189-192.

Hiemenz, P.C.; Rajagopalan, R. *Principles of Colloid and Surface Chemistry*; Marcel Dekker Inc: New York, 1997.

Höglund, E. Influence of Lubricant Properties on Elastohydrodynamic Lubrication. *Wear.* **1999,** 232 176-184.

Hsu, S.M. Molecular Basis of Lubrication. *Tribol. Int.* **2004,** 37, 553-559.

Hsu, S.M. Fundamental Mechanisms of Friction and Lubrication of Materials. *Langmuir.* **1996,** 12, 4482-4485.

Hu, B.; Scott, K. Microfiltration of Water in Oil Emulsions and Evaluation of Fouling Mechanism. *Chem. Eng. J.* **2008**, 136, 210-22.

Hu, Z.S.; Lai, R.; Lou, F.; Wang, L.G.; Chen, Z.L.; Chen, G.X.; Dong, J.X. Preparation and Tribological Properties of Nanometer Magnesium Borate as Lubricating Oil Additive. *Wear.* **2002**, 252, 370-374.

Hu, Z.S.; Dong, J.X.; Chen, G.X.; He, J.Z. Preparation and Tribological Properties of Nanometer Lanthanum Borate. *Wear.* **2000,** 243, 43-47.

Hu, Z.S.; Dong, J.X.; Chen, G.X.; Lou, F. Preparation of Nanometer Copper Borate with Supercritical Carbon Dioxide Drying. *Powder Technol.* **1999,** 102, 171-176.

Hu, Z.S.; Dong, J.X. Study on Antiwear and Reducing Friction Additive of Nanometer Titanium Borate. *Wear.* **1998**, 216, 87-91.

Huang, H.D.; Tu, J.P.; Gan, L.P., Li, C.Z. An Investigation on Tribological Properties of Graphite Nanosheets as Oil Additive. *Wear.* **2006,** 261, 140-144.

Ichikawa, T. Electrical Demulsification of Oil-in-Water Emulsion, *Colloids Surf., A.* **2007**, 302, 581-586.

Jacobson, S.; Hogmark, S.; Surface Modifications in Tribological Contacts, *Wear.* **2009**, 266, 370-378.

Jafari, S.M.; Assadpoor, E.; He, Y.; Bhandari, B. Re-Coalescence of Emulsion Droplets during High Energy Emulsification. *Food Hydrocolloids.* **2008,** 22, 1191-1202.

Jallad, K.N.; Ben-Amatz, D.B.; Erdemir, A. Raman Chemical lmaging of Tribological Surfaces. *Tribol Transactions.* **2002**, 45, 239-245.

Januszkiewicz, K.R.; Riahi, A.R.; Barakat, S. High Temperature Tribological Behaviour of Lubricating Emulsions. *Wear.* **2004,** 256, 1050-1061.

Jun, L., Shupping, X., Shiyang, G. FT-IR and Raman Spectroscopic Study of Hydrated Borates. *Spectrochimica Acta.* **1995,** 51A (4), 519-532.

Ke-long, H.; Liang-guo, Y.; Su-qin, L.; Chao-jian, L. Preparation and Formation Mechanism of Al_2O_3 Nanoparticles by Reverse Microemulsion. *Trans. Nonferrous Met. Soc. China.* **2007,** 17, 633-637.

Kim, S.M.; Sit, C.Y.; Komvopoulos, K.; Yamaguchi, E.S.; Ryason, P.R. Boundary Lubrication of Steel Surfaces with Borate, Phosphorus, and Sulfur Containing Lubricants at Relatively Low and Elevated Temperatures. *Tribol. Transactions.* **2000,** 43, 569-578.

Kimura, Y.; Wakabayashi, T.; Okada, K.; Wada, T.; Nishikawa, H. Boron Nitride as a Lubricant Additive. *Wear.* **1999**, 232, 199-206.

Klinegroup, Market Research, http://www.klinegroup.com/reports/emailings/newsletters/energy/september2009/timely_trends.asp (acessed May 13, 2010)

Korhonen, M.; Hirvonen, J.; Peltonen, L.; Antikainen, O.; Yrjänäinen.; Yliruusu, J. Formation and Characterization of Three-Component-Sorbitan Monoester Surfactant, Oil and Water-Creams. *Int. J. Pharm.* **2004**, 269, 227-239.

Koroleva, M.Y.; Yurtov, E.V. Water Mass Transfer in W/O Emulsions. *J. Colloid Interface Sci.* **2006.** 297, 778-784.

Köytepe, S.; Vural, S.; Seçkin, T. Molecular Design of Nanometric Zinc Borate-Containing Polyimide as a Route to Flame Retardant Materials. *Mater. Res. Bull.* **2009,** 44**,** 369-376.

Lee, K.; Hwang, Y.; Cheong, S.; Choi, Y.; Kwon, L.; Lee, J.; Kim, S.H. Understanding The Role of Nanoparticles in Nano-Oil Lubrication. *Tribol. Lett.* **2009**, 35, 127-131.

Lee, M.H.; Tai, C.Y.; Lu, C.H. Synthesis of Spherical Zirconia by Precipitation between Two Water/Oil Emulsions. *J. Eur. Ceram. Soc.* **1999,** 19, 2593-2603.

Leśniewski, T.; Krawiec, S. The Effect of Ball Hardness on Four-Ball Wear Test Results. *Wear.* **2008,** 264, 662-670.

Li, J.; Xu, X.; Wang, Y.; Ren, T. Tribological Studies on a Novel Borate Ester Containing Benzothiazol-2-Yl and Disulfide Groups as Multifunctional Additive. *Tribol. Int.* **2010,** 43. 1048-1053.

Li, S.; Long, B.; Wang, Z.; Tian, Y.; Zheng, Y.; Zhang, Q. Synthesis of Hydrophobic Zinc Borate Nanoflakes and Its Effect on Flame Retardant Properties of Polyethylene. *J. Solid State Chem.* **2010,** 183. 957-962.

Li, F.; Vipulanandan, C. Characterization of Y_2BaCuO_5 Nanoparticles Synthesized by Nano-Emulsion Method. *J. Nanopart. Res.* **2007,** 9, 841-852.

Li, B.; Wang, X.; Liu, W.; Xue, Q. Tribochemistry and Antiwear Mechanism of Organic-Inorganic Nanoparticles as Lubricant Additives. *Tribol. Lett.* **2006,** 22, 79-84.

Lin, T.L.; Hu, Y.; EE, .T. The Effect of Alcohols on the Size of Water-in-Oil Microemulsion Droplets. *Progr Colloid Polym Sci.* **1997**. 105. 268-271.

Liu, N.; Tian, Y.; Yu, L.; Li, Q.; Meng, F.; Zheng, Y.; Zhang, G.; Liu, Z.; Li, J.; Jiang, F. Synthesis and Surface Modification of Uniform Barium Borate Nanorods for Lubrication. *J. Alloys Compd.* **2008,** 266, L11-L14.

Liu, Q.; Xiao, Y.; Rong, W.; Yuan, L. Large-Scale Synthesis of Monodsiperse $2ZnO \cdot 2B_2O_3 \cdot 3H_2O$ Micro/Nano Single Crystals and Their Effect in Polypropylene. *Soft Mater.* **2009,** 7, 67-78.

Lopez, F.; Cinelli, G.; Ambrosone, L.; Colafemmina, G.; Ceglie, A.; Palazzo, G. Role of the Cosurfactant in Water-in-Oil Microemulsion: Interfacial Properties Tune the Enzymatic Activity of Lipase. *Colloids Surf. A.* **2004,** 237, 49-59.

Lu, Y.; GuO, T. Phase Behaviour of Microemulsions with Lubricant Base Oil as the Oil Phase. *Lubr. Sci.* **2009**, 21. 289-296.

Luo, Z.H.; Zhan, X.L.; Yu, P.Y. Effect of Addition Cosurfactant on the Phase Behavior of Oil-in-Water Aminosilicone Oil Microemulsion. *Chin. Chem. Lett.* **2004.** 15, 1101-1104.

Mang, T.; Dresel, W. *Lubricants and Lubrication;* Wiley VCH: Weinheim, 2001; pp 6-184.

Marsh, K.N.; Kandil, M.E. Review of Thermodynamic Properties of Refrigerants + Lubricant Oils. *Fluid Phase Equilib.* **2002,** 199, 319-334.

Masjuki, H.H.; Maleque, M.A. Investigation of Anti-Wear Characteristics of Palm Oil Methyl Ester using a Four Ball Tribometer-Test. *Wear.* **1997,** 206, 179-186.

Mazuyer, D.; Tonck, A.; Bec, S.; Loubet, J.L.; Georges, M. Nanoscale Surface Rheology in Tribology. *Tribol. Interface Eng. Ser.* **2001,** 39**,** 273-282.

Myers, D. *Surfaces, Interfaces, and Colloids Principles and Applications*; VCH Publishers Inc: New York, 1991.

Myshkin, N.K. Friction Transfer Film Formation in Boundary Lubrication. *Wear.* **2000,** 245, 116-124.

Nassar, N.N.; Husein, M.M. Effect of Microemulsion Variables on Copper Oxide Nanoparticles Uptake by AOT Microemulsions. *J. Colloid Interface Sci.* **2007,** 316, 442-450.

Neale, M.J. *Tribology Handbook;* Antony Rowe Ltd: Eastbourne, 1995; pp E6.1-E6.4

Nicholls, M.A.; Do, T.; Norton, P.R.; Kasrai, M.; Bancrof,t G.M. Review of Lubrication of Metallic Surfaces by Zinc Dialkyl-Dithiophosphates. *Tribol. Int.* **2005,** 38, 15-39.

Niemann, B.; Sundmacher, K. Nanoparticle Precipitation in Microemulsions: Population Balance Model and Identification of Bivariate Droplet Excahange Kernel. *J. Colloid Interface Sci.* **2010,** 342, 361-371.

Nies, N.; Beach, L.; Hulbert, R.W. Zinc Borate of Low Hydration and Method for Preparing Same. U.S. Patent 3,649,172, 1972.

Öncü,l A.A.; Niemann, B.; Sundmacher, K.; Thévenin, D. CFD Modelling of $BaSO_4$ Precipitation Inside Microemulsion Droplets In a Semi-Batch Reactor. *Chem. Eng. J.* **2008,** 138, 498-509.,,

Palla, B.J.; Shah, D.O. Preparation of Nanoparticles of Barium Ferrite from Precipitation in Microemulsions. *J. Nanopart. Res.* **1999**, 1, 215-221.

Pawlak, Z.; Kaldonski, T.; Pai, R.; Bayraktar, E.; Oloyede, A. A Comparative Study on the Tribological Behaviour of Hexagonal Boron Nitride (h-BN) as Lubricating Micro-Particles—An Additive in Porous Sliding Bearings for a Car Clutch. *Wear.* **2009**, 267, 1198- 1202.

Peltonen, L.; Hirvonen, J.; Yliruusi, J. The Effect of Temperature on Sorbitan Surfactant Monolayers. *J. Colloid Interface Sci* .**2001**, 239, 134-138.

Peltonen, L.; Yliruusi, J. Surface Pressure, Hysteresis, Interfacial Tension, and CMC of Four Sorbitan Monoesters at Water–Air, Water–Hexane, and Hexane–Air Interfaces. *J. Colloid Interface Sci.* **2000,** 227, 1-6.

Pi, H.; Guo, S.; Ning, Y. Mechanochemical Improvement of the Flame-Retardant and Mechanical Properties of Zinc Borate and Zinc Borate-Aluminum Trihydrate-Filled Poly(Vinyl Chloride). *J. Appl. Biol. Sci.* **2002**, 89, 753-762.

Porras, M.; Solans, C.; González, C.; Gutiérrez, J.M. Properties of Water-in-Oil (W/O) Nano-Emulsions Prepared by a Low-Energy Emulsification Method, *Colloids Surf., A*. **2008**, 324, 181-188.

Pulcu, G. Effect of Production Processes Mineral Base Oils On Quality and Sludge Formation of Hydraulic System Oils. MSc Thesis, Ege University, 2008.

Qiao, Y.; Liu, W.; Xu, B.; Ma, S.; Xue, Q. The Tribological Performance of Nano/Micrometre Borate Modified By an N-Containing Compound as an Oil Additive. *Lubr. Sci.* **2003**, 15. 369-379.

Qiu, S.; Dong, J.; Chen, G. Preparation of Cu Nanoparticles from Water-in-Oil Microemulsions. *J. Colloid Interface Sci.* **1999,** 216, 230-234.

Rao, K.P.; Xie, C.L. A Comparative Study on the Performance of Boric Acid with Several Conventional Lubricants in Metal Forming Processes. *Tribol. Int.* **2006,** 39, 663-668.

ResearchWikis, **2010,** Lubricants Marketing Research, http://researchwikis.com/Lubricants_Marketing_Research (Accessed May 13, 2010)

Rosen, M.J. *Surfactants and Interfacial Phenomena*; John Wiley & Sons: Canada, 1989; pp 305.

Ruina, A.; Pratap R. *Introduction to Statics and Dynamics;* Oxford University Press: Oxford, 2002; pp 713-721.

Sathyan, K.; Hsu, H.Y.; Lee, S.H.; Gopinath, K. Long-Term Lubrication of Momentum Wheels Used in Spacecrafts—An Overview. *Tribol. Int.* **2009,** 43, 259-267.

Schick, M.J.; Fowkers, F.M. *Nonionic Surfactants*; Marcel Dekker Inc: New York, 1966.

Schubert, D.M.; Alam, F.; Visi, M.Z.; Knobler, C.B. Structural Characterization and Chemistry of Industrially Important Zinc Borate $Zn[B_3O_4(OH)_3]$, *Chem. Mater.* **2003,** 15, 866-871.

Schubert, D. M. Zinc Borate. U.S. Patent 5,472,644, December 5, 1995.

Sedlaček, M.; Podgornik, B.; Vižintin, J. Influence of Surface Preparation on Roughness Parameters, Friction and Wear. *Wear.* **2009,** 266, 482-487.

Shen, G.; Zheng, Z.; Wan, Y.; Xu, X.; Cao, L.; Yue, Q.; Sun, T.; Liu, A. Synergistic Lubricating Effects of Borate Ester with Heterocyclic Compound. *Wear.* **2000,** 246, 55-58.

Shete, A.P.; Sawant, S.B.; Pangarkar, V.G. Kinetics of Fluid–Solid Reaction with An Insoluble Product: Zinc Borate by the Reaction of Boric Acid and Zinc Oxide. *J. Chem. Technol. Biotechnol.* **2004,** 79, 526-532.

Shi, X.; Xiao, Y.; Yuan, L.; Sun, J. Hydrothermal Synthesis and Characterizations of 2D and 3D $4ZnO \cdot B_2O_3 \cdot H_2O$ Nano/Microstructures with Different Morphologies. *Powder Technol.* **2009**, 189, 462-465.

Shi, X.; Wang, S.; Yang, H.; Duan, X.; Dong, X. Fabrication and Characterization of Hexagonal Boron Nitride Powder by Spray Drying and Calcining–Nitriding Technology. *J. Solid State Chem.* **2008,** 181, 2274-2278.

Shi, J.; Weweij, H. Synthesis and Purification of Oxide Nanoparticle Dispersions by Modified Emulsion Precipitation. *Langmiur.* **2005**, 21, 5570-5575.

Smiechowski, M.F.; Lvovich, V.F. Electrochemical Monitoring of Water-Surfactant Interactions in Industrial Lubricants. *J. Electroanal. Chem.* **2002**, 534, 171-180.

Stachowiak, G.W.; Batchelor, A.W. *Engineering Tribology*; Elsevier Inc: New York, 2005; pp 2-3.

Sun, L.; Tao, X.; Zhao, Y.; Zhang, Z. Synthesis and Tribology Properties of Stearate-Coated Ag Nanoparticles. *Tribol. Transactions.* **2010,** 53, 174-178.

Surh, J.; Vladisavljevi, G.T.; Mun, S.; McClements, J. Preparation and Characterization of Water/Oil and Water/Oil/Water Emulsions Containing Biopolymer-Gelled Water Droplets. *J. Agric. Food. Chem.* **2007**, 55, 175-184.

Tai, C.Y.; Chen, C.K. Particle Morphology, Habit and Size Control of $CaCO_3$ Using Reverse Microemulsion Technique, *Chem. Eng. Sci.* **2008,** 63, 3632-3642.

Tıhmınlıoğlu, F.; Ülkü, S. Use of Clinotilolite in Ethanol Dehydration. *Sep. Sci. Technol.* **1996,** 31, 2855-2865.

Tian, Y.; He, Y.; Yu, L.; Deng, Y.; Zheng, Y.; Sun, F.; Liu, Z.; Wang, Z. In Situ and One-Step Syntheis of Hydrophobic Zinc Borate Nanoplatelets. *Colloids Surf., A.* **2008,** 312, 99-103.

Tian, Y.; Guo, Y.; Jiang, M.; Sheng, Y.; Hari, B.; Zhang, G.; Jiang, Y.; Zhou, B.; Zhu, Y.; Wang, Z. Synthesis of Hydrophobic Zinc Borate Nanodiscs for Lubrication, *Mater. Lett.* **2006,** 60, 2511-2515.

Ting, C.; Cheng, D.J.; Shuo, W.L.; Gang, F. Preparation and Characterization of Nano-Zinc Borate by a New Method. *J. Mater. Process. Technol.* **2009,** 209. 4076-4079.

Tüpraş, Safety Data Sheet Light Neutral Base Oil, http://www.tupras.com.tr/file.debug.php?lFileID=1511 (Accessed May 27, 2010).

Ulmeanu, M. Preparation and Characterization of Water in Oil Emulsion via Drop Break-Off. *Colloids Surf., A.* **2008**, 316, 119-124.

Varlot, K.; Kasrai, M.; Bancroft, G.M.; Yamaguchi, E.S.; Ryason, P.R.; Igarashi, J. X-Ray Absorption Study of Antiwear Films Generated from ZDDP and Borate Micelles. *Wear.* **2001**, 249, 1029-1035.

Wakabayashi, T. Viscosity Correlation with Specific Gravity and Molecular Weight of Crude oil Fractions. *Fuel.* **1997,** 76, 1049-1056.

Wang, S.; Ge, S.; Zhang, D. Comparison of Tribological Behavior of Nylon Composites Filled With Zinc Oxide Particles and Whiskers. *Wear.* **2009,** 266, 248-254.

Wasilewski, T.; Sulek, M.W. Paraffin Oil Solutions of the Mixture of Sorbitan Monolaurate-Ethoxylated Sorbitan Monolaurate as Lubricants. *Wear.* **2006,** 261, 230-234.

Wikipedia, Solubility Table**,** http://en.wikipedia.org/wiki/Solubility_table (Accessed June 3, 2010).

Windhab, E.J.; Dressler, M.; Feigl, K.; Fischer, P.; Megias-Alguacil, D. Emulsion Processing-from Single Drop Formation to Design of Complex Processes and Products. *Chem. Eng. Sci.* **2005,** 60, 2101-2113.

Wood, G.L.; Janik, J.F.; Visi, M.Z.; Schubert, D.M.; Paine, R.T. New Borate Precursors for Boron Nitride Powder Synthesis. *Chem. Mater.* **2005,** 17, 1855-1859.

Xue, Q.; Liu, W.; Zhang, Z. Friction and Wear Properties of a Surface-Modified TiO_2 Nanoparticle as an Additive in Liquid Parafin. *Wear.* **1997,** 213, 29-32.

Yan, S.; Kuroda, S. Lubrication with Emulsion: First Report, the Extended Reynolds Equation. *Wear.* **1997,** 206, 230-237.

Yu, H.L.; Xu, Y.; Shi, P.J.; Wang, H.M.; Zhao, Y.; Xu, B.S.; Bai, Z.M. Tribological Behaviors of Surface-Coated Serpentine Ultrafine Powders as Lubricant Additive. *Tribol. Int.,* **2010**, 43, 667-675.

Yu, H.; Xu, Y.; Shi, P.; Xu, B.; Wang, X.; Liu, Q. Tribological Properties and Lubricating Machanisms of Cu Nanoparticles in Lubricant. *Trans. Nonferrous Met. Soc. China.* **2008,** 18, 636-641.

Zhang, M.; Wang, X.; Fu, X. Performance and Anti-Wear Mechanism of $CaCO_3$ Nanoparticles as a Green Additive in Poly-Alpha-Olefin. *Tribol. Int.* **2009,** 42, 1029-1039.

Zhang, W.; Qiao, X.; Chen, J. Synthesis of Silver Nanoparticles-Effect of Concerned Parameters in Water/Oil Microemulsion. *Mater. Sci. Eng. B.* **2007,** 142, 1-15.

Zeng, Y.; Yang, H.; Fu, W.; Qiao, L.; Chang, L.; Chen, L., Zhu, H.; Li, M.; Zou, G. Synthesis of Magnesium Borate ($Mg_2B_2O_5$) Nanowires, Growth Mechanism and Their Lubricating Properties. *Mater. Res. Bull.* **2008,** 43, 2239-2247.

Zheng, Y.; Tian, Y.; Ma, H.; Qu, Y.; Wang, Z.; An, D.; Guan, S.; Gao, X. Synthesis and Performance Study of Zinc Borate Nanowhiskers. *Colloids Surf., A.* **2009,** 339, 178-184.

Zheng, Z.; Shen, G.; Wan, Y.; Cao, L.; Xu, X.; Yue, Q.; Sun, T. Synthesis, Hydrolytic Stability and Tribological Properties of Novel Borate Esters Containing Nitrogen as Lubricant Additives. *Wear.* **1998,** 222, 135-144.

Zhao, Y.P.; Turay, R.; Hundley, L. Monitoring and Predicting Emulsion Stability of Metal Working Fluids by Salt Titration and Turbiscan. *Nalco Company*, **2006**.

Zimmerman, J.B.; Clarens, A.F.; Hayes, K.F.; Skerlos, S.J. Design of Hard Water Stable Emulsifier Systems for Petroleumand Bio-Based Semi-Synthetic Metalworking Fluids. *Environ. Sci. Technol.* **2003**, 37, 5278-5288.

Zhou, Z.R.; Vincent, L. Lubrication in Fretting-A Review. *Wear.* **1999**, 225-229, 962-967.

APPENDIX A

FTIR SPECTRA OF LUBRICANTS
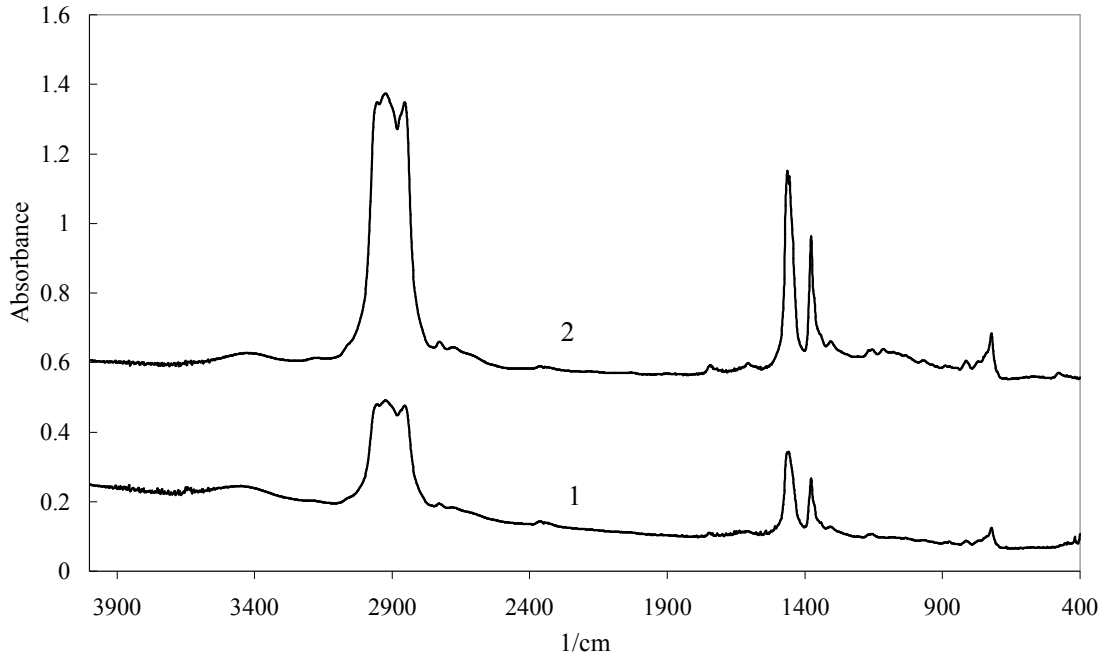
Figure A.1. FTIR spectrum of L2 lubricant containing only sorbitan monostearate 1) before 2) after four ball wear test.
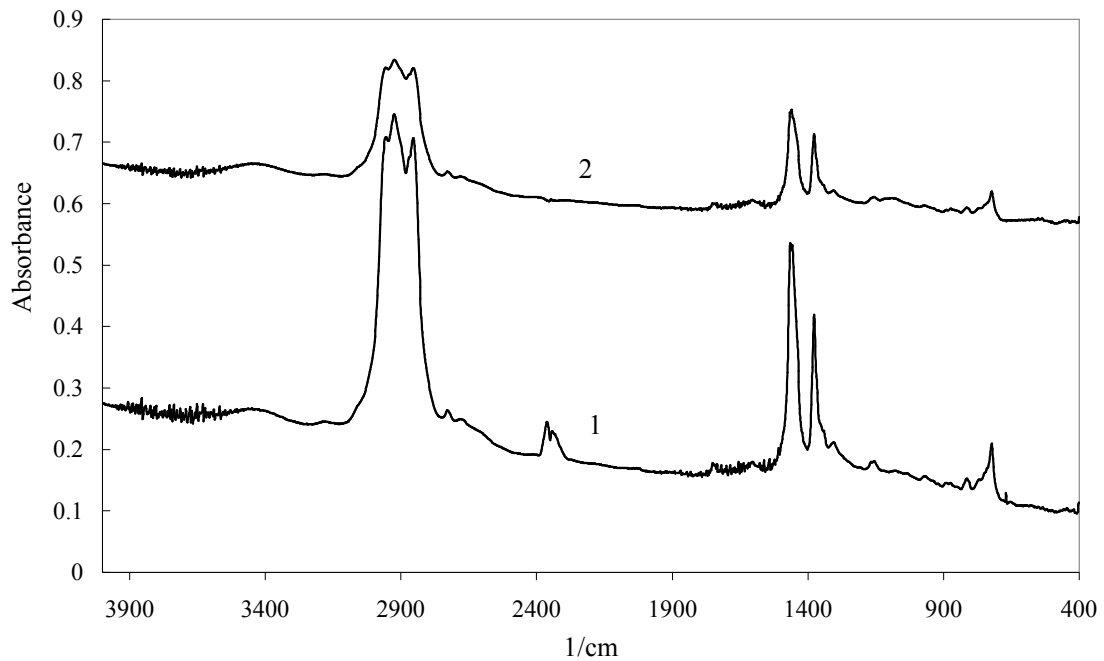
Figure A.2. FTIR spectra of L10 lubricant containing sorbitan monostearate and zinc borate prepared by coordination homogeneous precipitataion and mixed for 15 h 1) before and 2) after four ball wear test.
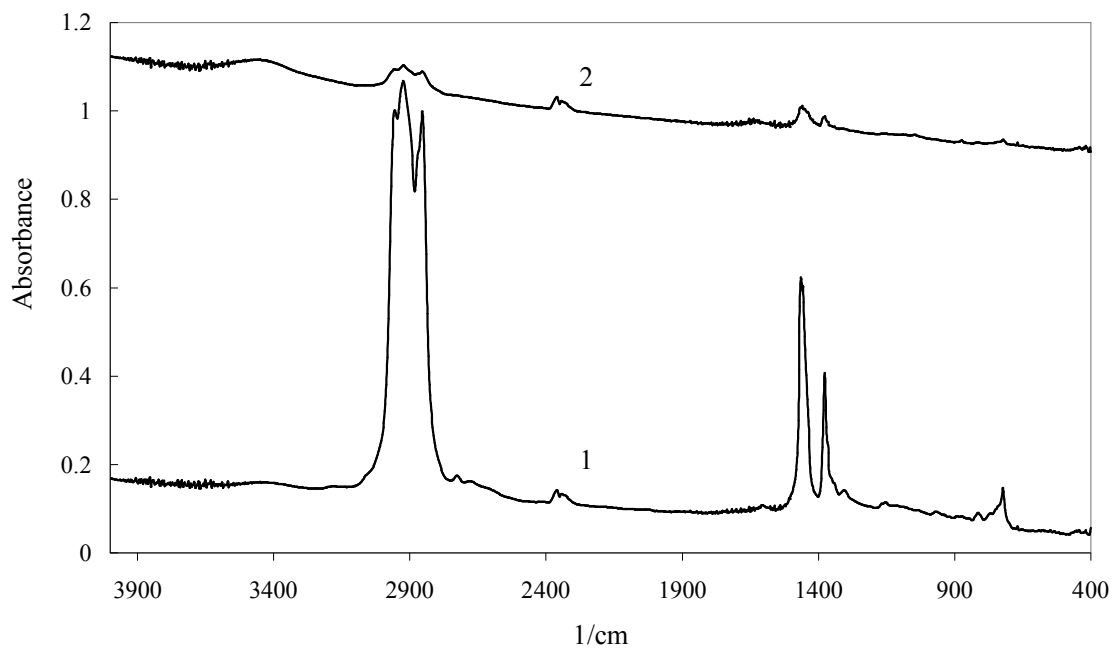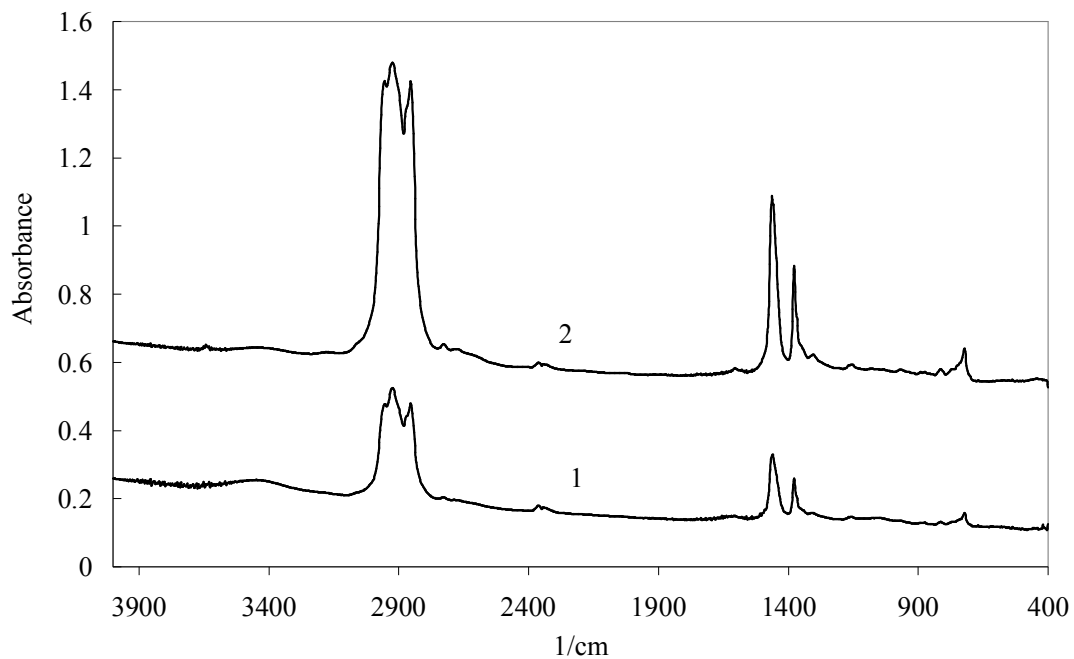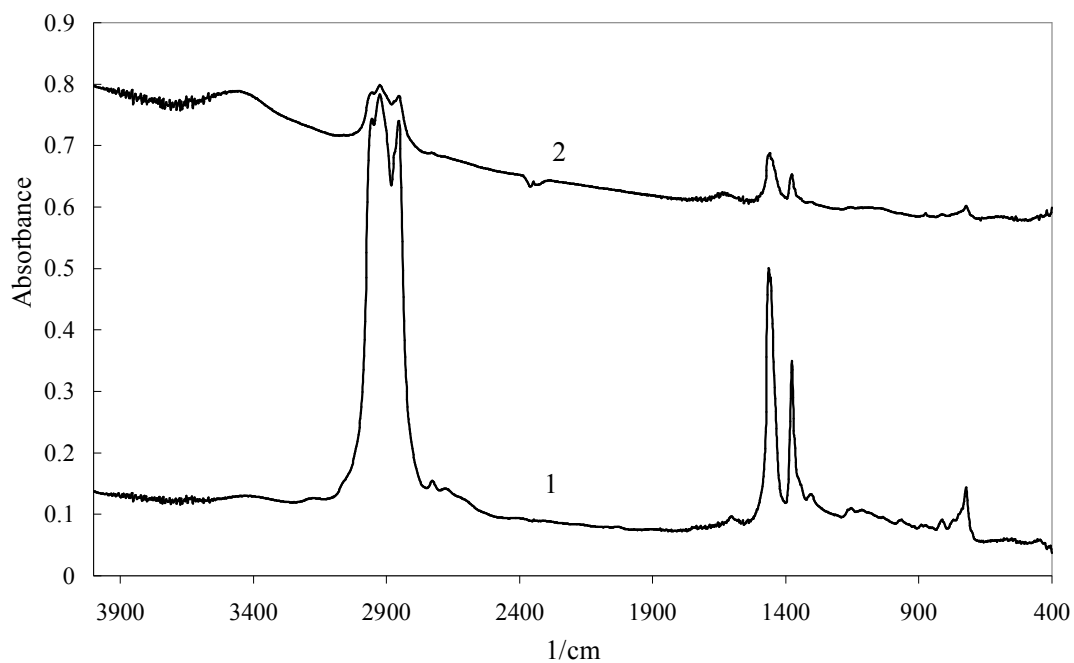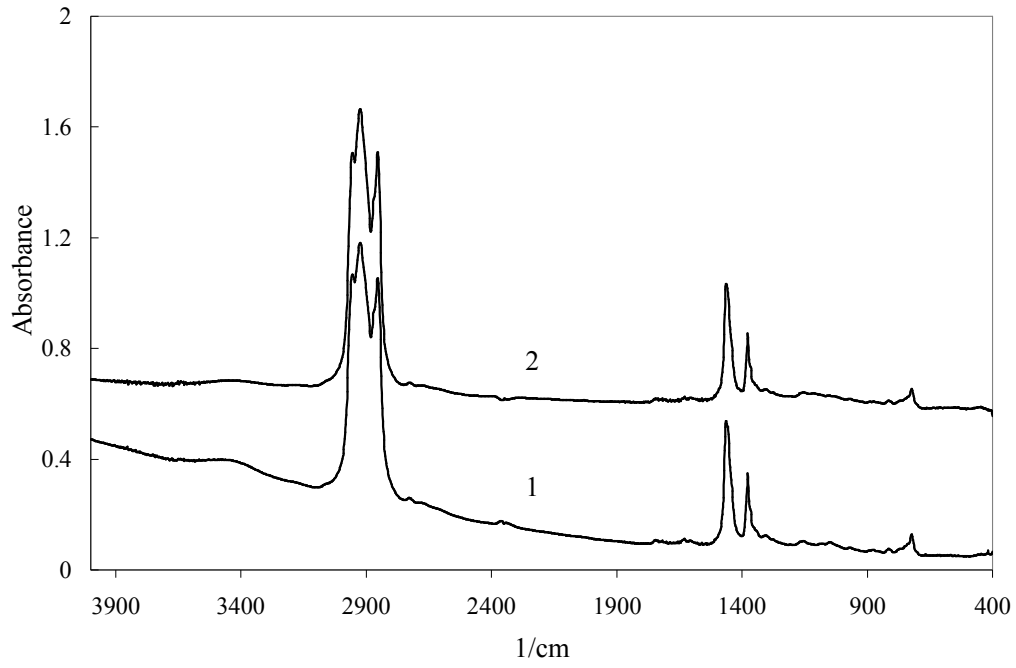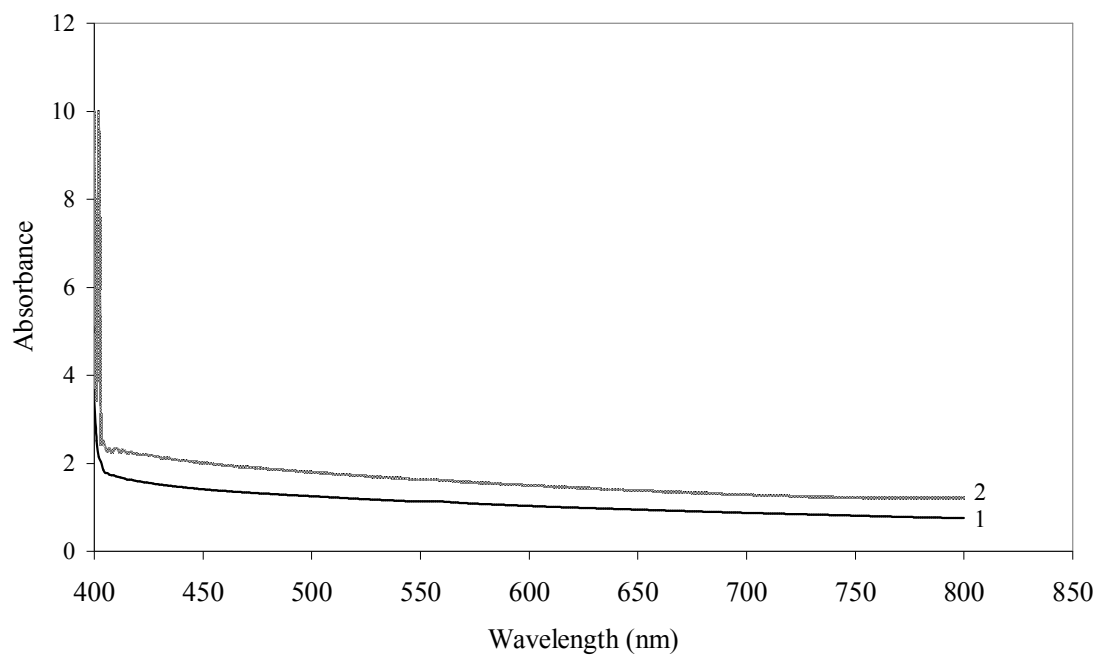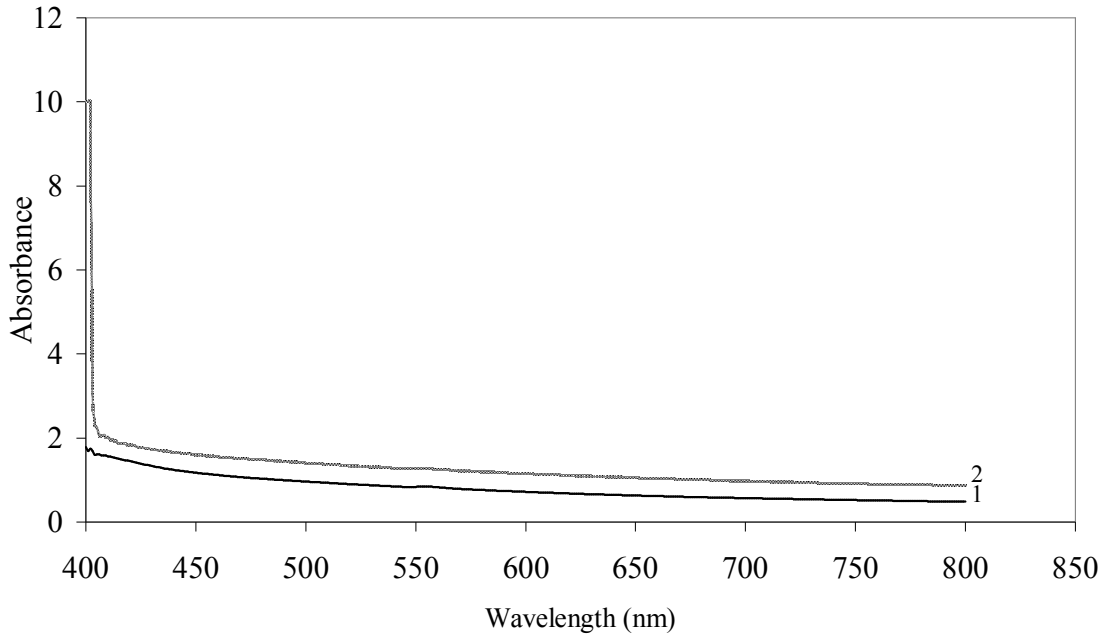

Figure A.3. FTIR spectrum of L11 lubricant containing sorbitan monostearate and zinc borate prepared by coordination homogeneous precipitataion and mixed for 12 h 1) before and 2) after four ball wear test.

237

Figure A.4. FTIR spectrum of L12 lubricant containing 0.00005 g sorbitan monostearate and zinc borate prepared by coordination homogeneous precipitataion and mixed for 12 h 1) before and 2) after four ball wear test.

Figure A.5. FTIR spectrum of L13 lubricant containing 0.1 g sorbitan monostearate and zinc borate prepared by coordination homogeneous precipitataion and mixed for 12 h 1) before and 2) after four ball wear test.

Figure A.6. FTIR spectrum of inverse emulsion heated up to 160 °C (L16) 1) before and 2) after four ball wear test.

APPENDIX B

UV SPECTRA OF LUBRICANTS

Figure B.1. UV spectra of the lubricant containing sorbitan monostearate and zinc borate synthesized by coordination homogeneous precipitation technique, mixed for 6 h 1) before four ball wear test 2) after four ball wear test.
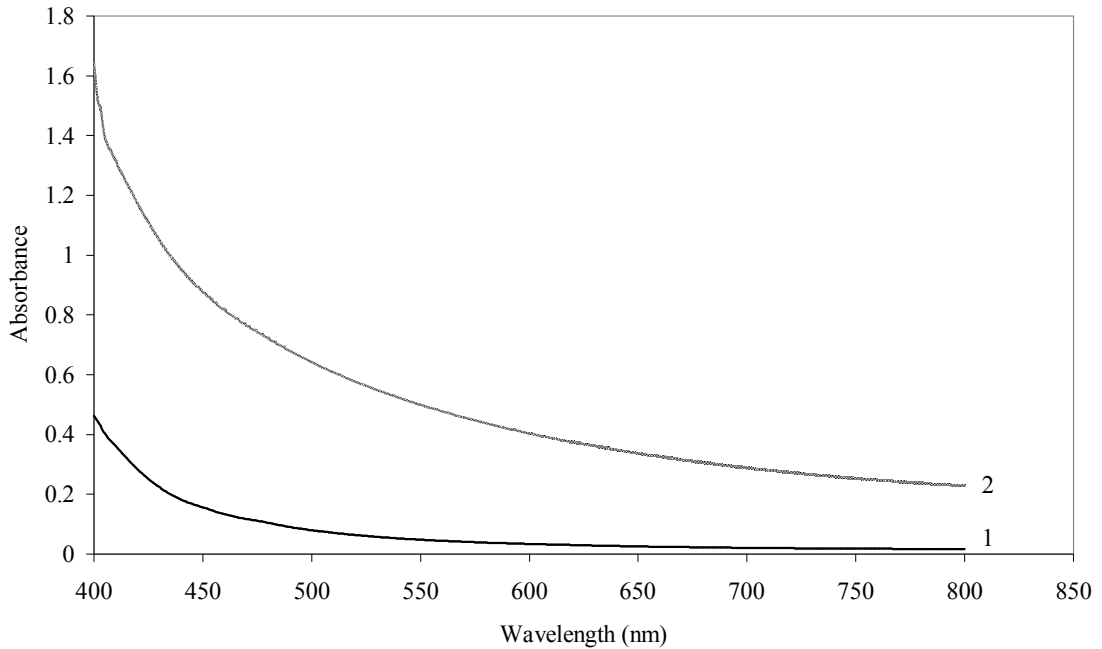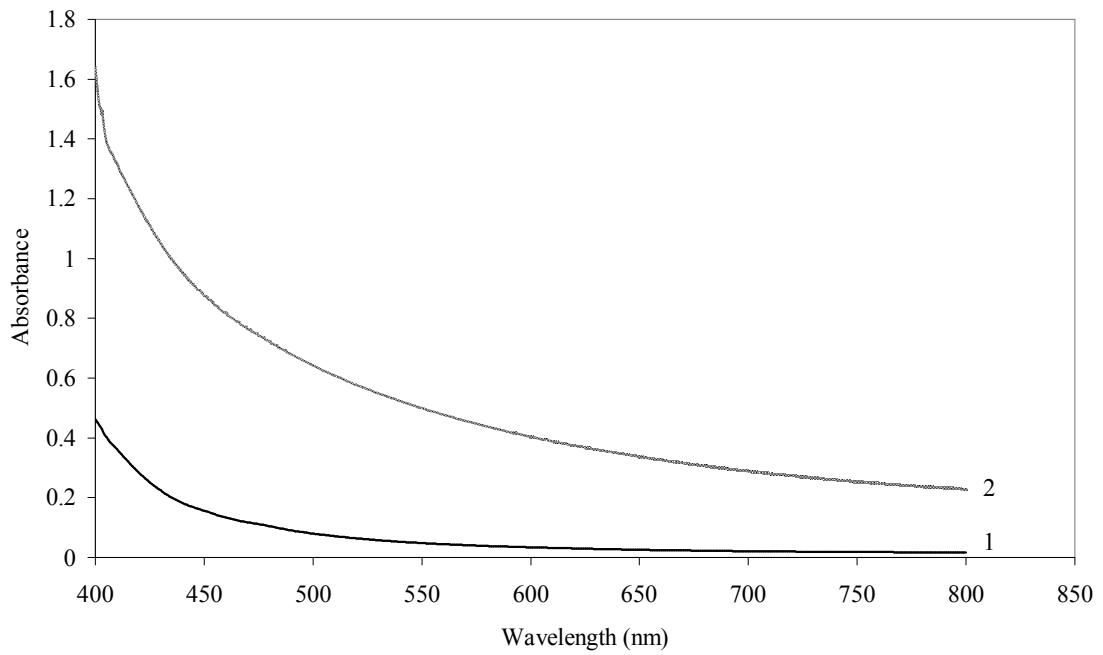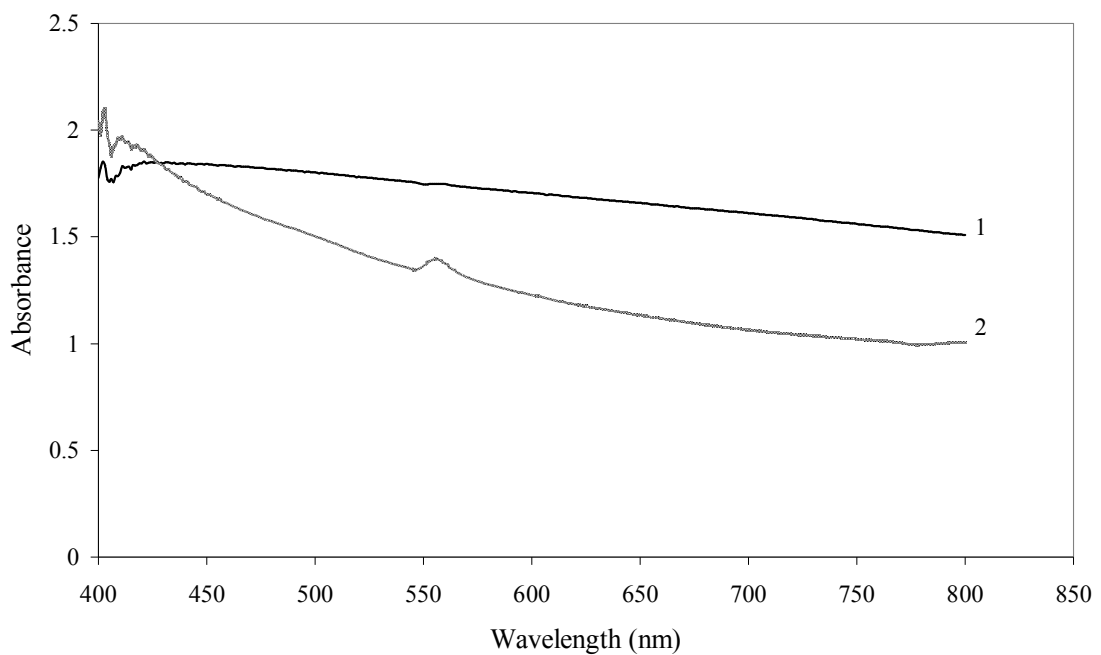
Figure B.2. UV spectra of the lubricant containing sorbitan monostearate and zinc borate synthesized by coordination homogeneous precipitation technique, mixed for 12 h 1) before four ball wear test 2) after four ball wear test.

Figure B.3. UV spectra of the lubricants containing 0.00005 g sorbitan monostearate and zinc borate synthesized by coordination homogeneous precipitation technique, mixed for 12 h 1) before four ball wear test 2) after four ball wear test.

Figure B.4. UV spectra of the lubricant containing 0.1 g sorbitan monostearate and zinc borate synthesized by coordination homogeneous precipitation technique, mixed for 12 h 1) before four ball wear test 2) after four ball wear test.

Figure B.5. UV spectra of the lubricant containing precipitate obtained by the microemulsion having 30% propanaol-2 1) before four ball wear test 2) after four ball wear test.
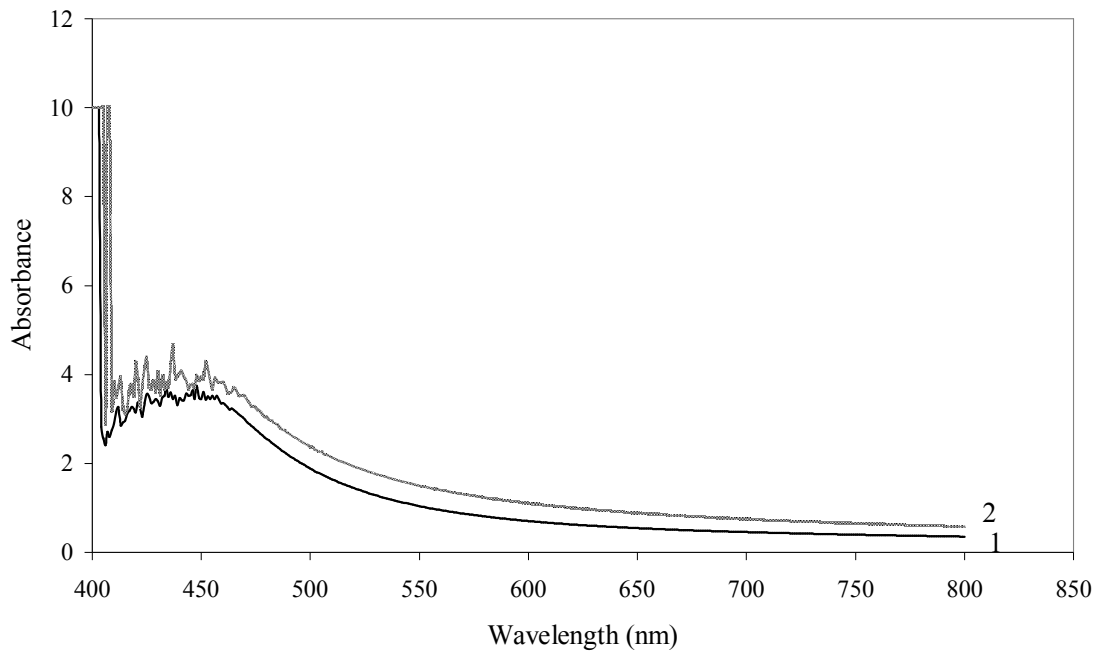
Figure B.6. UV spectra of the lubricant containing sorbitan monostearate and clinoptilolite rich mineral 1) before four ball wear test 2) after four ball wear test.

APPENDIX C
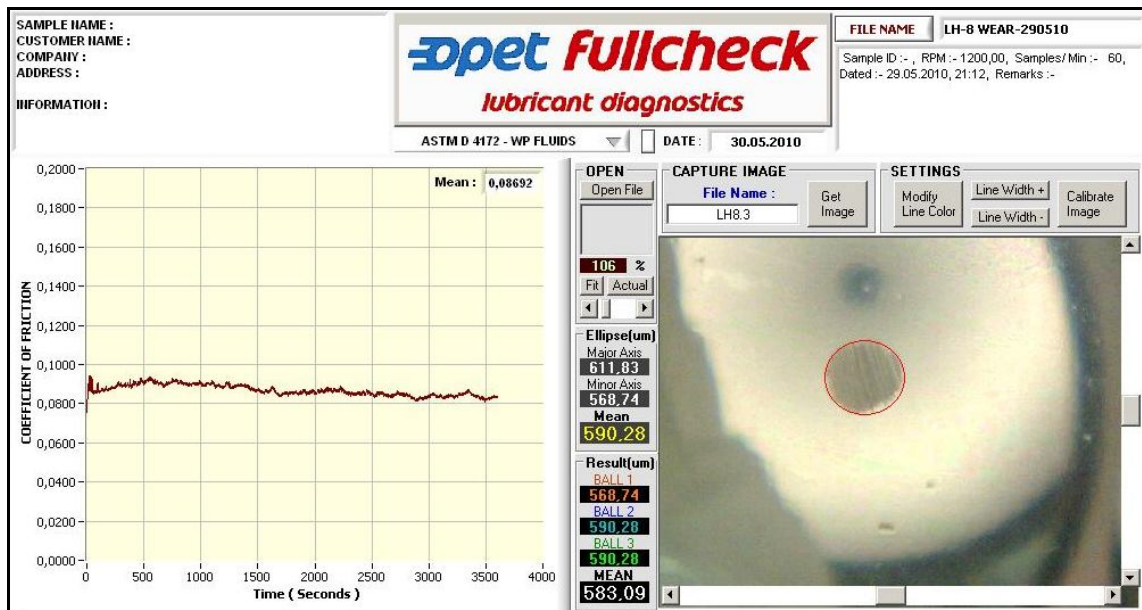
WEAR AND FRICTION BEHAVIOR OF LUBRICANTS

Figure C.1. The wear and friction behavior of the mineral oil having sorbitan monostearate and zinc borate synthesized by coordination homogeneous precipitation technique, mixed for 6 h and washed by ethanol.
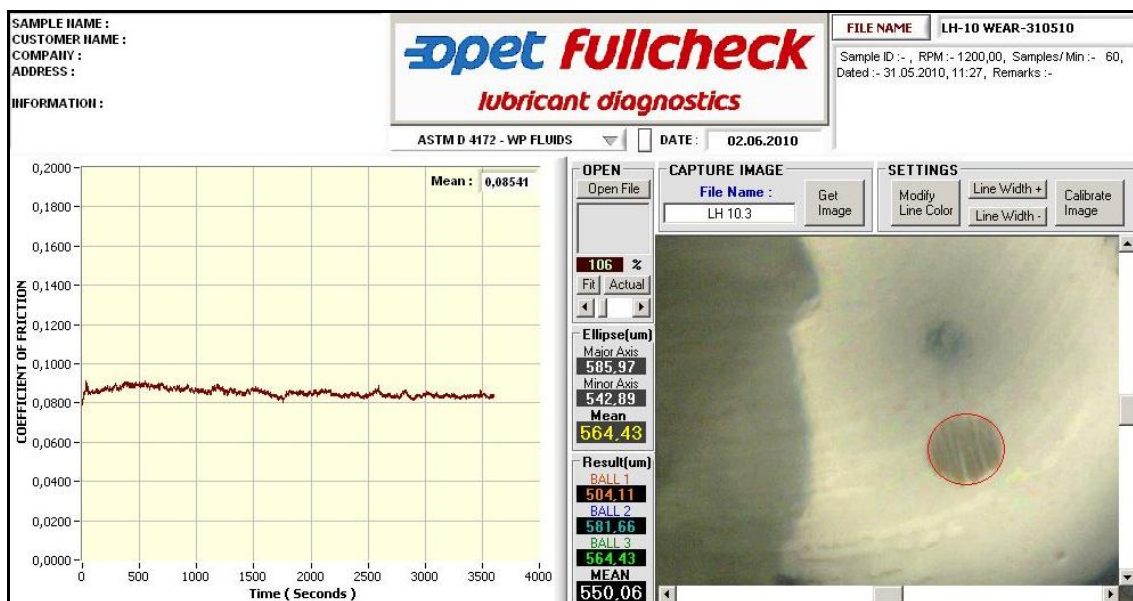
Figure C.2. The wear and friction behavior of the mineral oil having sorbitan monostearate and zinc borate synthesized by coordination homogeneous precipitation technique, mixed for 12 h and washed by water and ethanol.
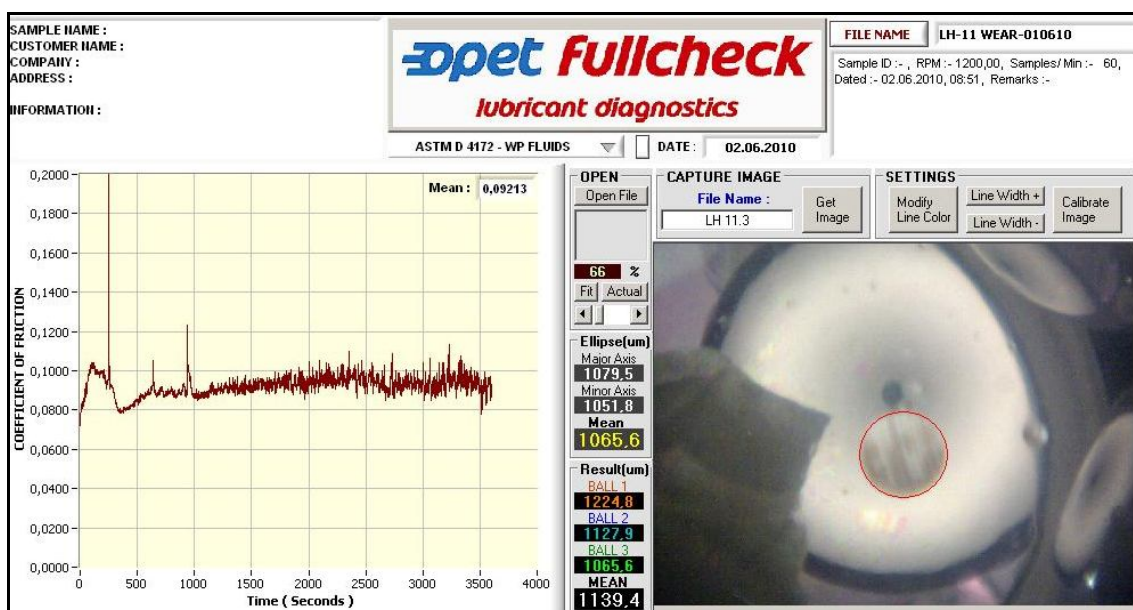

Figure C.3. The wear and friction behavior of the mineral oil having sorbitan monostearate and zinc borate synthesized by coordination homogeneous precipitation technique, mixed for 12 h and washed by water and ethanol. and 0.00005 g sorbitan monostearate.
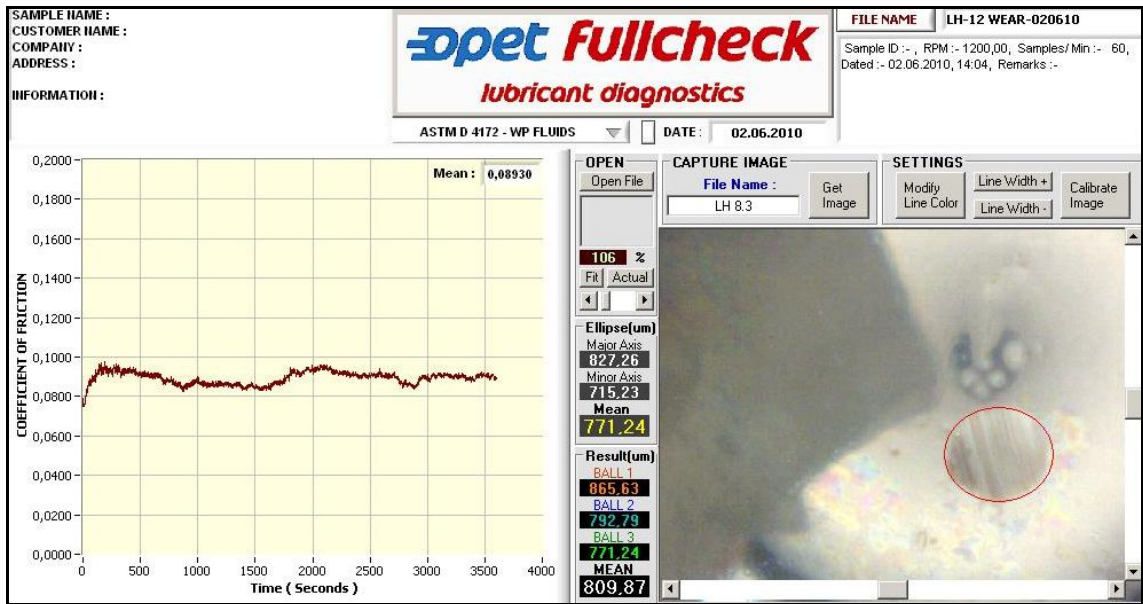
Figure C.4. The wear and friction behavior of the mineral oil having sorbitan monostearate and zinc borate synthesized by coordination homogeneous precipitation technique, mixed for 6 h and washed by water and ethanol. and 0.1 g sorbitan monostearate.
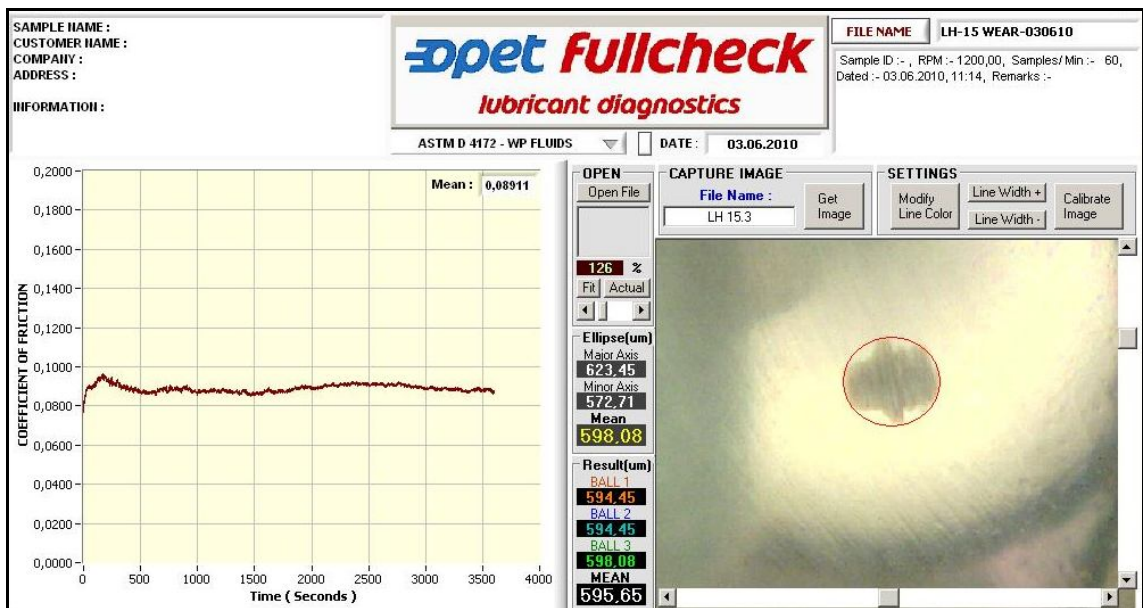

Figure C.5. The wear and friction behavior of the inverse emulsion of which water content was removed by heating up to 160 ^{o}C.
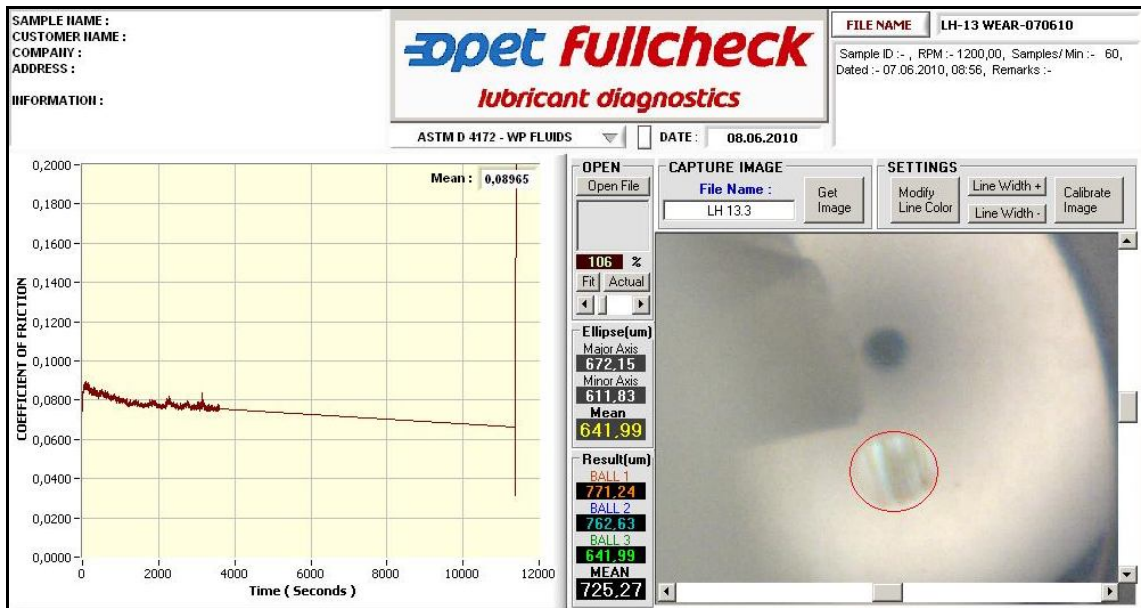
Figure C.6. The wear and friction behavior of the lubricant containing the precipitate of the microemulsion having 30% propanol-2.
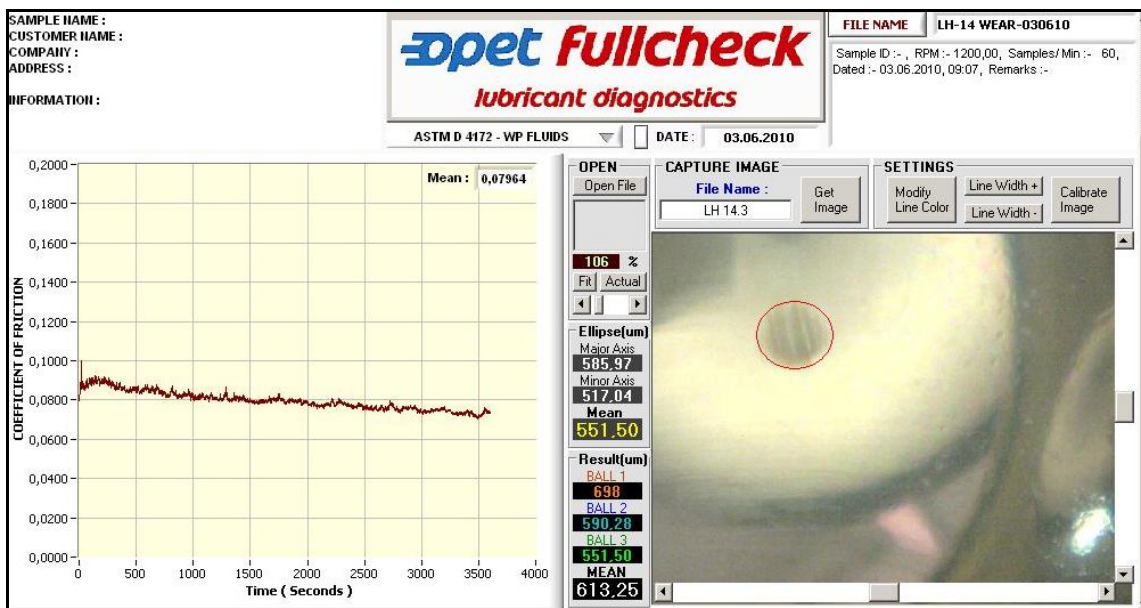

Figure C.7. The wear and friction behavior of the mineral oil having sorbitan monostearate and clinoptilolite rich mineral.
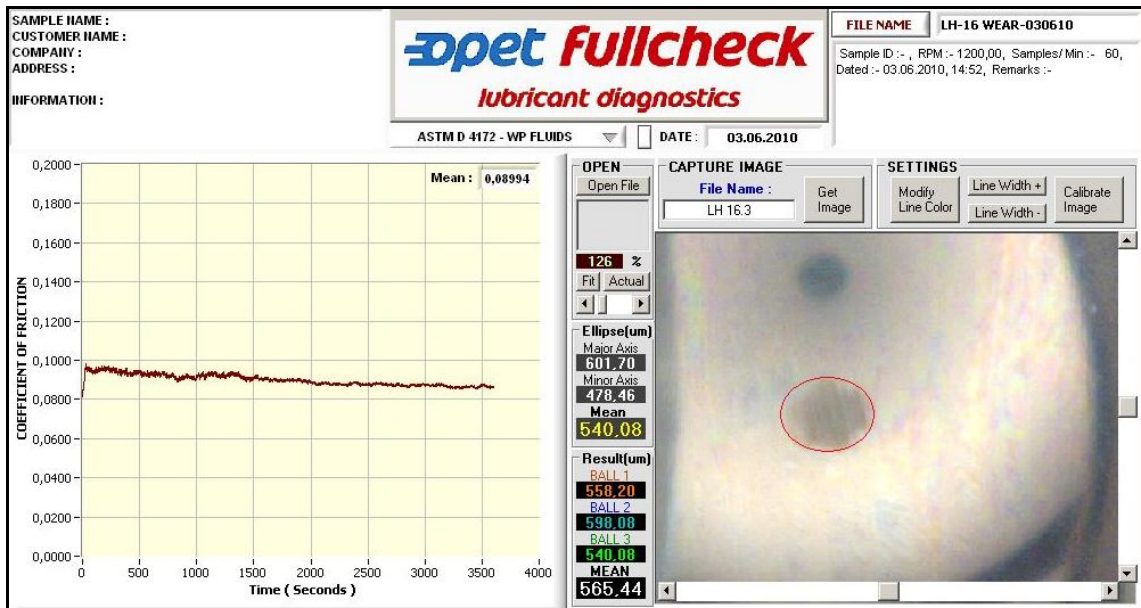
Figure C.9. The wear and friction behavior of the inverse emulsion of which water content was removed by clinoptilolite rich mineral.

VITA

PERSONALITY

Date of Birth: May 29, 1978

Place of Birth: İzmir

EDUCATION

2004 **Master of Science (M.S.)** İzmir Institute of Technology, Department of Chemical Engineering

2001 **Bachelor of Science (B.S.)** Hacettepe University, Department of Chemical Engineering.

PUBLICATIONS

S.A.Savrık, D. Balköse, S. Ülkü, "Synthesis of Zinc Borate by Inverse Emulsion Technique for Lubrication", submitted to *. J. Therm. Anal. Calorim., 2010.*

PRESENTATIONS

S.A. Savrık, M.Gönen, D.Balköse, S.Ülkü, Performance of Zinc Borate Nanoparticles as an Antiwear Additive in Mineral oil, *6th Nanoscience and Nanotechnology Conference*, 15-18 June, 2010.

S.A. Savrık, D.Balköse, S.Ülkü, "Synthesis of Zinc Borate in Inverse Microemulsion", *6th Chemical Engineering Conference for Collaborative Research in Eastern Mediterranean Countries*, Antalya, Turkey, 7-12 March, 2010

S.A. Savrık, M.Gönen, F.B. Alp, D.Balköse, S.Ülkü, "Zinc Borate Lubricant Production by Inverse Emulsion Technique", *Fourth International Boron Symposium*, Eskişehir, Turkey, 15-17 October, 2009

M. Gönen, D. Balköse, F.B. Alp, S.A. Savrık, S. Ülkü, "Supercritical Ethanol Drying of Zinc Borates", *Fourth International Boron Symposium*, Eskişehir, Turkey, 15-17 October, 2009.

S.A. Savrık, M.Gönen, F.B. Alp, D.Balköse, S.Ülkü, "Nano-Size Zinc Borate Production from Borax Decahydrate and Zinc Nitrate", *5th Chemical Engineering Conference for Collaborative Research in Eastern Mediterranean Countries*, Cetraro, Italy, 24-29 May, 2008.

MEMBERSHIP

Chamber of Chemical Engineers